University of Reading
Department of Meteorology

in association with Rothamsted Research

The biometeorology of high-altitude insect layers

Curtis Ron Wood

A thesis submitted for the degree of Doctor of Philosophy

March 2007

Declaration

I confirm that this is my own work and the use of all material from other sources has been properly and fully acknowledged.

Curtis Wood

Abstract

Flight at high altitude is part of a migration strategy that maximises insect population displacement. This thesis represents the first substantial analysis of insect migration and layering in Europe. Vertical-looking entomological radar has revealed specific characteristics of high-altitude flight: in particular layering (where a large proportion of the migrating insects are concentrated in a narrow altitude band). The meteorological mechanisms underpinning the formation of these layers are the focus of this thesis.

Aerial netting samples and radar data revealed four distinct periods of high-altitude insect migration: dawn, daytime, dusk, and night-time. The most frequently observed nocturnal profiles during the summertime were layers. It is hypothesised that nocturnal layers initiate at a critical altitude (200–500 m above ground level) and time (20:00–22:00 hours UTC).

Case study analysis, statistical analysis, and a Lagrangian trajectory model showed that nocturnal insect layers probably result from the insects' response to meteorological conditions. Temperature was the variable most correlated with nocturnal insect layer presence and intensity because insects are poikilothermic, and temperatures experienced during high-altitude migration in temperate climates are expected to be marginal for many insects' flight. Hierarchical effects were detected such that other variables—specifically wind speed—were only correlated with insect layer presence and intensity once temperatures were warm.

The trajectory model developed comprised: (*i*) insect flight characteristics; (*ii*) turbulent winds (which cause vertical spread of the layer); and (*iii*) mean wind speed, which normally leads to horizontal displacements of hundreds of kilometres in a single migratory flight.

This thesis has revealed that there is considerable migratory activity over the UK in the summer months, and a range of fascinating phenomena can be observed (including layers). The UK has moved from one of the least studied to perhaps the best studied environments of aerial insect migration and layering in the world.

Occam's razor (lex parsimoniae)

"Entia non sunt multiplicanda praeter necessitatem"
'Entities should not be multiplied unnecessarily'

William of Occam (c. 1285–1350)

Acknowledgments

Particular thanks must go to the following people and organisations. **Janet Barlow** for providing guidance in such subtle and tactful ways that I rarely knew that I was being directed; also for witty sidetracks. **Jason Chapman** and **Ian Woiwod**, of Rothamsted Research, for supervision of entomological material. **Pete Clark** for providing UM data and advice on modelling; plus tangential humour during meetings. **Sue Gray** and **Paul Mason** for academic guidance through the monitoring committee. **Paul Mason, John Gloster,** and **Anthony Illingworth** (chair) for examining me and the thesis in the PhD *viva voce* examination. **Don Reynolds** for guidance and humour, particularly during field work. **Alan Smith** for technical expertise, assistance, and lodgings. **Dave Thomson** and **Andy Reynolds** for comments on Lagrangian modelling. **Suzanne Clark** and **Sue Welham** for statistical advice. **Richard Harrington** and **Kelvin Conrad** for conducting a 2-year VIVA. **Stephen Belcher** and the **boundary-layer meteorology group** for constructive academic (and otherwise) discussions. The **Meteorology Department** for its elite qualities both academically and, most particularly, social aspects. Departmental **PhD students** for a friendly network of support and banter. **Officemates** for procrastinations when needed. **Jon Shonk** for sharing pedantry remarks on life, the universe, and everything. **Duncan Ackerley**, and other housemates, for supporting me. **Rob Thompson, Ewan O'Conner**, and **Matt Sapiano** for MATLAB help. **Genstat**, **Matlab**, **UNIX**, **Google,** and **Amazon** for making my life much easier. **Microsoft** for both making my life easier and testing my temper at the same time. **The Concise Oxford Dictionary**, which I have aimed to heed in the writing of this thesis. **BBSRC** & the **Met Office** for funding. **RMetS** for providing bursaries for conferences and fieldwork alike, for providing a strong community in the UK of atmospheric scientists, and for the opportunity to serve as chair of the Student Conference 2006. **Kevin Waters** and **Hugo Ricketts** for always being supportive friends. **My family**, parents in particular, for financial and emotional support.

Contents

1: An introduction to the biometeorology of high-altitude insect layers

This chapter first considers what insect migration is and which meteorological processes are likely to affect airborne insect movements. A review of the literature on layer concentrations of insects in the atmosphere will then be presented.

1·1 An introduction to the insects

The insects (Phylum Arthropoda, Class Insecta) are the most dominant group of land animals on the Earth. There are about one million named species, and 80 % of all known animals are insects, and it is estimated that up to ten million insect species exist. The UK alone has over 20,000 species, more than all its other terrestrial organisms put together (Chinery 1993). Insects have many advantages that have led to them becoming so successful, but perhaps it is their widespread ability to fly during the adult stage of life that is most important. Flight enables insects to (*i*) escape predators; (*ii*) find mates, food, and other resources; and (*iii*) move from unsuitable to suitable habitats (*i.e.* to migrate), often covering distances which would be impossible by terrestrial locomotion. Insects are found all over the globe in all climates, in all terrestrial and freshwater habitats, and in the lower regions of the atmosphere (usually up to 1 – 2 km above ground level) where many species spend appreciable amounts of time (hours, or even days in some cases) during their migratory flights. The size range of insects varies through orders of magnitude, the body-mass of airborne insects in the UK varies massively: 0.1 mg – 2 g (*e.g.* Johnson 1969, Chapman *et al.* 2004a). The existence of

this enormous aerial insect fauna is often overlooked, and it is this area of insect ecology that forms the focus of this chapter.

1·2 The aerial insect fauna

1·2·1 Introduction

At any given moment, there is an enormous diversity of insects in Earth's atmosphere that are engaged in windborne migration (Johnson 1969, Chapman *et al.* 2003). For example, over southern England in a typical summer's month, in the region of three billion insects (*c.* 1 tonne) will fly through a 1 km² 'window' of the atmosphere (Chapman *et al.* 2003). Large numbers of day-flying insects have been observed as high as 2.5 km above ground level (a.g.l.) in many regions of the world (Campistron 1975). Many species-rich and economically important insect orders regularly fly at high altitudes[*].

Migrant insect populations around the world have been observed to travel distances of up to 150 – 350 km in a single flight (Greenbank *et al.* 1980, Drake and Farrow 1983), although some individuals in a migrating population may only be airborne for short periods and migrate smaller distances, *e.g.* in the range of 20 km.

The most successful long-distance migrants are often serious pests to agriculture and humans: *e.g.* locusts, armyworm moths, and rice planthoppers (Pedgley 1993, Riley *et al.* 1995, Feng *et al.* 2003). For reviews on the pest status and zoogeography of some migrant Lepidoptera, see Fitt (1989) for *Helicoverpa* species and Showers (1997) for the black cutworm *Agrotis ipsilon*. Indeed, 10 % of the world's food production is destroyed annually by insect pests (Chinery 1993). Some airborne insects are virus vectors (*e.g.* the bluetongue[†] virus is carried

[*] High-altitudes are those that are well above an insect's flight boundary layer (FBL); for a definition of the FBL see §1·5·1.
[†] Bluetongue is a disease that affects livestock, often resulting in death.

particularly by the midge *Culicoides imicola*, there was an outbreak of this, typically Mediterranean-based, virus in northern Europe in the summer of 2006 (Enserink 2006)). Clearly, in order to protect crops and livestock better, an improved understanding of insect migration patterns and their implications is required. Insect migration studies are logistically challenging to carry out, but can supply useful information on population dynamics, investigate physiological and genetic traits, and work towards pest-outbreak prediction systems.

The aerial insect fauna in the UK atmopshere are studied further in Chapter 2.

1·2·2 Migration

Migration can be divided into **passive** and **active** movements. Some wingless arthropods (*i.e.* spiders, mites, and some insect larvae such as scale-insect 'crawlers') can partake in purely passive migration in the wind, although even here they often have special adaptations to facilitate this: *e.g.* spider ballooning (by controlling the release of silk thread, see Freeman (1946)). However, all flight by winged adult insects is active movement, where individuals have a large control over at least take-off and landing.

Another (and perhaps more fundamental) way in which movements can be discriminated is as **vegetative** (or **trivial**) movements and **migratory** movements (Kennedy 1985, Dingle 1996). Vegetative flight movements are usually over short distances close to the ground, and are concerned with the exploitation of resources for growth and reproduction, *e.g.* searching for food, mates, and egg-laying sites. Migratory movement implies movement of a portion of a population from one breeding or diapause site to another, sometimes involving displacements over tens or hundreds of kilometres. During migratory flight, vegetative forms of behaviour are temporarily suppressed (Taylor 1974, Matthews and Matthews 1978, Kennedy 1985). In many species, migratory flights are restricted to a distinct phase of the life cycle: often immediately after adult emergence. This distinction between discrete parts of the adult life cycle, of the

migratory phase preceding sexual maturation, is known as the **oogenesis-flight syndrome** (Johnson 1969).

The classic migration definition, which is most applicable to insects, is by Kennedy (1961):

> *"Migration is persistent, straightened-out movement with some internal inhibition of the responses that will eventually arrest it. It may be effected by the insect's own locomotory exertions or by its embarkation on some transporting vehicle, and in common with diapause involves a phase of depression of "vegetative" (growth-promoting) functions as a condition for their resumption."*

Insects migrate in order to find suitable habitats for feeding, mating, and producing the next generation. If their preferred habitat changes in quality throughout the season, then migrant species can attempt to locate areas that are more suitable. The alternative to migration is to enter a diapause (such as hibernation or aestivation[*]) to await suitable conditions. Overall, by being able to travel long distances, migrants are able to exploit resources that vary in space and time (Southwood 1977). A more complicated model of the components of a migration system was proposed in which the components comprised migration syndrome, migration arena, population trajectory, and genetic complex (Dingle and Drake 2007); this is not considered any further here.

Migration is a costly behaviour. Firstly, aerial migration is very energy consuming: flight is $50-200$ times more energetic than resting (Dudley 2001). Migration is hazardous, due to the increased risk of predation. Furthermore, migrant individuals may not find suitable new resources or even end up in completely unfavourable areas, such as the sea or cold mountain tops. However, for many species, the advantages manifestly outweigh the disadvantages and it has clearly proved a very successful lifestyle in evolutionary terms: many highly migratory species are extremely abundant and some have a cosmopolitan distribution (*e.g.* the diamond-back moth, *Plutella xylostella*).

[*] A prolonged dormancy in adverse heat and dryness.

1·2·3 Migratory flight periodicity

Four phases of high-altitude migratory flight activity throughout the diel[*] have been observed by radar and aerial netting in the UK (Smith *et al.* 2000, Chapman *et al.* 2002a, plus see Chapter 2 of this thesis). Peaks in aerial insect abundance have been observed in each of the dawn, day, dusk, and night periods. Every insect species has a preferred time of flight, thus different insect species are active in different phases (Lewis and Taylor 1964, Chapman *et al.* 2004a). For example, nocturnal migrants frequently take off during dusk, such as the dusk-peak of grasshoppers observed in Mali (Riley and Reynolds 1979), which took off $17-23$ minutes after sunset resulting in a $2-3$ order of magnitude increase in insect numbers $35-50$ minutes after sunset. Take-off within an hour of sunset has also been observed frequently elsewhere (*e.g.* Schaefer 1976, Drake 1984). Noteworthy exceptions, where insects bridge two phases, include micro-insects[†] that continue daytime migrations into dark (Farrow 1986, Chapman *et al.* 2004a) and a continued flight of nocturnal migrants that were over the sea at dawn (Wolf *et al.* 1986). Migrations starting at dusk typically last from a fraction of an hour up to the whole night *i.e.* $8-10$ hours (Greenbank *et al.* 1980, Feng *et al.* 2004a). Flight periodicity in the UK is the focus of Chapter 2.

1·3 Environmental responses

Insect flight in the atmosphere is typically within the **atmospheric boundary layer** (ABL) (see §1·4): both active and passive movements are affected (to a lesser or greater extent) by ABL processes. Firstly, to aid the understanding of high-altitude insect migration, it is necessary to consider how an insect might respond to its ambient environmental conditions.

[*] A biological term denoting 24 hours.
[†] There is no universally accepted limit, but micro-insects are defined in this thesis as insects too small to be individually observed by the vertical-looking radar (see Chapter 2), hence micro-insects are typically less than *c.* 1–10 mg.

1·3·1 Effects of temperature on take-off and flight in migrants

Insects are cold-blooded (**poikilothermic**), which means that they do not keep their internal body temperature constant. The physiology of many species in temperate countries (such as the UK) will be such that insects are limited by temperature. For example, winged insects will remain grounded unless their flight muscles reach warm enough temperatures for take-off. Once airborne, migrating insects might have an 'optimum' preferred temperature for flight, which is often above the air temperatures usually experienced in the UK (*e.g.* Chapman *et al.* 2003). Hence, one would expect such insects to tend to fly in warmer levels of the atmosphere if the atmosphere is too cool. It is likely that the response is more likely to be a positive **thermokinesis** (undirected stimulus) than a **thermotaxis** (directed stimulus): so that insects become less active in cool areas of the atmosphere and are thus less abundant. It seems unlikely that insects can detect temperature gradients and thus move toward higher temperatures by such a mechanism.

Some insects can partake in **endothermic** warming (*i.e.* alter their internal temperature). Primarily this is done by flapping their wings (94 % of energy supplied to wings goes to heat (Gullan and Cranston 2000)). Endothermic insects are typically larger and can raise body temperatures to $5-10\,^{\circ}C$ warmer than their environment (Matthews and Matthews 1978). Such warming can take place on the ground prior to flight, but thoracic warming will also occur due to wing-flapping during the aerial migration itself. This extra source of warming means some species might be able to stay airborne even when environmental temperatures fall below the minimum take-off threshold for the species concerned.

Insects that are more massive have a higher thermal inertia (Gullan and Cranston 2000) and can hence maintain their internal temperature for longer than less massive insects (*i.e.* the more massive an insect is, the further it is likely to be from ambient temperature). Perhaps this implies that more massive insects are less constrained by temperature than smaller insects. A budget of all energy sinks

and sources for an individual insect has been produced by Rainey (1989), but this will not be further considered here.

In summary, it is likely that temperatures are a large constraint on insect flight and temperatures are often sub-optimal for migrating insects in the UK, particularly at night when temperatures are typically cooler than by day. Consequently, migrants will prefer to fly in the warmest air, although thermal inertia and endothermy will complicate the relationships between temperature and insect flight.

1·3·2 Effects of vision on migratory behaviour

Insect vision might have a role to play in the orientation and navigation of migrants, particularly via the **optomotor** effect (Riley and Reynolds 1986). The optomotor response is a reflex feedback system by which animals adjust their position with respect to a moving background. In laboratory experiments, a cylinder with striped walls can be rotated around an insect. The individual often responds by turning its body in the opposite direction, as though it is attempting to stabilize the image of the cylinder's stripes on its retina (Götz 1972). Airborne insects are hypothesized to have a preferred speed of images moving across the retina, *i.e.* the **preferred retinal velocity**, and they will manoeuvre to attempt to achieve this velocity (Johnson 1969). Optomotor responses to ground patterns are an essential component of flight stabilization and many orientation mechanisms in low-flying insects (although other stimuli might be involved). There is much less information about optomotor reactions in high-flying insects; indeed some authors propose a **maximum compensatory height**, above which the optomotor response no longer occurs. The maximum compensatory height might be approximately the same altitude as the top of the flight boundary layer, FBL (see §1·5·1, Johnson 1969). For insects migrating at night, particularly on moonless nights, it is not thought that the migrants would be able to perceive the ground patterns and/or whether they would react to the very small angular velocities involved at these high altitudes. However, the response must be considered as a

possible mechanism when trying to explain wind-related orientation of high-flying insects observed by radar (Riley and Reynolds 1986, Riley 1989).

1·3·3 Chemical cues

Insects engaged in vegetative flight are highly responsive to chemical cues: for instance, the well-known upwind movement in response to sex pheromones (*e.g.* Gullan and Cranston 2000). During migration, reactions to vegetative cues are inhibited (Kennedy 1985), and no evidence has been presented that migrating insects land due to the influence of large-scale plumes from the ground. Thus, chemical responses are not considered further in this thesis.

* * * * *

In summary, it appears that migrating insects are primarily sensitive to temperature and wind; reactions to the latter being detectable through the movement of ground patterns (although direct responses to wind through the detection of turbulence might also be possible, see §1·6). Hence, it is now convenient to consider the environmental conditions imposed upon migrating insects by exploring the nature of the atmosphere in the ABL.

1·4 The atmospheric boundary layer

The 'atmospheric boundary layer' (ABL) is a general term for a layer of atmosphere next to the ground, of typically a few hundred metres depth, that is greatly affected by the Earth's surface. The ABL often takes different names depending on the current atmospheric conditions. For example, under idealised clear-sky conditions, a day-time boundary layer is convective (*i.e.* a CBL), and a nocturnal boundary layer (NBL) is stable. This section will highlight the processes governing ABL structure (which varies in space and time) that will be most relevant to high-altitude insect migrations. Throughout this review—unless otherwise stated—the ABL is assumed to form in response to idealised conditions: *i.e.* at an inland location with flat terrain and clear-sky conditions.

Comprehensive texts on ABLs are many, and form the source of the review of boundary layer theory discussed in the following sub-sections (Arya 1988, Stull 1997, Garratt 1992, Kaimal and Finnigan 1994).

1·4·1 Introduction

The ABL is the layer of the atmosphere next to, and directly affected by, its physical boundary: the surface of the Earth. The ABL is the most turbulent part of the atmosphere, due to it being in contact with the Earth's surface (where turbulent exchanges take place: primarily of heat, momentum, and moisture). ABL depths are highly variable (*e.g.* 50 m – 3 km), dependent upon conditions. The key sub-layers, *i.e.* within the ABL, are listed below (additionally, see Figure 1·1).

- The **laminar sublayer** is directly adjacent to the surface and is a few millimetres in depth where flow is determined by molecular viscosity / diffusion.

- Air flows around individual objects in the **roughness sublayer**, the 'roughness elements' comprise macroscopic objects such as grass, trees, and buildings.

- The **surface layer** occupies approximately the lowest 10 % of the ABL. Vertical fluxes of heat and momentum are approximately constant with altitude.

- The **mixed layer** consists of turbulent eddies, the size of which are typically constrained by the mixed layer depth. The turbulence comprises rising buoyant plumes (convection) and wind-driven (mechanical) mixing; hence, many quantities are well mixed (such as heat, humidity, and tracers). Mixed layers only occur within a **convective boundary layer** (CBL).

- A **capping inversion**: at the top of a CBL there is a strong inversion[*], which is *c.* 50 – 100 m thick and located above the mixed layer. The inversion is stable (see §1·4·3) and thus buoyant plumes rise no further in altitude, which confines air to the CBL. However, more energetic thermals will overshoot their level of neutral buoyancy, hence the capping inversion is also referred to as an **entrainment zone** due to the mixing caused by overshooting (*i.e.* air is entrained from the free atmosphere into the ABL). The altitude of the capping inversion is often used as an estimation of CBL depth: there is often a marked change in temperature and humidity across this inversion layer.

- The air above the capping inversion is known as the **free atmosphere**. Flow is almost entirely unaffected by frictional forces due to the Earth's surface, but instead only affected by the coriolis force (*i.e.* due to Earth's rotation) and the pressure gradient force[†]; the balance of these two forces is denoted '**geostrophic**': so that geostrophic winds flow *parallel* to isobars (lines of equal pressure).

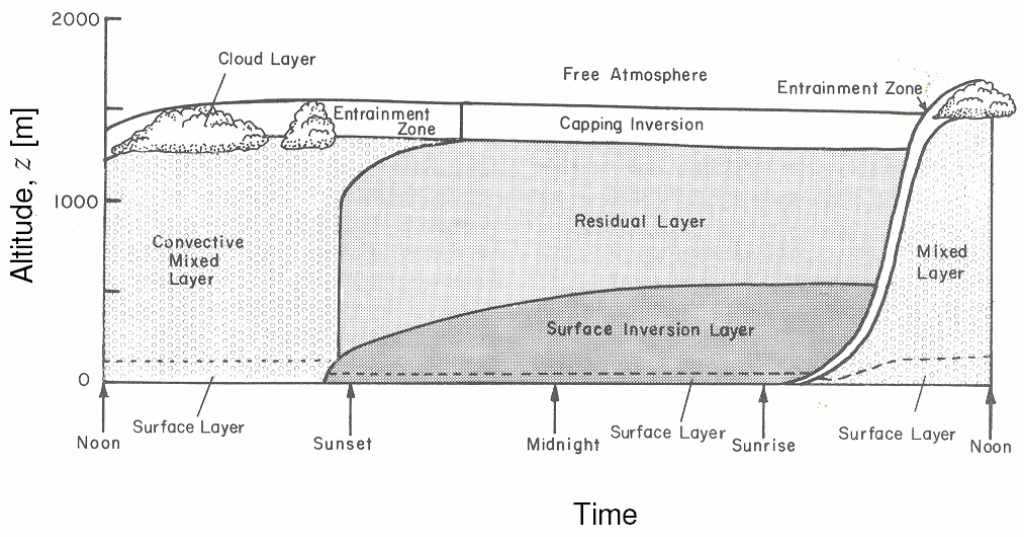

Figure 1·1 – *Diurnal evolution of the ABL (after Arya 1988). Lines represent the boundaries between layers.*

[*] A temperature *increase* with altitude.

[†] There is also a third force for highly curved flow on a large scale (*e.g.* hundreds of kilometres): centripetal acceleration. This is not considered in this thesis because—as shall be shown later—most interest is in situations of high atmospheric pressure, when the flow is not very curved on a large scale. For further information see 'gradient wind' in McIlveen (1992).

1·4·2 Diurnal cycle

The ABL diurnal cycle is driven by the balance of incoming and outgoing energy at the surface. A surface energy budget is shown in Figure 1·2 (*e.g.* Arya 1988), and balanced as follows:

$$R_n - G = H + \lambda E\,. \qquad (1{\cdot}1)$$

The net radiation, R_n, at the surface comprises up- and down-welling long- and short-wave radiation; R_n is defined as positive towards the surface. The ground heat flux, G, is positive away from the surface, as heat is conducted down into the soil. The energy available to the atmosphere is hence $R_n - G$, which is used by two different turbulent flux processes. Firstly there is heating of the overlying air by turbulent exchange of heat: sensible heat flux, H. Secondly, evaporation* leads to a vertical gradient of moisture, hence turbulent exchange of moisture: the latent heat flux, λE (where λ is the latent heat of evaporation and E is the amount of evaporation). All are usually expressed in units of W m^{-2}.

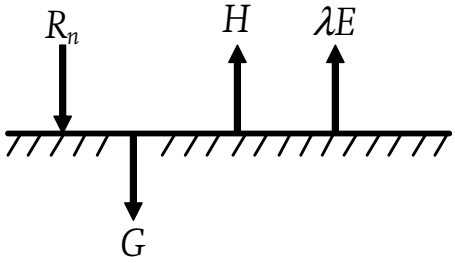

Figure 1·2 – *Surface energy balance at the Earth's surface during the daytime.*

Long-wave radiative cooling of the surface occurs by both night and day, but is often a negligible fraction of the net radiation by day because of the larger down-welling solar (short-wave) radiation. Hence, the night-time ABL is dominated by the energy removed from the surface via long-wave radiative cooling, giving a negative net radiation. Hence, under clear-sky conditions, as the surface temperature becomes higher or lower than the air temperature, the sensible heat flux has an approximately sinusoidal variation: a positive maximum during the daytime and a negative minimum during the night-time. The form of the NBL is explored further in §1·4·7.

* Becomes evapotranspiration for vegetated surfaces.

Figure 1·1 shows the typical diurnal variation of an ABL in fair-weather conditions. A daytime ABL is convective (*i.e.* a CBL) when turbulence is dominated by buoyant forces. Positive sensible heat flux implies upward motion: hence, as the sun increases in intensity during the day, the vertical plumes of air increase in frequency, magnitude, and energy. The air parcels rise until the surrounding air is sufficiently cool so that the air parcel no longer has an upward buoyancy force. Consequently, the CBL deepens throughout the daytime (Carson 1973). At night, the negative sensible heat flux allows the development of a shallow (typically $50-300\,\mathrm{m}$) stable **nocturnal boundary layer** (NBL), which leaves the remnants of the previous day's CBL aloft as a **residual layer** (RL).

1·4·3 Static stability

An introduction to potential temperature is provided here in order to consider **atmospheric stability** (see *e.g.* Stull 1997). The temperature at some altitude above the Earth's surface is affected by cooling due to expansion, because the atmospheric pressure is lower than at the surface. Potential temperature, θ, corrects for this effect by defining a measure of temperature that is referenced by pressure,

$$\theta = T\left(\frac{p_0}{p}\right)^{R/c_p}, \tag{1·2}$$

where p_0 is a constant reference pressure ($1000\,\mathrm{hPa}$), p is atmospheric pressure, T is absolute temperature, R is the dry gas constant, and c_p is specific heat at constant pressure (*e.g.* Stull 2000).

From vertical profiles of θ in the atmosphere, the **static stability** of the atmosphere can be inferred. An increase of θ with altitude indicates stable conditions (Figure 1·3). Colder air has a higher density than warmer air and hence stability prevents vertical motion of air when more dense air lies below less dense air (denser air has a greater gravitational force acting on it than less dense air does). A decrease of θ with altitude (super-adiabatic) indicates unstable conditions because less dense air is below denser air and hence has a buoyant

force pushing it upward in the atmosphere. The dry adiabatic lapse rate (DALR) in the atmosphere ($9.8\,\mathrm{K\,km^{-1}}$) means that potential temperature is constant with altitude and the static stability is neutral (*i.e.* neither stable nor unstable). An inversion profile is the most stable one.

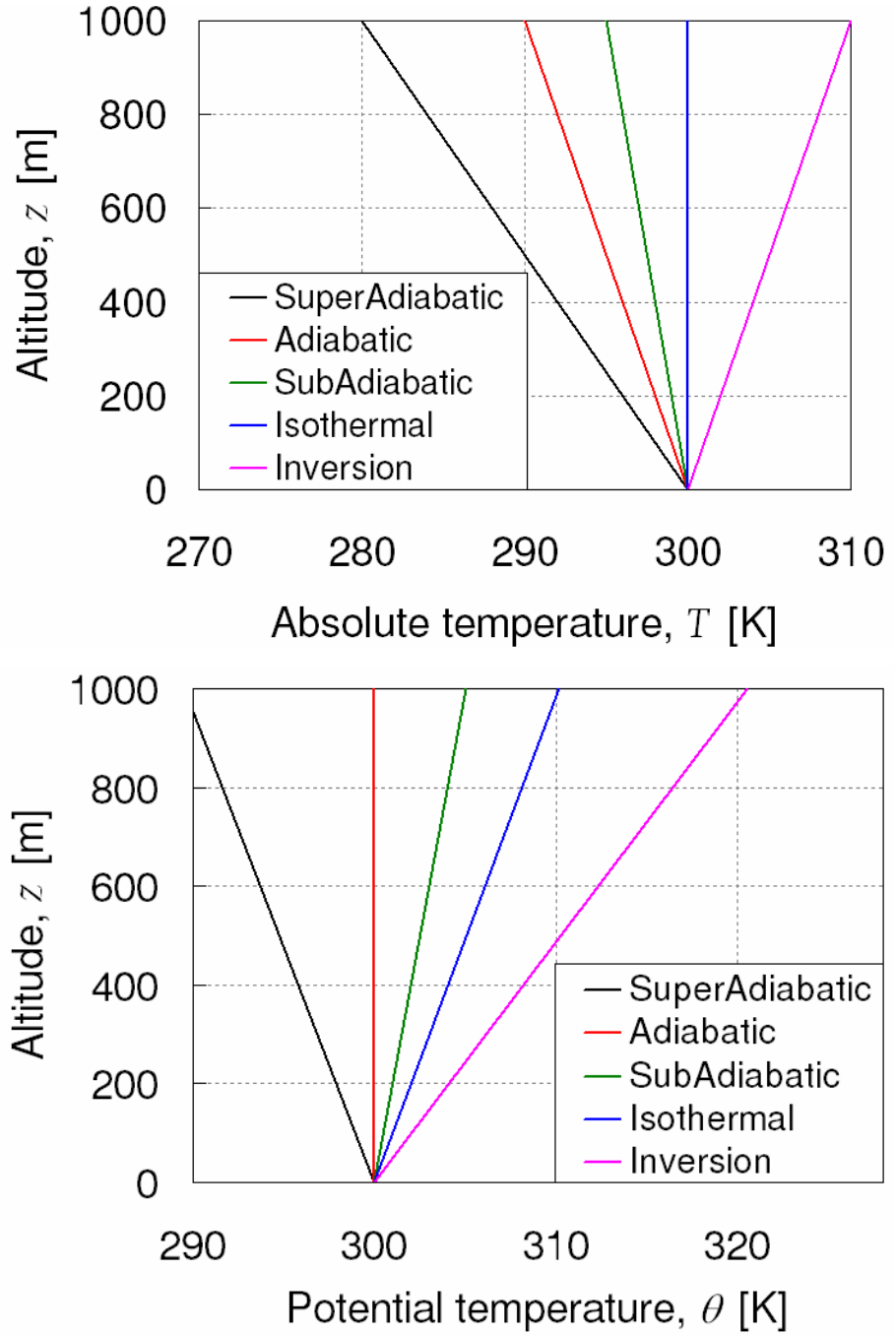

Figure 1·3 – *Temperature profiles showing different conditions of static stability, for absolute temperature (above) profiles, $T(z)$; and the corresponding profiles are presented (below that) using potential temperature, $\theta(z)$.*

In super-adiabatic profiles, parcels* of air can rise to form convective structures: thermals, plumes, jets, and bubbles (Garratt 1992). Such structures merge as they rise to form coherent structures such as large eddies, which can transport air directly from the ground up to the capping inversion. Updraughts are of order $2\,\mathrm{m\,s^{-1}}$ in the CBL; hence, a mixing time of 20 minutes is typical in a $1\,\mathrm{km}$ deep CBL. A useful distinction can be made between turbulence dominated by buoyant convective processes (**free convection**) and turbulence dominated by mechanical processes (**forced convection**).

1·4·4 Vertical neutral profiles of meteorological variables

Figure 1·4 shows typical profiles in the daytime CBL. Profiles of θ are typically super-adiabatic in the surface layer and neutral throughout the mixed layer. The capping inversion is $1-2\,\mathrm{km}$ high in UK summer daytime and is seen as a temperature inversion, but changes in the vertical profiles of wind and humidity are also observed at that altitude. The super-adiabatic profile in the SL is caused by the fact that the energy source for convective motions in the CBL is supplied at the surface. The surface subsequently heats layers of air above via longwave radiative emission, conduction (a poor method of heat transfer), and convection.

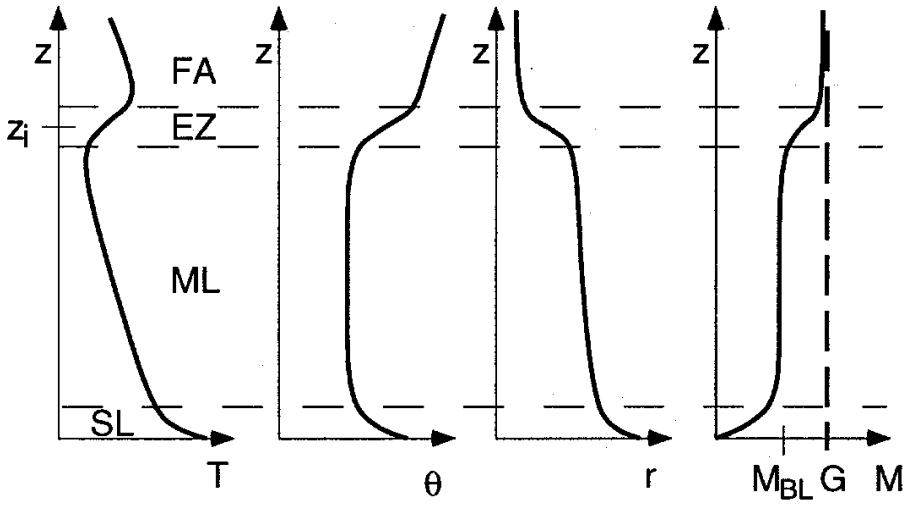

Figure 1·4 – *Typical daytime profiles in the CBL of temperature (T), potential temperature (θ), humidity mixing ratio (r), and horizontal wind speed (M). Geostrophic wind is denoted as G. Altitude is z, and inversion height is z_i. From Stull (2000).*

* An arbitrary volume of air that can be traced in space and time. Its environment properties are typically thought to remain constant with time.

In the free atmosphere, where frictional forces are negligible, wind velocities are geostrophic (Figure 1·4). Throughout the ABL, wind speed is sub-geostrophic due to the frictional force, but momentum is evenly distributed in the mixed layer causing wind speed to be constant with altitude. In the surface layer, air is less affected by surface friction with increasing altitude, hence the wind speed increases with altitude. The increase of wind speed with altitude is thus dependent upon surface friction and altitude a.g.l., hence in a neutral surface layer a scaling analysis yields the following expression for vertical gradient of wind speed (wind speed shear) in neutral conditions:

$$\frac{\partial u}{\partial z} = \frac{u_*}{kz}, \tag{1·3}$$

where u is wind speed, k is von Kármáns constant (0.41) and z is the altitude a.g.l. Friction velocity (u_*) represents the magnitude of wind-shear generated turbulence as a scaled velocity variable and is given by,

$$u_* = \left(\frac{\tau_s}{\rho_a}\right)^{1/2}, \tag{1·4}$$

where ρ_a is air density and τ_s is the surface drag force (flux of horizontal momentum toward the surface, see equation 1·9). Integration of 1·3 yields the wind speed profile in the surface layer:

$$u(z) = \frac{u_*}{k} \ln\left(\frac{z}{z_0}\right), \tag{1·5}$$

where z_0 is the aerodynamic roughness length, the altitude where the mean wind speed falls to zero, typical values range from 10^{-4} m for smooth ice and water surfaces to several metres for urban areas (Arya 1988).

The frictional force not only alters the wind speed, but the direction. Wind direction turns clockwise (veer) with increasing altitude until the geostrophic wind direction is reached: this is known as an **Ekman spiral**.

Sources of trace gases (*e.g.* pollutants) and water vapour are located at the Earth's surface. Hence, high values are found in the surface layer and low values in the

free atmosphere (see r in Figure 1·4). In between, in the mixed layer, turbulent plumes mix the gases evenly throughout depth. The nature of mixing and turbulence is discussed further in §1·4·5.

Equations for theoretical vertical profiles for wind speed and potential temperature can be modified for stable and unstable conditions by using Monin-Obukhov theory (*e.g.* Garratt 1992), but this is considered no further here.

1·4·5 Turbulent fluxes

In space and time, wind varies in magnitude and direction. The rapid and apparently random component of the wind is due to **turbulence**. The individual swirls of turbulence are called **eddies**, which can be visualised as vortices of varying sizes. The size of an eddy is constrained partly by its proximity to the ground (*i.e.* the need to fit a roughly spherical eddy in the space between a given altitude and the ground), hence eddies are typically larger at higher altitudes.

Figure 1·5 shows the spectral energy density associated with variations in wind speed at a range of timescales. There are essentially two timescales of wind speed variation: a smaller turbulent timescale and a larger 'synoptic' one. There is a **spectral gap** between the two peaks, where there are few processes creating variability. The *turbulent* (small) timescales vary irregularly in time from seconds to minutes, and in space from molecular lengths to the size of the mixed layer. Variations on scales of hundreds of kilometres and several hours correspond to *synoptic* scale variability, *i.e.* weather systems and fronts.

Because there is a 'spectral gap', it is useful to decompose local wind speeds into an averaged part (which varies only over synoptic timescales) and an instantaneous fluctuation corresponding to turbulence (small scale). Wind speed at a point location is hence composed of a mean wind speed, $\overline{u}$, plus a turbulent component, $u'(t)$. This is called Reynolds' decomposition (Figure 1·6),

$$u(t) = \overline{u} + u'(t). \qquad (1·6)$$

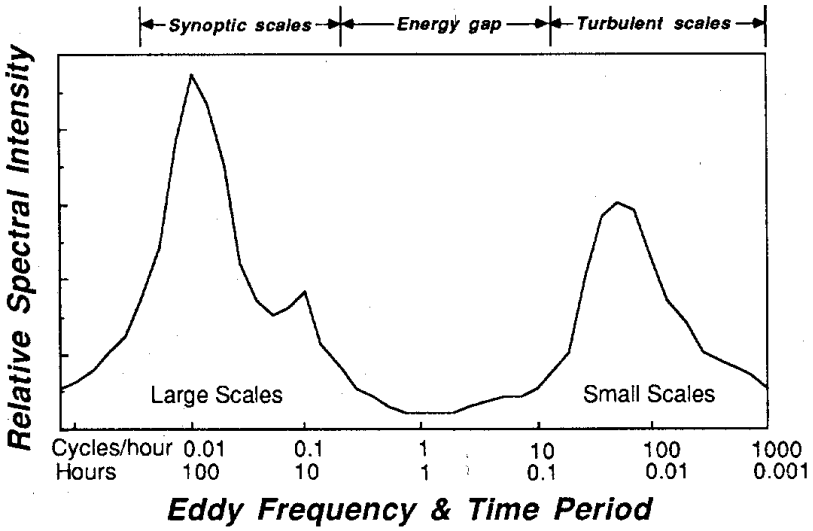

Figure 1·5 – *Horizontal wind speed spectrum from Stull (1997), after Van der Hoven (1957). The peak at 100 hours time period corresponds to synoptic scale winds and the peak at 0.01 hours corresponds to turbulent winds. The low spectral densities of period near 1 are time periods corresponding to the 'spectral gap'.*

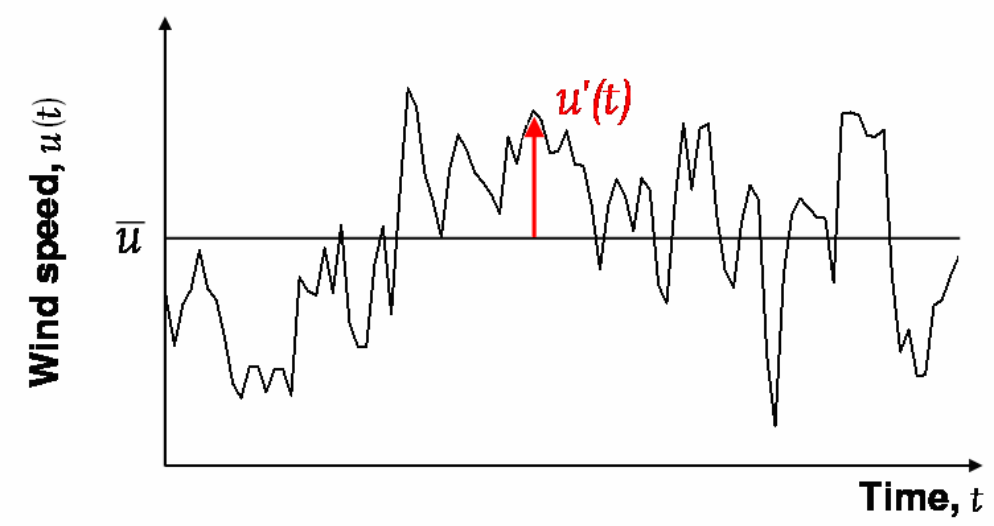

Figure 1·6 – *Variation of wind speed with time can be decomposed by taking a mean and thus finding the instantaneous deviation from the mean—the turbulent contribution—at each time step.* $\bar{u}$ *is mean wind speed, t is time, and* u' *is the turbulent fluctuation.*

Averaging over 10 – 100 minutes produces mean flow at a point location (averaging over longer timescales could inadvertently encompass synoptic scale variability, see Figure 1·5). In addition to transporting momentum, turbulent eddies also transport temperature, humidity, and other substances (*e.g.* gases and particles in the air). Any variable, *e.g.* ψ, can be decomposed in the same way, *i.e.*,

$$\psi(t) = \bar{\psi} + \psi'(t). \qquad (1\cdot7)$$

Turbulent diffusion is much more effective than molecular diffusion at causing vertical fluxes. The turbulent transport of temperature is given by a heat flux:

$$H = \rho_a c_p \overline{w'T'}. \tag{1·8}$$

The heat flux term represents a transport of heat vertically from the surface (H is positive upward). The $\overline{w'T'}$ term is known as a covariance, in this case between vertical wind speed and temperature (*i.e.* updraughts transport warm air upwards).

The vertical transport of horizontal momentum is known as Reynolds' stress, τ_s, which is positive for a *downward* flux of momentum,

$$\tau_s = -\rho_a \overline{u'w'} = \rho_a u_*^2, \tag{1·9}$$

where u is defined in the direction of mean horizontal wind speed.

The covariance terms can only be directly evaluated via use of fast-response equipment (*i.e.* high temporal resolution to capture fast fluctuations). So-called '*K*-theory' (or the flux-gradient method) assumes that covariances are proportional to the gradients of the respective variables:

$$\overline{u'w'} = -K_M \frac{\partial u}{\partial z}, \tag{1·10}$$

$$\overline{\theta'w'} = -K_H \frac{\partial \theta}{\partial z}, \tag{1·11}$$

where K_M and K_H are eddy viscosity (or eddy diffusivity) terms for momentum and heat respectively. By combining equations 1·3, 1·9, and 1·10, it can be seen that eddy viscosity for momentum varies with surface stress and altitude:

$$K_M = k u_* z. \tag{1·12}$$

Often $K_M \sim K_H$, because it is assumed that heat and momentum are transported in a similar way by turbulence.

1·4·6 Turbulence

Turbulence at a location is produced mainly by two mechanisms: wind shear (mechanical production) and buoyancy (*e.g.* convective plumes) (*e.g.* see Garratt

1992). The ratio of buoyant to shear production of turbulent kinetic energy* is a dynamic stability variable and is a measure of local turbulence, which is enhanced by unstable conditions and suppressed by stable conditions. The flux Richardson number is defined as:

$$Ri_f = \frac{\frac{g}{\overline{\theta}_0}\overline{w'\theta'}}{\overline{u'w'}\frac{\partial \overline{u}}{\partial z}}, \qquad (1{\cdot}13)$$

in which θ_0 is surface potential temperature. Flow is turbulent for $Ri_f < 1$ and flow is laminar†, for $Ri_f > 1$. K-theory represents the covariance terms (see equations 1·10, 1·11) instead in terms of gradients: hence, the same ratio becomes the gradient Richardson number,

$$Ri = \frac{\frac{g}{\overline{\theta}_0}\frac{\partial \overline{\theta}}{\partial z}}{\left(\frac{\partial \overline{u}}{\partial z}\right)^2} = \frac{\text{static stability}}{(\text{wind speed shear})^2}, \qquad (1{\cdot}14)$$

where $K_M = K_H$ has been assumed. Here, laminar flow becomes turbulent when $Ri < Ri_c$ and turbulent flow becomes laminar when $Ri > Ri_T$; $Ri \sim 0$ represents neutral flow. Typically $Ri_T = 1$ and $Ri_c = 0.25$ (Stull 1997).

When the gradient terms in equation 1·14 are discretised‡ with altitude, the value obtained is referred to as a bulk Richardson number, Ri_B. Hence, small scale turbulence might not be resolved. As vertical resolution in numerical models can be quite coarse, Ri_C values are artificially increased in an attempt to resolve turbulence (Lee *et al.* 1979).

* Turbulent kinetic energy is the variance of wind speed in directions *x*, *y*, and *z*.
† Smooth, viscosity-dominated flow.
‡ Averaged over finite steps, *i.e.* $\partial u / \partial z$ becomes $\Delta u / \Delta z = (u_2 - u_1)/(z_2 - z_1)$.

1·4·7 The nocturnal boundary layer (NBL)

Radiation

All matter above 0 K constantly emits radiation (*e.g.* Petty 2004). Wein's displacement law can be used to show that at temperatures of around 200–350 K (*e.g.* the Earth's surface, atmosphere, and clouds), the emitted radiation is longwave (the peak intensity is around 8–15 microns, in the near infra-red). At temperatures of 6000 K, the surface of the Sun emits radiation that is shorter in wavelength (peak intensity at 0.5 microns, in the visible). Hence, an important distinction is made between longwave and shortwave radiation.

The net longwave radiation near the Earth's surface is a combination of up-welling longwave radiative emission from the Earth's surface, plus the down-welling long-wave radiation from any clouds and the air itself. The net shortwave radiation is a combination of down-welling solar radiation, plus up-welling reflected solar radiation. The only source of shortwave radiation in the atmosphere is from the Sun. Hence, during darkness, the net shortwave radiation is zero and so the radiation budget is controlled by the net longwave radiation (*e.g.* Andre and Mahrt 1982).

The NBL

The net longwave radiation is relatively constant throughout the diurnal cycle ($100\ \mathrm{Wm^{-2}}$) compared to the larger change in shortwave radiation. Due to the strong diurnal cycle in solar radiation, at about 0.5–1 hours before sunset the net radiation becomes negative. The longwave radiative cooling from the surface exceeds that of the air itself, which leads to a stable temperature profile next to the ground, the 'SBL' (Figure 1·7), and hence there is typically a layer of warm air. As the cooling continues, this inversion layer deepens with time. This means that buoyant plumes can no longer exist: hence, turbulence in the SBL is only formed mechanically, *i.e.* by wind shear.

The cooling-rate within the surface inversion layer is faster within about $0-2$ hours after sunset than later in the night (Saunders 1952). Once the cooling has reduced to its second rate, the NBL is said to be 'well-developed', and steady state is often assumed for idealised cases. However, local-scale topographical features can create local-scale winds, which leads to alteration in cooling rates. For instance, slopes of just $0.1-1$ % can create katabatic (down-slope) winds that can alter local temperatures by $\pm 2\,\mathrm{K\,hr^{-1}}$, and wind speeds by $1-2\,\mathrm{m\,s^{-1}}$ (Mahrt 1981).

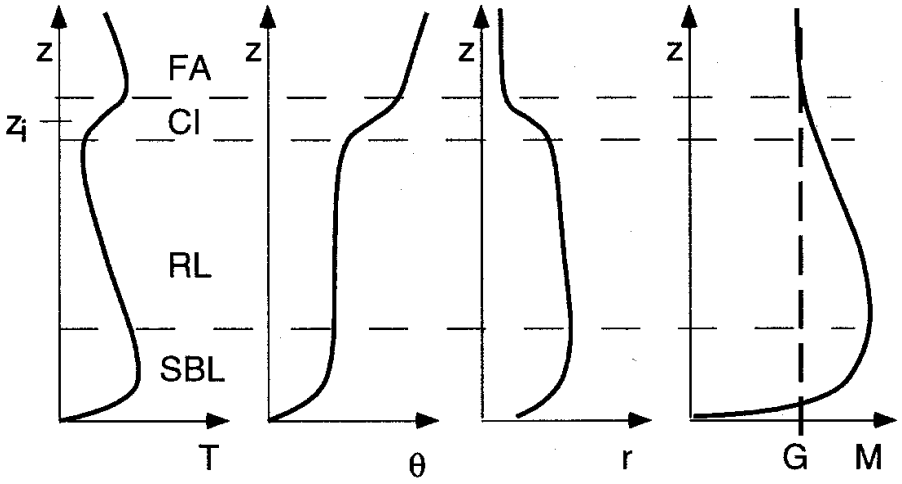

Figure 1·7 – *Typical nocturnal profiles in the NBL of temperature(T), potential temperature(θ), humidity mixing ratio(r), and horizontal wind speed(M). Geostrophic wind is denoted as G. Dashed horizontal lines indicate the boundaries between layers. Layers are stable boundary layer (SBL), residual layer (RL), capping inversion (CI), and free atmosphere (FA). Altitude is z, inversion altitude is z_i. From Stull (1997).*

Above the surface inversion, throughout the residual layer (RL), the potential temperature profile is neutral (*i.e.* an adiabatic cooling of temperature with altitude). Above that, the capping inversion (CI) from the previous day's convection can often be observed for many hours because there are no rapid processes that can erode the CI.

The humidity mixing ratio, r, is low in the SBL because evapotranspiration is reduced at night (firstly plants close their stomata, secondly reduced temperature and wind speeds leads to less evaporation). Additionally, there can be condensation of water vapour (dew) at the Earth's surface, hence reducing atmospheric water content. Values of humidity mixing ratio throughout the RL

remain similar to the previous day, because there are few sinks and sources for water vapour. Above the capping inversion, there is little source for water vapour, which accordingly reduces with altitude sharply through the capping inversion.

Shortly after sunset, when free convection ceases, there is no vertical transfer of horizontal momentum by buoyant plumes and hence only a shallow layer near the surface directly experiences the frictional forces (SBL). The daytime ML aloft is now replaced by a residual layer (RL) which is 'decoupled' from the surface, separated by the temperature inversion. The RL is a layer that is no longer in equilibrium with the surface (*i.e.* not in steady state): wind velocity accelerates, usually leading to the formation of a boundary layer nocturnal jet (Figure 1·7). At the jet's central altitude the flow becomes **super-geostrophic** (*i.e.* faster than geostrophic) for much of the night (Figure 1·8). The inertial oscillation leads to a change in wind speed and direction with time that can be mathematically derived (*e.g.* Thorpe and Guymer 1977, Davies 2000). A typical vertical structure of wind speed in the NBL is shown in Figure 1·9. Nocturnal wind maxima occur just above the temperature inversion in the nocturnal jet. The inertial oscillation starts at sunset with a time-period of $2\pi/f$ (f is the coriolis parameter); which is about 17 hours in mid-latitudes. The oscillation and jet are typically interrupted by thermals initiated by the following day's CBL, causing a 're-coupling' of air with the surface.

Within the RL, any turbulence is often intermittent. Large wind speed shear just above and below the jet reduce Ri (see equation 1·14). As Ri drops below Ri_c, turbulence starts to occur, thus causing mixing. Subsequently, vertical mixing of momentum smoothes the wind profile, thus reducing the vertical wind speed shear, which eventually results in Ri becoming larger than Ri_T: causing turbulence to stop and flow to become laminar once more. This effect can cause turbulence to be sporadic in space and time. The timescale of nocturnal turbulence is of the order of $6-30$ hours (Stull 1997).

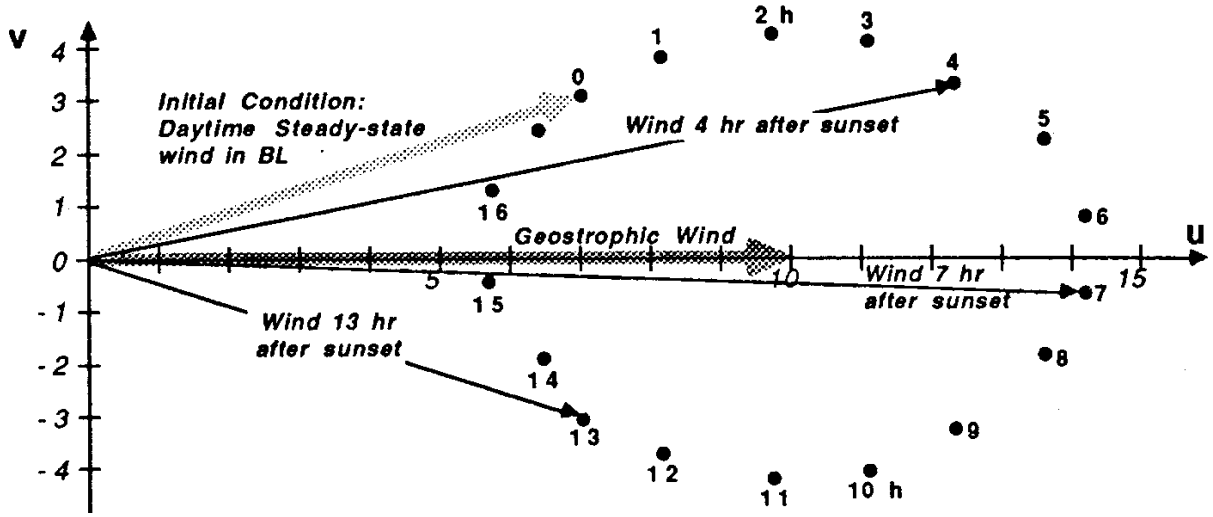

Figure 1·8 – *Inertial oscillation of wind speed in a nocturnal jet. From Stull (1988).*

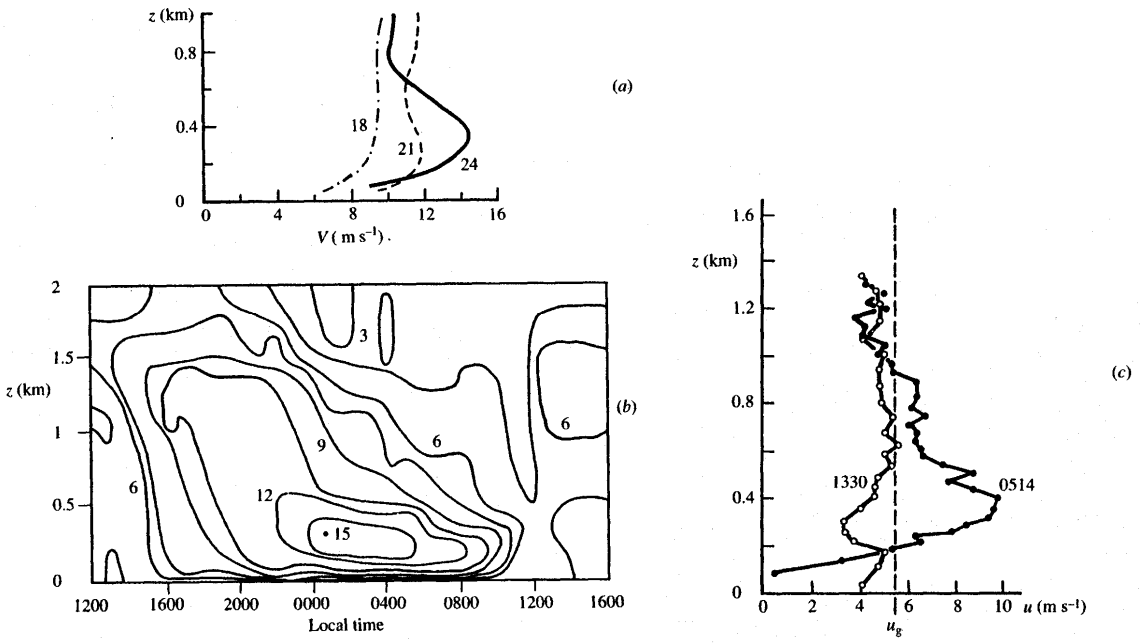

Figure 1·9 – *Spatial and temporal variation of an observed nocturnal jet during the 'WANGARA' experiment for (a) and (b) and (c) from Thorpe and Guymer (1977). After Garratt (1992).*

Various important depths can be defined within the NBL (Garratt 1992). The inversion altitude is generally defined as the altitude where $\partial\theta/\partial z = 0$, *i.e.* based on static stability. Sometimes $\partial T/\partial z = 0$ is used. The altitude below which there is substantial turbulent kinetic energy ($e = 0$ or $e = 0.05e_s$, where '$_s$' represents near-surface values) is used to denote where mixing is occurring. Alternatively, NBL mixing depth can be defined as the depth within which horizontal

momentum is vertically transferred: the altitude where $\overline{u'w'} = 0$ or $\overline{u'w'} = 0.05\left(\overline{u'w'}_s\right)$. A final useful altitude is the altitude of nocturnal jet (maximum $\bar{u}$).

Summary

Atmospheric boundary layers are typically divided into sub-layers, which are defined in terms of the profiles of the variables within the sub-layers. Within the ABL, these gradients can lead to environmental conditions at particular altitudes that are more favourable for insect migratory flight than other altitudes. If insects have the ability to detect these conditions, they might prefer flying at such altitudes (as is observed, see §1·6).

1·5 Migratory flight profiles

Until now in this chapter, migrating insects and their aerial environment have been considered separately. Hence, the following sections discuss how migrants can interact with their environment.

1·5·1 The insect flight boundary layer (FBL)

The insect FBL is a layer of air, extending a variable distance upwards from the ground, where the wind speed is lower than the insect's flight speed (Taylor 1974). Within this layer, insects are able to control their displacement direction by flying upwind, downwind, or crosswind. Hence, all vegetative movements associated with mate-finding or food-location (Kennedy 1985) are carried out within the FBL. It is typically only a few metres high for many small, weak-flying insects. The FBL will vary with prevailing meteorological conditions, so that on some days it is just a few cm (Taylor 1974) while on others it may be tens of metres high (or very occasionally hundreds of metres high (Riley 1975)). While some migrants carry out their long-range movements within the FBL (*e.g.* butterflies), so that they have more control over their flight track, the majority of

insect migrants fly above the FBL and thus utilise faster wind speeds to migrate further distances. The insect FBL must not be confused with the atmospheric boundary layer (ABL), which was discussed in detail in §1·4.

It was shown (§1·4·4) that wind speeds increase logarithmically with altitude in the surface layer, and in stable nocturnal situations the wind speed can increase dramatically up to a maximum at altitudes of $100-300\,\mathrm{m}$ if a nocturnal jet is present. Hence, insects flying above the FBL will experience fast wind speeds: a disadvantages being that insects have less control over their tracks. Of course, such fast winds are ideal for facilitating rapid windborne migrations.

Sometimes the aerial fauna above the FBL have been referred to as 'aerial plankton', implying passive flight. However, it seems possible that insects actively seek out specific altitudes for migration and partake in active flight. Even though the horizontal wind speed above the FBL is greater than the insect's flight speed, the insect's horizontal flight still contributes to the net horizontal insect movement as long as the insect is orientated approximately downwind. Surprisingly perhaps, high-flying insects frequently show a **common orientation** phenomenon (Riley 1975, Riley and Reynolds 1986, Chapman *et al.* 2003), where a population of migrating insects all fly with a common angle of deviation from the wind direction. Clearly, insects use the horizontal wind to facilitate rapid migration but in order to do so, insects need firstly to ascend to higher altitudes where wind speed and temperatures might be favourable.

1·5·2 Vertical movements

Synoptic vertical wind speed is of the order of typically $0.01-0.1\,\mathrm{m\,s^{-1}}$ in non frontal or non convective conditions (*e.g.* Stull 2000), which is small compared to horizontal wind speed (exceptions occur most notably in the up- and downdraughts of convective storms). Emigrating insects typically fly upwards with a vertical speed of $0.1-0.5\,\mathrm{m\,s^{-1}}$ (Schaefer 1979, Riley *et al.* 1991) and hence clearly have control over their vertical displacements in many situations. Meteorological radar has reported individual insects with an average upward

speed of 2.5 m s^{-1} (Bean *et al.* 1971); though this speed was likely to have been a combination of active flight plus a passive component due to convective plumes in the ABL.

Downward motion of insects can be much faster than upward motion due to the termination of intense wing beating. For example, in laboratory experiments, anaesthetized aphids of 0.49 mg reached terminal velocities of 0.82 m s^{-1} and 1.78 m s^{-1}, with wings fully extended and closed respectively (Thomas *et al.* 1977).

In summary, migrating insects are able to control their flight altitude during conditions of weak vertical motion, but there might be a few occasions (such as in violent updraughts associated with convective storms) when they are carried up to unfavourable altitudes (as shown by an insect embedded in a hail-stone (Browning 1981)).

1·5·3 Vertical distribution of insects in the atmosphere

It has been known for over 70 years (Coad 1931) that insect abundance usually reduces monotonically with altitude. This relationship might be more relevant for micro-insects, such as aphids (particularly during turbulent daytime conditions), than for larger species which are better able to control their vertical movements, or for insects flying at night. A continuous diffusion system has been suggested where individuals may be climbing or falling but the overall vertical structure remains constant (Johnson 1969). Although this has been mostly for day flyers, large night-flying insects have been observed with a monotonically decreasing profile of insect numbers for a period after dusk when emigration was occurring (Drake 1984).

The monotonic decrease of insect numbers with altitude has been represented by a power-law relationship (Johnson 1957a). The relationship was formed empirically after analysis of many major aerial trapping studies prior to 1957, and is applicable up to 5000 feet (*c.* 1.7 km). The use of the equation is demonstrated for experimental data in Figure 1·10.

A quantitative description of the monotonic insect decrease with altitude is thus provided by analysing data obtained by trapping mainly small insects (*e.g.* aphids) over several hours. It rarely reflects instantaneous vertical profiles of insects, particularly insects with large mass.

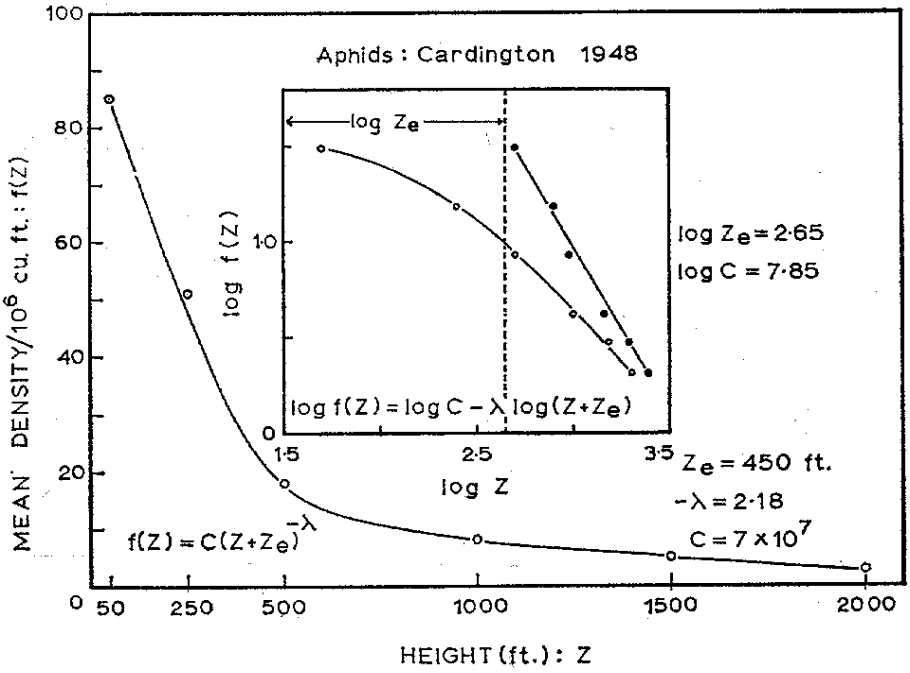

Figure 1·10 – *Mean profile of aphids at Cardington airfield, 1948 (from Johnson, 1969). The insert demonstrates a log-log transformation.*

One particular deviation from the monotonic profile is observed when a layer of insects can be observed for several hours, such that many individuals will concentrate at a particular altitude. This is particularly notable in stable atmospheric conditions where insects have excellent control of their vertical speed (and thus altitude of migration). Consequently, in these situations, it is possible that insects accumulate in the favourable conditions—*e.g.* the altitude of temperature inversion top—and so frequently, concentration of insects are observed in a layer of specific altitude. Insect layering is a migration phenomenon that is hence reviewed in detail for the remainder of this chapter.

1·6 Layer concentrations

1·6·1 Layer concentrations overview

One of the first reports of layering of insects in the atmosphere was in the 1930s in the USSR (Mel'nichenko 1936). Studies have since found insect layer structures throughout the world, more particularly since the advent of entomological radar (Schaefer 1976). Layers have been observed at altitudes from 75 m (Mel'nichenko 1936) to 2900 m a.g.l. (Drake and Farrow 1985) during both night and daytime (Chapman *et al.* 2003). Occasionally multiple layers (up to five), one above the other, have been observed using entomological radars (Schaefer 1976). Layer thicknesses range from 50 to 200 m (although higher altitude layers tend to be thinner in vertical extent) and have maximum densities that are several orders of magnitude higher than at altitudes immediately above and below the layer. The layers' lower boundaries frequently show a sharper decrease in insect density than upper boundaries—sometimes appearing discontinuous (Drake 1984). Layering can occur for short periods (*e.g.* 30 minutes) or for several hours, although sometimes a vertical shift of the layer is observed with time. In most cases, work has attempted to relate layer dynamics to meteorological conditions; most notably temperature and wind speed (Drake and Farrow 1988).

There are comprehensive recent reviews on insect migration biometeorology (Drake and Farrow 1988, Burt and Pedgley 1997), where many aspects of the relationship between aerial insect activity and meteorology are explored. These include not only the effect of atmospheric structure on aerial insect activity (*e.g.* layering), but also subjects outside the scope of this thesis such as the effect of atmospheric motions on insects (*e.g.* sea breeze fronts, mountain winds).

1·6·2 Daytime layering

Daytime layering has been observed at altitudes up to 2900 m (Drake and Farrow 1985). Typically, daytime layering appears to be strongly influenced by ABL

processes; it has been proposed that insects make use of rising thermals to gain high altitudes where they stay (Geerts *et al.* 2005a). It is not fully clear how and why insects at high-altitude remain there. It is possible that insects remain at the CBL top using their own flight power, the warm air of updraughts could provide favourable conditions, or the insects might favour less turbulent air at the CBL top. Daytime layers—of what are almost certainly insects—are frequently observed around $1-2$ km at the CBL top in the UK (Wood *et al.* manuscript in preparation) and the USA (Gallagher *et al.* 2004). Daytime layering requires further research.

Morning layers (soon after dawn or later in the morning) are rarely reported, but Irwin and Thresh (1988) describe three layers at and after dawn, one from the surface to *c.* 200 m, one from $500-650$ m, and another from $900-1200$ m. A strong subsidence inversion near 600 m was proposed as the cause for the middle layer, since temperature maximum and insect density maximum occurred at the same altitude. The isothermal temperature profile above 1100 m and maximum in wind speed occurred at a similar altitude as the upper layer. In the UK, a summary of dawn layers has been made over 2000–2004 at altitudes of $240-700$ m a.g.l. (Reynolds *et al.* 2007). In the summertime, 69 % of occasions had a dawn peak of high-altitude activity, but only some of these profiles subsequently became layered (10 occasions were significant enough for analysis). Temperature was analysed as the best explanatory factor in determining layer altitude. These layers became dispersed from 06:00–08:00 onwards in conjunction with the development of daytime convective motions.

1·6·3 Nocturnal layering

Nocturnal migrations have presumably evolved because the risk of bird predation is diminished at night (Drake and Farrow 1988), thermal stress can be prevented (Rainey 1974), and horizontal transport at night may be greater due to the rectilinear nature of flight in the NBL caused by the lack of thermals. Many night-time atmospheres are stable: leading to low vertical wind speeds. It is thought that this leads to greater control over insects' vertical flight and thus the

likelihood of higher concentrations in favourable conditions (*e.g.* Reynolds *et al.* 2005).

Most nocturnal layering has been observed at lower altitudes than the day-time layering: between 75 and 500 m. The majority of studies have linked nocturnal insect layering to surface temperature inversions (Riley and Reynolds 1979, Drake and Farrow 1983, Drake 1984, Hobbs and Wolf 1989, Feng *et al.* 2003). Some authors, instead, identified wind speed as the most likely meteorological variable associated with layers at lower altitudes (Sparks *et al.* 1985, Beerwinkle *et al.* 1994, Riley *et al.* 1995). In some reports, however, not all the relevant meteorological variables were measured and so, although layers were associated with an inversion, one cannot unambiguously identify the particular variable (temperature, wind velocity, humidity) responsible for the formation and maintenance of the layer. It should also be noted that these studies were typically carried out in warm regions of the world, where insect flight was probably not as limited by cool night-time temperatures as in the UK, and hence the migrants did not necessarily need to seek the warmest air. Overall, it is plausible that the formation of layers might have a hierarchical basis: they might be related to vertical temperature profiles when temperature is a limiting factor, and might be affected by wind speed or direction when temperatures are not limiting. In the case of *Plutella xylostella* observed in southern England (Chapman *et al.* 2002b), the moths flew in the warmest air at the top of a deep nocturnal surface inversion. The optimum temperature for flight in this species is 26 °C, which is above temperatures found at any altitude in the case study and perhaps explains why the species would concentrate in the layer of warmest atmospheric air.

In some studies, however, low-level nocturnal layering could not be strongly related to any meteorological factors (Sparks *et al.* 1985, Riley *et al.* 1995). A detailed meteorological analysis for one case study (Wolf *et al.* 1986) ruled out absolute, potential, and dew-point temperature; relative humidity; and wind direction as explanatory variables (based on statistical significance tests). However, an association was observed between layering and stable potential

temperature vertical structure (*cf.* static stability) and low wind shear. Clearly, there is no consensus concerning the factors controlling the altitude of low-level nocturnal layers, and further study is needed to clarify fully the meteorological factors underpinning this important phenomenon.

Upper-level nocturnal layers (*i.e.* those above *c.* 500 m a.g.l.) are far less common. The colder air at higher altitudes is generally less suitable for insect flight: which will lead to an overall decrease in aerial insect activity, and thus fewer insects will be available to form layers. In some scenarios, favourable conditions might have already been discovered by insects at a lower altitude and hence there might be little reason for insects to fly higher. A final hypothesis is that when a nocturnal layer occurs at high altitude, it might represent a 'ceiling layer', especially when it does not appear to coincide with any particular meteorological features. As discussed in §1·4, temperature cools with altitude in the absence of inversions. Each insect has a 'minimum threshold' for flight: the temperature below which the insect will not fly. Consequently, insects flying upward will reach their minimum threshold at a particular altitude. Insects can then concentrate below this 'ceiling' into a ceiling layer. Different insect species are likely to have different flight thresholds, thus: well-defined ceiling layers are more likely to occur where there is a dominant species (Riley *et al.* 1991) or a few dominant species if these have widely separated flight thresholds. If the observed aerial population is very diverse, the vertical distribution might approach a monotonic reduction with altitude and ceiling layers of individual species will be masked.

Layering has been observed nocturnally at altitudes as high as 1900 m (Drake and Farrow 1985) where a flight ceiling was proposed as an explanation. Layers between 400 and 1000 m have been observed for the brown planthopper, *Nilaparvata lugens*, in China (Riley *et al.* 1991) and these were defined as ceiling layers because they occurred between 15.2 and 17.0 °C, which was similar to known temperature thresholds for flight in the planthoppers. In this case, humidity profiles showed no correlation with layer altitudes. An intense

nocturnal layer at 800 m (Hobbs and Wolf 1996) was not related to wind speed or temperature, but was located below a region of wind directional shear. It is hence plausible that insects at different altitudes were from different source locations; so if the different locations had different quantities of insects, it would explain why layers occurred at that particular altitude. Wolf *et al.* (1990) observed a large cloud of moths (*Heliocoverpa zea* and *Spodoptera frugiperda*) at 400 – 500 m and observed that fine scale alterations in the vertical profile of insects occurred at the same time as turbulence. In summary, most high-altitude nocturnal layering tends to be classed as ceiling layers, but some observed layers had no meteorological explanation.

1·6·4 Summary of insect layering

Most observed layering appears to be related to meteorological conditions: temperature and wind speed are apparently the two most important variables. Daytime layering appears to be strongly aided by convective plumes. Night-time layering at lower altitudes is sometimes associated with surface temperature inversions and, at upper levels, with ceiling layers; but in other cases wind speed is strongly correlated with the presence of insect layers. Few layers showed no relationship with meteorological variables. However, there is no consensus for the cause of layering, in many cases not all the relevant variables have been measured, and so further work is clearly required. In particular, a thorough meteorological analysis is required in order to investigate insect layering in the UK.

1·7 Motivation and thesis plan

Many questions have emerged, as follows. The four diel periods are clearly important and study of them in the UK has been rare. With the focus on the nocturnal period, it is necessary to ascertain how the atmosphere can affect insect flight: in particular to investigate under which conditions airborne insect migration is passive or active. It is necessary to study the properties of nocturnal insect layers in the UK (in particular to ascertain values for layer duration,

intensity, and spatial variability), and the effect the atmosphere has on nocturnal insect layers. Finally, the composition of the migrating fauna is of interest for contextualising the importance of the results (*e.g.* the pest nature of migrants).

Many assumptions are to be made in this thesis, based on the literature above. It shall be assumed that all flight above the FBL is migratory, non-migratory flight will not be considered. Hence, chemical cues via the oogenesis flight syndrome can be ruled out.

Thesis aims are thus to:

- investigate the diel cycle in UK high-altitude insect migration;
- investigate the likely fauna comprising UK nocturnal layers;
- investigate if and how insect response to environmental conditions can lead to nocturnal layers;
- use continuous data-sets to study layering over several years, rather than just the traditional approach of study via case studies for single occasions;
- investigate the influence of atmospheric turbulence on nocturnal layers of insects.

A range of techniques will be used to investigate these aims. Entomological radar will be used to establish a 'climatology' of UK high-altitude insect movements. A numerical weather-prediction model (UK Met Office's Mesoscale Unified Model: UM) will be used, although radiosonde weather balloons will be used for specific occasions. These data-sets will be compared on a case study basis, followed by a longer-term statistical study. Finally, a numerical modelling approach capable of simulating turbulent motions will be used to aid understanding of processes leading to nocturnal insect layers in the UK.

The diel cycle for UK aerial migration is investigated in Chapter 2, including a UK layering frequency summary. Then the meteorological data is introduced in Chapter 3. Three case studies of UK nocturnal layering (from Wood *et al.* 2006) are presented in Chapter 4. Chapter 5 is a statistical analysis of several years' radar data to investigate the impact of meteorology on nocturnal layer initiation and

intensity. The numerical modelling of insect-flight is effected in Chapter 6. Finally, Chapter 7 contains discussion, conclusions, and future work.

2: Monitoring of airborne insect populations

There have been few studies of high-altitude insect migrants in the UK due to the need for specialized technology such as aerial sampling platforms or remote sensing. In this chapter, three methods of collecting entomological data have been utilised: remote sensing of insects migrating at high-altitude using vertical-looking entomological radar (VLR); aerial netting of insects migrating at high-altitude using a tethered blimp; and ground-based light-traps. Results in this chapter show the diel periodicity of high-altitude insect migration in the UK, and more specifically the temporal and vertical variability of layering.

2·1 Introduction

In Chapter 1, it was shown that the migration of most insect species occurs by active flight. The analysis of flight periodicity is most easily carried out near to the ground, and periodicity analyses for *c.* 400 insect* taxa in the UK were carried out using data from low-level suction-traps (Lewis and Taylor 1964). These data showed that individual species generally fly at certain times of the day. Hence, because thousands of species are flying at their preferred time throughout the diel cycle, then there are always considerable numbers of insects flying at any given period of the day/night. However, Lewis and Taylor's low-level samples were likely to have been a combination of vegetative and migratory fliers. Although a few insect species migrate at low levels within their FBL—particularly

* Although this thesis is based on airborne insect behaviour, most traps catch a wider range of fauna in the Phylum Arthropda (especially ballooning spiders), but in this thesis focus is restricted to the Class Insecta.

some species of butterflies and dragonflies (Williams 1930, 1958)—such low-level flights are not considered in this thesis. Insects flying at high altitudes are less well studied, and are certainly migrants: they are capable of traversing tens or even hundreds of kilometres in a few hours flight (*e.g.* Chapman *et al.* 2002b).

It is very difficult to study high-altitude insect migration directly because many species fly high above the ground and—because insects are rather small—they are difficult to observe (Chapman *et al.* 2003). Hence, the study of UK aerial insect abundance has been very limited, and is therefore the focus of this thesis. The primary method for direct sampling of high-altitude arthropod migration is by conducting aerial trapping using a net on a tethered blimp[*] (*e.g.* Chapman *et al.* 2004a). These data are very useful in determining abundances of high-altitude fauna, assuming there is enough wind to fill the net (> 3 m s^{-1}). However, entomological radar is the only effective method to obtain a superior temporal and vertical resolution by directly observing the *behaviour* of migrating insects at high altitude (see reviews in Vaughn 1985, Drake and Farrow 1988, Reynolds and Riley 1997, Smith *et al.* 2000; also the radar-entomology website[†]). The primary shortcoming of entomological radar is that individual insects cannot be unambiguously identified to species level. Nonetheless, data from insect-monitoring radars can be analysed to produce diel cycles of flight periodicity for all insect species averaged over several years (see later; §2·2·3). Scanning radars have been used elsewhere in the world, but in the UK the operational vertical-looking radar (VLR) system provides an unparalleled opportunity to observe high-altitude insect migration over a period of several years. Furthermore, given that aerial populations are often horizontally homogeneous—particularly at night (Schaefer 1976, Drake 1984, Wolf *et al.* 1990)—samples taken by a remotely sensed vertical profile sampled at one location, or by traps attached to an aerial platform, can be representative of populations over tens of square kilometres.

[*] Sometimes called a kytoon (as a hybrid between aerodynamically-shaped balloon and kite).
[†] http://www.pems.adfa.edu.au/~adrake/trews/

The literature on vertical profiles of airborne insects was reviewed in Chapter 1 (§1·6 and 1·5). It has been shown previously that typical daytime profiles exhibit a monotonic decrease with altitude. Layered profiles are most commonly seen at altitudes of 75–400 m a.g.l. at night (maximum observed 1900 m), dawn layers are rare, and layers during the daytime (seen up to 2500 m) are probably influenced by thermal plumes in the CBL. Radar is an excellent tool for expanding the work on insect layers and in helping to elucidate the mechanisms for their formation.

Chapter aims

In this chapter, aerial and ground-based trapping data will be used to analyse the composition of the airborne insect fauna in the UK. The diel cycle of flight periodicity of high-altitude insects is to be analysed using vertical-looking radar data. Finally, profile types will be analysed to observe the temporal and vertical variability of layering.

2·2 Methods

2·2·1 Ground trapping

Ground-based traps can provide information on the relative abundances of various taxa of airborne insects. Data from the internationally renowned Rothamsted Insect Survey's (RIS) UK-wide network (Woiwod and Harrington 1994) are particularly valuable in providing abundance and phenology data for common species across the UK. Traps are emptied on a daily basis for much of the year. There are 16 suction-traps (each 12.2 m tall) across England and Scotland for aphid monitoring; and nearly 100 light traps across Great Britain that provide daily counts of species of macro moths caught. The traps' biggest advantages are their ease of access (being at ground level), their widespread distribution, and the fact that catches (at least of some taxa) are identified to species level.

2·2·2 High-altitude netting

Ground-based trapping data might include many non-migrants (*i.e.* insects on vegetative flights). Therefore, to obtain catches that contain purely migrants, high-altitude netting is required. Sampling of windborne arthropods was undertaken at about 200 m a.g.l. at Cardington Airfield (Bedfordshire, UK: 52.10 °N / 4.20 °W). Four samples were normally taken per day: morning (09:00–13:00 hours UTC), afternoon (13:00–17:00), dusk (*c.* 20:00–21:00), and night (21:00–dawn). Dusk is defined here as the same as civil twilight: *i.e.* from sunset until the centre of the sun is 6° below the horizon; in the UK, civil twilight is typically 30–40 minutes in length. The field campaigns were supported by the Rothamsted Radar Entomology Unit (RREU) and carried out for about 4 weeks during each of the summers of 2003–2006 inclusive. A net was fixed below a tethered helium-filled blimp (Figure 2·1). The net aperture had a cross-sectional area of 0.64 m^2, which is capable of sampling quite large volumes of air (*e.g.* for 1 hour sampling with a mean wind-speed of 10 m s^{-1}, $\sim 2.3\times10^4$ m^3 of air is sampled). The net was fitted with a radio-controlled closing device to prevent contamination of the collected high-altitude samples with low-flying fauna during the winching down process (see Chapman *et al.* 2004a for further details about the aerial netting system).

The aerial sampling data are useful for obtaining estimates of the relative abundances of high-altitude migrating fauna, the only disadvantage being the integrated temporal resolution of several hours (compared to the radar's 5 minutes integrated temporal resolution, see later). All catches were sorted to order level. Some individuals were identified to lower taxonomic levels (normally at a later date by Rothamsted personnel) and their fresh body masses were measured on site using a microbalance.

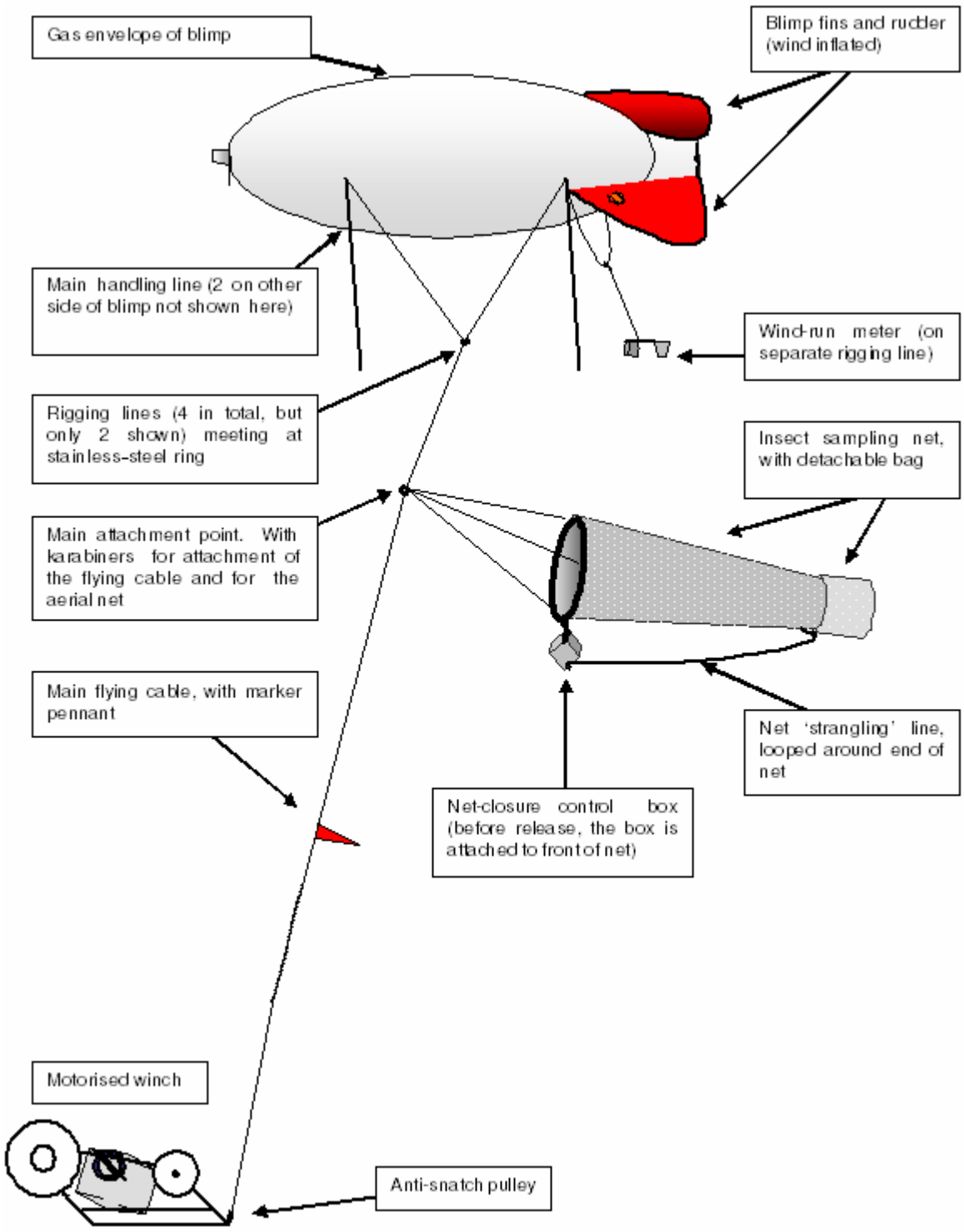

Figure 2·1 – *Schematic diagram of RREU aerial insect sampling equipment (items not to scale).*

2·2·3 Radar entomology

Netting campaigns are rather laborious, only yield samples at one altitude, and have a poor temporal resolution. Therefore, in order to obtain frequent observations of vertical profiles, the recently-developed vertical-looking insect-monitoring radar (VLR[*]) was used (Smith *et al.* 1993; Drake 2002; Chapman *et al.* 2002a, 2003). VLR gives instantaneous vertical profiles of insect aerial density (macro-insects[†] only) over virtually all migration altitudes to be expected over the UK. The RREU owns and maintains two operational insect-monitoring radars (Table 2·1, Figure 2·2). Full details of their operation can be found in Chapman *et al.* (2002a), but a summary is provided in the following paragraphs.

Table 2·1 – *Entomological radar locations.*

Radar	Location	Operational start	Turn-off date
1	Rothamsted, Harpenden 51.81 °N / 0.36 °W	June 1999	(Currently operational)
2	Malvern, north site 52.10 °N / 2.32 °W	October 1999[‡]	19 September 2001
	Malvern, south site 52.13 °N / 2.33 °W	19 September 2001	19 April 2004
	Chilbolton Observatory 51.20 °N / 1.80 °W	21 June 2004	(Currently operational)

[‡] Some preliminary operations in 1995, running continuously from October 1999

The 3.2 cm wavelength (X-band) radar-beam is circularly-symmetric and zenith-pointing. The plane of linear polarisation is continuously rotated at 5.8 Hz . Additionally, the beam nutates due to a slight offset (0.1 beam widths) in the antenna feed, producing a narrow-angle conical scan. The 1.5 m diameter parabolic antenna gives a half-power beam-width of 1.4 ° . The pulse duration is 100 ns , and the peak pulse power is 25 kW .

[*] Henceforth in this thesis, all references to radar will mean the VLR system, unless otherwise stated.

[†] In this thesis: macro-insects are defined as those that are detectable by the radar (*i.e.* of mass > 1–10 mg), and micro-insects are those that are not detectable by the radar.

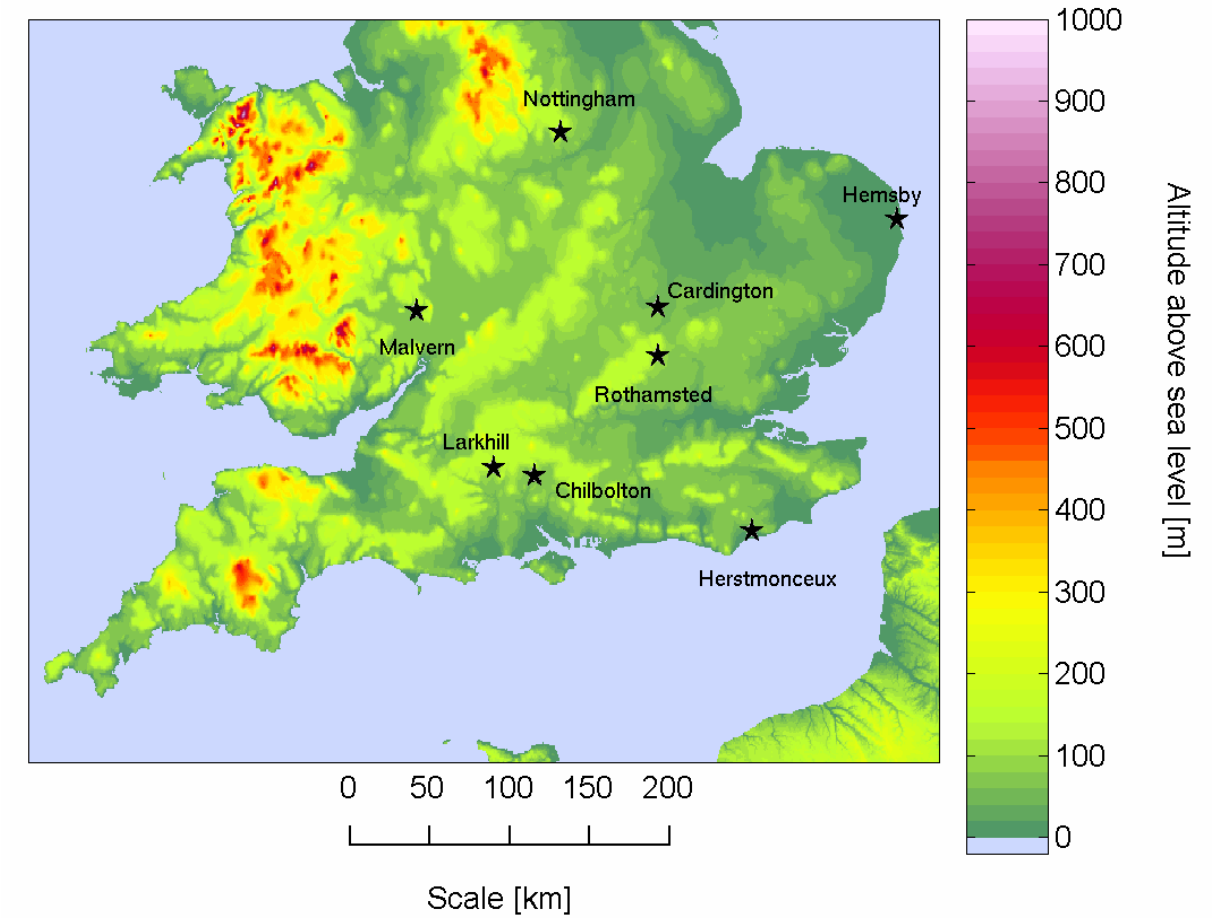

Figure 2·2 – *UK map with relief. Radar sites are Chilbolton, Rothamsted, and Malvern. Cardington is the site of radiosonde release and aerial netting. Nottingham, Hemsby, Larkhill, and Herstmonceux are radiosonde release sites.*

Return signals from individual insect targets flying through the radar beam are detected in fifteen 'range gates' (the sampling volumes), each 45 m deep with 26 m non-sampled intervals (Figure 2·3). Coverage above the radar is 180 – 1218 m for the Malvern/Chilbolton radar and 150 – 1166 m for the Rothamsted radar*. Data are recorded during 5-minute sampling periods, repeated every 15 minutes, 24 hours a day, giving 96 profiles per day. The computer and radar system routinely extract several variables (using Fourier transformation theory (Smith *et al.* 1993) calibrated by laboratory data): the target's distance of closest approach to the beam's central axis, horizontal speed, displacement direction, body alignment, and three terms that describe the radar back scattering properties of the target.

* The Rothamsted radar was located on the roof of a building until 20 October 2004: hence, sampling range whilst on the roof was 165 – 1203 m a.g.l.

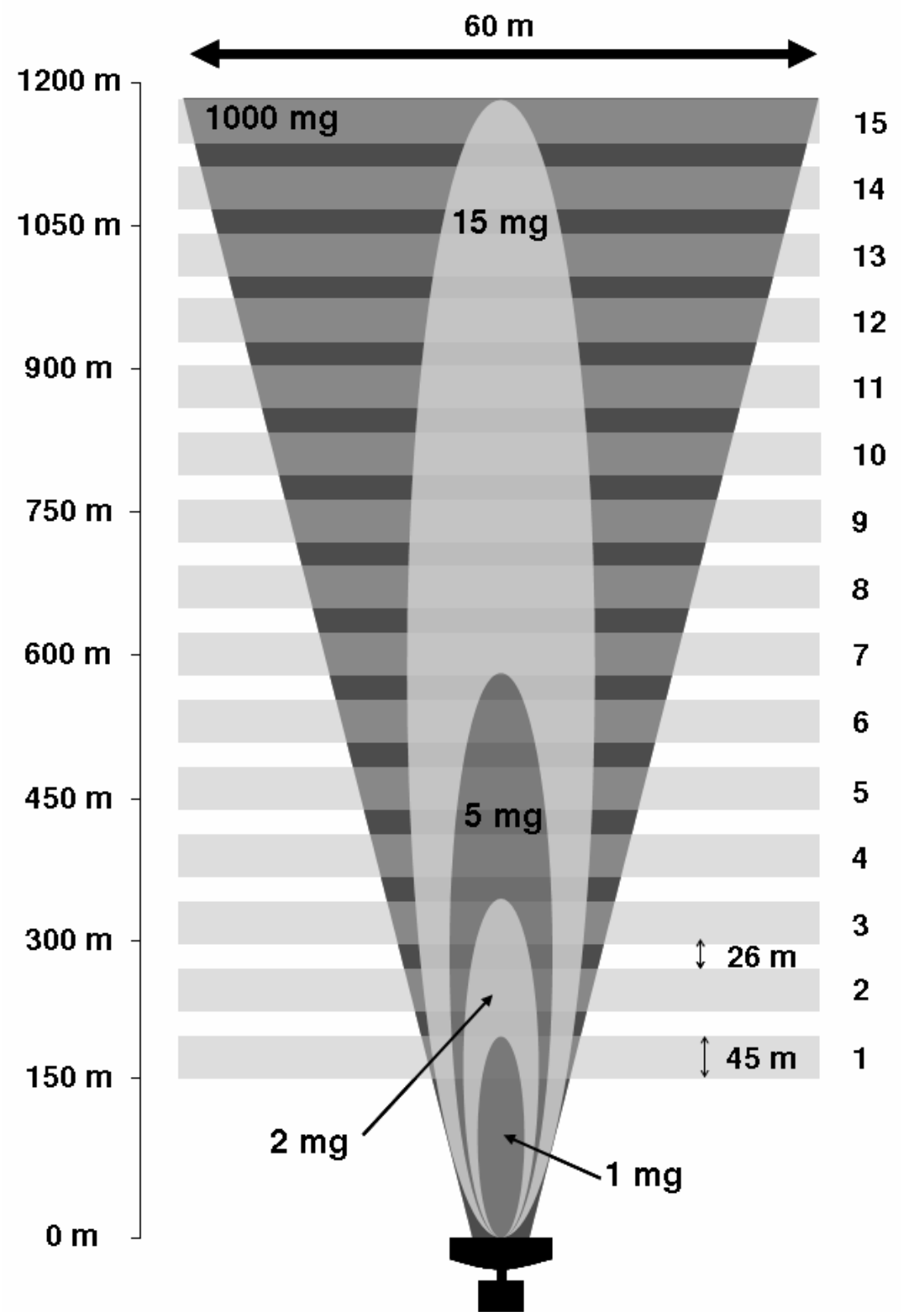

Figure 2·3 – *Sampling regime of the Rothamsted radar showing the 15 altitude range gates between 150 and 1166 m above the radar within which over-flying insects are sampled. The maximum altitude of detection and the volume sensed by the radar for targets with a range of body masses are shown diagrammatically. The vertical components of the diagram have been drawn to scale, but the beam width has been exaggerated to the make the geometry clear. From Chapman et al. (2002a).*

However, these variables can prove only of limited use in identifying radar-detected targets, *e.g.* only a narrowing of the taxonomic groups can typically be performed. Further aids to target identification can be obtained by relating radar-derived variables to data collected during aerial netting studies and ground-based insect trapping networks.

Using laboratory measurements of the radar cross-sections of insects, the radar back scattering coefficients are routinely used to estimate the targets' mass and shape (Chapman *et al.* 2002a). This is only possible when there is just one insect in the beam, otherwise the inter-target interference causes the primary analysis algorithm to fail. When this effect occurs almost constantly in a range gate, it is called 'saturation', *i.e.* almost all information on *individual* targets is lost.

The smallest detectable mass of insect varies with altitude (Figure 2·3), such that a 1 mg insect can barely be detected in the lowest radar range gate, and only insects larger than 15 mg can be reliably detected in all 15 range gates. This means that of the high-altitude migrants, many of the Diptera, Hemiptera, and Hymenoptera are unseen by the radar. Only orders that contain species with a large mass are seen by the radar (*e.g.* Lepidoptera, Coleoptera, Neuroptera). High-altitude arthropod composition is analysed in §2·3·3.

Insect concentration definitions

For a basic quantification of radar data, the term 'target numbers' is used, which is the number of insects detected in a particular range gate during a sampling period. The primary shortcoming of this variable is that the range gates vary in volume with altitude, and the sampled volume depends on the size of the target (Smith *et al.* 2000). Hence, an alternative variable (aerial density) is calculated to allow fairer comparison between different range gates. Furthermore, occasionally targets that do not match the analysis model are recorded—this is detected by calculating the correlation coefficient (C = 0–1) between the received signal and one simulated from the analysis results. A standard expression for the number of airborne insects is 'aerial density', defined in this thesis as the number of insects

per 10^7 m^3. Aerial density can only be calculated by the RREU system for targets that are well described by the analysis model (Chapman *et al.* 2002a), and where estimated masses and other radar-derived variables are expected to be reliable. Therefore, during periods of high-intensity migration—when there are many occasions with multiple insects passing through the range gate (resulting in high levels of multi-target interference)—the aerial density calculations will underestimate the true values because the algorithms are designed to retrieve information only when there is just one insect in a range gate at a time.

The analysis program also routinely records another (more basic) method of expressing aerial insect biomass: by recording the percentage of time the received signal power is above a certain power level. Here, the 'percentage-above-threshold' value is defined as the percentage of time that the return signal was above the -80 dBm (10^{-11} W) level*; which is ~ 10 dB over the noise floor of the radar receiver. The percentage-above-threshold values are particularly useful in situations where aerial densities are too high for individual targets to be resolved by the radar. Figure 2·4 shows that when percentage-above-threshold values are large, then the target numbers appear to fall because multiple targets cannot be resolved. A somewhat arbitrary threshold is needed, beyond which the target number values have a spread. For consistency with other RREU studies (*e.g.* Reynolds *et al.* 2005), a value of 10 % was used; beyond which the return power was too intense, and one expects target numbers to become unreliable.

Further details of the radar system, its mode of operation, and analysis protocols—including target identification procedures to deal with non-insect targets, such as precipitation, 'chaff', birds, and bats—have been described elsewhere (Smith *et al.* 1993; Smith *et al.* 2000; Chapman *et al.* 2002a, 2003).

* dBm: power level in decibels, referenced to 1 mW

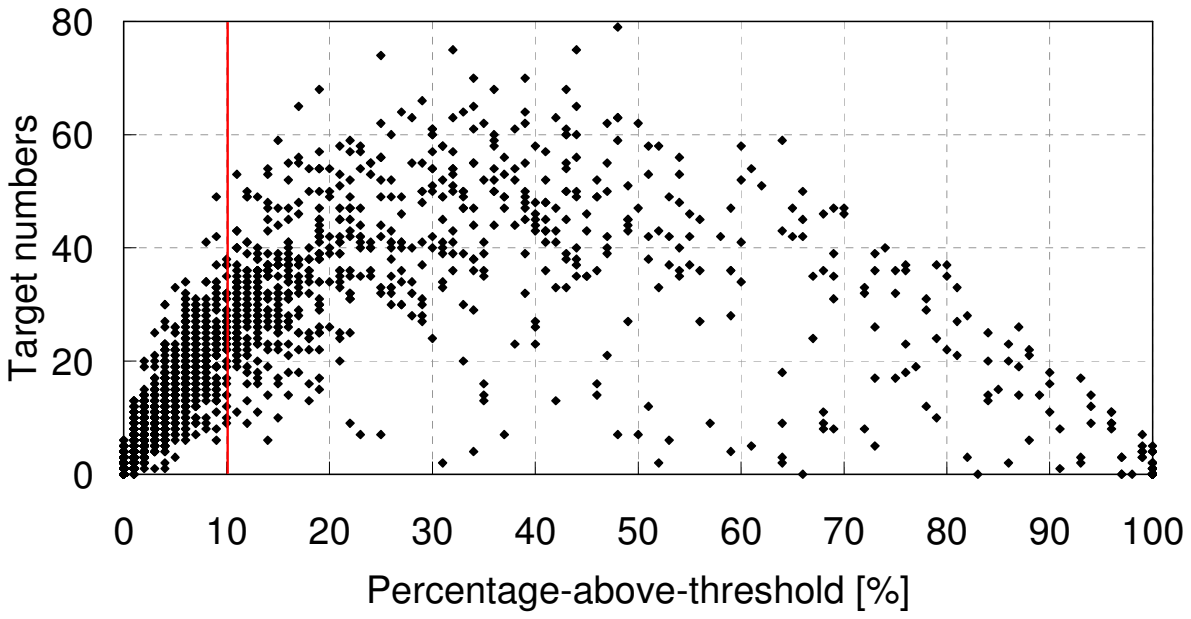

Figure 2·4 – *Comparison of target numbers with percentage-above-threshold for the results from range gate 1 in the Malvern radar for the month of August 2003. The red line at 10 % shows the threshold used for cases where multi-target interference becomes problematic.*

2·3 Analysis

2·3·1 Periodicity of high-altitude macro-insect flight

The regular times in the diel cycle within which insects fly, or 'periodicity', has been analysed for insects caught at low altitudes (Lewis and Taylor 1964). Periodicity of high-altitude migrants is less well studied (Chapman *et al.* 2004a). A long-term set of radar data (first 4 complete years' operational radar data, 2000–2003 inclusive) is used as the 'core data-set' for analysis in this section.

A visual database (dubbed 'Quickview') of radar data was prepared. This database comprises a succession of daily time-vs-altitude plots for several years of radar data, by using html to organise the colour-filled contour plots[*]. Plots of both 'target numbers' and 'percentage-above-threshold' values were made. The Quickview database can be used to identify noteworthy events for case study analysis (Chapter 4). An example is shown of how each day is seen in Appendix A.

[*] Jpeg-images created in Matlab®.

For the high-altitude diel periodicity analysis, an example of a particular diel cycle was examined in detail: 16 June 2000 at Malvern (Figure 2·5). A variety of profile shapes were seen throughout the day/night sequence. High-altitude peaks of activity at dawn (*c.* 03:00–04:00) and dusk (*c.* 20:00–22:00) can be seen, with as many as 60 macro-insect targets per range gate per 5-minute sample period in the dusk peak. Daytime profiles tend to have more variation in both altitude and time, probably associated with convective plumes in the daytime BL. It is also worth recalling that on hot summer days, with high insect aerial densities, multi-target interference in the radar data becomes more common, and this will result in unreliably low 'target number' data. For example in a case of high percentage-above-threshold values with a monotonic reduction with altitude, the target numbers sometimes shows apparent layering due to a reduction in resolved target numbers in range gates 1 and 2.

On this particular occasion (Figure 2·5), there was a continuation of activity from the dusk peak (about 21:00 hours UTC[*]) into a nocturnal layering event (*i.e.* where the peak numbers occurred above the lowest range gate) with concentrations of 20–50 targets (per range gate per 5-minute sample period). In this example, the layering event occurred with a slight delay after the dusk peak. Qualitative analysis of the Quickview database revealed that most layering events arose through a continuation of activity from dusk into a layer, so that the two events are *not* often discernable from each other. The dusk peak probably comprised both dusk fliers and nocturnal fliers that took off at the surface near dusk. Many dusk-only (crepuscular) fliers will have descended back to the surface within 1–2 hours of dusk (resulting in a drop in insect concentrations), while nocturnal migrants will continue to fly for several more hours, and occasionally through the whole night.

[*] All times in this thesis are in hours UTC (*i.e.* co-ordinated universal time). This is the same as GMT (Greenwich mean time).

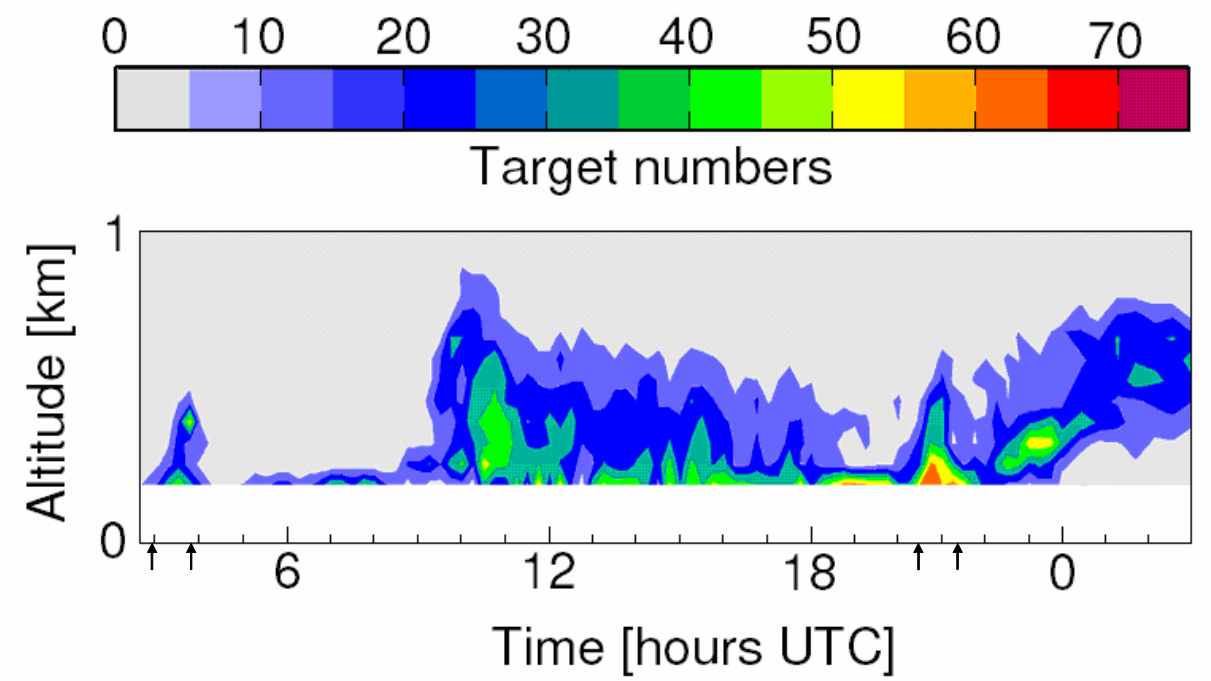

Figure 2·5 – *Target numbers (coloured key) on 16–17 June 2000 at the Malvern radar. This diurnal cycle shows many of the observed vertical profile structures seen. The start of civil twilight and sunrise are marked at 02:59 and 03:48 respectively. Sunset and the end of civil twilight are marked at 20:31 and 21:20 respectively.*

Integrating data from the complete core data-set, mean target numbers for the entire summertime period (June, July, and August) were produced (Figure 2·6). The key difference between Figure 2·5 and the average pattern displayed in Figure 2·6 is that because nocturnal layers are a comparatively rare phenomenon (see later, §2·3·2), they do not appear in the mean. The lowest target numbers throughout the diel cycle in range gate 1 occurred at about 01:00–02:00. As expected, the greatest altitudes were reached during the daytime (up to 850 m): daytime activity reached a peak altitude during 09:00–10:00, although the denser concentrations were observed near 11:00–14:30. The dawn peak reached an altitude of 400 m, whilst the dusk peak reached 600 m. The greatest densities were found to be in range gate 1, particularly during the dusk peak (~ 24 targets). It is worth noting that the dusk peak in activity did not correspond with the temperature maximum, in fact it is at dusk that the near-surface (*e.g.* 1.5 m) air temperature typically has the most rapid cooling of the diurnal cycle (Saunders 1952). At all times the *mean* profile (Figure 2·6) showed a monotonic decrease of insect concentration with altitude. The rate of decrease with altitude is larger at dusk than it is by day.

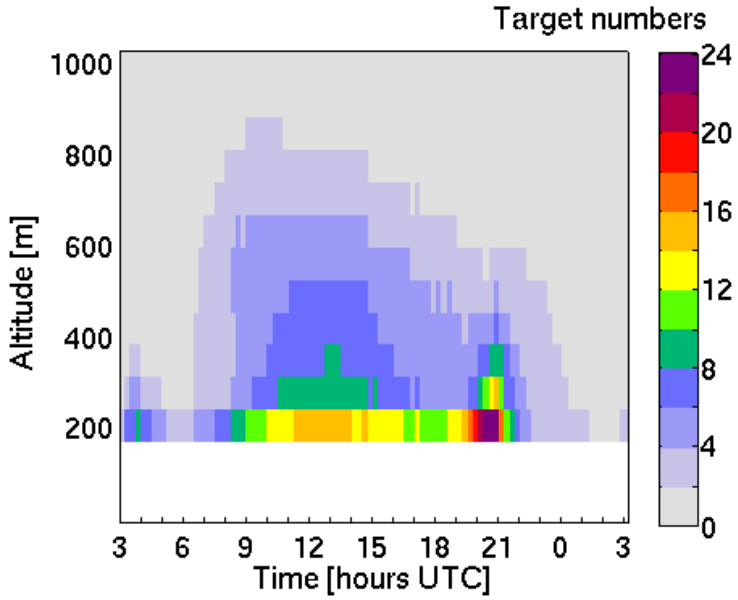

Figure 2·6 – *Target numbers per 5-min sampling period per range gate: Jun–Aug, 2000–2003 inclusive for both radars. No interpolation is used for the contours.*

Summation of the entire column's targets shows clearly three of the diel flight phases: dawn, daytime, and dusk (Figure 2·7). Some of the seasonal cycle can be identified. Of the months shown, July has the greatest aerial insect activity, and June the least. The mean maximum temperatures in the Midlands of the UK (Met Office website) were 19.3 °C, 20.7 °C, and 21.7 °C for June, July, and August respectively. The coolest month (June) had the least daytime aerial insect, but the warmest month (August) did not have the greatest aerial insect populations.

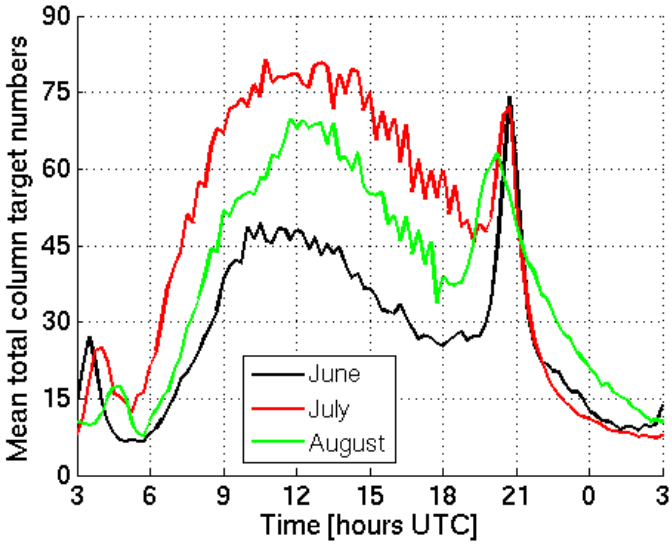

Figure 2·7 – *Total column target numbers in radar profile per 5-min sampling period, averaged 2000–2003 for Jun–Aug individually for both radars.*

The dusk peak has a similar column total in June and July, with a reduction in August (mean ~ 70 targets). The progression of the dusk and dawn peak timings towards the centre of the daytime from June–July–August illustrates the dependence of the peaks' timing on sunset and sunrise respectively (the time of sunset and sunrise approaches midday once the summer solstice has passed). The peak in daytime activity occurred at 10:00–13:00: often, curiously, before the hottest part of the day. Perhaps little can be concluded from this; however, target numbers might have been reduced due to multi-target interference later in the day.

It is worth re-stating that target number values can be unreliable during very high insect densities due to inter-target interference. Nevertheless, a similar distribution to Figure 2·7 was observed when using aerial density (not shown). Besides, attention is focussed on *nocturnal* layering events in this thesis. Night-time aerial insect densities are low compared to at dusk and during the daytime, hence nocturnal radar data are highly unlikely to be affected by saturation.

2·3·2 High-altitude macro-insect layers

Layered profiles were identified using a Visual Basic* module, which returned an insect 'layer quality' (LQ) code (a number from $LQ = 0 - 7$; see Reynolds *et al.* (2005)) that indicated the presence and strength of layering in each vertical profile. The algorithm analyses target numbers and additionally takes into account the percentage-above-threshold values (see Appendix B for full definitions), briefly:

- $LQ = 0$: radar not operating;
- $LQ = 1$: 'percentage-above-threshold' values > 10 % in all range gates (probably rain);
- $LQ = 2$: monotonic decrease with altitude;
- $LQ = 3$: variation in profile, but no significant layer;

* A programming language; often used in Microsoft® applications, *e.g.* Access.

- LQ = 4 : weak layer (range gate with maximum contains < 15 % of profile targets);
- LQ = 5 : layer;
- LQ = 6 : strong layer (range gate with maximum contains > 25 % of profile targets);
- LQ = 7 : probable layer in a situation where saturation in radar data was likely ('percentage-above-threshold' values > 10 % in all range-gates, but there is a rise of > 10 % within the profile). Note that isolated occurrences of LQ = 7 may be due to rain, so that one must consider *sequences* of LQ values, rather than isolated values.

An example of the temporal variation in LQ is shown in Figure 2·8. The layering scheme was analysed for June 16–17 2000, Malvern. LQ = 4 can happen spontaneously, and can occur when there is no temporally consistent layering (*i.e.* an isolated value). Experience of radar profiles and their LQ values has informed RREU staff (D. R. Reynolds, pers. comm.) that LQ = 4 does not produce layering occasions that are recognisable as temporally consistent and intense, unless those values are temporally interspersed with values of 5, 6, or 7. The running mean clearly shows three layering occasions in this diel. Near dawn (03:30–04:30), there is a short-lived layer. Equally, a short-lived layer is seen between 09:00 and 10:00. The nocturnal layer, from 21:00–00:00, is clearer because there is a continuous increase in LQ values from dusk (LQ = 3 before 21:00) towards 23:00 (LQ = 6); equally there are no LQ < 5 values after 21:00.

Analysis of LQ numbers in the first profile after dusk in the core data-set revealed that 43 % of summertime (June, July, and August) profiles exhibited some evidence of nocturnal layering (defined where LQ was 4, 5, or 6). The vertical profiles during the other seasons were layered on only 14 %, 2 %, and 11 % of occasions for Autumn, Winter, and Spring respectively. Therefore, for the purpose of this work, focus is on the three months of summertime, which has many more layering events because insect abundance and flight activity are much higher during the summer (because of higher temperatures). Thus, the

period of June–August 2000–2003 (inclusive) at both Malvern and Rothamsted radars is to be used as the 'core data-set' for statistical study (specifically in Chapter 5). This set comprises 736 24-hour-periods for study (*i.e.* from 3 months over 4 years and 2 radars).

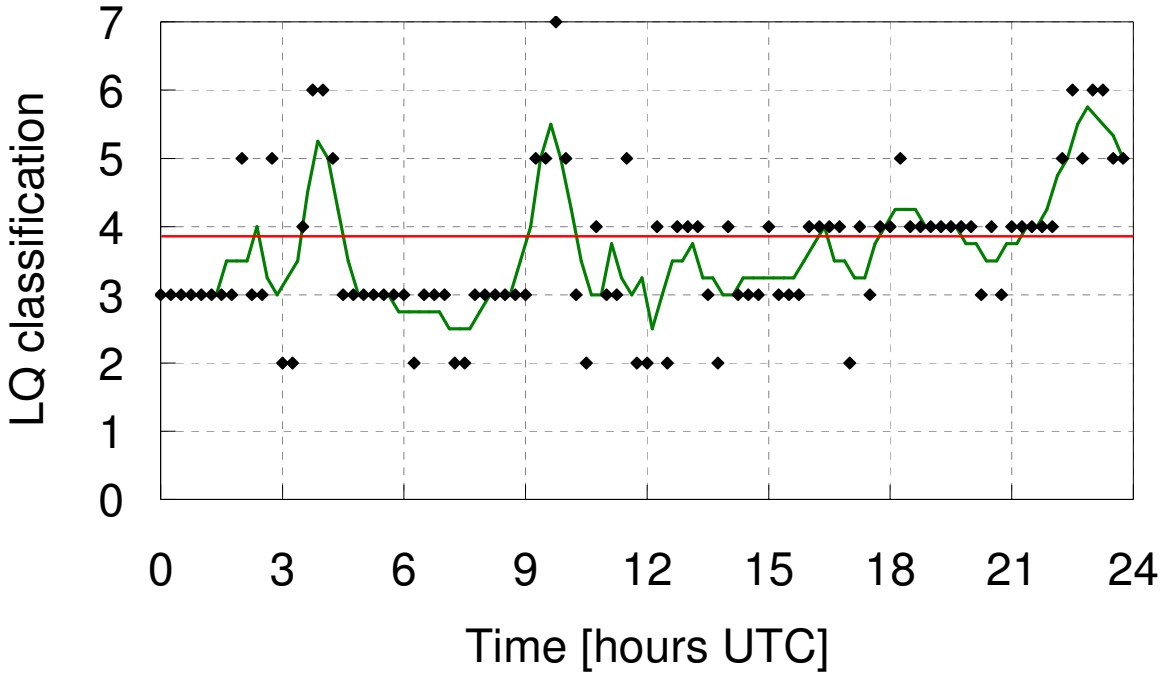

Figure 2·8 – *Time evolution of LQ values (black diamonds) for June 16 2000, Malvern. A red horizontal line is drawn below LQ = 4 to separate layered profiles from non-layered profiles. The green line is a running-mean over an hour (four points).*

Figure 2·6 suggests that there was frequently high insect activity in radar range gates 1 and 2 in the 1–2 hours around dusk. Subsequent to the dusk peak, insect numbers decreased and typically remained low for the remainder of the night. Substantial nocturnal insect activity was only associated with the presence of a strong dusk-peak.

Layer cessation typically occurred between 23:00 and 03:00, see Figure 2·7. In order to understand mechanisms for the cessation of nocturnal layering, it is necessary to focus on the period from dusk until cessation of nocturnal activity.

Temporal layer variability

To contextualise the importance of layering events, it is necessary to analyse the times of the day when layering occurs and how frequently they occur. The distribution of events for each of the LQ values at each time of day was calculated by dividing the number of occurrences of a given LQ value by 736, the total number of 5-minute samples at each time of day in the core data-set (Figure 2·9). For example, at 21:15 there were 221 occasions where LQ = 5 occurred out of the possible 736 occasions; thus 221/736 = 0.3 or 30 % of the profiles at 21:25 had an LQ = 5 classification.

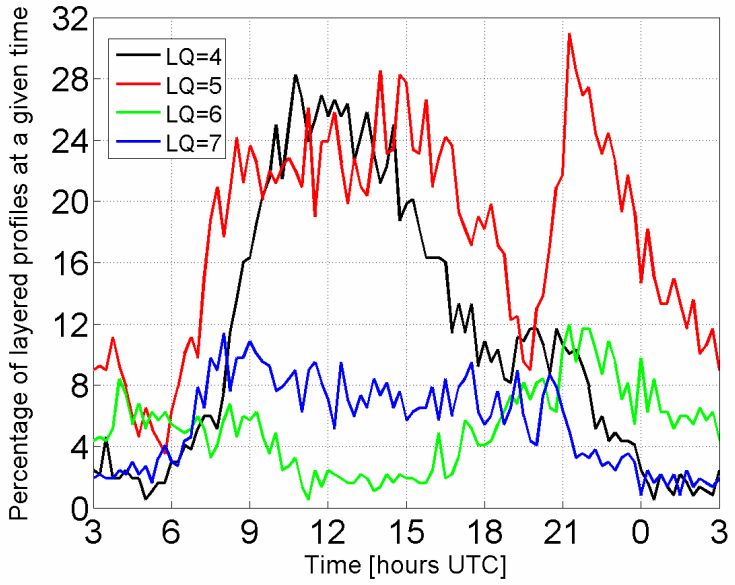

Figure 2·9 – *Layering likelihood (%) in each temporal profile (hours UTC); core data-set (Jun–Aug, 2000–2003). Layer quality (LQ 4–7) values indicate layers of increasing intensity.*

For weak to moderate layers (LQ = 4 or 5) there is considerable layering during the daytime: particularly from 08:00–17:00, when up to 50 % of the profiles have weak to moderate layering. However, much of this might be due to artefacts caused by multi-target interference. For moderate to strong layers (LQ = 5 or 6), there are peaks at 21:15 (of 30 % and 11 % for LQ of 5 and 6 respectively). At 21:15, 60 % of the profiles are layered (using LQ 4–7). There is a large dip in LQ = 5 and 7 from 19:00–20:00: *i.e.* during the dusk peak, when a monotonically decreasing concentration profile is typically seen. These findings also show that nocturnal layers are more intense than daytime layers, because LQ values of 5

and 6 have peaks at night, while LQ = 4 events are most common during the daytime.

In this study, the focus will be primarily on nocturnal layering events. They are stronger, more reliable events, and a frequently occurring nocturnal profile type. But additionally, because daytime layers are less often observed in case studies than nocturnal layers, it seems likely that daytime layers are not as temporally and spatially continuous as nocturnal layers due to the influence of convective boundary-layer (CBL) turbulence and updraughts (Chapter 1). At dusk, there is an increase in frequency of target numbers during 20:00–21:00. Subsequently, the nocturnal layering is most common at 21:15, and it becomes less common with time after this.

Finally, the fact that LQ = 7 is most common by day and rarer at night, highlights the fact that multi-target interference occurs most often during the day and rarely at night (< 4 % of profiles at night, and up to 11 % of daytime profiles).

Nocturnal layers

At this stage, it is necessary to define nocturnal layering more precisely. An assessment was made of whether a particular evening had a layering event or not by consideration of the LQ numbers of the several profiles in a nocturnal period (*i.e.* from 21:00–23:59). A new variable, NLQ, was created to indicate how much of each nocturnal period was layered. Different schemes were trialled, and the following method was chosen. NLQ was created by using the LQ values that were equal to 4, 5, or 6; and calculating their mean over the time range of 21:00–23:45; *i.e.* 12 early evening profiles. This time-range was chosen because it is during those times that LQ = 5 and 6 have their frequency peaks. Furthermore, using LQ numbers later in the night seems unnecessary because Figure 2·9 reveals that nocturnal layers decrease in frequency with time, and layers appear to originate only from the dusk peak. Furthermore, insect take-off from the surface occurs primarily at dusk, and there is no evidence of mass emigration later in the night

presumably because nocturnal near-surface temperatures have cooled to levels that are too low for take-off.

NLQ has a range between 0 and 6. If LQ = 6 for all 12 profiles, then a value of NLQ = 6 is returned. If LQ does not equal 4, 5, or 6 in any of the 12 profiles, then a value of NLQ = 0 is returned. Mid-range NLQ values can be produced by either temporally consistent layers of intermediate intensity, or very intense but short-lived layers. The example in Figure 2·5 has an NLQ = 4.8. It is also worth noting that since insect numbers are low at night (Figure 2·6), inter-target interference is not usually an issue: hence, the fact that NLQ is based on target numbers is highly unlikely to be influenced by saturation. Qualitative confirmation that this definition gave temporally consistent and strong layers was made by manually comparing the Quickview database with NLQ values.

So far, temporal variability of layering has been discussed. For occasions when nocturnal layering occurred (defined as NLQ > 1), the layer altitudes were extracted to test whether there was a preferred altitude for layering. Figure 2·10 shows the range gates in which nocturnal layering was most commonly observed. It can be seen that most nocturnal layering (76 % at Malvern, 73 % at Rothamsted) occurs in range gates 2–5, *i.e.* below 500 m a.g.l. It is worth noting that, by definition, a layer cannot occur in range gate 1 of the radar because layers can only be defined in a given range gate when there are reduced numbers in the gates both above and below it. Thus, due to the sampling range of the VLRs (~150 m and above), it is quite possible that layering frequently occurs at lower altitudes than range gate 2 (~265 m) but with the current system it is not possible to corroborate this; and no UK studies have been able to provide data on layers at these low altitudes. A peak in layering occurs in radar range gate 3 at Malvern (*c.* 300 m). However, at Rothamsted most layering occurs at the lowest discernable altitude (range gate 2, *c.* 259 m). Overall, the radar-observed nocturnal layers most frequently occur between 200 and 500 m.

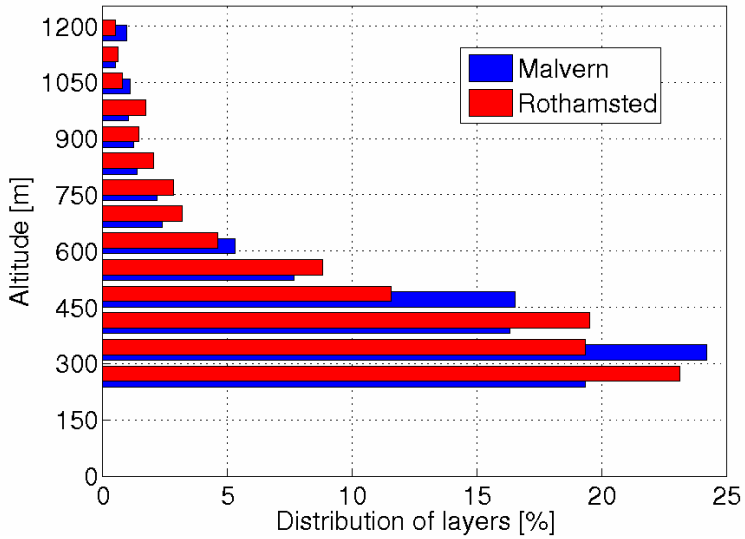

Figure 2·10 – *Altitude at which nocturnal (21:00–23:45 hours UTC) layers occur in the core data-set (Jun–Aug, 2000–2003). Centre of range gates are used.*

The 'critical region' for layer initiation is therefore defined as (*i*) during the summertime (because that is when most layers occur), (*ii*) at 200–500 m (because nocturnal layers are most frequently observed at these altitudes), and (*iii*) from 20:00–22:00, the reason 20:00 was used as a starting time-period is in order to capture the conditions in the dusk-peak. From 20:00 onwards, the meteorological conditions might be critical in determining if a layer will be initiated or not. The end of the critical period was designated as 22:00, when the dusk peak will be long-past and any layer that might have formed will have already appeared.

Emphasis is required in analysing the meteorological conditions in the critical region, which are presumably important in determining whether insect layering will be initiated. Meteorological conditions might also have an influence on the layer intensity, duration, and altitude. Hence, to allow analysis of the entire data-set in a systematic fashion, the meteorological variables in the critical region will be analysed and compared to layer quality as determined from radar data (see Chapter 5).

2·3·3 Airborne arthropod composition

Radar data

Identification of radar-detected insects in individual case studies can be relatively straightforward because ground-based trap data, if available, can complement the analysis and provide an indication of the most likely candidates. However, for a generalised analysis, it is impossible to identify radar-detected insects to species-level. The identity of certain subsets of radar targets can often be narrowed to particular taxonomic groups (such as "noctuid moths" or "green lacewings") by the creation of radar target mass distributions and comparison with masses of known insect species. Figure 2·11 shows a mass frequency distribution for the month of August 2000. There is a reduction in insect numbers with increasing mass. No reduction is seen in the data for smaller masses, because the radar can only detect larger insects (larger than ~ 1 mg in range gate 1). No generalised information on identity can be made. Hence, it is useful to analyse the insect orders and families that are abundant at hundreds of metres above the ground and large enough to be detected by the radar, by direct sampling of the aerial arthropod fauna.

Ground-based data

The abundance of insects in each size group—caught at 3 m a.g.l. in the UK—is shown in Figure 2·12 (Johnson 1969). This size distribution shows that over half the population are in the 3 – 10 mm² group, which comprised mostly aphids in high-altitude netting studies (*e.g.* Chapman *et al.* 2004a). The radar only can observe the largest of these groups (few generalised mass-to-size conversions are available in the published literature, but the radar's observable targets almost certainly are in the 100–1000 mm² range). Hence, the radar is sampling only around 2 % of aerial arthropod numbers (*i.e.* the largest targets). However, the Johnson data are ground-based, and so might include many non-migrant species: in this thesis, it is necessary to obtain information on the high-altitude fauna, which are certainly migratory species.

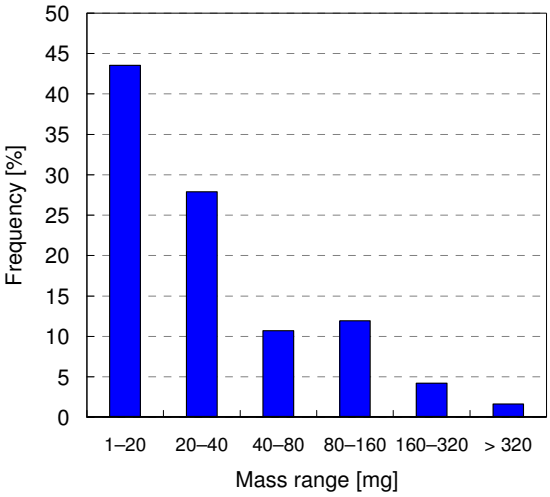

Figure 2·11 – *Mass distributions of insects in all range gates for the month of August 2000 in the Malvern radar for all times of day. No insects below 1 mg are observed by the radar.*

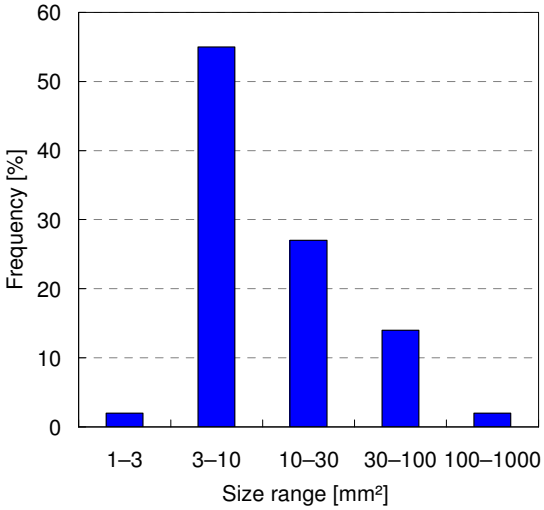

Figure 2·12 – *Abundance of insects of different sizes estimated from the total catch of 51,671 insects, trapped in very large suction traps in the UK at 3 m a.g.l. From Johnson (1969).*

High-altitude data

The aerial netting data, collected at Cardington from 2003–2006 inclusive, show the proportions of each order (see Table 2·2). Hemiptera, Hymenoptera, and Diptera together comprised 91 % of the total catch. Lepidoptera are less populous than aphids by around 3 orders of magnitude. This dominance reduces to around a factor of 40 in the night samples. The only insects with masses above 100 mg that were caught at night in the aerial netting campaign were all noctuid moths, and so this group are highly likely to be responsible for the large insects detected by the radar in nocturnal layers. Only two species of noctuid moth have been caught during the aerial netting campaigns: several *Autographa gamma* (the silver Y moth, a well-known migrant), and a single *Noctua pronuba* (the large yellow underwing, another species which is thought to be migratory). Furthermore, several species of micro-moths, including the well-known migrant pest *Plutella xylostella*, have also been caught, but these are too small to be detected by the radar throughout its sampling range.

Table 2·2 – *Cardington catches from 2003–2006 inclusive. Mean aerial densities for each order caught. A total of $0.64 \times 10^7\ m^3$ of air was sampled; $0.12 \times 10^7\ m^3$ of which was at night.*

Insect order	Mean aerial density (insects per 10^7 m^3)	Percentage of total catch	Mean aerial density at night† (insects per 10^7 m^3)	Percentage of night catch
Hemiptera	73.3	59.4 %	19.5	46.1 %
Aphididae	68.2	55.3 %	19.0	44.7 %
Psocoptera	1.1	0.9 %	0.44	1.0 %
Thysanoptera	0.41	0.3 %	0	0 %
Neuroptera	1.67	1.4 %	2.1	5.0 %
Lepidoptera	0.18	0.15 %	0.49	1.1 %
Coleoptera	4.0	3.2 %	0.88	2.1 %
Diptera	16.9	13.7 %	16.9	39.9 %
Hymenoptera	21.6	17.5 %	2.0	4.8 %
(Arachnidae)	4.15	3.4 %	0	0 %

† The night samples started at 22:00, and lasted for between 1 and 5 hours.

Noctuid moths

Because the only large nocturnal insects caught at high-altitude are noctuid moths, it is necessary to focus on noctuids when considering the composition of nocturnal layers. Noctuids are the most speciose of the Lepidopteran families, with around 400 UK species (Chinery 1993) including many highly abundant species that are long-range migrants (*e.g.* Fitt 1989, Showers 1997). For case study analysis, radar estimates of the mass, size, and shape of the insect target can be used with trap data to aid identification of targets by the radar that appear to be moths.

Noctuid moths were caught in a mercury-vapour light-trap at Rothamsted during 1999 and 2000 at ground level (data collected by J. W. Chapman, unpublished). These data are analysed here. Fresh body-mass and wing lengths* of 209 noctuid moths were recorded. The sample included two well-known migrant noctuid species: 11 *Autographa gamma* and 51 *Agrotis exclamationis* (Figure 2·13). There is a strong positive relationship between mass and wing length, with different linear

* Defined as thoracic centre to wing-tip.

regression coefficients for each species. A generalised relationship can be shown for all 209 samples (Figure 2·14), the linear regression is:

$$m_i = 20.9 l_w - 215\,, \qquad (2\cdot1)$$

in which m_i is the mass of a noctuid moth, in mg, and l_w is length of wing, in mm.

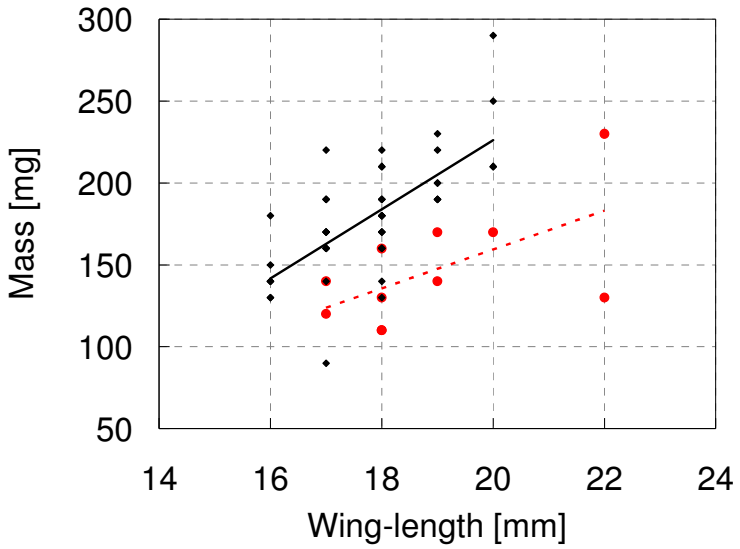

Figure 2·13 – *Mass against wing-length for 51 A. exclamationis (black) and 11 A. gamma (red) noctuid moths. Linear regression fits are shown: coefficient of determination (R^2) values are 0.5 and 0.4 respectively.*

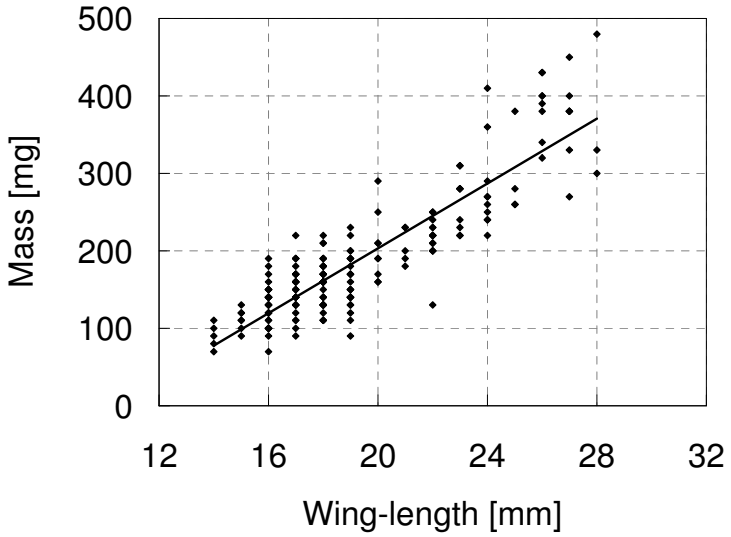

Figure 2·14 – *Mass against wing-length for 209 noctuid moths of 16 species. A linear regression is shown, the coefficient of determination (R^2) was 0.8.*

For the purpose of this thesis, further body dimensions were obtained from 9 samples of each of four common species of noctuid (*A. exclamations, A. gamma*,

Xestia c-nigrum, Mythimna pallens), using a preserved collection at the Plant and Invertebrate Ecology (PIE) division of Rothamsted Research, UK (Table 2·3). Because no fresh mass information was available for *X. c-nigrum* and *M. pallens*, equation 2·1 was used to provide estimates of their masses.

Overall, these data on noctuid mass and size are useful for both parametrizing insects in the trajectory model (Chapter 6) and for helping to find the probable identity of radar-observed insects during nocturnal layer events (Chapter 4).

Table 2·3 – *Dimensions, mass, and cross-sectional area for 4 species of noctuid moth. Values shown are mean ± standard deviation for 9 moths of each species.*

	A. exclamations	*A. gamma*	*X. c-nigrum*	*M. pallens*
Body length [mm]	16 ± 1.0	14 ± 1.6	14 ± 1.0	13 ± 1.1
Wing length [mm]	19 ± 1.1	19 ± 1.4	19 ± 1.0	18 ± 1.1
Insect size [mm²]	595 ± 54	542 ± 87	507 ± 58	446 ± 64
Thorax width [mm]	5 ± 0.3	4 ± 0.3	4 ± 0.6	4 ± 0.5
Mass, m_i [mg]	194 ± 23	142 ± 16	† *171 ± 22*	† *151 ± 24*

†Fresh masses of these species were not available, the mass values are estimates based on equation 2·1.

2·4 Discussion

Catch data

Near ground-level catches of airborne arthropods showed strong diel periodicity, especially when analysing just one species (Lewis and Taylor 1964). Time of flight was found to be a function of illumination level, whilst concentrations were primarily a function of temperature (Lewis and Taylor 1964). These low-level catches are likely to have been a combination of migratory flight and vegetative flight. Hence, an analysis of diel periodicity patterns of high-altitude insects will reveal the effect of time-of-day on the flight activity of migrants alone.

Catches from the Cardington aerial netting campaign (2003–2006) revealed that the most abundant high-altitude migrants observed in the UK are Hemiptera (the

true bugs, including aphids), Diptera (true flies), and Hymenoptera (parasitic wasps and ants). Together these groups comprised 57.9 % of the aerial fauna caught over the entire period, compared to 89 % of the aerial fauna caught in more restricted period studied in Chapman *et al.* (2004a). The remainder of the catch comprised Orthoptera (grasshoppers), Neuroptera (lacewings), Coleoptera (beetles), Lepidoptera (moths), Aranea (spiders), Thysanoptera (thrips), and Psocoptera (booklice). The catches of Lepidoptera have included important crop pests, such as the diamondback moth *Plutella xylostella* (Yponomeutidae), the large yellow underwing *Noctua pronuba* and the silver Y *Autographa gamma* (both Noctuidae).

In particular, the abundance of Lepidoptera caught in the 2003–2006 campaigns were less than one percent by night or day. Near-ground catches of Lepidoptera were similarly small by day, but were hugely abundant at night: 82 % of small (< 30 mm^2) fliers at night were Lepidoptera (Lewis and Taylor 1964). The reason that a low proportion of the high-altitude catches (here and in Chapman *et al.* 2004a) were Lepidoptera compared to the vast low-level catches in Lewis and Taylor (1964) is probably because the vast majority of the Lepidoptera collected in the 3 m suction traps were not migrants. Furthermore, the numbers of Lepidoptera caught were low due to the relatively small net aperture: the small number of catches means that the sample number is more susceptible to natural random variations in catch numbers. The reason that the net aperture was made as small as it was is that the small blimp cannot carry a larger net due to lack of static lift.

High-altitude concentrations of Lepidoptera were low compared to other orders. Nonetheless, moths are highly suitable for study for two main reasons. Firstly, many Lepidoptera are larger than many of the migrant species found in other orders and can hence easily be detected by radar. Secondly, because Lepidoptera are less numerous, more effort can be focussed on the individuals sampled or detected, for example in ascertaining the species and its characteristics (*e.g.* mass, wing-length, *etc*: see §2·2·3).

Noctuids are the most speciose of the Lepidopteran families, with around 400 UK species (Chinery 1993). Many noctuid larvae are known as cutworms, owing to the damage they can cause to crops: reviews can be found on the pest status and zoogeography of *Helicoverpa* species (Fitt 1989) and the black cutworm *Agrotis ipsilon* (Showers 1997). Analysis of radar and aerial netting data—complemented by ground-based trap data (Chapter 4; Chapman *et al.* 2002, Reynolds *et al.* 2005)—suggested that the following species of moths were migrants at high-altitude: the noctuids beet armyworm (S*podoptera exigua*) and silver y (*Autographa gamma*); the pyralids rush veneer (*Nomophilia noctuella*) and rusty dot pearl (*Udea ferrugalis*); and the yponomeutid diamondback moth (*Plutella xylostella*). Often these species have the migratory potential to cover hundreds of kilometres and, for example, can easily fly to the UK from continental Europe. For instance, see Chapman *et al.* (2002b) for the migration capabilities of the diamondback moth *P. xylostella*, and French (1969) for the migration of *Spodoptera exigua* noctuid moths from North Africa to the British Isles.

Masses and sizes of noctuid moths were taken from ground-trap data to obtain typical noctuid moth characteristics, particularly useful for comparison with radar data when attempting target identification. A strong relationship was found between noctuid mass and wing-length, with noctuid masses in the range 70–490 mg and wing-lengths of 13–28 mm. The sizes of these noctuids corresponds to Johnson's (1969) group where body area was 100–1000 mm², comprising just 2 % of the population at 2 m a.g.l.

Diel periodicity

Analysis of high-altitude migrations of insects above the UK is, not surprisingly, very sparse, but a new era has now begun through the deployment of continuously-operating vertical-looking radars. Operational VLRs are effective tools for the monitoring of aerial migrant insect activity for altitudes of flight above ~ 180 m. In fact, it is the only effective method of observing vertical structure in high-altitude insect activity, and in particular, insect layers.

The diel periodicity of flight was analysed for high-altitude UK migrant macro-insects averaged over 4 years of the three summer months, at a high resolution of 15 minutes; overall this gives a total of over half a million samples (15 range gates, 12 months, 96 profiles per day). This includes more data than any other previous UK study. Insect taxa have not been identified by the radar, but instead a general approach to patterns in insect abundance has been taken. For case studies, probable species can be identified using mass, shape, and size variables derived from radar data along with trapping data (see Chapter 4).

The overall diel cycle in insect numbers showed a similar pattern to that found in other studies (*e.g.* Chapman *et al.* 2003). Four well-defined diel phases were observed: dawn, day, dusk, and night. Flight behaviour is constrained primarily by light and a noticeable change with seasons was observed, particularly with the dawn and dusk peaks; this was also noted in Lewis and Taylor (1964). Most activity was observed by day, where there are several hours of high temperatures and insect abundance at altitude was presumably assisted by CBL motions. The dusk peak is the most consistent and strongest feature of the diel cycle. On average, nocturnal activity was low and became less intense with time. But on certain occasions, layering occurred, and 60 % of profiles just after dusk (21:15) were found to be layered.

The daytime peak in insect numbers was reached between 11:00 and 13:00, with a drop in numbers thereafter. The hottest part of the day occurs typically from 12:00 to 15:00. Furthermore, it is curious that the average profile showed that the highest altitudes were reached during 09:00–10:00, with a drop in height thereafter. Clearly, most insects respond to variations in sunlight (Lewis and Taylor 1964). But perhaps the existence of thermals in the CBL is partially a cue in addition to providing extra upward motion. A detailed investigation of the CBL and daytime insect flight is needed to elucidate this; but it is not considered further in this thesis.

Vertical profiles

The mean profiles throughout the diel showed a monotonic decrease of insect number with altitude at all times. This is consistent with the profiles observed in Johnson (1969), where a power-law relationship was proposed. This profile type indicates that layering is a less frequent event, and requires a more sophisticated analysis to identify layering events.

Daytime layers are less often reported in the literature than nocturnal layers (but Chapman *et al.* (2002a) shows a good example). It seems likely that daytime layers are not as temporally and spatially continuous as nocturnal layers due to the influence of turbulence and updraughts in the CBL (see Chapter 1), whereas the atmosphere is generally more stratified at night. Indeed, layering by day is generally weaker than nocturnal layering. A recent study using modelling (Geerts and Miao 2005b) and radar observations (Geerts and Miao 2005a) showed that some insects detect updraughts and adjust their flight accordingly, *e.g.* by opposing upward motion: hence, numbers were sometimes found towards the top of CBLs. Again, this will not be covered in this thesis, but further work on insect flight in the CBL is required.

A peak in layering occurrence was observed at 21:15, following the dusk peak in insect numbers at 20:45. This has been previously noted on a case study basis (*e.g.* Reynolds *et al.* 2005), but the present work (covering 4 years of data) clearly confirms that nocturnal layering follows the dusk peak in insect density. Subsequently, insect concentrations reduce with time through the night: presumably because airborne insects cease flight at various times throughout the night, with the added assumption that there is no further insect take-off following dusk (because temperature has usually fallen too much and the necessary decreasing light cue at dusk has passed).

In the core data-set, the lowest column-integrated aerial activity is seen at 02:30–02:45. The dawn peak in activity occurs between 03:30 and 03:45. Subsequently, 22 % of occasions had a dawn layer, where layer frequency was centred in time at

04:00. Dawn layering was short-lived; indeed, the time of the diel cycle with least layering is 05:15. Dawn layers are not considered in this thesis, and are rarely mentioned in the published literature; the only comprehensive study is Reynolds *et al.* (2007).

Nocturnal layers, the focus of this thesis, were observed mostly at altitudes of 200–500 m. The peak of layering was observed in radar range gate 2 or 3 (*c.* 300–400 m) at both locations studied. There remains uncertainty in how many insect layers form beneath the lowest radar-detection altitude, *i.e.* below around 165–180 m.

Most nocturnal layering followed from mass emigration at dusk (*i.e.* dusk peak in insect numbers), and layers occurred at relatively low altitudes (200–500 m). Therefore, a critical region has been defined (as 200–500 m a.g.l., at 20:00–22:00; summertime) in which meteorological variables might have a key influence on nocturnal layer initiation. The meteorological variables in the critical region are compared to the intensity of nocturnal layers, in Chapter 5.

In this chapter, progress has been made in describing a 'climatology' of insect layering, which Drake and Rochester (1994) identified as essential to the study of insect layering. Layering has been observed in all diel periods, with a low frequency at dawn or in the morning. In this thesis, focus is made on nocturnal layers occurring during summer nights, when insects forming the layers were able to undertake extended migrations. Case studies of typical nocturnal layering events are discussed in Chapter 4.

3: Meteorological data

3·1 Background

The evolution of meteorological conditions over a diurnal cycle was reviewed in §1·4. Data are required in this thesis to test the hypotheses that meteorological conditions are critical for nocturnal insect layer formation. In this chapter, the sources of meteorological data are described, and any limitations highlighted. Finally, the UK Met Office's numerical weather prediction model—the Unified Model (UM)—will be validated against radiosonde (weather balloon) data for nocturnal occasions.

3·2 Sources of data

3·2·1 Radiosondes

A radiosonde[*] is a package of instrumentation suspended from a helium-filled balloon, which is released into the atmosphere. The radiosonde transmits data to a ground-based receiver as the balloon rises, which gives an atmospheric profile for each of its recorded variables: wind speed and direction[†], temperature, humidity, and pressure.

There is a worldwide 'upper-air station' network of ground-stations, from which radiosondes are launched operationally at 00:00, 06:00, 12:00, and 18:00 hours UTC (although some stations might not release radiosondes at all of these times). The southern England locations are shown in Table 3·1 and Figure 2·2. The vertical resolution of radiosonde data as the balloon rises is typically between 2 and 12 m (this variation is dependent upon atmospheric conditions and the amount of helium in the balloon).

[*] The word radiosonde is composed of 'radio' for radio communication (transmitting frequency, circa 403 MHz) and 'sonde', which is a German word for probe.
[†] Wind data are obtained by global positioning satellite (GPS) tracking.

The radiosonde data are sparse both temporally and spatially: *i.e.* just one profile in space (with large spacing between stations), and only for one time (spaced by at least 6 hourly intervals). Hence, for many uses—particularly for systematic studies (to be conducted in Chapter 5)—there is a requirement for data that have a higher resolution in time and lateral space.

Table 3·1 – *Network (operational) stations for radiosonde release in southern England.*

WMO† station number	Location	Latitude / longitude	Altitude a.s.l.‡
03808	Cambourne	50.22 °N / 5.32 °W	87 m
03496	Hemsby *	52.68 °N / 1.68 °E	14 m
03882	Herstmonceux	50.90 °N / 0.32 °E	52 m
03743	Larkhill **	51.20 °N / 1.80 °W	122 m
03354	Nottingham	53.00 °N / 1.15 °W	117 m

† World Meteorological Organisation ‡ Above sea level * Station closed in March 2001

** Soundings made to satisfy Firing Range commitments.

3·2·2 Numerical weather prediction data

Numerical weather prediction (NWP) models numerically solve the equations of fluid dynamics to predict meteorological variables in 3D space and their evolution in time. In addition to geophysical dynamics theory, NWP models assimilate measured meteorological data to constrain the numerical predictions. Atmospheric profiles are simulated at various locations (grid-boxes) across the globe (or within a given region) with a certain fixed spatial resolution between grid-points. These NWP data can be used as a surrogate for measured data; this is particularly in situations when there is no nearby radiosonde launch, or when a network radiosonde is not released at a required time.

The UK Met Office's operational NWP model—the Unified Model (UM)—provides the main source of meteorological data used in this thesis. The UM (version 5 onwards) solves non-hydrostatic, deep-atmosphere dynamics using a semi-implicit, semi-Lagrangian numerical scheme (Cullen *et al.* 1997). The model

includes a comprehensive set of parametrizations*, particularly for surface fluxes (Essery *et al.* 2001), boundary layer (Lock *et al.* 2000), mixed phase cloud microphysics (Wilson and Ballard 1999), and convection (Gregory and Rowntree 1990): with additional downdraft and momentum transport parametrizations.

Operationally, a 'mesoscale' domain is run by the Met Office, which covers the UK and north-western Europe. Its horizontal resolution is 0.11° (approximately 12.5 km). The profiles of meteorological variables in this thesis were interpolated between grid-points to specific sites of interest (*i.e.* Cardington, Chilbolton, Rothamsted, and Malvern). The model runs with 38 levels spaced non-uniformly with altitude (Figure 3·1), which gives a resolution of 40 m at the lowest levels, up to a resolution of 280 m around 1 km. Data were extracted every hour. Meteorological variables archived were temperature, wind speed, wind direction, humidity, and pressure.

Boundary layer mixing schemes

The components of the UM that are most relevant in this thesis are those describing boundary layer dynamics (*cf.* §1·4). Boundary layer mixing schemes are classified as one of seven types (Lock *et al.* 2000), depending upon the sign of the surface temperature gradient† and cloud conditions. Two of these schemes are used for stable boundary layers: with and without cloud.

The state of the nocturnal boundary layer, and its vertical profiles, depend greatly on local turbulent mixing. Excessive mixing smoothes gradients; weak mixing allows strong gradients to remain. Hence, the mixing scheme in the UM is critical for accurate prediction of boundary layer profiles. Turbulent fluxes are estimated by using local mean gradients of relevant variables such as temperature and wind

* There are differences in spelling which provide subtle differences in meaning to some authors. *Parametrizations* are the attempt to represent sub-gridscale features (*i.e.* those that are too small in spatial or temporal extent) in the gridscale variables. A *parameterization* is to describe in terms of parameters.

† Vertical gradients of temperature (strictly, virtual potential temperature) at the lowest model level are used to select a boundary layer type.

speed (see flux theory in §1·4·5). This method of calculating fluxes works best in moderately stable conditions, but the theory used is probably less certain for very stable conditions with large positive Richardson number (Lock *et al.* 2000).

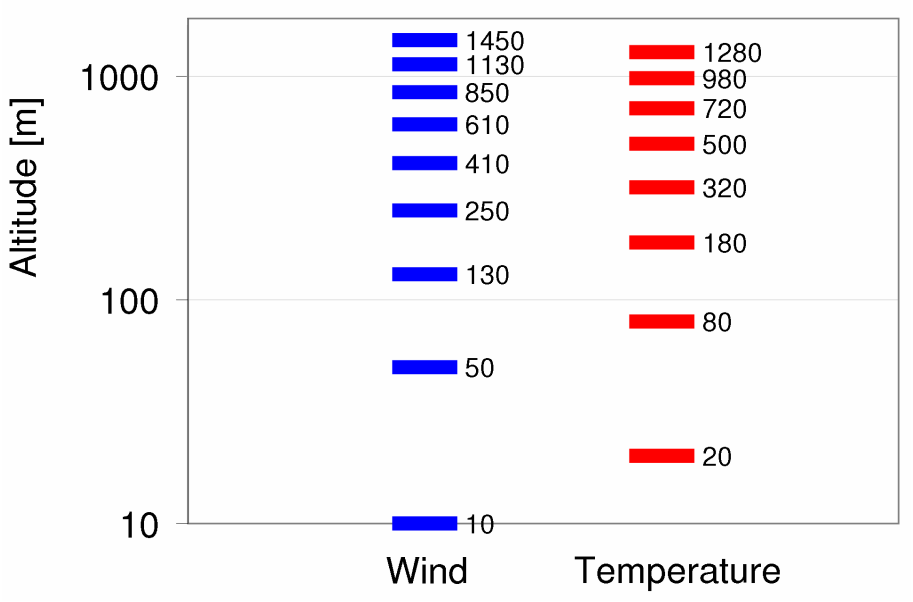

Figure 3·1 – *The lowest few levels of the mesoscale UM. The Charney-Phillips staggering solves wind speed and direction on one set of levels, and temperature and humidity on a different set of levels.*

The simulation of mixing is clearly important. A cut-off threshold for turbulent mixing is often used (*e.g.* $Ri = 0.25$), but experimental studies (*e.g.* Kondo *et al.* 1978) have shown that there is often no cut-off value for turbulence. Hence, a continuous function can be defined for the decrease in intensity of turbulence. K-theory is used to estimate vertical fluxes by using the gradients of variables and using eddy diffusivities (see §1·4·5). This is the basis of turbulent mixing in the UM. The first-order* mixing scheme defines eddy-diffusivity values that are dependent on mixing-length, vertical shear of wind, and Richardson number (Edwards *et al.* 2006). Such mixing schemes are based on empirical studies. The form used in the UM is summarised thus (see Edwards *et al.* 2006 for further details):

$$K_H = l_M l_H \left| \frac{\partial U}{\partial z} \right| f_H^n(Ri), \qquad (3·1)$$

* Turbulence parametrizations experience so-called 'closure' problems that are hard to solve because of non-linearity and that there are more unknowns than equations. First-order schemes use only *first* derivatives.

$$K_M = l_M^2 \left| \frac{\partial U}{\partial z} \right| f_M^n(Ri), \tag{3·2}$$

where U is the mean wind speed, l_M is the mixing length for momentum, and l_H is the mixing length for heat. Mixing lengths are an estimate of the travelled distance for which an air-parcel retains its characteristics before given quantities are mixed out of the air-parcel into its surroundings. Mixing lengths are typically modelled as a function of altitude and boundary layer depth (*e.g.* Edwards *et al.* 2006), and can hence vary with time as the boundary layer evolves. The stability functions, $f_H^n(Ri)$ and $f_M^n(Ri)$, are functions of Richardson number: there are three main functional forms:

(*i*) that introduced by Louis (1979),

$$f_H^n = f_M^n = (1 + 5Ri)^{-2}; \tag{3·3}$$

(*ii*) the long-tailed function,

$$f_H^n = f_M^n = (1 + 10Ri)^{-1}; \tag{3·4}$$

(*iii*) the sharp-tailed function,

$$f_H^n = f_M^n = \begin{cases} (1 - 5Ri)^2 & 0 \le Ri \le 0.1 \\ (20Ri)^{-2} & Ri \ge 0.1 \end{cases}. \tag{3·5}$$

In the mesoscale UM, a hybrid has been employed that interpolates between the Louis form near the ground and the sharp-tailed functions above 200 m (Edwards *et al.* 2006). Each form has advantages and disadvantages in simulating observed turbulence statistics and for numerical stability. Hence, pragmatic decisions are required to decide which one to implement. The sharp-tailed function underestimates mixing near the surface and overestimates at altitude. Long-tailed functions give surface heat fluxes that are too high.

A study has shown that the stable boundary layer scheme itself performs well in isolation, but occasionally the surface-flux scheme provides poor predictions due to incorrect modelling of radiative emission (Edwards *et al.* 2006). The surface-flux scheme provides data needed to operate the boundary layer scheme: hence, errors in the former will cascade into the latter scheme. For field campaigns,

measured surface fluxes could replace the surface-flux scheme (*i.e.* model-predicted fluxes) to give a better UM performance.

3·2·3 Trajectory model

To improve the ecological understanding of a given migration event, it is necessary to estimate the probable take-off locations of insects observed above the insect-monitoring radars. For particular cases (in Chapter 4), back-trajectories are produced by a configuration of NAME (Numerical Atmospheric dispersion Modelling Environment, Maryon *et al.* 1999). NAME can be used for a wide range of applications in the prediction of medium- to long-range spread of pollutants. Its general uses include air quality prediction, emergency response, and tracking of chemical species.

NAME uses advection terms (*i.e.* large-scale winds, typically taken from the UM) to calculate a trajectory for a parcel of air. Turbulent dispersion is effected using Monte Carlo methods: *i.e.* 'units of air' (or particles) undergo a random walk using turbulent statistics specific to the conditions. In Monte Carlo methods, a large number (an ensemble) of particles are released at a given location and the resultant plume is analysed. In this thesis, NAME has been used only in its trajectory configuration to estimate the likely source of insects for case study occasions in Chapter 4. In Chapter 6, a trajectory model based on Monte Carlo methods will be developed.

3·3 Validation of nocturnal UM profiles

3·3·1 Motivation

Because the radiosonde data are sparse in space and time, they are often not very useful for comparison with data from the entomological radars. The UM data have a much better temporal and horizontal resolution and can be used for case study occasions as well as analysis over long-term data-sets. It is obviously important to know the accuracy of the UM data during nocturnal occasions if it is

to be used as a surrogate for measured data. In this section, literature on previous analyses of UM accuracy is reviewed, and then a validation study between UM and radiosonde data is carried out. There is particular focus on the altitudes of 200 – 500 m a.g.l. and times around 20:00–22:00 because that is when conditions might be critical for nocturnal insect layer formation (§2·3·2).

3·3·2 Background

In a single-column* version of the UM, comparison of UM data was made with data measured at Cardington from a meteorological tethered-blimp (Edwards *et al.* 2006). The UM's surface inversions were found to be too shallow during the nocturnal transition. However, on 20 % of occasions, very rapid and intense cooling was observed in measured data that was not observed in the UM data. This was probably caused by surface heat fluxes that were too large in the UM; this subsequently resulted in surface temperature minima that were not cool enough in the UM (Edwards *et al.* 2006). In the developed phase of the NBL, performance was generally better than in the transition period (Edwards *et al.* 2006). However, in general, the potential temperature profiles in the UM exhibited curvature that was "too negative" (*i.e.* too statically stable), leading to shallow and cool boundary layers.

3·3·3 Comparison of UM data with radiosonde releases

Experimental background and methods

For validation of the UM data used in this thesis, 17 radiosondes were released during two consecutive summers' field campaigns (July 2004 and June–July 2005). Release sites were: Chilbolton Observatory (51.14 °N / 1.40 °W, 81 m a.s.l.), Cardington Airfield (52.10 °N / 0.42 °W, 28 m a.s.l.), and the network station at Larkhill (Table 3·1). Radiosondes were released on clear-sky, non-frontal, and low synoptic-wind conditions. These conditions were chosen so that the nocturnal boundary layer was in a near-idealised state; hence, complications caused by cloud (radiative effects) or rapidly changing synoptic conditions were negligible.

* Single column modelling is a simplification of an NWP model by representing just a single column of the atmosphere, thereby assuming horizontally homogeneous flow.

Radiosondes were released during the critical time for insect layering (§2·4), *i.e.* releases were made within around $0-3$ hours after sunset (Table 3·2).

Larkhill lies 32 km to the West of Chilbolton Observatory (Figure 2.2 and Figure 3·2); there is enough variability in the relief to suggest that the near-surface meteorology might be different in some situations. In general, the slopes are of order $0.1-1\,\%$ at both sites. At Cardington, there is a particularly pronounced ridge 2.5 km to the south-east of the site that has a maximum gradient of about $5\,\%$ (but more typically $1\,\%$) and rises to 50 m above the site (Figure 3·3; Grant 1994). While there are no mountains in the south-east of England, the relief has still enough undulation to cause katabatic flows at night to be present (which are sometimes called drainage or gravity currents). Katabatic winds are caused because the cold air near the surface at night (due to radiative cooling, see §1·4·7) will roll down slopes due its increased density. These downslope flows can give peak winds of up to $4\,\mathrm{ms^{-1}}$, although $1-2\,\mathrm{ms^{-1}}$ is a more likely value for slopes of order $0.1-1\,\%$ (Mahrt 1981). The temperatures are altered by up to $\pm 2\,\mathrm{K\,hr^{-1}}$. These katabatic currents vary in depth with slope and weather conditions from a few metres to 150 m, a formula suggested for their depth is (Stull 2000):

$$h_d = 0.037(\sin\alpha)^{2/3} x\,, \qquad (3{\cdot}6)$$

in which h_d is depth of current, α is angle of slope, and x is the downslope distance. Given the data in Figure 3·3, a depth of 8 m can be predicted for katabatic flow depth below the ridge at Cardington (assuming that $\alpha = 0.7°$, $x = 4\,\mathrm{km}$). It is therefore worth noting that any topographical features (and furthermore land-use types) that are unresolved in the UM are likely to cause an error in the low-level variables in the UM.

Table 3·2 – *Summary of seventeen radiosonde releases on evenings with a stable boundary*

No.	Location	Date	Release time [hours, UTC]	Release time after sunset [hours]	Inversion-top temperature [°C]		Inversion top altitude [m]		Jet [m
					UM	R.†	UM	R.	UM
1	Cardington	28 July 2004	21:45	1:46	19.2	18.1	20	54	12.1
2	Cardington	30 July 2004	21:42	1:46	20.7	19.5	80	71	6.2
3	Cardington	08 June 2005	21:12	0:55	15.3	15.4	300	277	7.7
4	Cardington	21 June 2005	21:45	1:21	19.7	19.3	20	144	3.0
5	Cardington	22 June 2005	21:38	1:14	23.9	23.1	50	108	None
6	Cardington	10 July 2005	21:44	1:25	22.3	22.0	80	110	4.3
7‡	Cardington	11 July 2005	21:53	1:35	17.3 16.0	17.6 16.6	20 600	23 441	None
8	Cardington	12 July 2005	21:31	1:13	21.0	20.8	20	83	3.6
9	Cardington	12 July 2005	23:05	2:47	19.6	20.2	300	174	3.3
10	Cardington	17 July 2005	22:52	2:39	21.2	21.3	80	80	8.0
11	Chilbolton	23 July 2004	22:00	1:52	15.1	16.2	495	330	8.9
12	Chilbolton	28 July 2004	21:26	1:25	20.9	19.6	79	54	8.3
13	Larkhill	05 August 2003	20:00	0:11	None	25.0	None	80	13.9
14	Larkhill	01 September 2003	21:00	2:05	15.0	14.4	80	80	6.8
15	Larkhill	01 September 2003	23:00	4:05	13.8	14.0	80	80	7.0
16	Larkhill	04 September 2003	20:00	1:11	18.8	17.5	80	180	8.1
17	Larkhill	13 May 2004	20:00	0:13	None	13.5	None	80	None

† Radiosonde ‡ Case 7 had two inversions in the profile

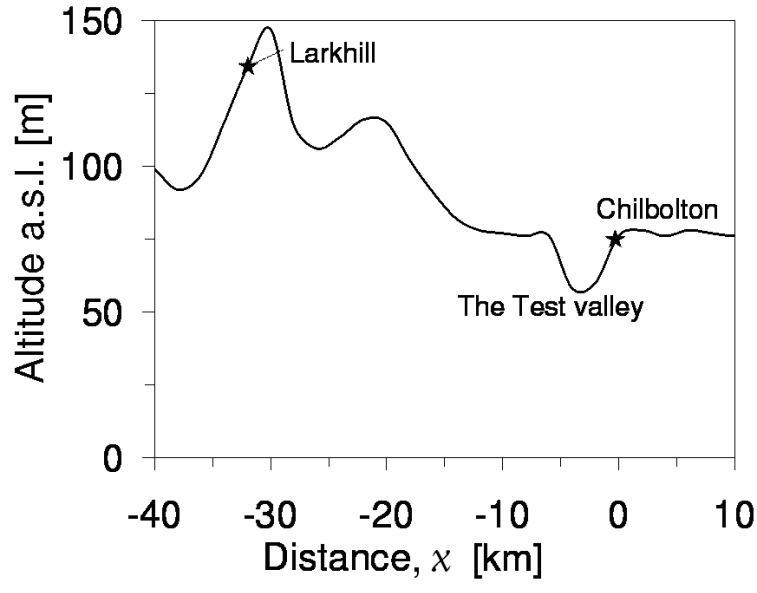

Figure 3·2 – *Orography cross-section through Chilbolton Observatory (x = 0 km) heading through Larkhill. Taken from digital elevation model (DEM) of the US National Geophysical Data Center. Altitude is metres above sea level (a.s.l.).*

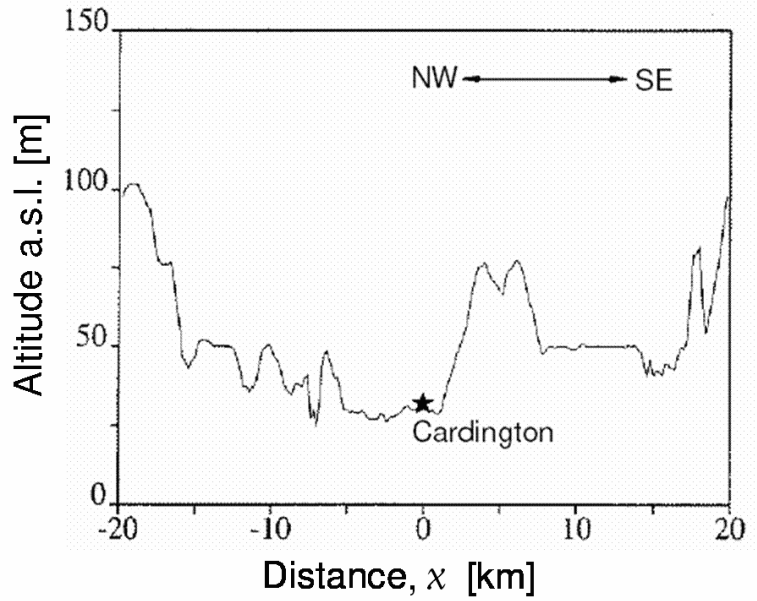

Figure 3·3 – *Orography cross-section through Cardington airfield (x = 0 km) in a north-west to south-east plane. From Grant (1994).*

Radiosonde data were assumed as 'truth' for comparison with the UM. It is worth noting, however, that radiosondes drift due to the horizontal winds: typically 3 km horizontally within the first 1 km of ascent, which takes *c.* 7 minutes. Firstly, this horizontal drift is of reduced importance because as the balloon is advected by the wind, so are the air parcels (hence, as the radiosonde drifts it is

sampling air that was above the release site even at later times). Secondly, the UM horizontal resolution is coarser than the radiosonde drift.

The UM horizontal resolution is 12 km. Any site-specific biases in the forthcoming validation might be reduced by using more than one site in the evaluation (*i.e.* two comparison sites: Chilbolton and Cardington). The UM data had hourly temporal resolution, but linear interpolation of this hourly data was performed to create a profile that matched the time of radiosonde launches.

Because the radiosonde data are much finer in resolution than the UM, the radiosonde data have increased fluctuations in the measured variables. Hence, the data were smoothed using a running mean of 7 values (except for the first 7 values of the ascent which were unsmoothed, *i.e.* until approximately 40 m). Subsequently, the nearest radiosonde datum to the centre of each UM level in the database was chosen for validation.

Absolute errors were calculated as follows:

$$\varepsilon = \psi_{UM} - \psi_{sonde}\,, \tag{3·7}$$

where ψ is any variable. The relative, or fractional, errors were calculated as follows:

$$\varphi = \frac{\varepsilon}{|\psi_{sonde}|}\,. \tag{3·8}$$

Temperature

The mean profile of the absolute error is shown in Figure 3·4. There was an underestimation of temperature from $200-1000$ m by < 0.5 °C ; and the confidence intervals included a zero error, so perhaps the underestimation is not a consistent bias. However, below 200 m, warmer temperatures (most marked near the surface) were observed in the UM: the mean error was 1.8 °C at 10 m. Indeed, the confidence intervals are away from the zero error line, which indicates a consistent warm bias at low levels. Crucially, in the critical region

($z \approx 200 - 500$ m a.g.l.) mean temperature errors were less than 0.5 °C. The largest absolute temperature error across all radiosonde profiles was for case 5, when there was very little synoptically-driven wind and so more susceptibility to local-scale flows. There was a 4 °C overestimate of temperature by the UM at 20 m, which was possibly the effect of a katabatic current from the ridge to the SE of Cardington Airfield; though 4 °C is quite a large change for a katabatic flow over such a weak slope.

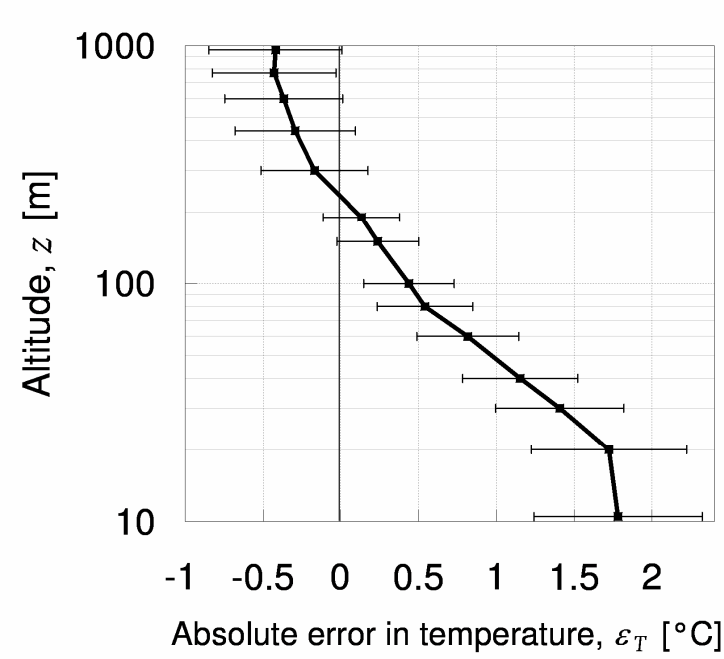

Figure 3·4 – *Mean profile of absolute error in UM temperature, compared with radiosonde data. Horizontal bars show the 95 % confidence interval.*

Inversion tops were defined as the altitude at which $\partial T / \partial z = 0$. For the seventeen occasions, eighteen inversions were observed in the radiosonde data (*i.e.* two inversions were observed in one profile: one surface and one upper inversion). The UM represented sixteen of these inversions: *i.e.* the UM failed to capture two inversions, which were both 80 m deep in the radiosonde data (and were the closest two releases to sunset, indicating a problem in representing the NBL transition). Of the sixteen inversions, thirteen inversions were low-level, *i.e.* below *c.* 200 m (Figure 3·5). For only three of these low-level inversions did the UM over-estimate inversion depth: the rest were either correct (three) or an under-estimate (seven). The mean magnitude error for low-level inversion depth was 57 m.

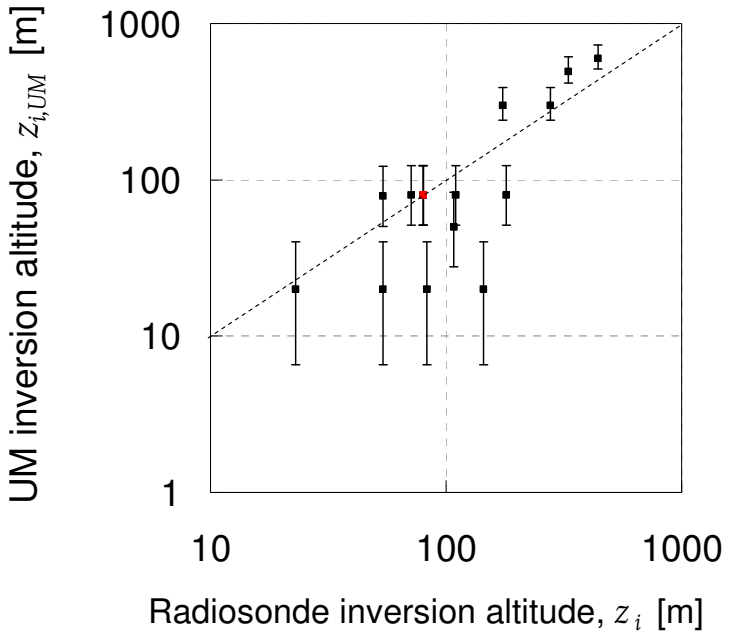

Figure 3·5 – *16 inversion-top altitude comparisons between UM and radiosonde. The red value represents three different occasions when both radiosonde and UM inversion altitudes were at 80 m. The vertical bars show the UM vertical resolution.*

There were only three cases in the radiosonde data where inversion tops were at higher altitude, *i.e.* $z_i > 200$ m. The UM overestimated z_i (z_i is inversion altitude) in all upper-inversion cases, and by an average of 116 m.

Inversion-top temperature was well modelled by the UM in all cases (Figure 3·6): showing a correlation of $r = 0.97$ between radiosonde and UM temperature. However, recall that on two occasions the UM diagnosed no inversion when one was detected by the radiosonde measurements. The mean absolute error magnitude of the temperature at inversion-top was 0.6 °C: the worst cases were where the UM overestimated by 1.3 °C (case 12), and underestimated by 1.1 °C (case 11). Inversions were simulated in the UM with warmer temperatures than the radiosonde data (9 occasions too warm, 7 occasions too cool). Exemplar profiles for accurate (Figure 3·7) and inaccurate (Figure 3·8) inversion simulations are shown. The inaccurate example shows a low-level inversion simulated by the UM which did not occur in the radiosonde observed profile. Furthermore although an inflection is seen in the UM profile at 300 m, no inversion was simulated, in contrast to the radiosonde data.

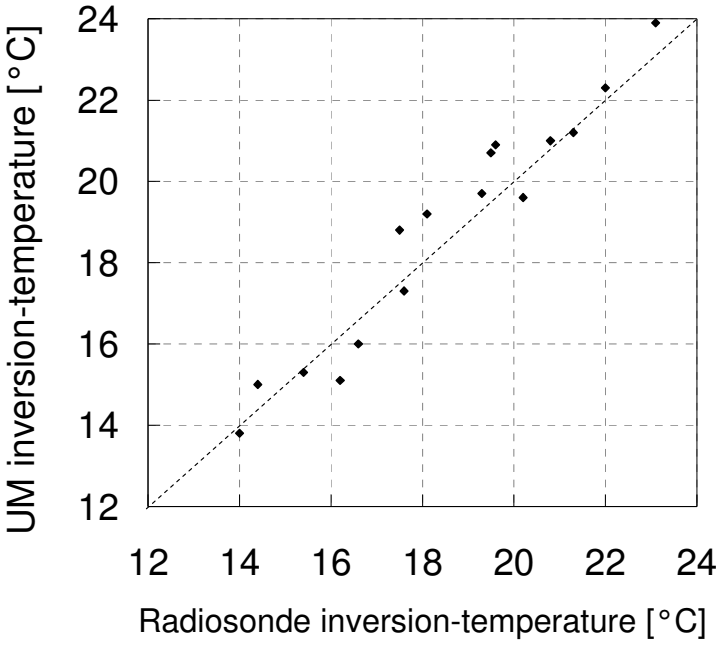

Figure 3·6 – *Inversion-top temperature for 16 inversions in UM and radiosonde data.*

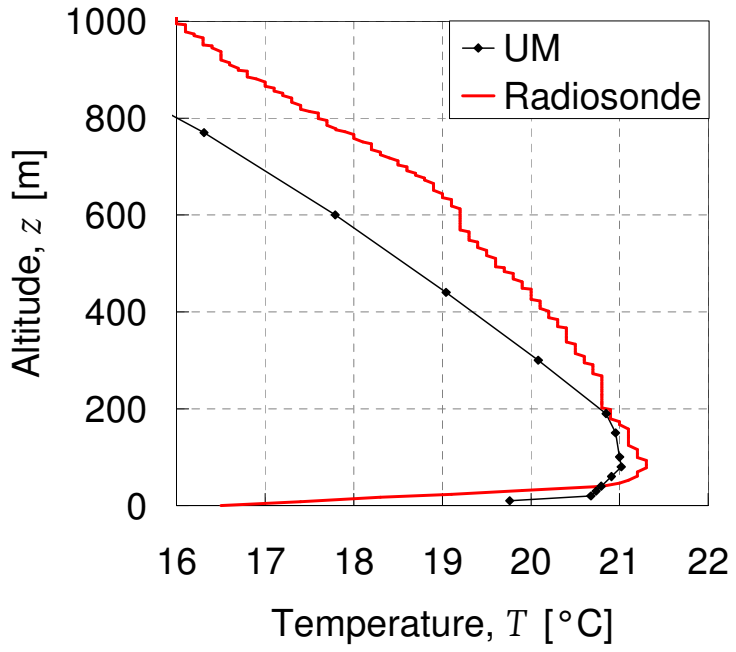

Figure 3·7 – *Example of accurate UM inversion simulation for case 10 (17 July 2005, Cardington). Radiosonde released at 22:52 hours UTC and UM profile at 23:00.*

It is important to diagnose the gradients of variables correctly in the NBL, especially for the calculation of the turbulence/stability variable, *Ri* (see §1.4.3). At the outset, it is worth noting that in the nocturnal boundary layer relatively

small errors in altitudes of features such as the nocturnal jet, capping inversion, and surface inversions can result in larger errors in gradient variables. This is because the vertical gradients themselves change rapidly in these regions of the atmosphere (see §1.4.8). The potential temperature gradient, $\partial\theta/\partial z$, is particularly sensitive to relative errors because profiles are typically close to neutral throughout the residual layer above the inversion (*i.e.* $\partial\theta/\partial z \approx 0$): hence any absolute errors in this variable lead to a larger relative error.

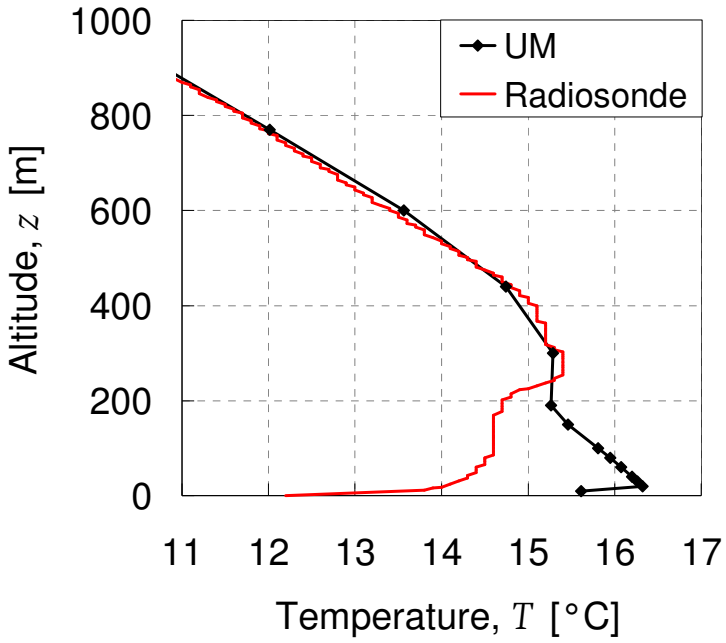

Figure 3·8 – *Example of a poor inversion capture by the UM (case 3, 8 June 2005, Cardington). Radiosonde released at 21:12 hours UTC and UM profile at 21:00.*

Throughout the lowest 1 km, $\partial\theta/\partial z$ is too positive (*i.e.* increased static stability) in the UM, by up to a mean value of 0.13 K km^{-1} (Figure 3·9). This caused a large relative error, particularly in cases 6 and 15 where the radiosonde $\partial\theta/\partial z$ values were very close to zero (*i.e.* neutral), but the UM had a slightly stable profile. The magnitude of the errors was largest at lower altitudes and was most accurate above 200 m. The best accuracy in the profile was from $70-400$ m, where $\varepsilon_{\partial\theta/\partial z} < 0.05$ K km^{-1}. In the $150-200$ m region, the confidence intervals overlapped the zero error line: which indicated that a consistent bias was not evident in that region.

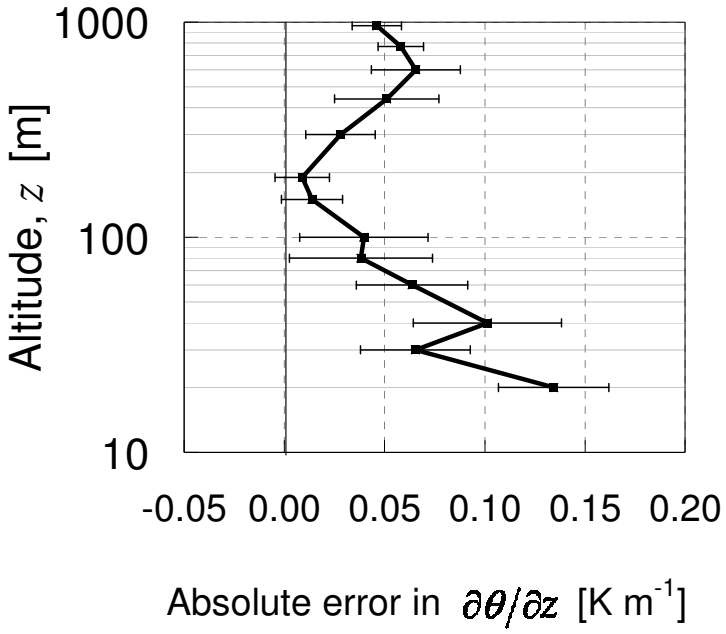

Figure 3·9 – *Mean profile of absolute error in UM's $\partial\theta/\partial z$, compared with radiosonde data. Horizontal bars show the 95 % confidence interval.*

For absolute error of $\partial T/\partial z$ (Figure 3·10) there is a trend for UM overestimation of $\partial T/\partial z$ at the lowest two altitudes and consistent underestimation above 200 m. In the region of 90 – 200 m there was no consistent bias in the errors, since the confidence intervals overlap the zero error line. Many of the inversion altitudes in this region are hence well simulated (*cf.* Figure 3·5).

Wind

The error in UM-diagnosed wind speeds throughout the mean profile shows no consistent bias (Figure 3·11) and the relative error was less than ~ 10 % throughout the mean profile. The spread of errors is up to 3 m s^{-1} and there appears to be no substantial variation in spread of error with altitude. The largest absolute mean errors were found between 30 and 190 m, with a mean underestimation of 0.4 – 0.6 m s^{-1}; and at 960 m, with a 0.6 m s^{-1} overestimate. The largest individual error, of magnitude 5.2 m s^{-1}, occurred when the jet was simulated too weakly in the UM (Figure 3·12).

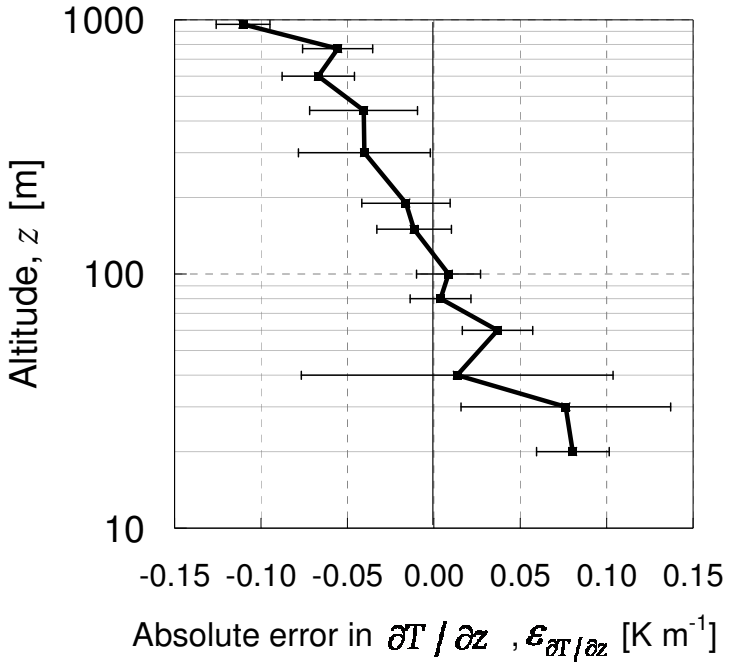

Figure 3·10 – *Mean profile of absolute error in UM's $\partial T/\partial z$, compared with radiosonde data. Horizontal bars show the 95 % confidence interval.*

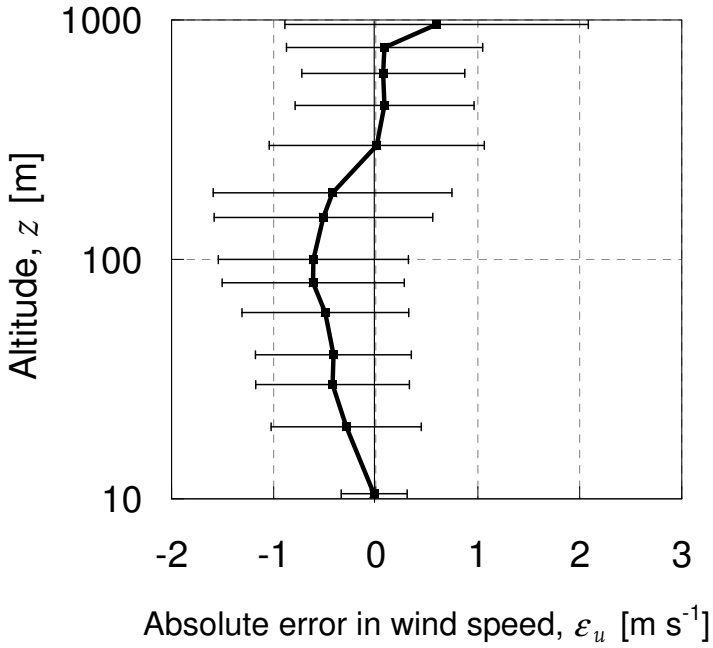

Figure 3·11 – *Mean profile of absolute error in UM wind speed, compared with radiosonde data. Horizontal bars show the 95 % confidence interval.*

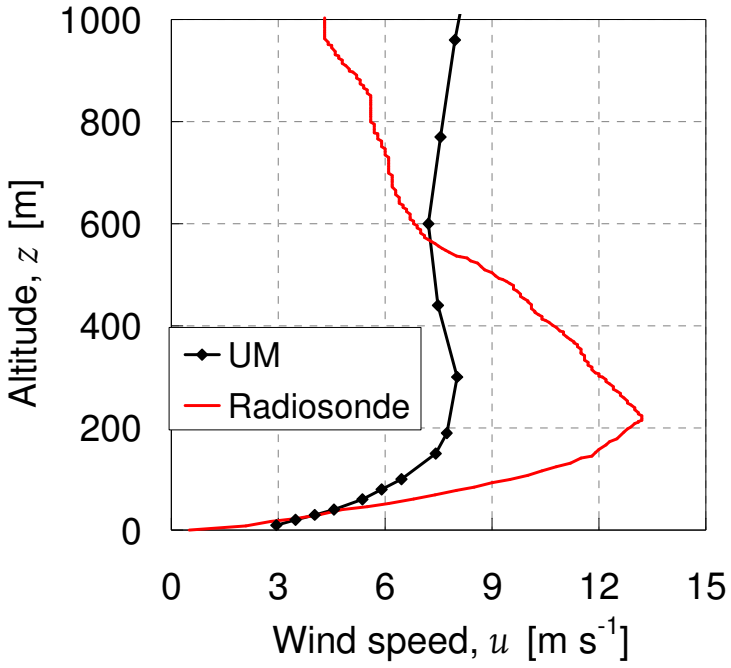

Figure 3·12 – *Example of a weak UM jet: case 10 (17 July 2005, Cardington). Radiosonde released at 22:52 hours UTC and UM profile at 23:00.*

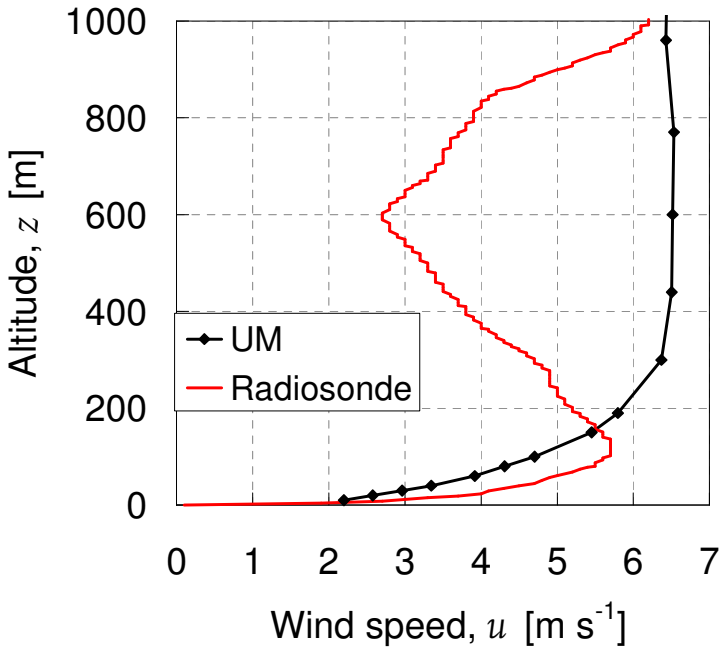

Figure 3·13 – *Example of an inaccurate jet simulation: case 5 (22 June 2005, Cardington). Radiosonde released at 21:38 hours UTC and UM profile at 22:00.*

For the seventeen occasions' wind-speed profiles, jets were observed in the radiosonde data on 15 occasions; on the remaining two occasions no jet was simulated by the UM (*e.g.* Figure 3·13). Nonetheless, in twelve cases jets were observed in both sets of data: ten cases where the UM accurately defined the jet

altitude (Figure 3·14), and two poorer cases (one an underestimate, one an overestimate). An example of accurate simulation in the UM is shown in Figure 3·15. The mean magnitude of the absolute error in the UM profile's jet altitude simulation was 80 m. The largest errors occurred at higher altitudes.

A correlation of $r = 0.89$ was found between radiosonde and UM data for jet speed (Figure 3·16). The UM quite consistently under-estimated wind speeds at jet maximum (in all but three cases): with a mean underestimation of 1.4 m s^{-1}. This is consistent with the observation that jet profiles were consistently too smooth in the UM (*e.g.* Figure 3·12).

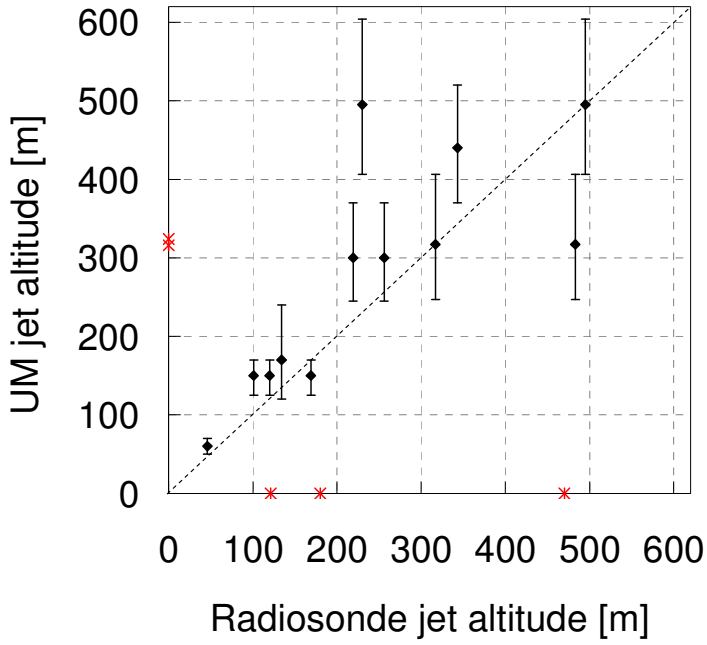

Figure 3·14 – *Jet altitude comparison between UM and radiosonde for 17 clear-sky occasions. Red asterisks are occasions where a jet was only found in either the radiosonde or UM. The vertical bars show the UM's vertical resolution.*

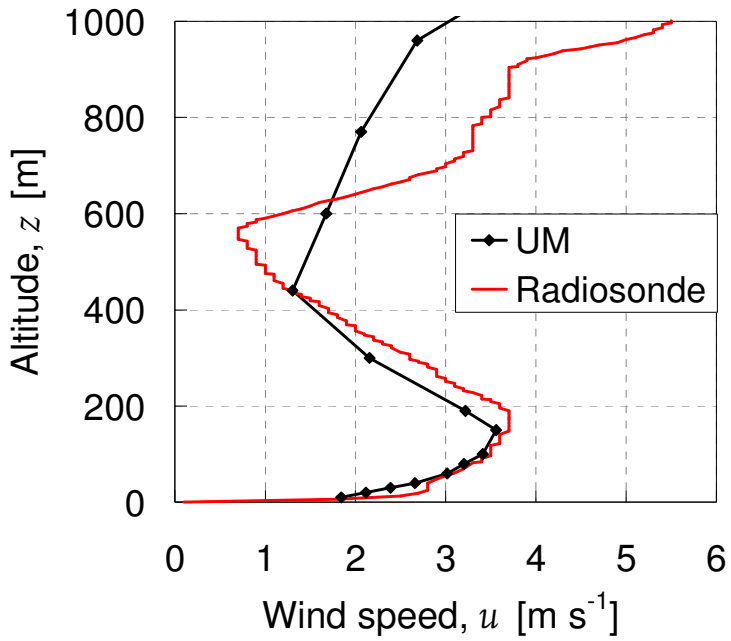

Figure 3·15 – *Example of an accurate jet capture: case 8 (12 July 2005, Cardington). Radiosonde released at 21:31 hours UTC and UM profile (mean of 21:00 and 22:00).*

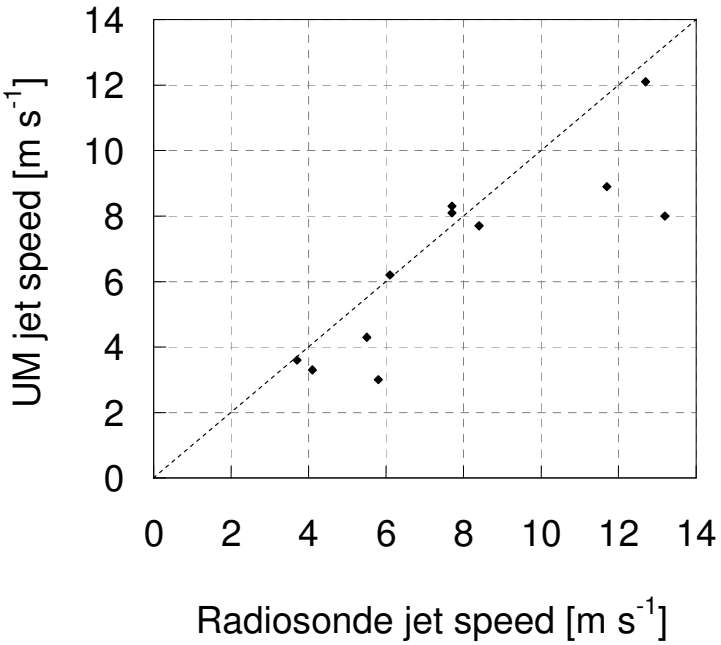

Figure 3·16 – *Jet speed comparison between UM and radiosonde for 10 clear-sky occasions at Cardington and Chilbolton in the summers of 2004 and 2005.*

A variable has been defined in this thesis to represent jet intensity in a given profile as a dimensionless ratio,

$$j = \frac{u_{jet}}{u_{min\uparrow}}, \tag{3·9}$$

where u_{jet} is the wind speed maximum of the nocturnal jet and $u_{min\uparrow}$ is the minimum wind speed above the jet (between the jet altitude and 2 km). An example of jet strength values can be seen for case 10: $j_{UM} = 1.1$ and $j_{sonde} = 3.25$ (Figure 3·12). Over all 17 cases (including cases where one data-set indicated no jet), there was a correlation of $r = 0.66$ between jet intensity calculated for UM and radiosonde profiles (Figure 3·17). Seven cases had an error of less than 30 % in *j*. Eleven of the seventeen cases had a *j*-value that was too low in the UM data (*i.e.* the wind profile was too smooth). On the other occasions the *j*-value was too large in the UM (*i.e.* the wind profile was too sharp). Overall, there is reasonable agreement between the model and measured data, but with a tendency for jets to be smoother in the UM than in the radiosonde profiles.

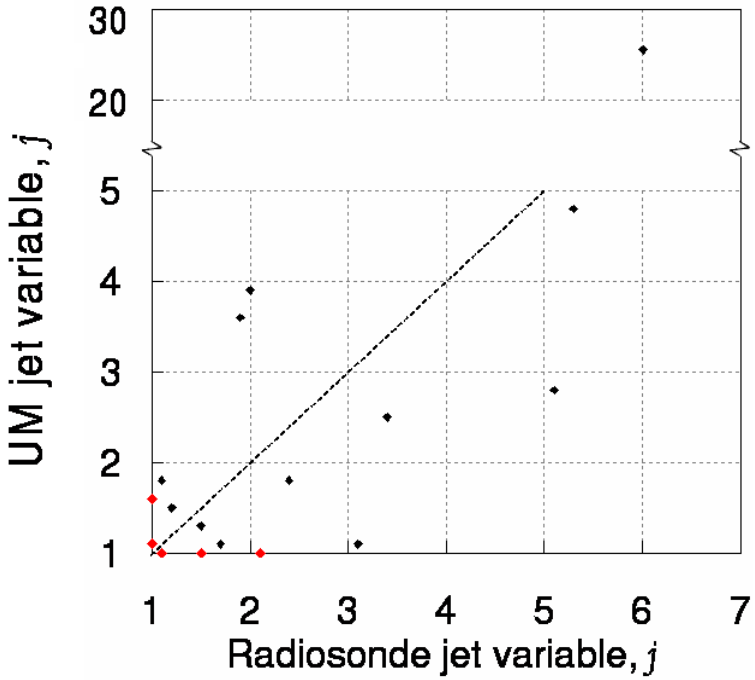

Figure 3·17 – *Jet strength variable comparison between UM and radiosonde for 17 clear-sky occasions at Cardington and Chilbolton in the summers of 2004 and 2005.*

The largest error in *j* was for case 3 ($j_{UM} = 25.1$). On this occasion the jet's wind-speed was accurately simulated (an absolute error of 0.7 m s^{-1}). The reason for the huge difference in *j* values is that above the jet, at around 700 – 800 m, the wind speed reduced to 1.5 m s^{-1} in the radiosonde profile, but the UM simulated a reduction to 0.3 m s^{-1}. Hence, the relatively small absolute error in wind speeds above the jet led to a large error in *j*.

The wind speed shear magnitude was underestimated for much of the altitudes below $\sim 350\,\mathrm{m}$ by up to $60\,\%$, or $0.11\,(\mathrm{m\,s^{-1}})\mathrm{m^{-1}}$ (Figure 3·18). This is consistent with jets that are simulated too weakly in the UM. In the altitude range of $350-750\,\mathrm{m}$ the confidence intervals indicated no consistent error bias in the UM data. Above $\sim 750\,\mathrm{m}$, there was too much wind-speed shear in the UM, but by a smaller amount than the underestimate at low levels.

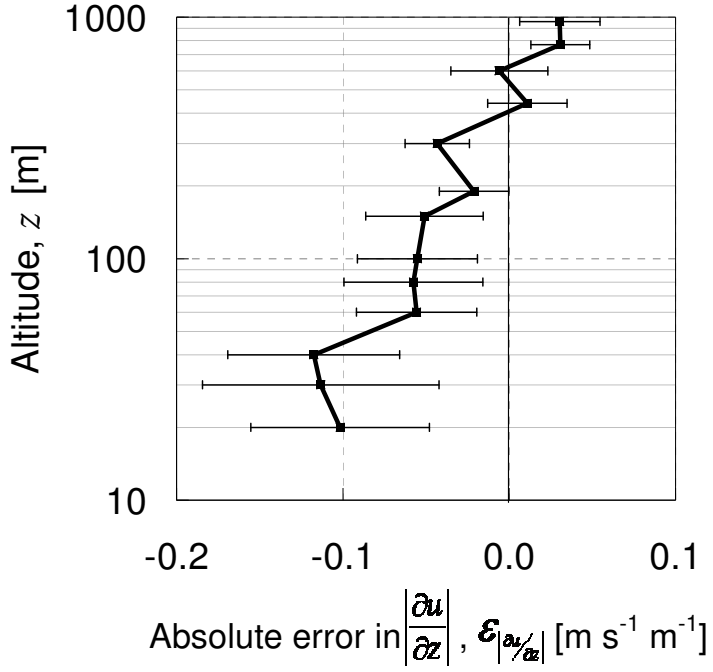

Figure 3·18 – *Mean profile of absolute error in UM wind speed shear magnitude, compared with radiosonde data. Horizontal bars show the 95 % confidence interval.*

The confidence intervals for wind direction (Figure 3·19) were large, with values of $7-25°$. Furthermore most of these confidence intervals encompass the zero error line, so there is no significantly consistent bias for most of the profile: except above 350 m and below 25 m. There is a notable shift in the error from $200-300\,\mathrm{m}$ (from a minimum to maximum mean error). The shift corresponds to the altitude below which most of the jets occurred. Overall the mean values show that the UM wind direction is backed* compared to the radiosonde with a mean of $8-21°$.

* Backed wind, anticlockwise turn, is the opposite of veered wind, which is clockwise turn.

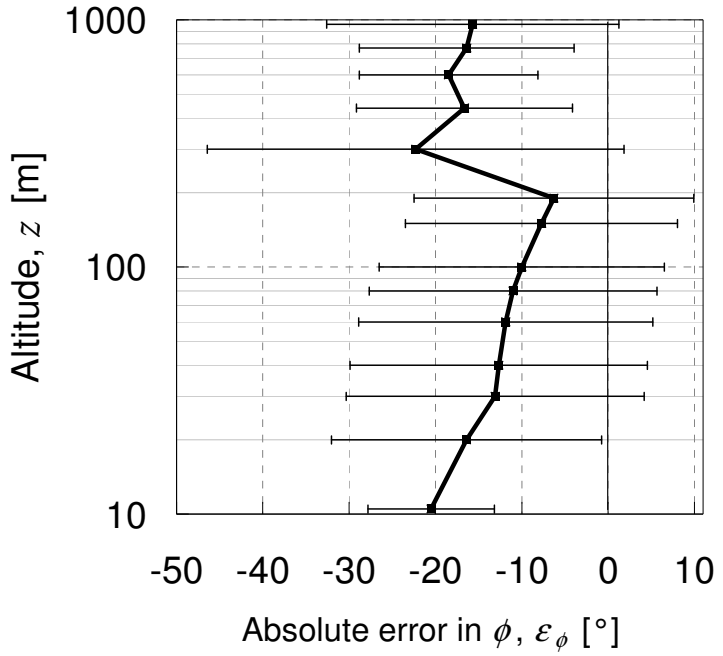

Figure 3·19 – *Mean profile of absolute error in UM wind direction, compared with radiosonde data. Horizontal bars show the 95 % confidence interval.*

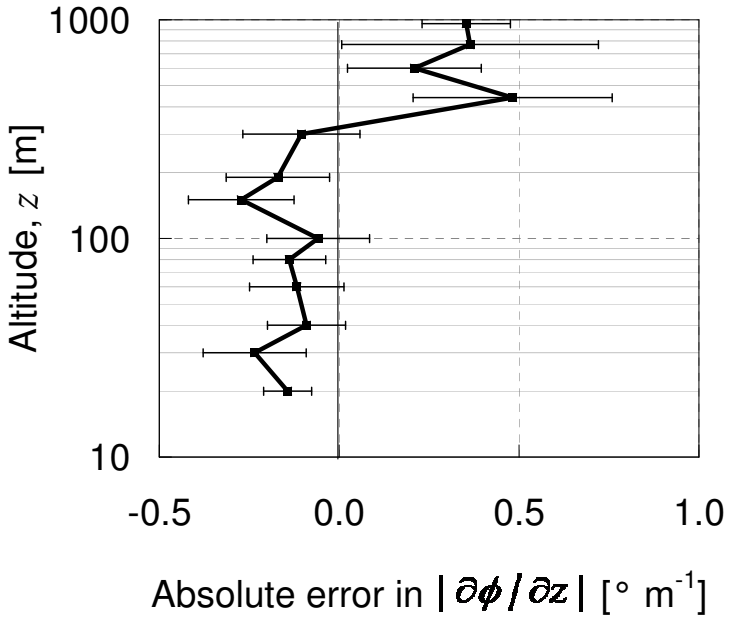

Figure 3·20 – *Mean profile of absolute error in UM wind direction shear, compared with radiosonde data. Horizontal bars show the 95 % confidence interval.*

Vertical shear of wind direction is important for identifying possible layering due to differential advection*. Below 300 m, the wind-direction shear is mostly underestimated in the UM (Figure 3·20). Above 300 m, the shear was mostly over-estimated in the UM: mean values were up to a factor of 4.3 in error. The changes in error occurred across $200-400$ m in both wind direction and its shear.

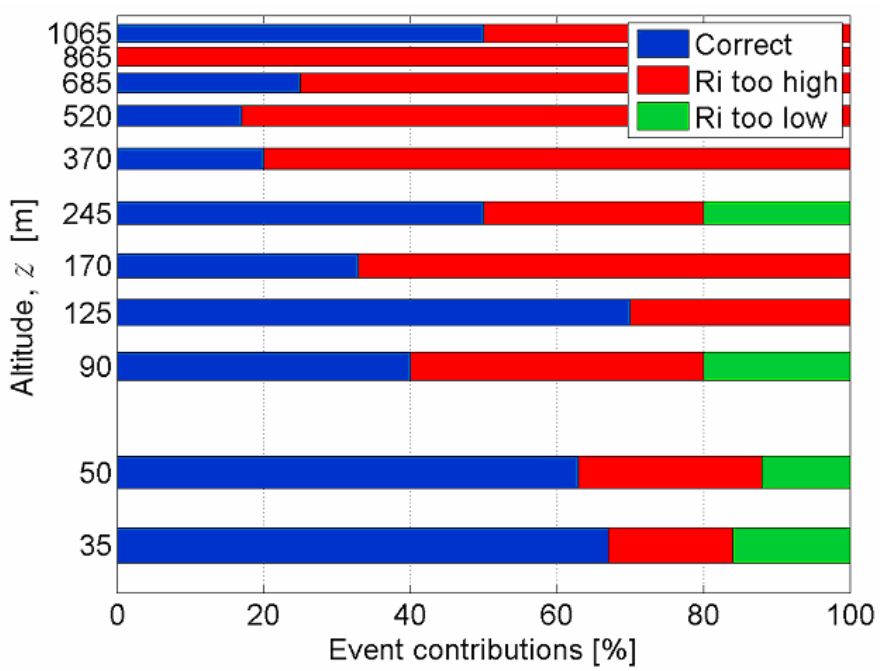

Figure 3·21 – *Absolute error in UM Ri, compared with radiosonde data. 'Correct' is where both UM and radiosonde data are above or below Ri = 0.25, 'Ri too high' is where Ri(UM) > 0.25 whilst Ri(sonde) < 0.25; 'Ri too low' is where Ri(UM) < 0.25 whilst Ri(sonde) > 0.25. Altitude is metres above ground level (a.g.l.).*

The ratio of the gradient of potential temperature to the square of the wind-speed gradient is the basis of the dynamic-stability variable, Richardson number Ri (§1·4·6). The error in these gradients has led to large errors in Ri above 300 m. Using $Ri = 0.25$ as the threshold (§1·4·6), the cases were grouped for their performance in predicting $Ri > 0.25$ (non-turbulent), or $Ri < 0.25$ (turbulent flow). Below 300 m, the regime of Ri was correctly predicted for $35-70$ % of cases. However, above 300 m, the UM over-predicts Ri on $50-100$ % of occasions. In general, the UM profiles indicated higher Ri (less turbulent flow) than was diagnosed from the radiosonde profiles. This was probably due to the weak jets in

* The process of layering of material (*e.g.* pollution) caused by shear in wind direction, which implies that air at different altitudes originated from different sources.

the UM caused by a smoother profile of wind speed (recall that *Ri* is inversely proportional to the square of wind speed shear).

Humidity

The UM underestimated both specific and relative humidity below 250 m (figure 3·22, figure 3·23): the mean of the absolute error was up to a 10 % underestimate in RH and up to a mean of 0.6 g kg^{-1} in q. The low relative humidity is consistent with the overestimation of temperatures near to the surface (see Figure 3·4). The overestimate at upper levels was observed above 250 m, with mean $RH < 5\,\%$ and $q < 0.4$ g kg^{-1}; this did not represent a significant bias (since the confidence intervals encompassed the zero error line).

The correlation coefficients between UM and radiosonde data were $r = 0.72$ and $r = 0.44$ for specific and relative humidity respectively.

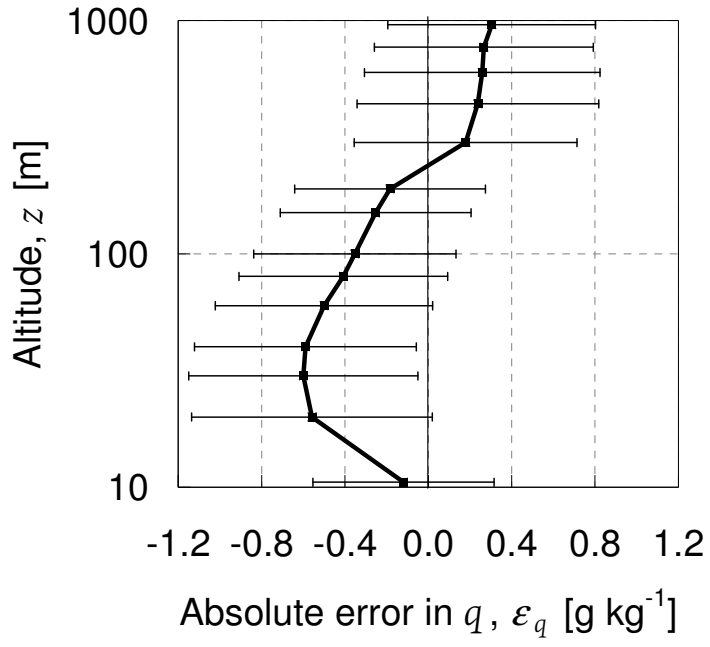

Figure 3·22 – *Mean profile of absolute error in UM specific humidity, compared with radiosonde data. Horizontal bars show the 95 % confidence interval.*

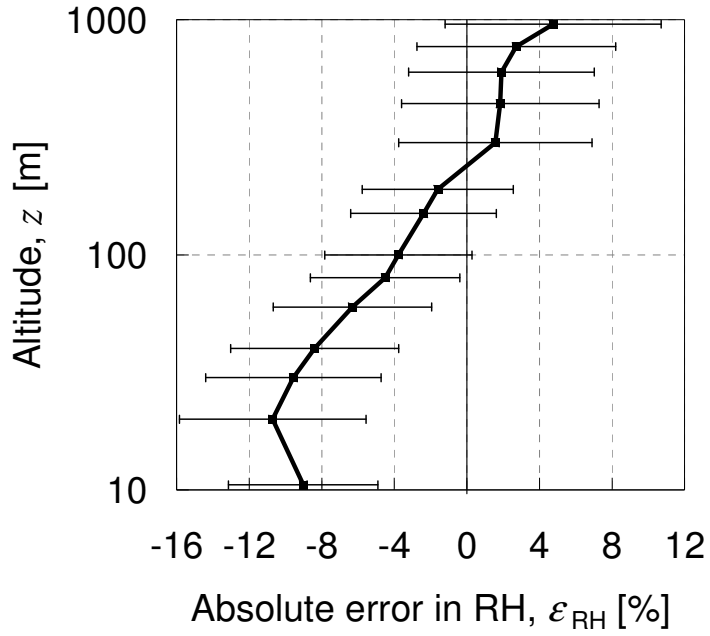

Figure 3·23 – *Mean profile of absolute error in UM relative humidity, compared with radiosonde data. Horizontal bars show the 95 % confidence interval.*

3·4 Discussion

The primary aim of this chapter has been to introduce and to assess the accuracy of the nocturnal meteorological data obtained from the UM. It is worth stating at the outset that there are some limitations with the results obtained in this chapter. Firstly, the 17 radiosondes were all released after implementation of the UM's 'new dynamics' scheme. Hence, these results are perhaps less relevant to the UM data prior to the change in summer 2002. Furthermore, the locations of validations were not the same as where the radars are located: hence there might be site-specific biases which cannot be assessed. In §1·4·8, it was noted that slopes of just 0.1–1% can create drainage currents, and therefore, the orography around both sites are susceptible to these. Consequently, the radiosonde profiles within 10s of metres of the surface might contain very localised meteorological features, whereas the UM profiles are more representative of the area as a whole. Regardless, local effects (topography and land-use) create differences in profiles primarily at low-levels (*e.g.* 10s of metres). It is likely that at the altitudes of the critical region (200–500 m), the effects of local features are unimportant, since katabatic flows are typically in the range of dozens of metres deep and not

hundreds. Finally it is worth noting that even small errors in the timing of features in the nocturnal UM might have resulted in errors in some variables. Many variables change rapidly around dusk and a single radiosonde profile is not adequate to inform whether errors are due to timing effects rather than an actual error in a given quantity. In particular, much research has been done on the nocturnal transition and it seems that the parametrizations in the UM are known to incorrectly simulate the transition. Hence, it is no surprise that for the profiles of the two radiosondes released closest in time to sunset (11 and 13 minutes after sunset), the UM failed to simulate the inversions seen in the radiosonde data.

It is worth noting that because the insect-monitoring radars' range gates start at $\sim 180\,\mathrm{m}$, the performance of the UM below $180\,\mathrm{m}$ is not of great concern. The critical region for nocturnal insect layering (identified in §2·4), means that there is particular interest in the accuracy of the UM in the first few hours after dusk and at $200-500\,\mathrm{m}$ a.g.l. The mean critical region errors are shown in Table 3·3. This chapter has indicated that the UM is a good proxy for real data for the variables most cited in the literature as explanatory variables for insect layering, *i.e.* temperature and wind speed. Furthermore, for most of the variables there are no significant biases from zero in the mean error—except for the temperature gradients: $\partial\theta/\partial z$ was too positive and $\partial T/\partial z$ was too negative.

Table 3·3 – *Mean absolute errors in the UM variables in the critical region (note that jet intensity, j, is not a critical region variable – but is a ratio from jet max to an upper level minimum wind speed). The confidence intervals (C.I.) are shown: hence, biases that are significantly positive or negative (at the 95 % level) are indicated with (*), all other differences are insignificant.*

	Wind speed, u [m s^{-1}]	Temperature, T [°C]	Relative humidity, RH [%]	Specific humidity, q [g kg^{-1}]	Potential temperature gradient, $\partial\theta/\partial z$ [K m^{-1}]	Magnitude of vertical shear of wind speed, $\lvert\partial u/\partial z\rvert$ [(m s^{-1})m^{-1}]	Jet intensity, j	Magnitude of vertical shear of wind direction, $\lvert\partial(\phi)/\partial z\rvert$ [° m^{-1}]	Wind direction, ϕ [°]	Temperature gradient, $\partial T/\partial z$ [K m^{-1}]
Mean	-0.1	-0.2	0.9	0.1	0.04*	-0.01	1.1	0.10	-16	-0.04*
C.I.	1.0	0.4	8.1	0.6	0.03	0.03	1.9	0.29	16	0.03

Above 100 m, all mean temperature errors were $< 0.5\,°C$. Below 100 m, the mean error was up to $1.7\,°C$ over-estimate. This over-estimate suggests that the cooling at the ground was not as strong in the UM as the radiosonde data showed. The overly warm surface was also seen in a longer-term study at Cardington, particularly during the nocturnal transition (Edwards *et al.* 2006). In this chapter, surface-based inversions were diagnosed accurately, but with a tendency for UM simulation of an inversion that was too shallow, which also agrees with Edwards *et al.* (2006). Results in this thesis showed that the $\partial T/\partial z$ gradients below 100 m in the UM data were more positive than those in radiosonde data, which agrees with the result that near-surface air temperatures were too warm in the UM data.

For wind speed, an error of $\pm 0.5\,m\,s^{-1}$ was seen throughout the mean profile with a mean relative error of 6.4 % in the critical region. Edwards *et al.* (2006) found that surface wind speed was too strongly simulated in the UM, contrary to the results found here. The jet altitudes were accurately diagnosed, but the jet maximum speed was often under-estimated in the UM, giving smoother profiles of wind speed. This is consistent with other studies (Lock *et al.* 2003). The wind direction showed a consistent backing in the UM data, by 16° in the critical region. Assuming a constant wind speed of 8 m s^{-1} and 4 hours flight, this error could give an error in backtracked source areas of 33 km. However, the confidence intervals for both wind speed and direction revealed that there was no significant bias (Table 3·3).

The humidity variables showed a small error: too dry below 100 m and too moist above 500 m. The humidity showed greatest accuracy over the critical region. It is worth noting that these discrepancies in humidity might have impacted upon the radiation scheme in the UM, because the effect of longwave radiative emission is sensitive to the amount of moisture in the atmosphere (since there is absorption of longwave radiation by water molecules). Accordingly, the observed temperature errors might have been caused by inaccuracies in the radiative parametrization.

Difficulties in error analysis arose. Firstly, when gradients near zero (such as potential temperature throughout the residual layer), smaller absolute errors can give apparently large relative errors. Secondly, vertical variation in the gradients can be large (*e.g.* across features such as inversion and jet altitude) and hence smaller errors in misdiagnosing jet and inversion altitudes can result in apparently large errors in the gradient variables. Finally, the UM resolution is coarser than the radiosonde resolution, and the coarse resolution might be acting like a low-pass filter, resulting in less pronounced features.

Potential temperature gradients in the critical region were too positive in the UM, leading to an overestimation of the static stability. The gradients in wind speed were often underestimated, but more accurate near the critical region. Wind direction shear was underestimated at lower altitudes and overestimated at higher altitudes. Combination of these variables indicated that Richardson number was too positive, indicating flow that was too laminar (though prediction was more accurate near to the surface).

* * * * *

The sources of data discussed in this chapter will be used in subsequent chapters of this thesis. The radiosonde data can be used for specific occasions; but the UM data will be more useful for case studies (Chapter 4), statistical analysis of layer initiation (Chapter 5), and in the trajectory modelling (Chapter 6). Finally, in Chapter 4, the NAME trajectories will be used to estimate source areas for the migrant insects on particular layering occasions.

4: Case studies

The majority of work in this chapter has been published through the peer-review process in the *International Journal of Biometeorology* (Wood *et al.* 2006). In that paper, I carried out all analyses except the figure on the common orientation phenomenon (Figure 4·9).

4·1 Introduction

The factors influencing the formation of insect layers were reviewed in Chapter 1. In the current chapter, analyses are carried out on case studies of nocturnal insect layers in the UK by comparing radar measurements of the vertical distribution of insect density (Chapter 2) with meteorological profiles generated by the UK Met Office's mesoscale Unified Model (UM, see Chapter 3). Radar-derived measurements of insect mass and displacement speed, along with data from Rothamsted Insect Survey (RIS) light-traps (Bredon Hill and Hereford) provided evidence on the likely identity of the macro moth species involved in the migrations (Chapter 2).

The key objective of the current chapter is to present case studies where meteorology apparently has an effect on nocturnal insect layering in the UK: an area virtually unstudied by entomological radar techniques and previously suspected to be climatically marginal for night-time migrations. Additionally, this chapter highlights that the relatively new insect-monitoring radars can be analysed alongside outputs from numerical weather prediction models (in this case the Unified Model, see Chapter 3) to investigate case studies in detail. Subsequently, a generalised approach is taken in Chapter 5 of several years' data.

4·2 Results

Three case studies of nocturnal layering events were selected from the entire radar data-set using the Quickview database (Chapter 2). Cases were chosen based on the presence of well defined and persistent insect layers, which occurred

during stable atmospheric conditions: specifically, high atmospheric pressure with largely clear skies.

4·2·1 Case study A: 22–23 August 2000

The evolution of the vertical profile of insect aerial density throughout the evening and night of 22–23 August at Malvern (Figure 4·1) includes only insects above 10 mg in mass (to ensure detection of insects up to 1 km above ground level (a.g.l.)). The figure shows a dusk take-off underway by about 19:30 hours UTC, with aerial densities up to 100 insects per 10^7 m^3. A distinct layer in the vertical profile of insects had formed by 21:00 at about 400 m a.g.l. The layer centre decreased in altitude by about 70 m from 23:00 to 01:00, after which the layer dissipated, and aerial densities then remained low for the rest of the night. Maximum densities recorded within the layer were ~ 100 insects per 10^7 m^3, and layer depth (defined using the 25 insects per 10^7 m^3 contour) varied between 250 and 400 m.

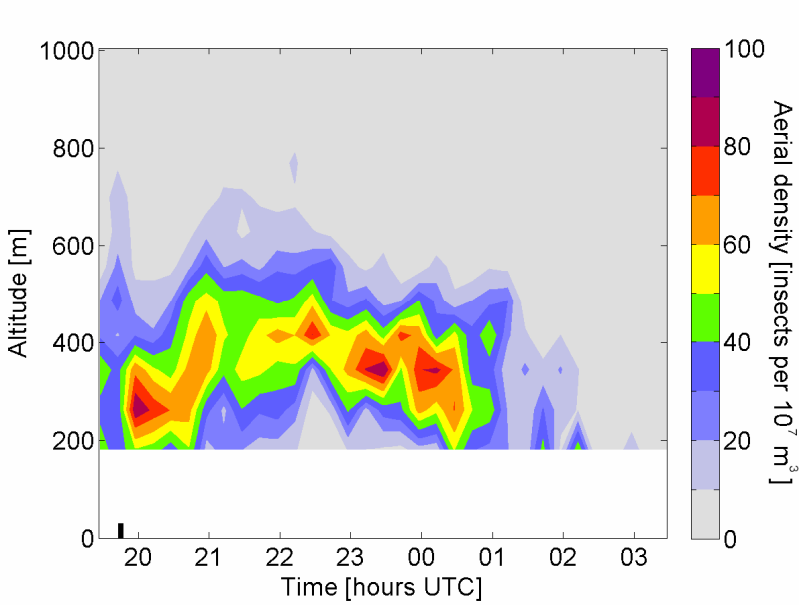

Figure 4·1 – *Evolution of insect aerial density (numbers per 10^7 m^3) with altitude and time for the night of 22–23 August 2000 at Malvern. Only insects with mass 10 mg or greater have been included. Sunset was at 19:18 hours UTC, and the end of dusk is represented by a marker on the time axis at 19:48.*

It is highly likely that the insects forming the layer took off at dusk and that no further significant take-off of insects occurred later in the night. Therefore, the insects observed at Malvern at 01:00 had probably been flying for about 5 hours.

Back-trajectory analysis using NAME (§3·2·3) revealed that a parcel of air at 300 m over Malvern at 01:00 would have been located around 150 km to the east at 20:00 (Figure 4·2, trajectory A). An additional component of ~ 3.5 m s^{-1} (taken from Lingren *et al.* (1995) for *Heliocoverpa zea*) representing the self-powered flight speed of the migrants can be added to the wind speed to estimate net speed relative to the ground. Thus, the insects may have travelled a further 63 km between 20:00 and 01:00, giving a total estimated migration distance of around 213 km. This almost corresponds to the distance to the east England coast, and the lack of further sources beyond this point may explain the sudden decline in insect numbers at 01:00. The maintenance of high insect numbers before 01:00 also suggests widespread source locations of the insect species concerned.

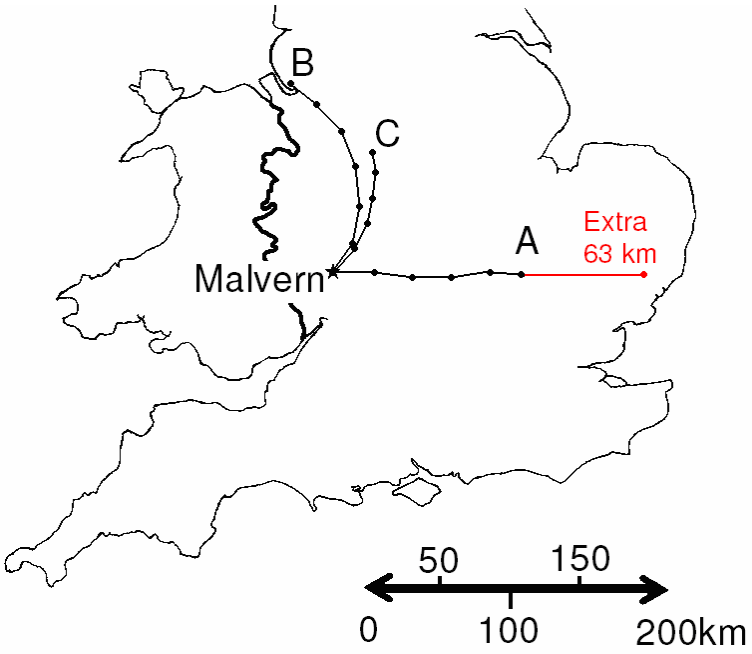

Figure 4·2 – *Back trajectories calculated for an air parcel located near the insect layer altitude (300 m a.g.l.) and crossing the Malvern site at the time of layer termination. The trajectories show the presumed origin of the air parcel at 20:00 UTC. (A) 22–23 August 2000, (B) 14–15 August 2003, (C) 23–24 August 2003. Most trajectories probably under estimate insect displacement, e.g. for case A, an additional distance is sketched to indicate the likely extra distance covered when including insect flight speed.*

The meteorological data generated from the UM at Malvern showed that a surface temperature inversion was present from 21:00 to 04:00 on 22–23 August (Figure 4·3). The top of the inversion (*i.e.* altitude of maximum temperature, depicted by the magenta line) was located near 300 m agl and showed a slight tendency to rise in altitude until 01:00. The temperature maximum decreased

from 16 to 14 °C between 21:00 and 01:00. For much of the night the centre of the insect layer was located ~ 50 m above the maximum temperature, implying that most insects were experiencing temperatures of at least 14 °C.

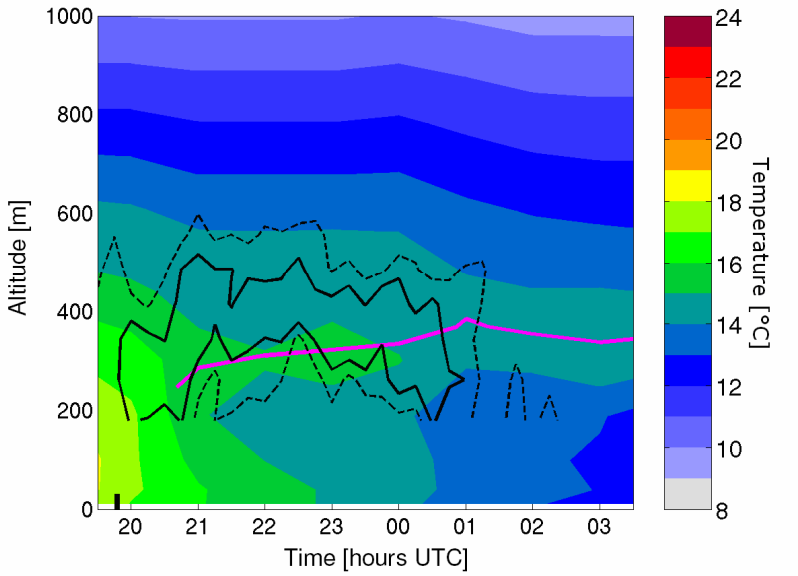

Figure 4·3 – *Evolution of temperature (°C) with altitude and time for the night of 22–23 August 2000 at Malvern. The magenta coloured line marks the top of the temperature inversion. Superimposed are the insect aerial density contours from Fig. 1 for 25 (– –) and 50 (—) insects per* 10^7 m^3.

The upper boundary of the insect layer, located at around 500–550 m, coincided approximately with the 14 °C isotherm throughout (see dashed line denoting the 25 insects per 10^7 m^3 contour in Figure 4·3). This may imply that the layer is a 'ceiling layer' with a threshold of minimum temperature for flight near 14 °C. However, as the threshold for sustained flight in at least some British noctuids is lower than 14 °C (*e.g.* 10.5 °C in the mouse moth, *Amphipyra tragopoginis*: Taylor and Carter 1961), the observed upper extent of the layer may be indicative of a preferred temperature rather than an absolute physiological threshold.

Both relative humidity, RH (Figure 4·4) and wind-speed shear featured high gradients near the altitude of 200 m throughout the migration period (the wind speed shear can be seen below the jet centre from 21:00–23:30 in Figure 4·5). The insect layer was located in a layer of less humid air (< 65 % RH), with higher values (up to 80 % RH) above and below the layer. These gradients are associated

with the NBL top (Garratt 1994) which indicates that migration was occurring in the residual layer above.

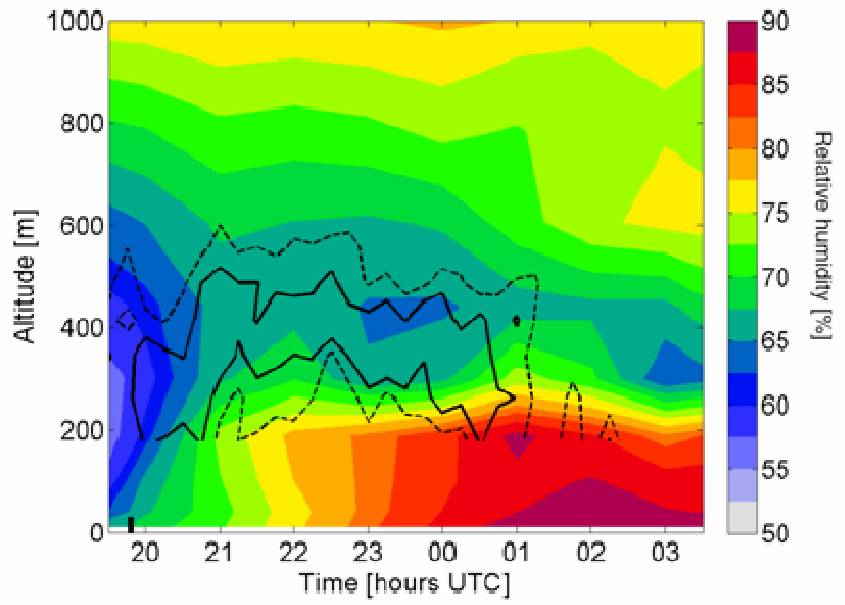

Figure 4·4 – *Evolution of relative humidity (%) with altitude and time for the night of 22–23 August 2000 at Malvern. Superimposed are the insect aerial density contours* from *Figure 4·1 for 25 (– –) and 50 (—) insects per* 10^7 m^3.

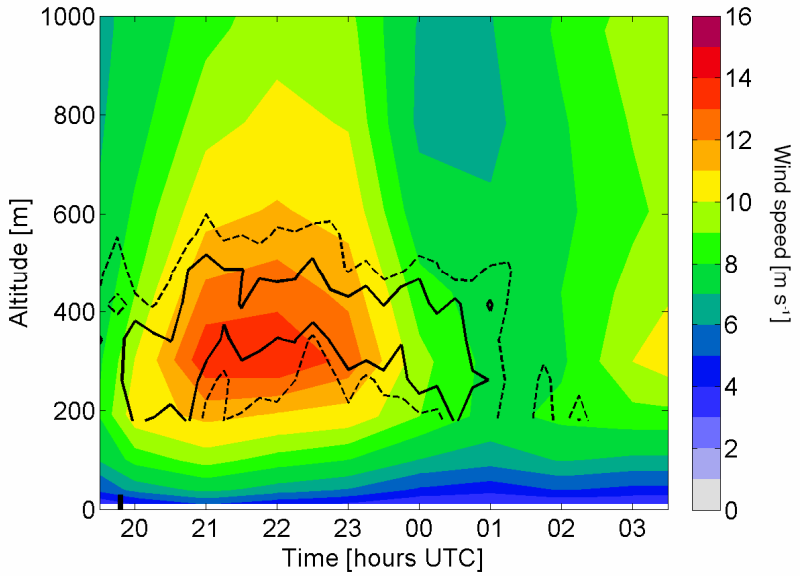

Figure 4·5 – *Evolution of wind speed (m* s^{-1}*) with altitude and time for the night of 22–23 August 2000 at Malvern. Superimposed are the insect aerial density contours from Fig.1 for 25 (– –) and 50 (—) insects per* 10^7 m^3.

UM data showed that a nocturnal jet formed from 20:00 to 00:00 (Figure 4·5). The wind speed maximum occurred at about 300 m, and was most intense (14 m s^{-1}) between 21:00 and 22:00. Radio-soundings at Herstmonceux, East Sussex (00:00)

and Larkhill, Wiltshire (06:00) also provided evidence for a jet, again with the strongest wind speeds ($14\,m\,s^{-1}$) at about 300 m. The centre of the insect layer observed at Malvern apparently remained no more than 50 m above the jet centre (Figure 4·5) and hence typical wind speeds experienced by the insects would have been $12-13\,m\,s^{-1}$.

The mean of the net speeds of insect flight relative to the ground recorded by the radar is shown in Figure 4·6. The highest radar-derived displacement speeds within the layer ($18-20\,m\,s^{-1}$) occurred between 21:00 and 22:00, *i.e.* they corresponded approximately to the maximum speeds in the nocturnal wind jet: the jet centre was around 50–100 m below the layer centre. However, Chapter 3 analyses revealed mean errors of 80 m in jet height, so given that fact—along with the radar's finite resolution (caused by range gate data)—one cannot make strong inferences about the fact that the altitudes of jet and layer centres are not perfectly coincident.

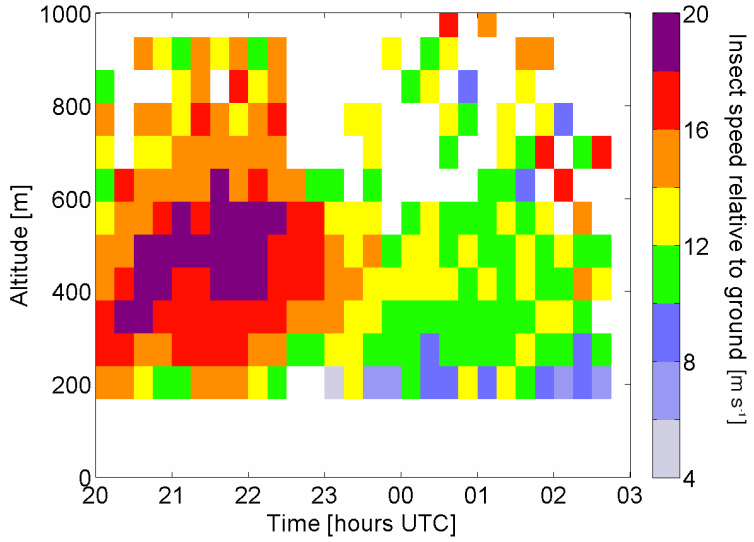

Figure 4·6 – *Evolution of insect speed relative to the ground ($m\,s^{-1}$) with altitude and time, on the night of 22–23 August 2000 at Malvern.*

Scalar subtraction of UM wind speeds from the radar-derived speed relative to ground can give an estimate of the insect flight speed (Figure 4·7). The flight speed largest groups were for $3.5-4.5\,m\,s^{-1}$ (Figure 4·8); these derived speeds are consistent with noctuid moth flight speed measurements. *Helicoverpa zea*, for

example, have mean flight speeds of 3.5 ± 0.3 m s^{-1} (± standard error); extremes were 0.4 m s^{-1} and 8.2 m s^{-1} (Lingren *et al.* 1995). However, some of the inferred insect speeds are probably incorrect (shown by the darker orange and blue colours). The most consistent error was from 20:00–22:00 (around 400–700 m a.g.l.), where the inferred speeds of 6 – 10 m s^{-1} are almost certainly too high for insects, and certainly so for the likely species migrating on this night. This indicates that the UM wind speeds were too slow both before the time of greatest speeds in the jet, and above the centre of the jet, by up to 4 m s^{-1} on this occasion. Analysis in Chapter 3 (Figure 3·12) suggested that the UM can under-predict the maximum jet speeds; mean error was an underestimation of 1.4 m s^{-1}, though there was an occasion where an underestimation of 5 m s^{-1} occurred (Figure 3·12). Hence, the suggestion of UM error of 4 m s^{-1} is probable. It is also possible that the error was contributed to by an error in jet altitude and the 1-hour time resolution of the UM, which might not have been adequate to capture the atmospheric conditions associated with the rapidly developing nocturnal jet.

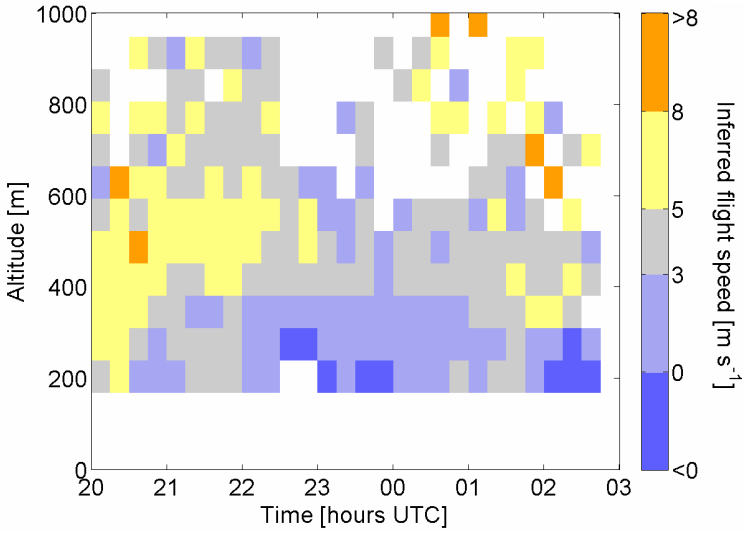

Figure 4·7 – *Evolution of inferred insect flight speed (i.e. relative to ground speed minus modelled wind speeds) (m s^{-1}) with altitude and time, on the night of 22–23 August 2000 at Malvern. Dark colours (orange and blue) represent values that are unrealistic for noctuid moths. The values represented by grey are consistent with noctuid moths, while the lighter shading is probably noctuid moths (yellow and cyan).*

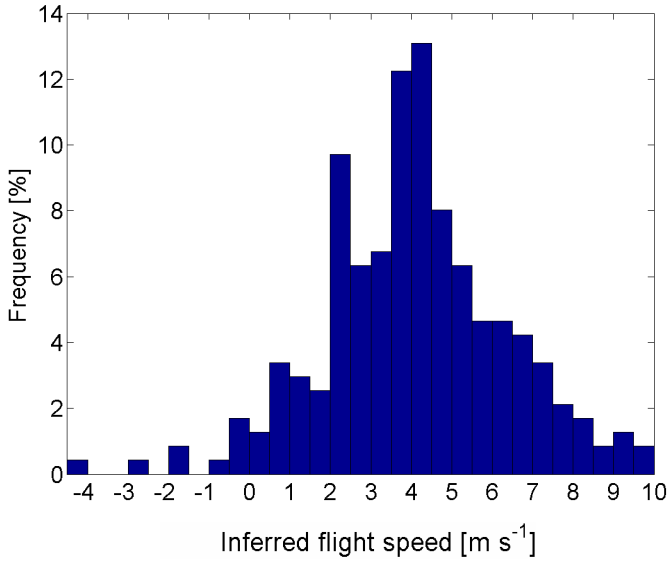

Figure 4·8 – *Frequency histogram of mean insect speeds in each radar range-gate, from data in Figure 4·7.*

The few regions of negative inferred insect speed (particularly around 22:30–00:00 in range gates 1 and 2) seem unlikely to be caused by insects flying upwind. Probably, either the UM over-predicted the winds by ~ 4 m s^{-1} (most likely), or radar calculations of the net speed relative to ground were incorrect. Perhaps the low numbers of insects at that time gave a small sample size that thence gave less reliable radar-derived displacement speeds. It is also worth noting that it is likely that not all the radar-observed fauna are noctuids.

Radar measurements of body alignment for insects in the layer showed evidence of the common orientation phenomenon (Riley and Reynolds 1986, Riley 1989) (see Figure 4·9). The analysis in Figure 4·9 was conducted in Wood *et al.* (2006) by a co-author using a method in Mardia (1972) for calculating circular standard deviations, the results are analysed here. There is a 180° ambiguity in the actual insect headings, but consideration of the insects' displacement vectors and flight speed make it clear that the mean orientation of bodies was towards the WSW. The mean orientation angle of 1,062 targets (14.9 % of targets) was 245° with a circular standard deviation (CSD) of 31°. The mean displacement direction was towards 263° (CSD = 26°) so that the insects were orientating at an angle slightly anti-clockwise from the downwind direction. Although there was evolution of the wind direction with time (Figure 4·10), the general pattern in the UM data was

that the wind direction veered with altitude from 50° near the surface through ~ 70° at jet altitude to 100° above 1 km (and 100° as low as 300 m after 00:30).

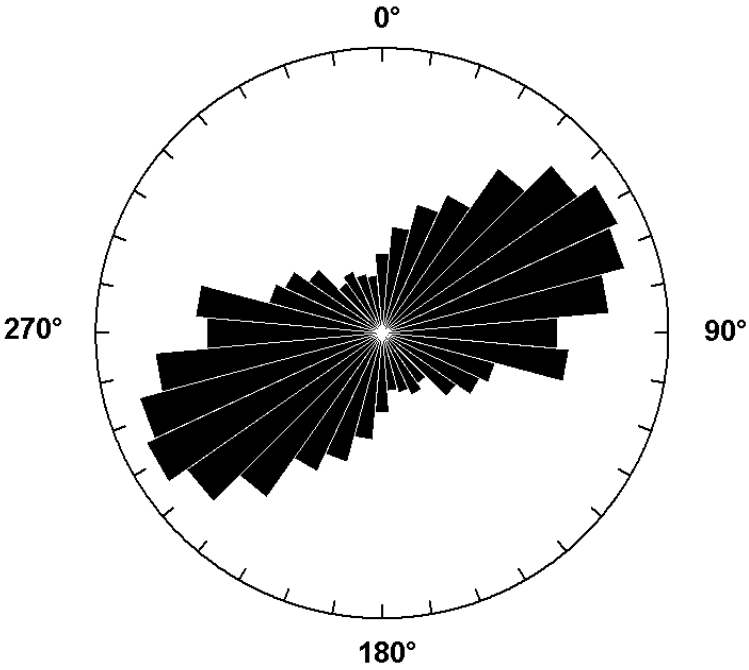

Figure 4·9 – *Equi-areal plot showing distribution of body alignments for insects flying in the layer in range-gates 3–5 at 290–480 m above ground from 21:00–01:00 hours UTC on 22–23 August 2000. 14.9 % of the targets were aligned along 60–240° axis. From Wood et al. (2006).*

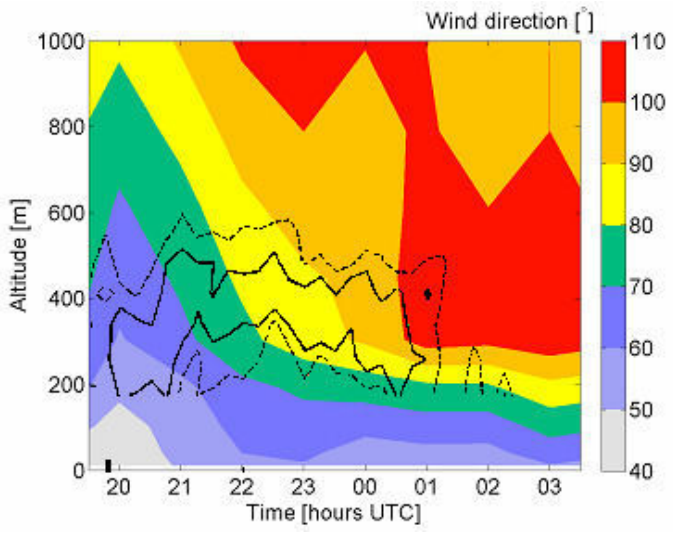

Figure 4·10 – *Evolution of wind direction (°) with altitude and time for the night of 22–23 August 2000 at Malvern. Wind direction is defined as the direction from which the wind blows.*

The radar-estimated masses of insects in the layer provide an aid to identification (Figure 4·11). The insect mass distribution remained almost unchanged throughout the duration of the layer (Figure 4·12): various sizes of insect were

present, but a large peak (comprising 35 % of the insects) occurred in the 80–160 mg group. Medium-sized noctuid moths are the most likely component of the nocturnally migrant insect fauna in this size range. The catch from the nearest RIS light trap to the Malvern radar—Bredon Hill, Worcestershire (20 km east of the radar)—was examined*. Analysis showed that the most common species of noctuid moths caught on this night were *Xestia c-nigrum* (setaceous Hebrew character) *Diarsia rubi* (small square-spot), *Mythimna pallens* (common wainscot), *Ochropleura plecta* (flame shoulder), *Luperina testacea* (flounced rustic), and *Autographa gamma* (silver Y). There is some evidence for windborne migration in *X. c-nigrum* and *M. pallens* (Reynolds *et al.* 2005). *A. gamma* is a well-known migrant (Taylor *et al.* 1973) and indeed it has been caught during high-altitude aerial samples (see Chapter 2): its mean mass (146 mg; n = 11) places it within the 80–160 mg peak observed for the insects forming the layer.

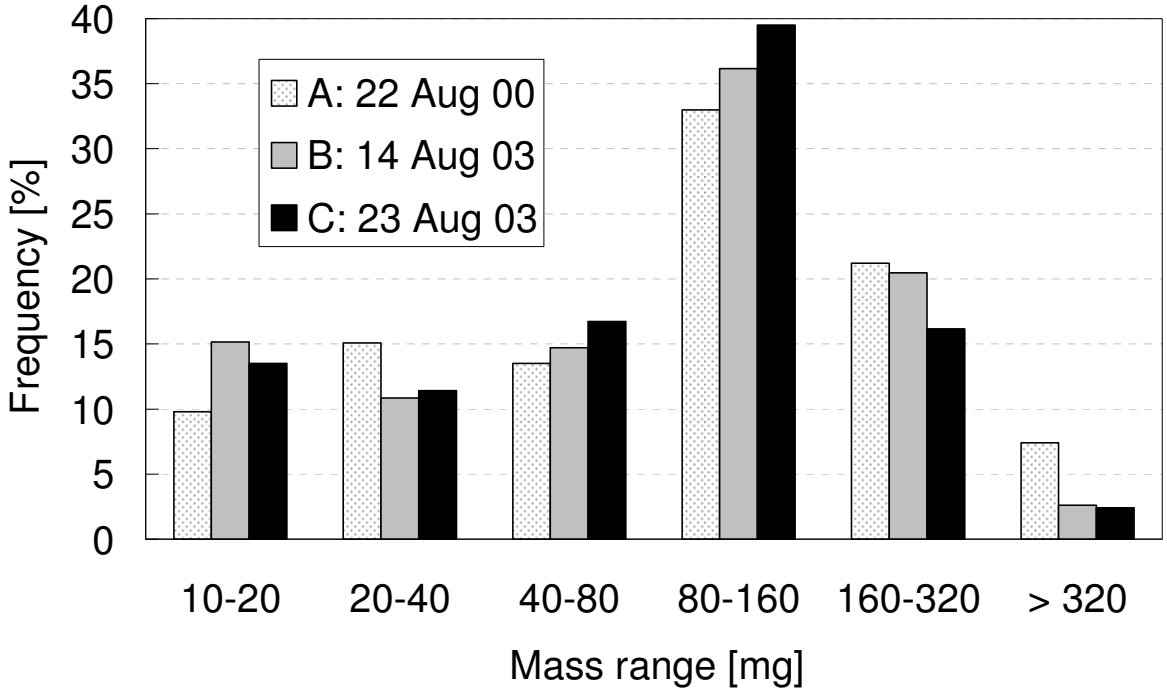

Figure 4·11 – *Mass distributions of insects in range-gates 2–5 inclusive at Malvern. (A) 20:00–01:00 hours UTC on 22–23 August 2000 (B) 21:00–01:00 on 14–15 August 2003 and (C) 21:00–01:00 on 23–24 August 2003. Only insects of mass 10 mg or greater have been included.*

* Rothamsted insect survey personnel sorted and identified the trap catches. The work of this thesis was to analyse the results of this identification.

The mass distribution was analysed at the start and end of the layering event (Figure 4·12). There was little change in the distribution, which suggests that the composition of the aerial fauna flying throughout the layering event remained the same.

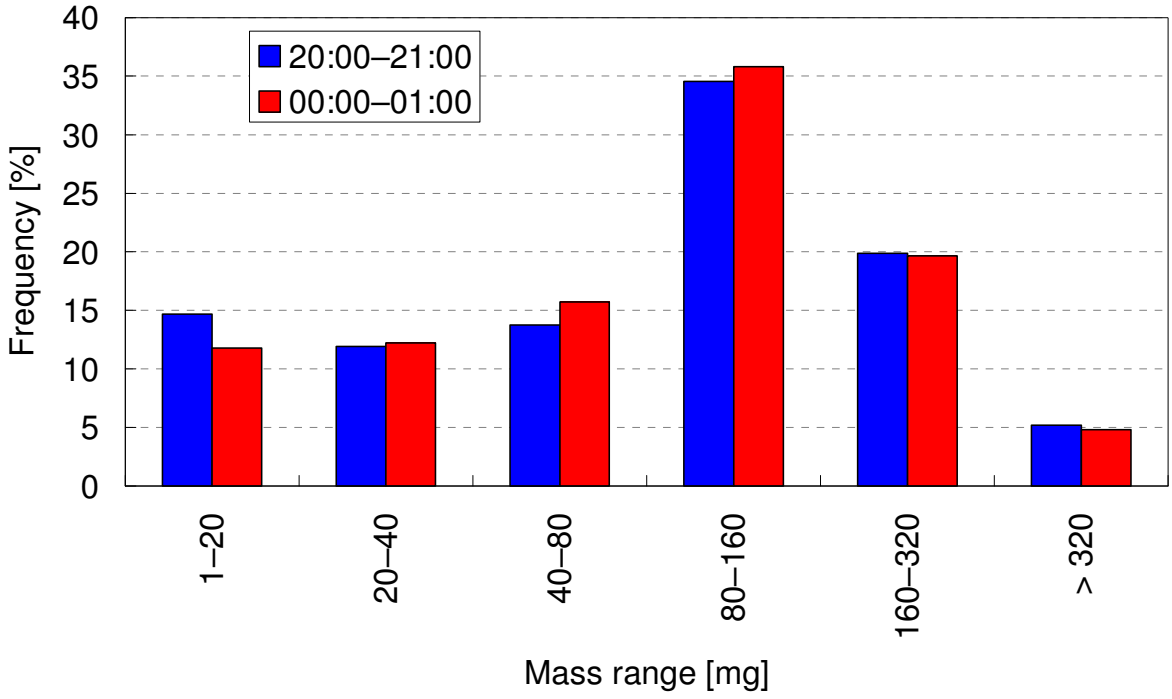

Figure 4·12 – *Mass distributions of insects in range-gates 2–5 inclusive at Malvern for case A (22 August 2000). Shown are distributions for the start of the layering event (20:00–21:00) and the end of the layering events (00:00–01:00).*

4·2·2 Case study B: 14–15 August 2003

The evolution of the vertical profile of insect aerial density throughout the evening and night of 14–15 August 2003 at Malvern is shown in Figure 4·13. Dusk take-off lasted until 20:45, and a distinct layer had formed by 21:30 at about $200-450$ m a.g.l. The layer rose in altitude until 23:30 when it was located at $300-500$ m, and then it decreased with altitude until 01:45, after which time the layer dissipated. Maximum densities of ~ 100 insects per 10^7 m^3 were recorded in the dusk emigration peak, but densities were always lower than 65 insects per 10^7 m^3 within the layer. Density values were thus less than in the layer described in case study A above. Layer depth—defined by the 25 insects per 10^7 m^3

contour—varied from < 70 m up to 200 m. The duration of migration is likely to have been about five hours (20:30 and 01:30).

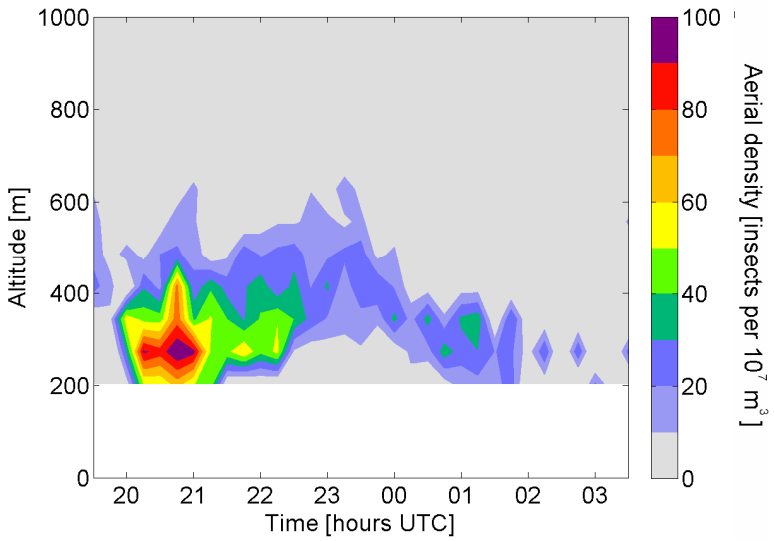

Figure 4·13 – *Evolution of insect aerial density (numbers per 10^7 m^3) with altitude and time for the night of 14–15 August 2003 at Malvern. Only insects with mass 10 mg or greater have been included. Sunset was at 19:36 hours UTC, and the end of dusk at 20:06.*

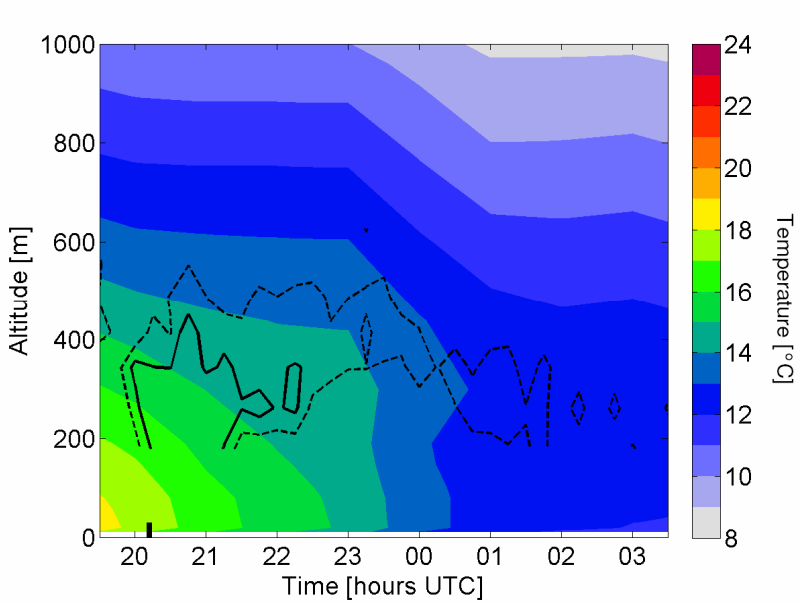

Figure 4·14 – *Evolution of temperature (°C) with altitude and time, on the night of 14–15 August 2003 at Malvern. Superimposed are the insect aerial density contours of 25 (– –) and 50 (—) insects per 10^7 m^3 as detected by the Malvern radar. Sunset was at 19:36 hours UTC, and the end of dusk is represented by a marker on the time axis at 20:06.*

Back-trajectory analysis showed that a parcel of air moving at an altitude of 300 m and arriving at Malvern at 01:30, would have originated at around 130 km north of the radar site at 20:30 (Figure 4·2, trajectory B). The back-trajectory has a

curved shape due to a high-pressure system centred to the west of the UK. The insects forming the layer again showed a tendency to orientate downwind: the mean orientation angle was 207.5° (CSD = 29.5°, 642 targets) and the mean displacement direction was towards 205.5° (CSD = 26.9°). Therefore, taking into consideration am estimated component of 3.5 m s^{-1} for the insect flight speed (see case study A), the flight distance may have been up to 63 km greater giving a total estimated migration distance of around 193 km. The fact that the source area of insect take-off is estimated to be near the coast is again a possible reason for the layer dissipation seen at Malvern after 01:45.

The evolution of the temperature profile on the night of 14–15 August is shown in Figure 4·14. Before about 23:00, the warmest temperatures occur quite close to the surface (within the first 100 m), and radiosonde ascents indicated that the top of the inversion was located at relatively low altitude on this night (*e.g.* 175 m at Nottingham at midnight). Therefore, it seems clear that, in this case, the insects were not concentrated at the altitude of the warmest air. The temperature profile suggests that up until 23:30 most insects flew in air of 14–16 °C, with the upper layer boundary located in the 12–14 °C region, suggesting a minimum temperature preference or threshold for flight near 12 °C. The majority of insects flew in air of less than 75 % RH and there was a general increase of RH with time at all altitudes (not shown). Figure 4·15 shows that wind speeds of up to 10 m s^{-1} were present in a nocturnal jet from 21:00 to 23:00 at 200–300 m, but insects still flying after 01:00 may have experienced winds as low as 5 m s^{-1}. The insect layer appeared to be centred slightly above the wind jet in a region of negative wind shear (*i.e.* wind speed decreased with altitude). This is similar to the observations in case study A.

The insect mass distribution again showed a peak in the 80–160 mg group (Figure 4·11), and medium-sized noctuid moths are the most likely component of the nocturnally migrant insect fauna in this size range. Examination of the RIS catch from Bredon Hill showed the most common species of noctuid moth caught on this night were *X. c-nigrum*, *M. pallens*, *O. plecta*, and *Thalpophila matura* (straw

underwing). The highly migratory species, *A. gamma* (silver Y), was caught in the light-trap in the days before and after this layering event. Further evidence for mass migration of this species was the capture of specimens in a balloon-supported net at 200 m above Cardington airfield on the evenings of 19, 20, and 24 August 2003 (see §2·3·3). Although the noctuids may have constituted a large portion of the radar-detected insects, three migratory micro-moth species were also found in trap catches, namely: *Plutella xylostella* (diamondback moth) (Yponomeutidae), *Nomophila noctuella* (rush veneer), and *Udea ferrugalis* (rusty dot pearl) (both Pyralidae). *Plutella xylostella* is too small (1–4 mg) to have been easily detectable in the layer (Chapman *et al.* 2002a), but *N. noctuella* (16–25 mg) and *U. ferrugalis* (~ 10 mg) could have been among the smaller insects detected by the radar in the 10–40 mg size groups (Figure 4·11). Altogether, these findings imply that good numbers of moths were migrating, and indeed migrations in mid to late August are likely to involve southward return movements to over-wintering sites in several species. Certainly, the northerly winds recorded on this night would have aided such a migration strategy.

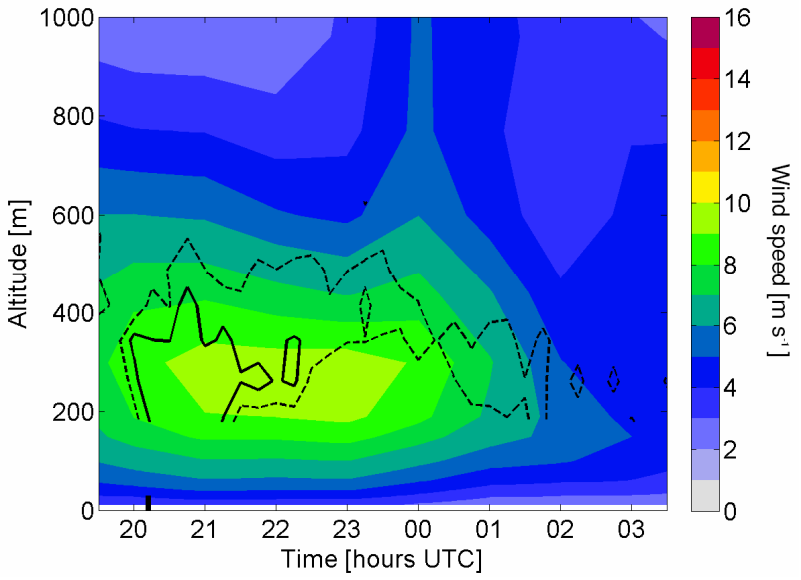

Figure 4·15 – *Evolution of wind speed ($m\ s^{-1}$) with altitude and time, on the night of 14–15 August 2003 at Malvern. Superimposed are the insect aerial density contours of 25 (– –) and 50 (—) insects per $10^7\ m^3$.*

4·2·3 Case study C: 23–24 August 2003

The evolution of the vertical profile of insect aerial density throughout the evening and night of 23–24 August at Malvern is shown in Figure 4·16. A distinct layer had formed by 20:30, in the region 200–600 m above ground. The lower edge of the layer was only just visible in the radar data, but its centre apparently showed little tendency to change in altitude and its depth was never less than 300 m. The layer dissipated at 00:45, and aerial densities then remained low for the rest of the night. Maximum densities of ~ 90 insects per 10^7 m^3 were recorded near 20:30, and densities above 50 insects per 10^7 m^3 occurred within the layer for much of its duration. Migration duration appeared to be about 5 hours, based on a take-off just before 20:00 and layer dissipation just before 01:00.

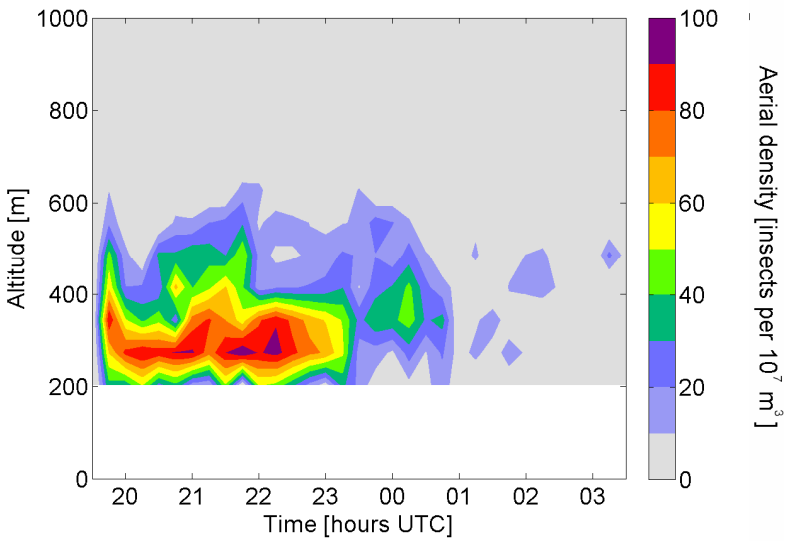

Figure 4·16 – *Evolution of insect aerial density (numbers per 10^7 m^3) with altitude and time for the night of 23–24 August 2003 at Malvern. Only insects with mass 10 mg or greater have been included. Sunset was at 19:18 hours UTC, and the end of dusk at 19:48.*

Back-trajectory analysis (Figure 4·2, trajectory C) reveals that a parcel of air at 300 m over Malvern at 01:00 would have originated at around 80 km to the north at 20:00. The mean orientation angle of insects forming the layer was 208.7° (CSD = 39.8°, 1461 targets) and their mean displacement direction was towards 210.3° (CSD = 28.7°). Thus an extra 70 km can be added to take account of the insect flight speed (see case study A), and this suggests an estimated migration distance

of around 150 km. Hence, the proposition that insects observed near the end of the layering event (01:00) took off near the coast cannot be discounted, particularly given the curvature of the horizontal wind field shown on back-trajectory C.

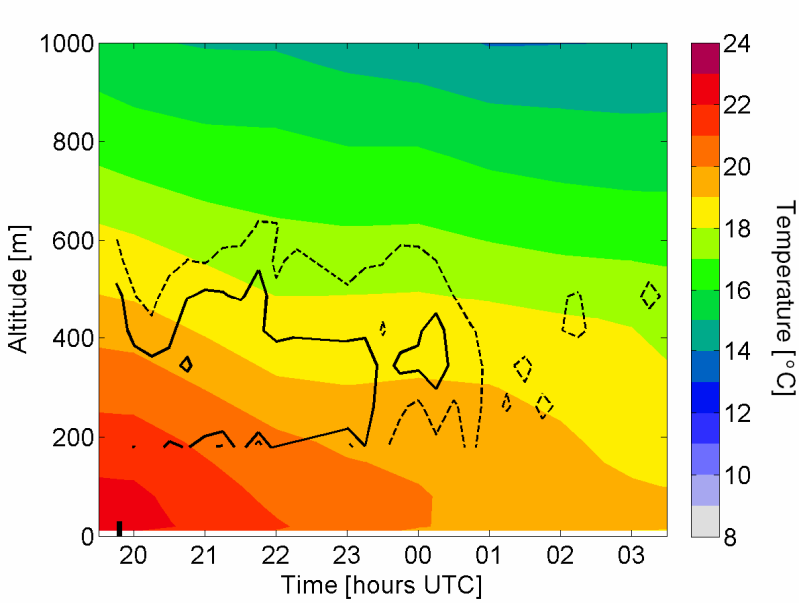

Figure 4·17 – *Evolution of temperature (°C) with altitude and time, on the night of 23–24 August 2003 at Malvern. Superimposed are the insect aerial density contours of 25 (– –) and 50 (—) insects per 10^7 m^3. Sunset was at 19:18 hours UTC, and the end of dusk is represented by a marker on the time axis at 19:48.*

The evolution of the temperature profile (Figure 4·17) shows that temperatures were distinctly warmer than in case studies A and B. Most insects flew above the altitude of the temperature maximum, in air of 18–21 °C throughout the night. The upper boundary of the layer was located at 17–18 °C: this is likely to be higher than the minimum temperature threshold for flight, given the likely species constituting the layer. This implies that temperature was not limiting insect flight altitude, as was suggested in cases A and B. It is possible that in this case maximum wind speed was the significant variable determining layer altitude. Figure 4·18 shows that a nocturnal jet was present, with maximum speeds of 8 m s^{-1} between 21:00 and 00:00 at an altitude of 200–300 m. The jet centre was located at the same altitude as the centre of the insect layer and most insects would have experienced wind speeds above 6 m s^{-1}.

The insect mass distribution again showed a peak in the 80–160 mg group (Figure 4·11). The nearest working RIS light-trap was at Hereford (30 km to the west of the radar). The noctuids caught included *X. c-nigrum*, *M. pallens*, and the rare UK migrant *Spodoptera exigua* (small mottled willow or beet armyworm). *A. gamma* (silver Y), was caught in the light-trap in the days before and after this layering event and in the net at 200 m above Cardington airfield. The northerly wind experienced in this migration event is consistent with southward return migrations to over-wintering sites. Catches of *S. exigua* in the RIS light-traps first appeared in June, probably indicating an early northward invasion of the species and subsequent return southwards (*cf.* Johnson 1969, p. 516).

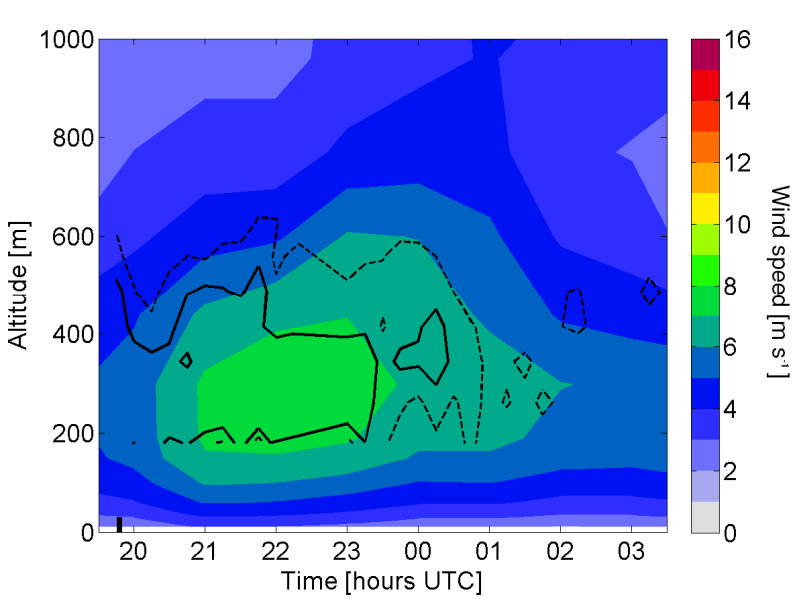

Figure 4·18 – *Evolution of wind speed ($m\ s^{-1}$) with altitude and time, on the night of 23–24 August 2003 at Malvern. Superimposed are the insect aerial density contours of 25 (– –) and 50 (—) insects per $10^7\ m^3$.*

4·3 Discussion

Large insects flying in the stable atmospheric boundary layer at night would be expected to have more control over their altitude of migration than, for example, small insects flying under convective conditions during the day (Gatehouse 1997). It seems likely that migrant moths (which form the subject of the present study) climb steeply after take-off in order to rise above their FBL (see Johnson 1969 p. 81, Lingren *et al.* 1995), and then ascend more gradually (at $\sim 0.5\ m\ s^{-1}$, Riley *et al.*

1983) until they reach altitudes of several hundred metres where conditions seem optimal for migratory flight. The migrants will then tend to accumulate at these altitudes, and if the resulting concentrations are relatively restricted in depth, they will be perceived as layers. Apart from the effects of atmospheric conditions on flight altitude (see below), there are presumably other limits on the vertical distance a large insect will climb before it stops flying upwards. These might be controlled by internal physiological restraints such as energy expended in climbing flight—or conceivably by optomotor reactions to ground patterns, of which little is known for high-flying insects (Riley 1989, §1·3), and certainly little is known for nocturnal flight when illumination is low. After reaching their 'cruising' altitude, nocturnal migrants will maintain steady and continuous flight, often for a period of several hours, during which time they will be displaced considerable horizontal distances in an approximately downwind direction. In southern Britain, migrations are usually over by about midnight or 01:00 (Figure 2·7 shows the lowest activity of the diurnal cycle from about 01:00–03:00). Flights of moths continuing throughout the whole night until dawn or beyond (which have been observed in other regions of the world; Drake *et al.* 1981, Drake 1985a, Drake 1985b, Wolf *et al.* 1990, Beerwinkle *et al.* 1994, Feng *et al.* 2004a) are apparently uncommon in the UK (Reynolds *et al.* 2007). Since Britain is an island, some of the more abrupt flight terminations may be due to a lack of source areas beyond the coasts—indeed this may have occurred in the current study—rather than because air temperatures have dropped below thresholds for sustained flight or because flight fuel reserves have been exhausted.

A key question is thus: *which environmental factors present in the first kilometre of the nocturnal atmosphere will have most influence on the migration altitude of large insects*? Temperature would be expected to be a primary influence, as this variable affects many other aspects of insect physiology and behaviour, and there are plenty of studies to support this view (Drake and Farrow 1988, Gatehouse 1997). The simplest case is where the insects have selected the altitude of the warmest air, often at the top of a surface temperature inversion (Schaefer 1976, Drake 1984, Drake and Farrow 1988, Feng *et al.* 2003, Reynolds *et al.* 2005) or occasionally a

higher-altitude temperature maximum, such as that due to a subsidence inversion (Reynolds *et al.* 2005). Selection of the warmest air by migrants appears to be most likely to occur in relatively cool conditions, and in taxa that have high optimum temperatures for migratory flight. For example, migratory acridoid insects (grasshoppers and locusts) have optimum temperature values for sustained flight of above 20 °C (Clark 1969, Riley and Reynolds 1979), which are much higher than for instance the noctuid moths studied here (see also Taylor and Carter 1961). Contrary to this, there are many references in the literature in which insects—particularly moths—have ascended above the altitude of the temperature maximum. On some of these occasions insects might be forming 'ceiling layers', *i.e.*, ascent has continued until insects reach an altitude corresponding to the lowest temperature at which they can sustain flight. A good example is the sharp upper boundary of layers of the brown planthopper, *Nilaparvata lugens*, in China (Riley *et al.* 1991): these layers were well above the altitude of the temperature maximum, but the layer tops corresponded to known temperature thresholds (*c.* 16 °C) for sustained flight in the planthoppers. Ceiling layers may also be implicated in cases of high-altitude layering where there is no obvious corresponding feature in the vertical profile of meteorological variables—(Drake and Farrow (1985a) observed one as high as 1900 m a.g.l. in eastern Australia)—and in cases where maximum flight altitudes of certain taxa (*e.g.* grasshoppers) show a general decrease as expected with seasonal air temperatures (Schaefer 1976, Reynolds and Riley 1997).

The observations in this chapter were in southern UK and hence in a cooler climate than most previous radar entomology studies, and it was thus expected that even noctuid moth migration would be strongly restrained by temperatures on many occasions. A good indication that temperatures were sub-optimal on many nights was the observation that when migratory activity occurred at dusk, it frequently did not persist for long after dark (Wood, Reynolds *et al.* unpublished data). When night-time layering did develop, moths were observed to fly at the altitude of the warmest air (Reynolds *et al.* 2005), but sometimes it may be difficult to distinguish (as in case study A above) between this effect of

temperature and the formation of a 'ceiling' layer. However, in case study B, the observed insect layer was well above the altitude of the temperature maximum, and was most easily explained by a restriction on migratory flight due to the cooler air at higher altitudes. It is worth noting that the UM validation (§3·2·2) showed generally good capture of temperature inversions, and one would not expect the UM to completely mis-diagnose an inversion. Hence, confidence can be expressed in the UM data.

Notwithstanding the above findings, there are many reports in the literature where the insect layers are closely associated with wind-related variables (*i.e.* wind velocity, shear zones, turbulence) and conspicuously unrelated to air temperature profiles (Wolf *et al.* 1986, Hobbs and Wolf 1989, Beerwinkle *et al.* 1994, Feng *et al.* 2004a). A necessary condition in these cases is presumably that night-time air temperatures need to be significantly above flight thresholds for the taxa concerned, thus freeing the insects of the need to migrate at the warmest altitudes. Examples where moths contributed to wind-related layers include *Helicoverpa zea*, *Helicoverpa virescens*, *Peridroma saucia,* and other species in the southern USA (Wolf *et al.* 1986, Beerwinkle *et al.* 1994); and *Loxostege sticticalis* and *Helicoverpa armigera* in north-eastern China (Feng *et al.* 2004b). It seems plausible that large insects—such as migratory noctuid moths—are able to detect zones of wind speed maxima, and to fly preferentially within them (Wolf *et al.* 1986), and this would appear to be an adaptive strategy for maximizing their displacement. Moreover, the migrants are often able either to align themselves in a downwind direction (as in the three case studies presented here), or to orient at an angle to the wind (but generally one which avoids backwards (tail-first) displacement: Riley and Reynolds 1986). The mechanism(s) and adaptive significance of this orientation behaviour are still unclear. In some cases, orientation occurs under severely reduced illumination, which may suggest that insects are able to use non-visual cues to detect wind speed and direction, such as anisotropies in turbulence due to Kelvin-Helmholtz waves (Riley 1989).

Because the boundary-layer wind speed maximum often occurs close to the top of the surface inversions, it can be difficult to distinguish the effects of wind speed from those of temperature. In case study C, however, an association with the nocturnal jet seemed likely, as the migrants were evidently flying above the level of the warmest temperatures, and 'ceiling layer' effects seemed unlikely because layers of similar species have been observed to migrate at much lower temperatures on previous nights (*cf.* case study B).

In summary, the results of the case study approach taken here indicates that the altitude of layers of migrating moths in the UK may be constrained by either (*i*) the altitude of the warmest air (case study A); (*ii*) the altitudes with temperatures which may represent flight thresholds and/or preferences (case studies A and B); (*iii*) or the altitude of regions of high wind speed when air temperatures are relatively high (case study C).

A case study approach is clearly useful for investigation of migration events involving a preponderance of particular species, as demonstrated by the recent studies of noctuid moths in the UK (this chapter; Reynolds *et al.* 2005) and elsewhere (Feng *et al.* 2003, 2004a). In the next chapter, a systematic study has been carried out of several years' radar data to elucidate the statistical relationships between meteorological variables and nocturnal insect layer formation and intensity.

5: Meteorological impacts on nocturnal insect layer formation and intensity

5·1 Introduction

This chapter entails an analysis of the effect of meteorological conditions on nocturnal insect layering: specifically the conditions that promote layer formation and intensity. It was shown in §2·4·1 that 60 % of the summertime radar profiles at 21:15 hours UTC were layered. This percentage reduces with time, hence a *critical region* for nocturnal layer formation was defined in §2·4 (of 20:00–22:00, 200–500 m a.g.l.). Hence, an analysis of the meteorological variables in the critical region associated with the formation and subsequent intensity of insect layers will be carried out.

5·2 Review of data

In this chapter, the same core data-set is used as throughout the thesis: 2000–2003 Jun–Aug inclusive at both Malvern and Rothamsted. Hence, 736 nights were available for analysis; however, missing UM data reduced the number to only 539 nocturnal events. The dataset was further reduced to 412 nights, to include only events when there was nocturnal activity, so that these analyses are revealing potential relationships between meteorological variables and *layering*, not just aerial activity. The definition used for activity was where the total number of insects detected in the radar data between 21:00 and 23:59 was greater than 75. This period is justified by observing Figure 2·9, in which most nocturnal insect activity was seen from 21:00 to 23:59 (before 21:00 is where the daytime activity merges into the dusk peak and hence unusable for *nocturnal* analysis).

The analyses presented here are investigations of the impacts of a range of meteorological variables on layer formation and intensity *given* that there was sufficiently high nocturnal insect activity. The analyses comprise: (*i*) **binary analysis of layer presence**: a comparison of a range of meteorological variables between layered and non-layered events; and (*ii*) **continuous-variable analysis of layer intensity:** variation of the continuous variable, NLQ (Nocturnal Layer Quality, see §2·3·2), is analysed for a range of meteorological variables.

5·2·1 Explanatory variables

A number of variables have previously been found to be correlated with the presence of insect layers: a full review was given in §1·4. The variables to be used in this chapter are now summarised.

Temperature

Temperature (T) is the meteorological variable which is most often attributed to be the cause of insect layers. In some cases, it is supposed that insects concentrate in the warm air at the top of nocturnal temperature inversions (case A in Chapter 4). It is also thought that insects might concentrate in ceiling layers (case B in Chapter 4); hence inclusion of the temperature gradient, $\partial T/\partial z$, in the analyses is required. Finally, the effect of atmospheric stability will be analysed: hence the need for potential temperature gradient, $\partial\theta/\partial z$, to be included (see §1·4·3 for definitions of stable, neutral, and unstable atmospheric profiles).

The mean UM errors (Chapter 3) in the critical region were: $\varepsilon_T = -0.2\,°\mathrm{C}$; $\varepsilon_{\partial\theta/\partial z} = 0.04\,\mathrm{K\,m^{-1}}$; and $\varepsilon_{\partial T/\partial z} = -0.04\,\mathrm{K\,m^{-1}}$.

Humidity

Both relative humidity, RH, and specific humidity, q, are analysed in this chapter. The mean UM errors (Chapter 3) in the critical region were not significant: $\varepsilon_q = 0.1\,\mathrm{g\,kg^{-1}}$ and $\varepsilon_{RH} = 0.9\,\%$. It is worth noting that RH, q, and T

are not independent. Given a mass of air with constant q, when cooled RH increases (this is described further later in this chapter). Therefore, all three variables should be analysed.

Wind

Wind speed, u, has also been reported to be important for insect layer formation (*e.g.* case C in Chapter 4). The mean UM errors (Chapter 3) in the critical region are: $\varepsilon_u = -0.1\,\mathrm{m\,s^{-1}}$; $\varepsilon_{\partial u/\partial z} = -0.01\left(\mathrm{m\,s^{-1}}\right)\mathrm{m^{-1}}$; and $\varepsilon_{\partial \phi/\partial z} = 0.10^\circ\,\mathrm{m^{-1}}$.

The nocturnal jet is often correlated with insect layers; hence, the jet intensity variable, j (see §3·2·2), is used in this chapter. Furthermore, the gradient of wind speed, $\partial u/\partial z$, is included because it is necessary to consider it for mechanical production of turbulence (§1·4·6). Note the interaction between these variables: fast wind speeds in the critical region are often due to nocturnal jets (Thorpe and Guymer 1977), which are typically accompanied by large wind shears above and below jet centre. Finally, the vertical shear of wind direction, $\partial \phi/\partial z$, has been widely reported to cause layering of passive material (*e.g.* Luhar 2002) and hence is worthy of investigation with respect to insect layering.

Turbulence is important because it might hinder insects' ability to layer. Hence, the Richardson number, Ri, is analysed. The definition of Ri (§1·4·6) showed a dependence of turbulence on $\partial u/\partial z$ and $\partial \theta/\partial z$; hence these variables—in addition to jet intensity—will not be independent.

Correlations between variables

One assumption of the ANOVA statistical method—used later in this chapter (see §5·6, 5·7)—is the use of independent explanatory variables. However, some of the aforementioned variables are not independent of each other. Hence, it is worth noting at the outset.

Table 5·1 shows the strongest correlations are between: T & q, q & RH, T & RH, T & $\partial\theta/\partial z$, and u & $\partial u/\partial z$. These co-dependencies are now summarised.

Temperature and humidity are strongly linked; indeed, one only needs two variables from $T, q,$ and RH in order to calculate the third: hence, we do not expect these variables to be independent. For the 412 nocturnal cases analysed, the co-dependencies are presented in Figure 5·9. From this, the relationship between temperature and humidity can be seen. For constant specific humidity, temperature increases give relative humidity decreases[†]. Hence, apparent relationships of decreasing relative humidity associated with high NLQ might actually be associated with increasing temperature. Also, if a line of constant relative humidity is followed, increases in temperature are accompanied by increases in specific humidity.

Table 5·1 – *Correlation (r) values for meteorological variables in the critical region for the 412-night data set.*

	A. Wind speed, u [m s^{-1}]	B. Temperature, T [°C]	C. Relative humidity, RH [%]	D. Specific humidity, q [g kg^{-1}]	E. Potential temperature gradient, $\partial\theta/\partial z$ [K km^{-1}]	F. Magnitude of vertical shear of wind speed, $\lvert\partial u/\partial z\rvert$ [m s^{-1} km^{-1}]	G. Richardson number, Ri	H. Jet intensity, j	I. Magnitude of vertical shear of wind direction, $\lvert\partial(\phi)/\partial z\rvert$ [° m^{-1}]
A	*(1)*	-	-	-	-	-	-	-	-
B	*-0.21*	*(1)*	-	-	-	-		-	-
C	*0.22*	*-0.57*	*(1)*	-	-	-	-	-	-
D	*-0.05*	*0.48*	*0.43*	*(1)*	-	-	-	-	-
E	*0.29*	*0.41*	*-0.20*	*0.20*	*(1)*	-	-	-	-
F	*0.75*	*-0.14*	*0.22*	*0.01*	*0.29*	*(1)*	-	-	-
G	*0.35*	*-0.04*	*0.04*	*0.00*	*0.20*	*0.27*	*(1)*	-	-
H	*-0.11*	*0.15*	*-0.26*	*-0.11*	*0.28*	*-0.07*	*0.06*	*(1)*	-
I	*0.00*	*0.05*	*0.05*	*0.09*	*0.12*	*0.06*	*0.03*	*0.00*	*(1)*

The high correlation between wind speed and wind speed shear is consistent with the fact that fast wind speeds in the critical region are often due to nocturnal jets, which are typically accompanied by large wind shears (Thorpe and Guymer 1977). It is worth noting that $\partial u/\partial z$ and j are not highly correlated, as might be expected; perhaps it is because both of these variables are averaged over a large vertical region and time (critical region) within which these variables

[†] RH is sometimes called the saturation ratio. For an decrease in T, assuming constant q, RH will increase because water vapour saturates more easily in colder air; eventually T will drop to its dew-point, water vapour condenses (*e.g.* fog, cloud), and RH = 100 %.

will vary; and because $\partial u/\partial z$ is in the critical region, whilst j is a ratio from jet altitude up to 2 km.

Finally, T and $\partial\theta/\partial z$ are not independent. Stable profiles are associated with warmer temperatures. This is to be expected, because the warmest temperature conditions during the summer occur during high atmospheric-pressure, hence clear-sky conditions. During clear-sky nights, potential temperature profiles are expected to be stable (or near neutral in the residual layer).

5·2·2 Calculations

GenStat® version 7 (Payne *et al.* 2003) was used to carry out the statistical tests in this chapter.

The UM calculates meteorological variables at several levels and at hourly time intervals (Chapter 3). The mean of each meteorological variable throughout the critical region was calculated. Using the mean of several data points is advantageous because of the inaccuracies of meteorological variables in the UM (particularly for gradient variables). Hence, a variable averaged over a region in space and time will be more representative of actual conditions in the critical region than a spot value.

The gradient variables were calculated at each time-step by first calculating local gradients across each vertical model level, then a vertical mean was taken, and then the time mean was calculated.

5·3 Binary analysis of layer formation

Statistical analyses of the variation of important meteorological variables between layered and non-layered occasions were carried out. Initially, a binary analysis approach was taken to assess if there were any gross statistical

differences of individual meteorological factors* between layered and non-layered events.

The 412 nocturnal events were split into layered profiles—where NLQ > 1 (59 events)—and weakly- or non-layered profiles (353 events). Mean meteorological factors in the critical region during layered and non-layered occasions were compared using binary statistical tests. The **null hypothesis** was that the means were the **same** in each population of layering and non-layering events. Refutation of the null hypothesis thus indicates that the relevant meteorological factor might be associated with layered occasions. However, due to the correlation of many meteorological factors with each other, a significant relationship between a particular meteorological factor and strong layering does not prove a causative effect. Rather, it indicates that this factor might have a role to play in layer formation, and is worthy of further analysis.

Table 5·2 shows the p-values for the factors analysed. These p-values represent significant differences at the $p \leq 0.05$ level, and highly significant differences at the $p < 0.001$ level. Parametric t-tests were used to test for significant differences in the sample means where the data were approximately normal (2-sample, 2-sided, unpaired with 95 % confidence interval). For data where there was a skewed distribution, the Mann-Whitney U-test was used to obtain a p-value. The usefulness of the U-test is that it can be used with skewed data because the test is non-parametric: it uses ranked rather than numerical values, as parametric tests do. Figure 5·1 shows box-plots only for the near-Gaussian (*i.e.* low skewness, of <1) factors in Table 5·2.

The mean temperature was higher during layering events than non-layering events by 2.5 °C ($p < 0.001$). Figure 5·1 shows that when layering occurred, the entire distribution was shifted to warmer temperatures.

* A factor is a statistical term for a variable whose values are independent of changes in other variables. For example, in this case, an assumption of the statistical tests is that temperature is independent of wind speed (which may not meteorologically be the case).

Table 5·2 – *Summary of averages of layered and non-layered factors. The Mann-Whitney U-test was used where the data were highly skewed; otherwise, the p-values were obtained using the standard t-test.*

	A. Wind speed, u [m s^{-1}]	B. Temperature, T [°C]	C. Relative humidity, RH [%]	D. Specific humidity, q [g kg^{-1}]	E. Potential temperature gradient, $\partial\theta/\partial z$ [K km^{-1}]	F. Magnitude of vertical shear of wind speed, $\lvert\partial u/\partial z\rvert$ [m s^{-1} km^{-1}]	G. Richardson number, Ri	H. Jet intensity, j	I. Magnitude of vertical shear of wind direction, $\lvert\partial(\phi)/\partial z\rvert$ [° m^{-1}]	J. Temperature gradient, dT/dz [K km^{-1}]
Skewness	*0.40*	*0.77*	*-0.39*	*0.46*	*2.89*	*1.27*	*-2.51*	*7.56*	*4.42*	*2.92*
Mean (layer)	*7.3*	*16.4*	*69*	*8.3*	*-6.0*	*4.6*	*n/a*[†]	*2.3*	*0.08*	*-6.5*
Mean (non-layer)	*7.8*	*13.9*	*74*	*7.7*	*-7.0*	*5.3*	*n/a*	*1.9*	*0.07*	*-7.4*
Median (layer)	*6.8*	*15.4*	*68*	*8.3*	*-6.9*	*3.0*	*-90*	*1.4*	*0.04*	*-7.0*
Median (non-layer)	*7.8*	*13.7*	*74*	*7.6*	*-7.0*	*4.0*	*-65*	*1.1*	*0.04*	*-8.0*
	Parametric (t-test, T-statistic)				**Non-parametric (U-test, W-statistic)**					
p-value	*0.065*	***<0.001***	***<0.001***	***<0.001***	***0.003***	***0.03***	*0.32*	***<0.001***	*0.726*	***0.018***
Test statistic	*-1.86*	*7.56*	*-3.80*	*4.11*	*42958*	*36834*	*38271*	*43815*	*39874*	*42288*

[†] *Because Ri is a ratio, it does not make sense to take its mean.*

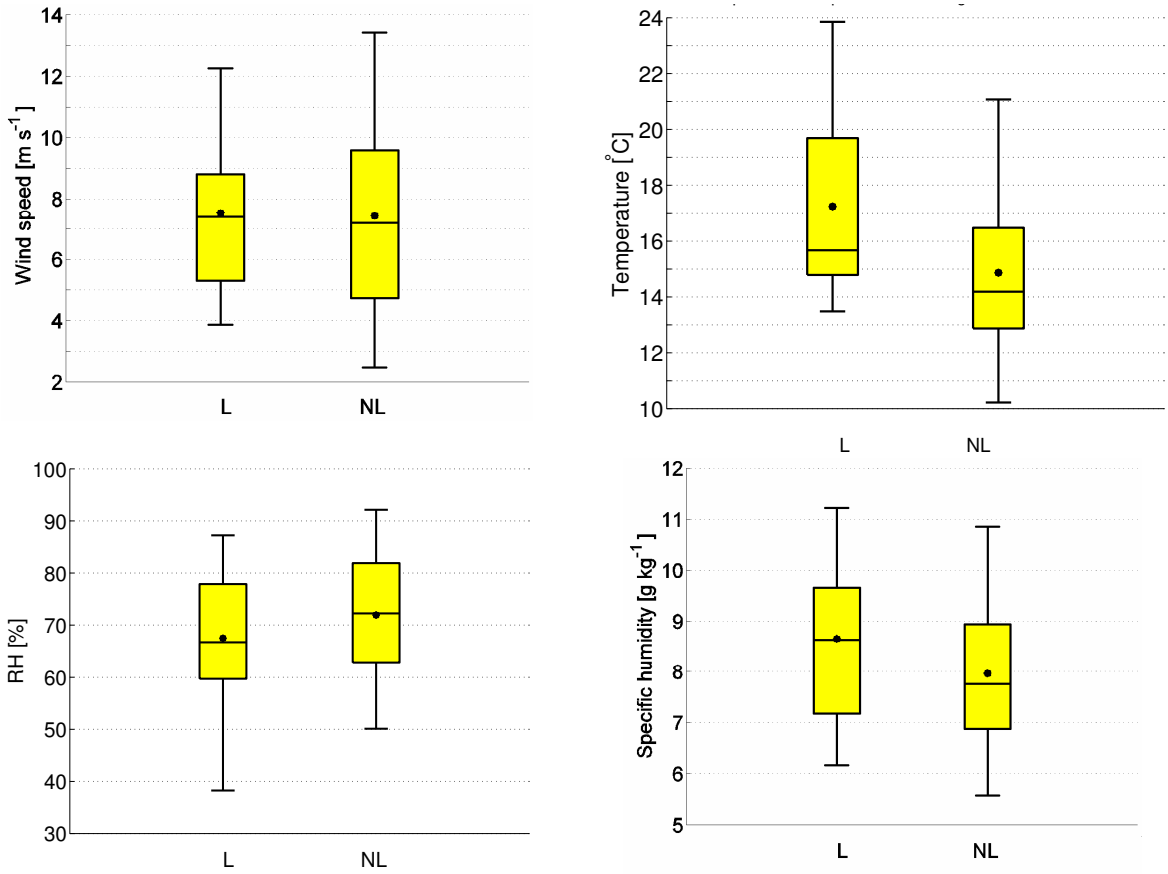

Figure 5·1 – *Box-plots for the meteorological factors with small skewness (u, T, RH, q). The dot is the mean, the bar is the median, the box is the inter-quartile range, and the whiskers extend to the 5/95th percentiles. Layered occasions (L = 59), non-layered occasions (NL = 353). p-values are shown in Table 5·2.*

Mean RH was 5 % lower for layered profiles ($p < 0.001$); and mean q was higher by 0.6 g kg^{-1} for layered profiles ($p < 0.001$). These results suggest that humidity might explain some of the variation in NLQ. There is interaction between

humidity, temperature, and NLQ which is analysed further in §5·4·3. Finally, it is worth noting from Figure 5·1 that when layering occurred the entire RH distribution was shifted to less humid air; but for q, the distribution barely shifted.

There was no significant difference in wind speed ($p = 0.065$) between the two distributions. Indeed, the distributions were not shifted, but the distribution for non-layered profiles was more spread. However, layering case studies in this thesis (Chapter 4) and in the literature have demonstrated a strong relationship between nocturnal insect layers and local maxima of wind speed in some cases. Hence, one might expect a significant relationship between the nocturnal jet intensity and layers, rather than with wind speed *per se*, and this appears to be the case. The mean jet intensity was higher by 0.4 during layered events ($p < 0.001$, Table 5·2); and it was the most significant of the non-parametrically-analysed factors. This indicates that wind speed does affect the formation of nocturnal insect layers, but that the relationship is not straightforward.

There was no significant difference between the medians of layering and non-layering populations for the turbulence factor, Ri ($p = 0.32$). However, gradients in both wind speed ($p = 0.03$) and potential temperature ($p = 0.003$) had significant differences in their medians. Hence, the conditions with less wind shear (small $|\partial u/\partial z|$) and more stable profiles (*i.e.* $\partial\theta/\partial z > 0$) were associated with layering. The directional shear of wind showed no difference in medians between layering and non-layering ($p = 0.726$); this result is discussed later.

Comparing meteorological factors for layered and non-layered occasions suggests that temperature is the most significant variable for the formation of insect layers, that humidity relationships cannot be ruled out (at this stage), and that insect layering is not affected by wind speed (but appears to be related to the presence of more intense nocturnal jets). There might also be some effect of gradients in potential temperature and wind speed.

5·4 Layer intensity

Now that the most important meteorological factors associated with the formation of nocturnal insect layers have been identified, the next task is to identify which factors promote high NLQ values (*i.e.* very intense and persistent layers) *given* that layering has occurred. High NLQ values are obtained from layers that have a pronounced profile maximum (high LQ value) and are temporally persistent.

The distribution for all cases (N = 412) is shown in Figure 5·2a (*i.e.* $NLQ \geq 0$). However, to compare meteorological conditions with layer *intensity*, the data were restricted to only occasions when layering occurred (*i.e.* $NLQ > 0$, N = 279, Figure 5·2b). For many statistical analyses, Gaussian distributions are assumed. A logarithmic transformation (Figure 5·2c) did not produce a closer approximation to a Gaussian distribution; in fact, the distribution was instead merely negatively skewed ($sk = -0.41$). Hence, in this chapter, an untransformed NLQ variable was used (*i.e.* the data in Figure 5·2b).

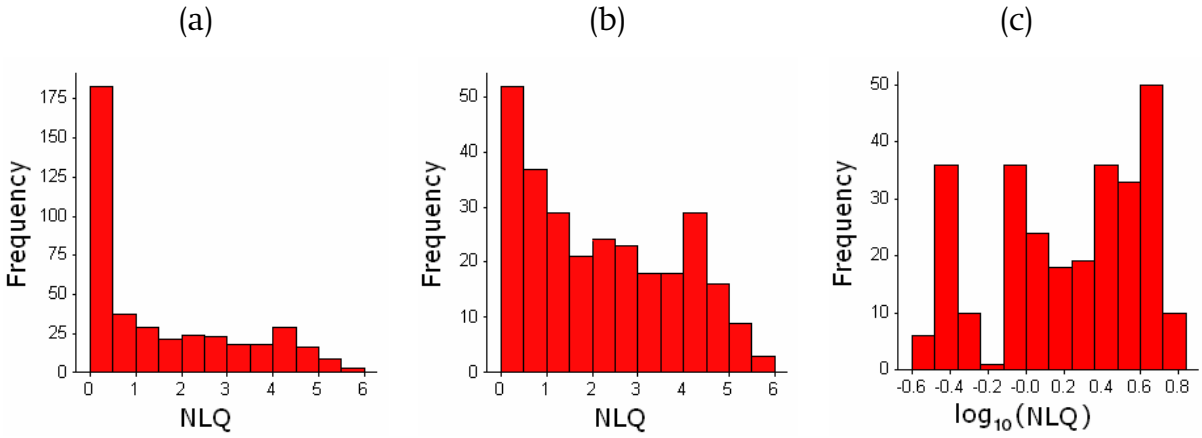

Figure 5·2 – *Frequency histograms (each with 12 bins) of NLQ for [a] all NLQ values (sk = 0.82), [b] NLQ > 0 only (sk = 0.42), and [c] logarithm of NLQ > 0 (sk = -0.41).*

To review, the data (N = 279, untransformed) was filtered to include only nights where: (*i*) UM and radar data were both available, (*ii*) there was a sufficient level of insect activity (> 75 radar targets), and (*iii*) layering had occurred (NLQ > 0). Thus, the dependence of layering intensity on meteorological conditions is now investigated.

5·4·1 Linear regression of layer intensity

A linear regression analysis model was used to relate NLQ to meteorological factors. Such a basic model often accounts for only a small percentage of the variability in the dependent factor (because it is a linear model and because it does not include interactions between factors). A further reason for the low amounts of explanatory variance found in these analyses is that although NLQ is a quantitative variable, there were ranking methods used in calculating LQ values (which NLQ is based upon). Nonetheless, linear regression is still helpful in identifying gross relationships.

A summary of the linear regression analyses for each meteorological factor is shown in Table 5·3; the correlation coefficient, r, if squared gives the coefficient of determination[†], r^2. Temperature had the highest $|r|$ value ($r = 0.31$, $p < 0.001$), and hence explained most variance in NLQ (10 %). Wind speed explained almost no variance in NLQ ($r = 0.02$, $p = 0.766$), however jet intensity explained 2.3 % of the variance in NLQ ($r = 0.15$, $p = 0.010$). Significant amounts of variance (at the 95 % confidence level) in NLQ were explained by both relative humidity (negative slope) and specific humidity (positive slope): 1.4 % ($p = 0.037$) and 4.4 % ($p < 0.001$) of the variance respectively. Hence, there is evidence that NLQ increases with decreasing RH and increasing q. Vertical shears of wind direction and speed did not explain any variance in layering ($r = 0.04$ and $r = 0.03$, $p = 0.493$ and $p = 0.604$), however this result is analysed further in §5·4·2. Richardson number did not explain any significant variance in NLQ. However, a linear regression between potential temperature gradient and NLQ showed a positive slope ($r = 0.24$, $p < 0.001$) which indicates that statically stable air was associated with layering. The positive slope of $\partial T/\partial z$ ($r = 0.15$, $p < 0.001$) indicates that gradients nearer to zero are associated with layering (NB. almost all of $\partial T/\partial z$ is negative[‡]).

[†] This value is the portion of variance in NLQ that can be accounted for by a given explanatory variable.

[‡] Positive potential temperature gradients only occur below the inversion, the inversion is usually in, or below, the critical region; hence, one would not expect a positive gradient averaged over the critical region.

Temperature gradient, $\partial T/\partial z$, is not being used in the subsequent ANOVA tests owing to its similarity to $\partial\theta/\partial z$.

Table 5·3 – *Summary of linear regression analysis for the identified factors. r is the correlation coefficient; r² is the coefficient of determination, which expresses the amount of variance in NLQ explained by the given factor. Data taken are for NLQ > 0 (N = 279).*

	A. Wind speed, u [m s^{-1}]	B. Temperature, T [°C]	C. Relative humidity, RH [%]	D. Specific humidity, q [g kg^{-1}]	E. Potential temperature gradient, $\partial\theta/\partial z$ [K km^{-1}]	F. Magnitude of vertical shear of wind speed , $\lvert\partial u/\partial z\rvert$ [m s^{-1} km^{-1}]	G. Richardson number, Ri	H. Jet intensity, j	I. Magnitude of vertical shear of wind direction, $\lvert\partial(\phi)/\partial z\rvert$ [° m^{-1}]	J. Temperature gradient, $\partial T/\partial z$ [K km^{-1}]
p	*0.766*	***<0.001***	***0.037***	***<0.001***	***<0.001***	*0.604*	*0.383*	***0.010***	*0.493*	***<0.001***
r	*0.02*	*0.31*	*-0.12*	*0.21*	*0.24*	*0.03*	*-0.05*	*0.15*	*0.04*	*0.15*
r²	*0 %*	*10 %*	*1.4 %*	*4.4 %*	*5.8 %*	*0.1 %*	*0.3 %*	*2.3 %*	*0.2 %*	*2.3 %*

Linear regression, as done here, assumes a very simple model for potential relationships between NLQ and meteorological factors. Hence, regression analyses are not likely to show strong relationships; this is consistent with the generally small $|r|$ values obtained. Multiple regression techniques allow the inclusion of several independent variables (factors) simultaneously. However, in the present case there are many variables, some of which are inter-related, leading to problems with interpretation. Grouping each of the factors into a few distinct categories and using analysis of variance (ANOVA) allows one to investigate potential relationships and interactions between the meteorological variables. Firstly, category means are compared for each factor separately using one-way ANOVA before moving to pair-wise analyses using two-way ANOVA.

5·4·2 One-way 'analysis of variance' for layer intensity

Each meteorological factor was divided into either two or three categories, and then analysed using the standard ANOVA technique (*e.g.* Fowler *et al.* 1998). Table 5·4 lists the chosen categories and gives the number of replicate events in each category. Wherever possible the number of replicates in each category was kept approximately equal, although some categories are larger or smaller than others are (based on physical constraints and the fact that UM data has a discrete resolution). Those categories based on physical limits were chosen as follows. Potential temperature gradient was split into three categories representing

'highly unstable', 'weakly unstable', and 'stable' (see §1·4·3 for definition). Vertical shear was split to represent small and large magnitude shears. Richardson number was split into two categories representing turbulent (Ri < 0.25) and non-turbulent (Ri > 0.25) flow conditions; Ri = 0.25 is the classical threshold (§1·4·6) for onset of turbulence when changing from stable to unstable conditions.

Table 5·4 – *Categorisation of meteorological factors for use in ANOVA, with number of replicates in each category.*

	categories			replicates		
	1	**2**	**3**	**1**	**2**	**3**
Wind speed [m s^{-1}]	< 6	6≤ u ≤8.5	> 8.5	99	81	89
Temperature [°C]	< 14	14≤ T ≤16.5	> 16.5	100	87	92
Relative humidity [%]	< 65	65≤ RH ≤80	> 80	71	104	105
Specific humidity [g kg^{-1}]	< 7.2	7.2≤ q ≤8.5	> 8.5	94	75	111
Potential temperature gradient [K km^{-1}]	< -5.0	-5.0≤ $\partial\theta/\partial z$ ≤0.0	> 0.0	216	54	9
Magnitude of vertical shear of wind speed [m s^{-1} km^{-1}]	< 2.0	$\lvert\partial u/\partial z\rvert$ ≥ 2.0	-	97	182	-
Richardson number	< 0.25	Ri ≥ 0.25	-	270	9	-
Jet intensity	< 1.0	1.0≤ j ≤2.7	> 2.7	91	110	78
Magnitude of vertical shear of wind direction [° m^{-1}]	< 0.04	0.04≤ $\lvert\partial\phi/\partial z\rvert$ ≤0.05	> 0.05	111	74	95

The results of nine one-way ANOVAs to compare mean NLQ values for each category are displayed in Figure 5·3 and the p-values for the parametric tests are summarised in Table 5·5 (full results in Appendix C).

There was an insignificant difference in the mean NLQ value between the three mean wind speed categories (p = 0.767). Furthermore, the mean NLQ did not differ between jet categories (p = 0.368), other than a small increase of 0.2 in NLQ from category one to two. This would suggest that wind speed is not a factor related to layer intensity.

Temperature had the strongest effect on NLQ and was highly significant (F = 11.71, p < 0.001); there was an increase in NLQ of 1.1 from the mean of category 1 to the mean of category 3. The gradient of potential temperature showed a significant effect (p = 0.003); high NLQ values hence appear to be associated with higher static stability.

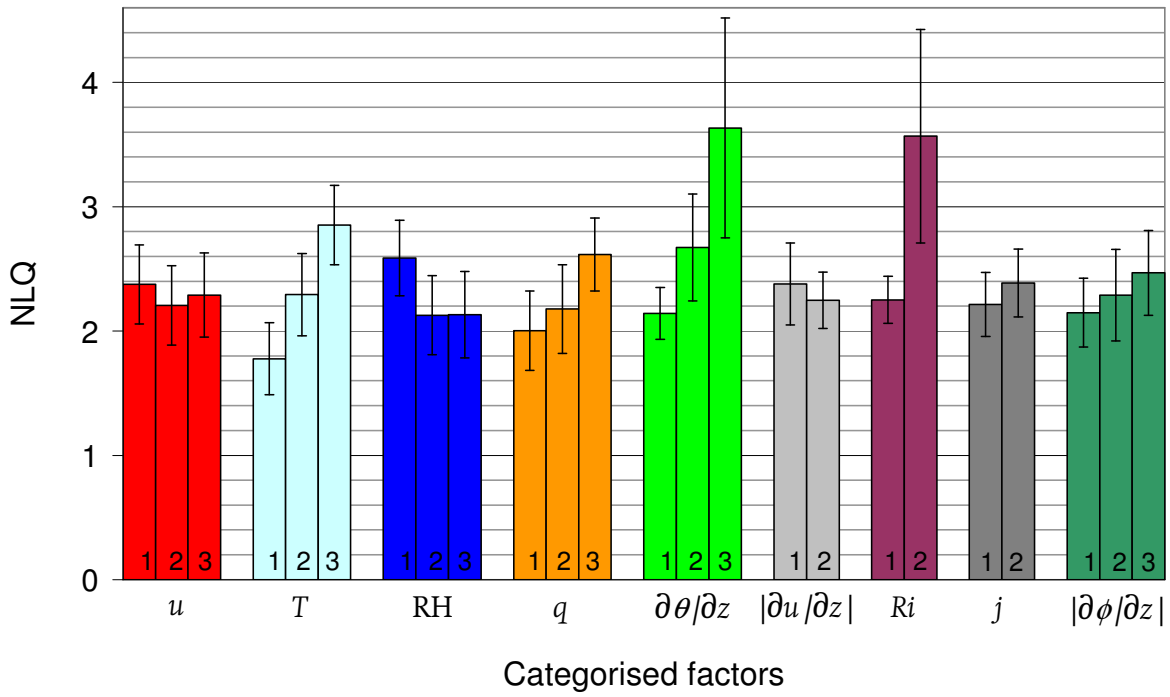

Figure 5·3 – *Comparison of mean NLQ value between categories in each factor. Confidence intervals (95 %) are plotted.*

Table 5·5 – *Summary of parametric ANOVA.*

Parameter	A. Wind speed, u [m s^{-1}]	B. Temperature, T [°C]	C. Relative humidity, RH [%]	D. Specific humidity, q [g kg^{-1}]	E. Potential temperature gradient, $\partial\theta/\partial z$ [K km^{-1}]	F. Magnitude of vertical shear of wind speed , $\lvert\partial u/\partial z\rvert$ [m s^{-1} km^{-1}]	G. Richardson number, Ri	H. Jet intensity, j	I. Magnitude of vertical shear of wind direction, $\lvert\partial(\phi)/\partial z\rvert$ [° m^{-1}]
p	0.767	**<.001**	0.389	**0.017**	**0.003**	0.511	**0.015**	0.368	0.359
F	0.27	11.71	0.95	4.11	5.86	0.43	6.03	0.81	1.03
Correlation	*n/a*	*+ve*	*-ve*	*+ve*	*+ve*	*-ve*	*+ve*	*+ve*	*+ve*

Wind directional shear had no significant effect on layer intensity (p = 0.359). A hypothetically sheared environment is discussed here to aid the interpretation of this result. Consider a moderate shear of 0.04° m^{-1} (which is the threshold between category 1 and 2); this is equivalent to an 8° change in the wind direction over 200 m vertically, as shown in Figure 5·4—which also includes a representative wind-*speed* shear of 10 (m s^{-1}) km^{-1}. By backtracking the insects that fly through the radar beam at a particular time by 2 hours it can be seen that the insects flying at 300 m have come from a west-north-west direction (path s_1),

whilst insects flying at 100 m above the radar have came from a westerly direction (path s_2). Hence, if insect layers were to form due to this differential advection effect alone, this would require surface insect source-populations to be highly heterogeneous, *i.e.* there would need to be a large difference in the density of insects taking-off from the ground below the end-points of s_1 and s_2. The results of this example therefore imply that a significant horizontal variation in source populations within x = 16 km would be required for wind directional shear to be an important factor in promoting insect layering. Analysis of the spread of data for the mean wind direction shear in the critical region revealed a mean x of 16 km due to differential advection (with extremes at 343 m and 139 km). The fact that wind directional shear has no significant effect on insect layering therefore implies that nocturnal migrating insect population sources are horizontally homogeneous over scales of at least tens of kilometres. This calculation (*i.e.* Figure 5·4) assumes an instantaneous scenario; however there is frequently an oscillation of the wind direction and speed with time (see Chapter 1) which has not been taken into account.

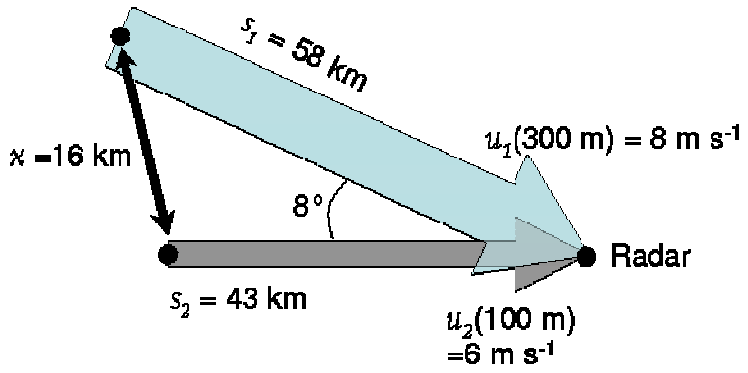

Figure 5·4 – *Schematic wind shear diagram (not to scale). The wind speeds and directions at 100 m and 300 m are shown by the thin grey arrow and the large blue arrow respectively, separated by 8° of directional shear. Assuming 2 hours of flight at dusk (and that insects take off and rise almost instantaneously to cruising altitude), the 's' values represent the distance of the paths to the sources. The distance between sources is given by x.*

Low relative humidity and high specific humidity were associated with high NLQ values. The variation in NLQ value for specific humidity has a significant difference in means (p = 0.017), but relative humidity is insignificant (p = 0.389).

The variance explained by Ri indicates a significant relationship (p = 0.015): there was an increase in mean NLQ of 1.2 from turbulent to non-turbulent occasions.

Hence, insect layering was more intense during non-turbulent conditions than turbulent conditions. The potential temperature gradient (a component of *Ri*) result showed that very statically stable conditions were associated with high NLQ values ($p = 0.003$): this indicates that layers were more intense during stable conditions. The wind speed shear (the other component of *Ri*) did not show any significant effect on NLQ ($p = 0.511$): so changes of wind speed with altitude appeared to have no correlation with insect layer intensity.

The most important relationship is clearly with temperature ($F = 11.71$). This result is consistent with the linear regressions ($r = 0.31$), which provides confidence that the ANOVA categorisations are not mis-representing the data. The remaining results in this chapter are two-way ANOVAs, which have been used to investigate interactions between NLQ, temperature, and other potentially important meteorological factors.

5·4·3 Two-way ANOVA: interaction effects

The meteorological factor that has the strongest relationship with layer intensity is temperature (one-way ANOVA: $p < 0.001$, $F = 11.71$). Hence, in this section inter-comparisons are made between (*i*) temperature, (*ii*) nocturnal layer intensity, and (*iii*) the other leading meteorological factors, each in turn. Two-way ANOVAs are usually *a-priori* designed experiments (particularly as used in agricultural and biological sciences) and are typically used to estimate the effects of two independent variables on a dependent variable; and variables should have Gaussian distributions (*e.g.* Fowler *et al.* 1998). This method allows the analyst to observe interaction effects, for example if there are any hierarchical effects. In this thesis, for example, a response to wind speed might occur only after a certain temperature threshold has been reached. The distribution of NLQ was closer to being Gaussian following the removal of NLQ = 0 values, but the categories do not have equal numbers of replicates and temperature is not independent of other variables (see Chapter 1 and

Table 5·1). Hence, an 'unbalanced*' ANOVA test was carried out (a function in GenStat, see Appendix D) in order to make some allowance for these shortcomings. The results of this analysis are summarised in Table 5·6.

Table 5·6 – *The p-values for two-way ANOVAs of NLQ as the dependent variable with temperature and a second factor. Significant results are emboldened.*

Analysis	Second factors					
	u	RH	q	$\partial\theta/\partial z$	j	Ri
1a Temperature factor ignoring second factor	**<0.001**	**<0.001**	**<0.001**	**<0.001**	**<0.001**	**<0.001**
1b Second factor allowing for temperature factor	0.713	0.720	0.647	0.075	0.351	0.131
2a Second factor ignoring temperature	0.750	0.059	**0.015**	**0.002**	0.624	**0.023**
2b Temperature factor allowing for second factor	**<0.001**	**<0.001**	**<0.001**	**<0.001**	**<0.001**	**<0.001**
+ Interaction	0.189	0.161	0.612	0.824	0.294	0.408

Temperature alone, whilst ignoring the effects of other factors (Table 5·6, row 1a), had a highly significant positive effect on NLQ ($p < 0.001$). Furthermore, when the effect due to temperature was taken into account after allowing for other factors first (2b), the effect of temperature was still highly significant for all factors ($p < 0.001$). Moreover, there were no significant p-values for any of the second factors where the temperature factor had first been taken into account (1b). It thus seems that temperature has by far the largest influence on NLQ of the meteorological variables studied here.

The other principal factors are considered in the following sub-sections.

Wind factors

After allowing for temperature, there appears to be no significant effect of wind speed ($p = 0.713$) on NLQ. Furthermore, allowing for wind speed whilst ignoring temperature also did not have a significant effect on explaining variance in NLQ ($p = 0.750$). Neither does there appear to be any significant interaction ($p = 0.189$). However, the actual pattern of the relationship observed is complicated. Figure 5·5 shows that at higher temperatures (T_2 and T_3), higher wind speeds are

* A balanced ANOVA is where the order of 'ignoring' or 'allowing for' does not matter, an unbalanced statistical test is performed in the same way as a standard balanced ANOVA – but the test result outcomes vary depending on which way the results are analysed. Table 5·6 has been split into several rows to show the results depending on order.

associated with higher NLQ values. However, at low temperatures (T_1) there appears to be an increase in NLQ associated with *low* wind speeds (u_1). This suggests a hierarchical effect: only during high temperatures do high wind speeds increase layer intensity. One possible mechanism is suggested here. Lower temperature conditions in the summertime typically occur with low-pressure systems, which are associated with higher winds at all altitudes and with rain: conditions unfavourable for insect migrations. Thus, it appears that during occasions with lower temperatures, lower wind speeds are *less* likely to be associated with unsuitable rainy conditions. A negative correlation between wind speed and temperature was indeed found in the data (Table 5·1), which is consistent with climatology: that colder summertime temperatures are associated with higher wind speeds. In summary, this result indicates a (non-significant) hierarchical effect: whereby higher wind speeds are associated with stronger layering only during higher temperatures.

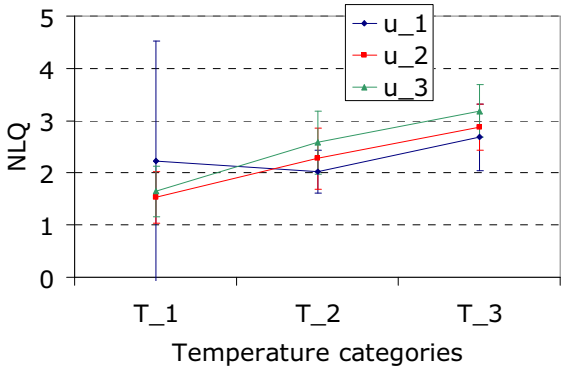

Figure 5·5 – *Two-way ANOVA for NLQ with temperature and wind speed. The means are shown with 95 % confidence interval.*

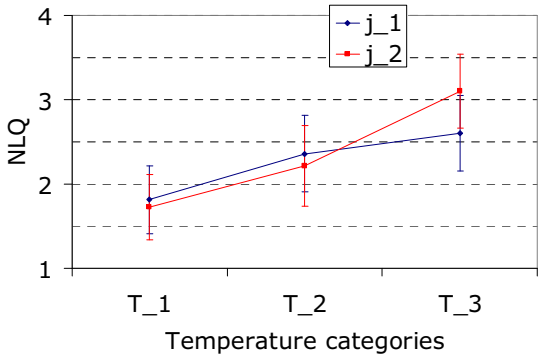

Figure 5·6 – *Two-way ANOVA for NLQ with temperature and nocturnal jet. The means are shown with 95 % confidence interval.*

The higher NLQ values for fast wind speeds during warm conditions are probably due to the presence of the nocturnal jet (Figure 5·6). The results for the jet factor show that mean NLQ has no significant difference between jet categories when ignoring temperature ($p = 0.624$) nor when variance due to temperature factor is explained first ($p = 0.351$). Nor was there any significant interaction ($p = 0.294$). It is worth noting that the linear regression analysis showed jet factor explained 2.3 % of the variance in NLQ ($p = 0.01$). The statistically non-significant interaction can be explained (Figure 5·6): an increase in NLQ of 0.5 occurred during warmer

temperatures (T_3) for jet presence (j_2) compared to no jet (j_1), which is consistent with the suggested hierarchical effect that during warmer temperatures the jet presence explains variance in NLQ. Furthermore, from the analyses of all two-way ANOVAs carried out (Appendix D) the smallest residual was found to be for the analysis of temperature and jet factors (*i.e.* to explain the most amount of variance with just two factors, then jet intensity and temperature would be used).

Humidity factors

The relationship between temperature and humidity is meteorologically complex: temperature and humidity are co-dependent (Figure 5·9). Analysing the interaction between these factors will illuminate the relationship between insect layering and humidity. When ignoring temperature, specific humidity had a significant positive effect on NLQ ($p = 0.015$), but the effect of relative humidity was not significant ($p = 0.059$). However, as second factors (allowing for variance in NLQ due to temperature) neither specific nor relative humidity showed a significant relationship ($p = 0.647$ and $p = 0.720$ respectively). It is likely that the apparent relationship with specific humidity is due to specific humidity tending to be higher in warmer temperatures. The interaction terms are also not significant; $p(q_{int}) = 0.612$, $p(RH_{int}) = 0.161$. Altogether, this is strong evidence that there is no link between insect layering and humidity *per se*. Figure 5·7 and Figure 5·8 show the two-way ANOVAS. There is no separation of the confidence intervals, indicating no significant interaction and the three lines almost collapse on each other, which suggests humidity has no effect on NLQ.

The temperature and specific humidity values for each NLQ value in the complete data-set are plotted (Figure 5·9), with relative humidity lines superimposed.

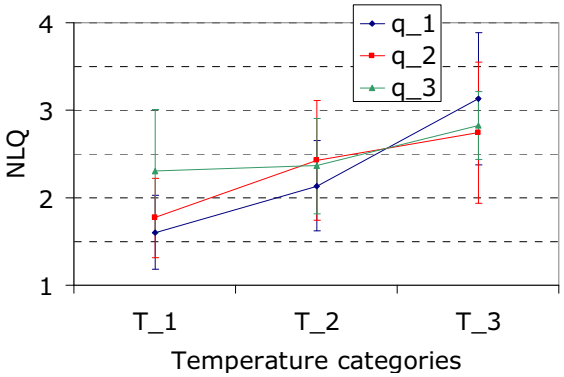

Figure 5·7 – *Two-way ANOVA for NLQ with temperature and specific humidity. The means are shown with 95 % confidence interval.*

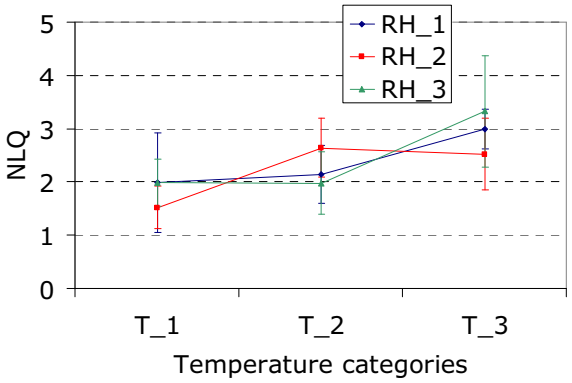

Figure 5·8 – *Two-way ANOVA for NLQ with temperature and potential temperature gradient. The means are shown with 95 % confidence interval.*

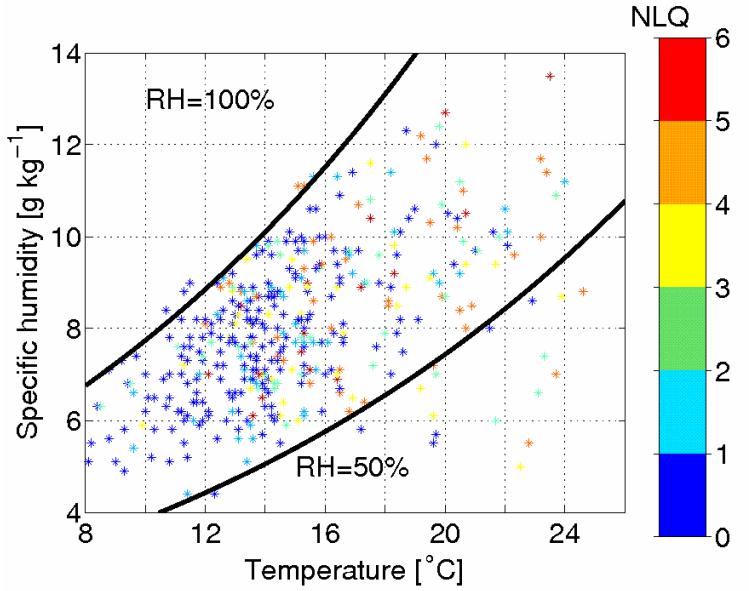

Figure 5·9 – *Specific humidity against temperature for all data from the nocturnal samples (from 412 nights data set). The coloured legend shows NLQ values for each case. Lines of constant relative humidity are also plotted.*

Stability and turbulence

Potential temperature gradient ($\partial\theta/\partial z$) explained a significant amount of variance in NLQ ($p = 0.002$). However, when variance due to potential temperature gradient is considered allowing for temperature, there was not a statistically significant amount of variance in NLQ explained ($p = 0.075$). Thus, much of the variance apparently explained by potential temperature gradient is actually explained by the effect of temperature. There is no significant interaction ($p = 0.824$). The third category of potential temperature gradient—representing positive static stability—had just 9 replicates, hence the results are

not as clear as they would have been if there were more replicates in this category. However, increased (or equal) NLQ occurred for higher potential temperature gradients at all temperatures.

For turbulence, the Richardson number, Ri, was split into two categories. The non-turbulent (laminar) category had only 9 replicates ($\partial\theta/\partial z$ was positive on only nine occasions). Hence, the results are not clear from so few replicates. Nonetheless mean NLQ was higher for laminar Ri compared to turbulent Ri ($p = 0.023$ ignoring temperature). There was no significant interaction between Ri and T.

5·5 Discussion

The key question which has been addressed is: *which environmental factors present in the critical region (20:00–22:00, 200–500 m a.g.l.) have most influence on the formation and intensity of nocturnal layers of large insects?* One might expect temperature to be a primary influence, as temperature affects many aspects of insect physiology and behaviour. Previous results have been analysed on a case study basis (Chapters 1 and 4). In this chapter, a unique systematic study over several years' data has been completed to elucidate the correlations between certain meteorological variables and nocturnal layer formation and intensity.

Temperature explained the largest amount of variance in NLQ ($p < 0.001$, $F = 11.71$). Even for analyses where variance due to each of the other meteorological factors was allowed for first, there was still a highly statistically significant amount of variance in NLQ explained by temperature ($p < 0.001$). Overall, temperature seems to be the most important meteorological variable affecting UK nocturnal insect layering. Confidence can be expressed in this result due to the accuracy of UM in modelling temperature. Nonetheless, other variables were worth investigating: in some cases to discount apparently significant variables associated with layering in case studies.

The majority of UK nocturnal layers examined so far have not been explained by wind speed profiles; this is presumably because on most occasions, UK temperatures are sub-optimal and *temperature* is first in the hierarchy of meteorological variables in UK nocturnal layering. Examples where noctuid moths contributed to layers where wind maxima were suggested as the layer cause include: *Helicoverpa zea*, *Heliothis virescens*, *Peridroma saucia*, and other species in the southern USA (Wolf *et al.* 1986, Beerwinkle *et al.* 1994); and *Loxostege sticticalis* (actually a pyralid micromoth) and *Helicoverpa armigera* in northeastern China (Feng *et al.* 2004a). However, wind speed magnitude appears not to be relevant for UK nocturnal layers ($p = 0.750$); except for a small hierarchical effect that wind speeds slightly promote layering once warm temperatures have been reached. A necessary condition in these cases is presumably that air temperatures at night were significantly above the flight thresholds for the taxa concerned: thus, freeing the insects of the need to migrate at the warmest altitudes. The UM's simulation of wind speed has an error of –0.1 m s^{-1}, with the confidence interval indicating no consistent bias.

If the optomotor effect were present (*i.e.* insects might be able to detect and fly at altitudes of the fastest moving air), then one would perhaps expect to see variance in NLQ explained by the jet or wind speed, and since this is not the case then the results suggest that the optomotor effect is not causing an increased frequency or concentration of layers in the UK. Note, however, that cloud cover and moonlight have not been taken into account in this analysis: such illumination conditions might influence the optomotor effect. Jet intensity explained just 2 % of the variance in NLQ in the linear regression ($p = 0.010$); furthermore in the two-way ANOVA, the largest amount of variance explained by just two factors was for temperature and jet intensity (Appendix D). Hence, the existence of the jet appears to have a weak positive effect on nocturnal layering.

The absolute temperature gradient result opposes the ceiling layer hypothesis (in the critical region) because the result showed that *low* NLQ values were associated with stronger reduction of temperature with height ($\partial T/\partial z << 0$). However, it is

worth noting that 19 % of nocturnal layers occurred outside the critical region (Chapter 5) at higher altitudes: so such upper layers might be ceiling layers, but the ones in the critical region appear not to be.

The stability of the atmosphere has been correlated with insect layers: the profiles of layers of noctuid moths in the USA (Wolf *et al.* 1986) were found to be associated with potential temperature gradients that were significantly more stable at layer altitude. Indeed, this is corroborated by the fact that in the critical region, positive potential temperature gradients were significantly associated with higher NLQ values (one-way ANOVA: $p = 0.003$). The vertical shear of wind speed in the critical region did not have an association with NLQ ($p = 0.511$): hence, it appears unlikely that insects can form layers based on the vertical shear of wind speed. It is worth noting now that the shear values calculated for the critical region might not always be representative because the critical region variables are a mean over four vertical levels. For instance, if a jet were centred in the critical region then the gradients would average to near zero due to a positive gradient below the jet maximum and negative gradient above the jet maximum. Therefore, it is possible that some significant results could be masked in the present analysis.

The combination of vertical gradients in wind speed and potential temperature provide an indicator of the turbulence of the local atmosphere using the Richardson number, Ri. In the critical region during this study, only 9 cases of non-turbulent air ($Ri > 0.25$) occurred. Non-turbulent cases gave a significant increase in NLQ of 1.4 compared to turbulent cases ($p = 0.015$). It seems unlikely that insects could respond directly to potential temperature, and even less likely to potential temperature gradient. Therefore, we might assume that any relationships could be due to insects' preference to fly in non-turbulent air. Alternatively, one can hypothesise that layers of any material (insects or otherwise) are more likely to persist in stable conditions and that in turbulent conditions, layers would be diffused vertically by the turbulence. Lagrangian modelling (Chapter 6) has been used to test this hypothesis further.

Studies of passive material with a heterogeneous source at the ground have shown that material can easily be layered in the vertical given that there is a vertical shear of wind direction; this effect is called **differential advection** (*e.g.* Bowen *et al.* 2000). Indeed, there is a small monotonic increase in NLQ from lower to higher shears (Figure 5·3); however, the difference is not significant ($p = 0.359$). This result suggests that layering is not affected by the vertical shear of wind direction. This indicates that the density of source populations of the migrants is homogenously distributed over large areas, as first postulated by Taylor (1973).

Vertical profiles of relative humidity often have a minimum near the altitude of insect layers; frequently, such minima in relative humidity also occur at the altitude of maxima in temperature (e.g. Wolf *et al.* 1986, Reynolds *et al.* 2005). Hence, it can be difficult to separate the two effects. The two-way ANOVA suggests that relative humidity is not significant and is a surrogate for temperature ($p = 0.720$, allowing for temperature). The physical relationship between temperature and relative humidity lead to investigation also of specific humidity. Specific humidity alone was positively correlated with NLQ ($p = 0.015$); but when allowing for temperature in the analysis, no significant relationship was found ($p = 0.647$). No literature exists to support a relationship between layering and humidity, indeed relative humidity and humidity mixing ratio were overtly refuted in the case of Wolf *et al.* (1986); and can be refuted here too.

It is worth noting that the gradient variables discussed above, as calculated from UM data, are less accurate than *T, u, q,* and RH (Chapter 3). Hence, any field campaigns that can accurately obtain gradient variables would elucidate further any relationships. Indeed, one method of conducting such experiments is via a numerical modelling exercise (see Chapter 6, where the effect of turbulence on layer intensity is investigated).

Finally, 19 % of radar-detected nocturnal layers occurred *above* the critical region and hence were not included in this analysis. Potential further work from this chapter could be the approach of analysing the meteorological conditions *at layer*

altitude in a systematic study (thus far only done on a case-study basis). Overall, the critical region analysis in this chapter has been very useful as a pioneering systematic analysis of layering (specifically in this chapter, nocturnal layers in the UK).

* * * * *

In summary, the results of the statistical analysis in the critical region suggest that the main meteorological explanatory variable for the formation and intensity of nocturnal layers of migrating moths in the UK is temperature. Atmospheric turbulence also provides some explanation of layer existence, and will be investigated further in the next chapter. No significant relationships between layer intensity and humidity or wind speed were found. Overall, temperature can be taken forward into a numerical modelling environment to elucidate further the effect of temperature on layers.

6: Stochastic Lagrangian insect modelling (SLIM) of nocturnal insect layers

6·1 Background

In previous chapters, the temporal and vertical variability of nocturnal insect layers has been explored, and the key mechanisms of their formation and maintenance have been hypothesised. This chapter will use information gathered in this thesis, and elsewhere, to model high-altitude insect flight in a stochastic Lagrangian insect model (SLIM). The aim will be to improve the understanding of the insect behaviours that lead to nocturnal insect layering. The model will predict layer altitude, spread, and cessation via representation of atmospheric turbulence and insects' response to the ambient temperature.

6·2 Introduction to modelling

6·2·1 Numerical flow modelling

The numerical model developed in this chapter is used to solve a mathematical equation that does not have an analytical solution. Numerical model output allows quantitative analysis to be made of layer characteristics such as altitude, duration, and intensity. 'Virtual' experiments will be performed in the numerical model's environment.

Numerical fluid dynamics models are typically based on a 'frame of reference' in the four space-time dimensions: co-ordinates x, y, z, and time t (Figure 6·3). Within this frame of reference, properties of a particle in the fluid can be monitored (such as temperature, velocity, *etc.*). Two general approaches are often

used for constructing numerical flow models. Firstly, by Eulerian modelling, where dynamic and thermodynamic environmental properties evolve in space and time (typically with use of the advection and diffusion equations, *e.g.* Holton 1992). This type of model can be run on a fixed Cartesian* geographical model-grid (its frame of reference). For example, the three orthogonal directions (x, y, z) are typically defined as being positive northward, eastward, and upward directions respectively. Particles to be modelled in Eulerian frames of reference can only be resolved via parametrization of a particle concentration variable located at each grid-point. Transportation of particles is effected by diffusion and advection between model timesteps (*i.e.* discrete steps in time, Δt).

A second approach to numerical flow modelling uses a Lagrangian frame of reference. In this technique, the trajectories of individual particles are traced through space and time. Lagrangian models often use 'stochastic Physics'†, such that each particle in a released ensemble has unique characteristics that have been randomly selected from within a pre-determined distribution. Turbulence is frequently explained by a stochastic approach because of the random nature of turbulence: turbulent fluctuations can only be represented statistically (unlike large-scale motions, which can be simulated deterministically).

The Lagrangian modelling technique is a more natural frame of reference for fluid dynamics in tracking individual particles. A disadvantage of the technique is that it is computationally expensive, because each particle must be traced individually from start to end. Eulerian frames of reference are less computationally expensive, but properties of individual particles cannot be modelled (only implied).

* The Cartesian co-ordinate system in 3D is three orthogonal axes: x, y, z. This is typically only used for small scales (*e.g.* less than tens of kilometre). On larger scales, the curvature of the Earth must be taken into account.

† Stochastic processes are those that contain inherent random processes.

6·2·2 Numerical models for aerial insect migration

In the simulation of aerial insect distributions, Eulerian modelling has been carried out by modifying numerical weather prediction (NWP) models. Long-distance (continental scale) insect transport has been modelled by adaptation of NWP models' diffusion and advection equations to account for 'swarming' (used here to mean coalescence of insects) and insect flight respectively (McCorcle and Fast 1989).

Eulerian modelling has been used in some studies on a more local scale: for example, radar observations of micro-insects in the convective boundary layer (Geerts *et al.* 2005a) were used to develop a mathematical model in which insects could respond to their environment by altering their vertical flight speed (Geerts *et al.* 2005b). The radar and model observations indicated that insects appeared to fly downwards when subjected to cold temperatures and/or in opposition to updraughts.

Trajectory analyses can be used to track insect paths, and are based on unmodified NWP data. Trajectory analyses have been the basis of most attempts at quantifying aerial insect migration since the 1960s (see the review by Scott and Achtemeier 1987). Such trajectory analyses can be used after an event to estimate from where insects have originated: this is called 'back-trajectory analysis'.

In Lagrangian models (sometimes called trajectory models) of insect migratory flight, it is necessary to prescribe a take-off time and duration—in nocturnal migration studies a dusk take-off lasting from twenty minutes to one hour is typically assumed—followed by upward flight (*e.g.* $0.2 - 2.0\ \mathrm{m\ s^{-1}}$). Subsequently, insects reach an altitude where they are assumed to have zero vertical flight and hence constant altitude. Subsequently, either (*i*) insects are transported only by atmospheric winds (Scott and Achtemeier 1987, Turner *et al.* 1999, Otuka 2000a, Gregg *et al.* 2001); or (*ii*) insect flight speed is simulated in trajectory models (Symmons and Luard 1982). A detailed analysis of the potential components of trajectory models revealed that the important components were found to be take-

off location and time, insect flight behaviour, and atmospheric motion (Rochester *et al.* 1996).

Components of velocity

A useful distinction has been made between two components of migratory insect flight: the *migration arena* (the wind field) and the *migration syndrome* (insect behaviour and physiology) (Rochester 1999). The migration arena comprises both the mean wind vector and evolving turbulent fluctuations (§1·4). Turbulence parametrization was identified as an important component in aerial biological transport by Nathan *et al.* (2005), however turbulent flow has seldom been considered in aerial insect migration models. The effect of turbulence on high-altitude insect migration will be studied later in this chapter.

6·3 Insect flight and response to environment

In this section, a review is made of the modelling of moth response to environmental conditions whilst in migratory flight. Firstly, an estimate of moth flight-speed is required for SLIM. Radar case studies (see Chapter 4) have indicated that high-flying medium-sized noctuid moths in the UK have horizontal flight-speeds (relative to the ground) in the range of $3-7\,\mathrm{m\,s^{-1}}$ (although their displacement speeds are often 2 or 3 times greater). Flight-speeds of $1.5-6.0\,\mathrm{m\,s^{-1}}$ have been recorded for noctuid moths in previous studies (Drake *et al.* 1981, Riley *et al.* 1983). Some individual moths have apparently been detected flying up to $10\,\mathrm{m\,s^{-1}}$ by radar (Rochester 1999); however, such high speeds are unlikely to be sustained for long.

Measurements of *vertical* flight speed in noctuid moths are few. Radar observations have been taken of the corn earworm moth (*Heliothis zea*) which show an initial climb rate of $1.7\,\mathrm{m\,s^{-1}}$ (Lingren *et al.* 1995), and of the armyworm moth (*Spodoptera exempta*) which show a climb rate of $0.4-0.8\,\mathrm{m\,s^{-1}}$ (Riley *et al.* 1981, 1983). Vertical flight speeds of moths in radar studies are typically

estimated via averages of a large number of insects flying together: thus, the vertical flight speeds of individuals might vary within the group.

Insects are poikilothermic (see §1.3) and therefore many insect processes are governed by temperature. Both wing-beat frequency and flight speed increase with ambient temperature for noctuid moths (Carpenter *et al.* 1981; see Figure 6·1). The data in Figure 6·1 are unique in providing laboratory data of flight speed variation with temperature, although the flight speeds appear to be rather low compared to other published data. Nonetheless, no flight occurred below 8 °C for the species studied, suggesting the presence of physiological temperature thresholds for flight. Previous studies of noctuids have estimated flight thresholds of $10-11\,°C$, with some individuals taking off in temperatures as low as $4-5\,°C$ after wing-shivering* (Taylor and Carter 1961, Taylor and Shields 1990, Coombs 1993). Take-off by noctuids in a migratory flight model (HEAPS) was only allowed on occasions when $T > 12\,°C$, among other parameters (Fitt *et al.* 1995). Asymptotes for flight speed and wing-beat frequency appear to be between 14 and 23 °C in the three species studied in Carpenter *et al.* (1981), although different for different species (Figure 6·1). These values seem to be distinct from the absolute physiological minima in the range $8-11\,°C$ (see above), and the asymptotes may be termed 'optimal flight temperatures' or 'temperature preferenda'.

Flight constraints produced by high-altitude temperature have previously been modelled via two approaches. Firstly, an overt flight ceiling can be used, whereby modelled insects stop flying at altitudes where temperatures are cooler than a ceiling threshold temperature (*e.g.* Symmons and Luard 1982, Otuka 2000b). Secondly, vertical flight speed can be prescribed as a function of ambient temperature throughout the entire flight (Achtemeier 1998, Geerts *et al.* 2006) and hence only by proxy is there a virtual ceiling for flight via the

* Thoracic muscle temperatures can be raised by shivering before flight, thus enabling flight at lower temperatures after shivering than if no shivering occurred.

parametrization of a preferential minimum where vertical flight speed becomes zero (*cf.* Figure 6·2).

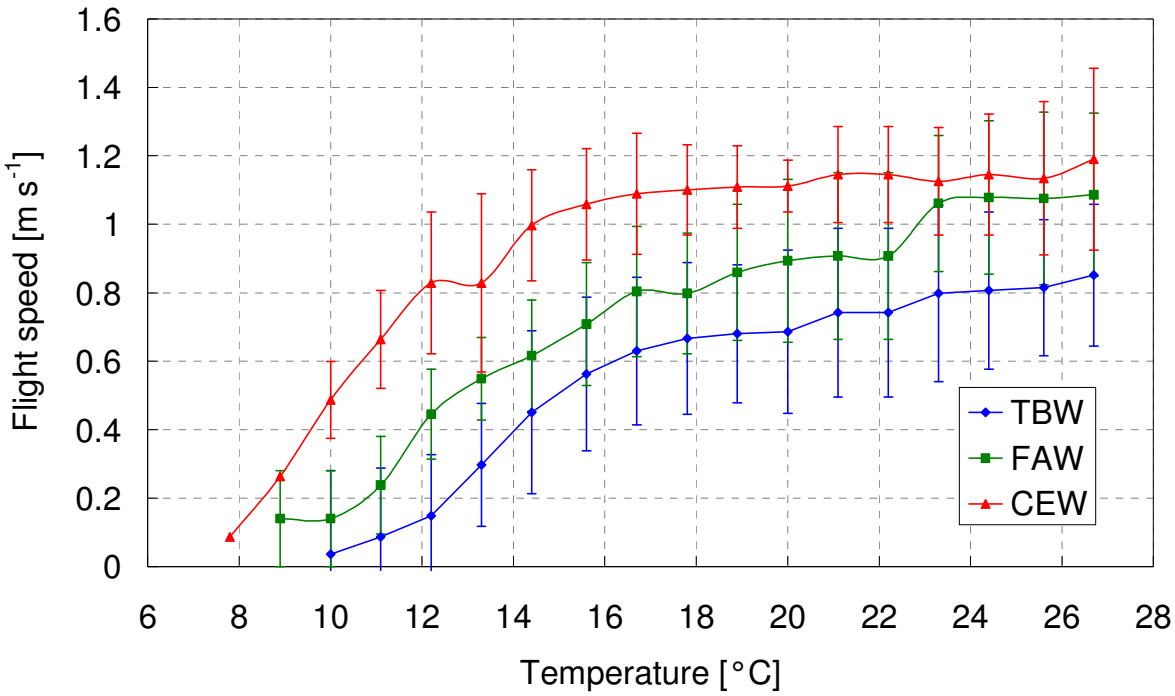

Figure 6·1 – *Flight speed against temperature for three species of noctuid moth: tobacco budworm (TBW), fall armyworm (FAW), and corn earworm (CEW). Vertical bars are the standard errors. Each point is a mean of 20 moths for the corn earworm and of 10 moths for the other species. Data taken from Carpenter et al. (1981).*

A good example of work incorporating both the wind field and insect behaviour was undertaken in Achtemeier (1998). A graphical schematic of the functional form is shown in Figure 6·2. The vertical flight speed was modelled as a function of ambient air temperature,

$$w_i = c(T_{amb} - T_0) + r_k \Delta w_i , \qquad (6\cdot1)$$

where w_i is insect vertical speed, T_{amb} is the ambient temperature, $c = 0.14\ \mathrm{m\ s^{-1}\ K^{-1}}$ (the rate of change of vertical speed with T_{amb}), T_0 is the temperature at which vertical flight speed is zero (a preferential minimum temperature), and Δw_i is a spread for weaker and stronger fliers of $0.5\ \mathrm{m\ s^{-1}}$. Each member of the ensemble has a unique speed, because r_k is a number randomly picked from $\pm 0.5\ \mathrm{m\ s^{-1}}$. Achtemeier's (1998) results clearly showed that an insect layer could be modelled in the case of a nocturnal temperature inversion; in fact, the layer was located above the temperature inversion.

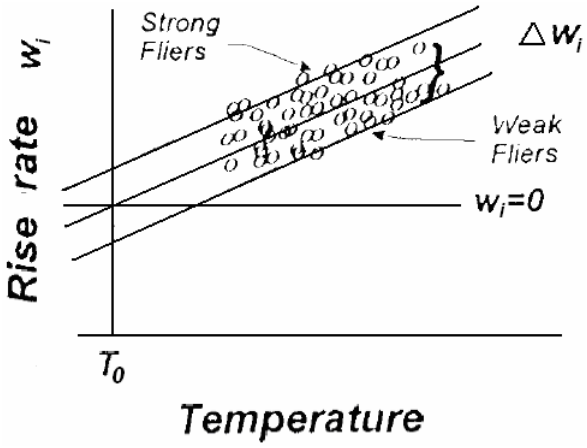

Figure 6·2 – *Rise rate (vertical flight) of insects as a function of ambient temperature (from Achtemeier 1998).*

Finally, it is worth noting that, on average, larger moths can fly in lower ambient temperatures than smaller moths due to their increased thoracic warming during flight (Bartholomew and Heinrich 1973, May 1979). Furthermore, it was observed in a nocturnal study that larger moths were more abundant in higher altitude traps than those traps nearer the ground (Taylor *et al.* 1979). Altogether, it seems that larger moths can fly to higher altitudes and in colder ambient temperatures; hence, this can form the basis of a spread in modelled flight characteristics based on moth mass (*cf.* weak/strong fliers in Figure 6·2).

6·4 Model equations and parameters

6·4·1 Introduction

The numerical model developed in this chapter, the stochastic Lagrangian insect model (or SLIM), is now described. It is a Lagrangian trajectory model for insect migratory flight, including both the migration arena (mean wind and turbulence) and aspects of the migration syndrome (moth flight behaviour, specifically the response to ambient temperature). In this model, an ensemble of insects is released into the same 'virtual' environment from a point in space and time. Resultant concentration profiles are then calculated from a vertical 1D cross-section through the ensemble.

Following Chapters 2 and 4, this thesis focuses on a particular family of moths that are a major constituent of the aerial nocturnal fauna in the UK: *i.e.* noctuid

moths Lepidoptera: Noctuidae (*cf.* Reynolds *et al.* 2005). There are approximately 400 species of noctuid moths in the UK (Chinery 1993), although the constituents of high-altitude layers during summer nights will be more limited in species diversity. Four noctuid species were assumed for SLIM that were previously identified as probable migrants in nocturnal layers detected by radar over the UK (Chapters 2 and 4; Reynolds *et al.* 2005): *Agrotis exclamationis* (Heart and Dart), *Xestia c-nigrum* (Setaceous Hebrew Character), *Mythimna pallens* (Common Wainscot), and *Autographa gamma* (Silver Y).

6·4·2 Model equation and setup

Displacement is a quantity that tracks insect position with time; it is a vector, $\underline{\mathbf{s}}$, comprising three orthogonal distances x, y, z (Figure 6·3). SLIM tracks the evolution of insect displacement with time from the initial position at $\underline{\mathbf{s}} = 0$.

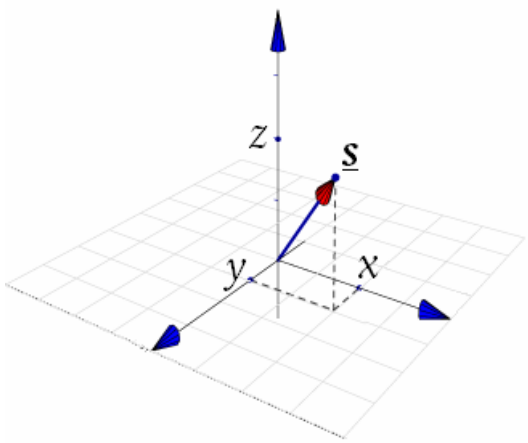

Figure 6·3 – *Schematic of the composition of the displacement vector.*

The evolution of the insect displacement vector is simulated using the following equation:

$$\Delta\underline{\mathbf{s}} = \underline{\mathbf{u}}\Delta t\,, \qquad (6\cdot2)$$

in which, $\underline{\mathbf{u}}$ is the velocity vector for speeds in three orthogonal directions (u, v, w). These speed components are defined as positive in the direction of the mean horizontal flow (u), cross-wise* to the mean horizontal flow (v), and

* Cross-wise means the component of wind in the horizontal plane that is in the direction perpendicular to mean horizontal flow.

upwards (w); and $\Delta\underline{\mathbf{s}}$ is the displacement within each timestep of the particle or insect. The trajectories in the model comprise a number of 'timesteps' (Δt)*. Time in the model is not a continuous quantity, but is represented as a number of small steps.

The total velocity vector varies as a function of time—$\underline{\mathbf{u}}(t)$—in the Lagrangian frame of reference and comprises four vectors:

$$\underline{\mathbf{u}}(t) = \underline{\mathbf{u}}_i(t) + \underline{\mathbf{u}}_{\mathrm{UM}}(t) + \underline{\mathbf{u}}'(t) + \underline{\mathbf{u}}_l(t), \qquad (6{\cdot}3)$$

where the subscripts of the parts are: i for insect flight; UM is model winds; l is low-frequency meanders; and the primed vector ($'$) is the turbulent fluctuation component (see §1.4.5). Low-frequency meanders are large mesoscale horizontal eddies acting cross-wise to the mean flow that produce a horizontal spread (often observed in studies of pollution/smoke plumes) and are observed particularly at night (Maryon 1998). The low-frequency meander term will not be considered in this model because there is little concern for the precise horizontal spread of moths; instead, the vertical profiles are of interest (in particular, insect layers).

The model was run in two dimensions only: the spatial dimension of altitude (z) and time (t). Hence, equation 6·2 becomes $\Delta z = w\Delta t$. Horizontal components were not modelled, since the main interest is in layers, which are a vertically-spaced phenomenon. Hence, the 'cross-wind' insect speed was assumed to be zero for all timesteps (*i.e.* $v_i = 0\ \mathrm{m\ s^{-1}}$). For this reason, the model provides no information on the common-orientation phenomenon (Riley 1975), but it was assumed that this horizontal-flight phenomenon would not alter the vertical profiles. The 'along-wind' insect speed (u_i) was not modelled, but instead assumed constant for all timesteps for each insect in the ensemble, and was randomly selected for each insect from a Gaussian distribution centred on $4\ \mathrm{m\ s^{-1}}$ (with a minimum value of $1\ \mathrm{m\ s^{-1}}$). The vertical flight speed, w_i, was modelled as being dependent upon ambient temperature (see §6·3). Two regimes from

* The Δ-notation (Greek letter: delta) is a mathematical term for discrete increments in a given quantity (in the above case, time).

equation 6·3 were thus defined: (*i*) insect flight (solved in SLIM), and (*ii*) free-fall (iteratively solved below in §6·4·3);

$$(i)\ w = w_i + w', \tag{6·4}$$

$$(ii)\ w = w_T + w', \tag{6·5}$$

in which w_T is the terminal velocity of a free-falling moth. For both cases the vertical atmospheric mean motion, w_{UM}, was assumed to be zero: since subsidence* is assumed small (*e.g.* $\sim 0.01\,\mathrm{m\,s^{-1}}$ in McIlveen 1992) and hence negligibly small compared to the other terms in equations 6·4 and 6·5.

For the purpose of SLIM, each insect was always assumed to be in the insect flight regime. The free-fall regime was only used to show what might happen to moths not engaged in flight.

Chapter 5 showed that once variance in NLQ (nocturnal layer quality) due to temperature had been analysed, none of the other meteorological variables studied explained any of the variance in NLQ. Hence, only the temperature response was modelled. No light-based behavioural cues have been used, such as moonlight, sun, or artificial light, except that insect take-off was set at a prescribed time, which was chosen based on field data—where moths take off at a certain irradiance† level (Riley *et al.* 1981). Any in-flight cues based on light would be rather complicated and beyond the scope of this thesis, but future work could incorporate research on the optomotor effect (see Götz 1972 and §1·3).

SLIM was used to investigate cases where there was significant dusk activity (see Chapter 3 for definition), which assumes that a sufficiently large population existed and that ground conditions were suitable for take-off. A take-off time of 19:30 hours was used because high-altitude nocturnal activity in the UK was detected by radar from this time onwards (see Chapter 3).

---

* The mean vertical downward atmospheric motion, typically over broad regions of synoptic scale under the influence of a high-pressure system.

† Defined in units of $\mathrm{W\,m^{-2}\,sr^{-1}}$, irradiance is a measure of light power per square metre per unit solid angle.

The *trapezoidal* timestepping scheme was used: both for its advantages of increased numerical stability and slightly increased accuracy (Appendix E). The timesteps used were set at least ten times smaller than the Lagrangian timescale for turbulence ($\Delta t \leq 0.1\tau_w$, see §6·4·5). This ensured that turbulent eddies were fully resolved (*e.g.* Maryon *et al.* 1999).

The three terms in the equations above (6·4 and 6·5) will be discussed in the subsequent sections.

6·4·3 Free-fall regime

If an insect stops flying it will fall; the free-fall speed is derived in this section and iteratively solved without the need for SLIM. Much of this free-fall derivation is standard and can be found in fluid mechanics textbooks, however the derivation is focussed here upon that needed to characterise the free-fall of moths in the atmosphere.

A particle in motion experiences a drag force (due to air resistance) that acts in the opposite direction of movement through a fluid. This causes a deceleration of the particle's speed, which would eventually slow the particle's speed to zero in the absence of further forces. A particle placed in the atmosphere experiences an initial downward acceleration under the force of gravity. Subsequently, the drag force—which is proportional to speed—increases until the drag and gravitational forces balance: then the particle is at its terminal velocity (*i.e.* it no longer accelerates towards the ground, but approaches it at constant speed). The gravitational force is given by:

$$F_g = m_i g\,, \tag{6·6}$$

in which, m_i is insect mass and g is gravitational acceleration. The drag-force at terminal velocity is given by:

$$F_d = \frac{\rho_a C_D A w_T^{\,2}}{2}\,, \tag{6·7}$$

in which ρ_a is air density, C_D is the dimensionless drag-coefficient, A is the cross-sectional surface area that is perpendicular to movement, and w_T is the terminal velocity.

Figure 6·4 – *Force diagram of a falling particle at terminal velocity, the downward gravitational force is balanced by the retarding (upward) drag force.*

At equilibrium, there is no net acceleration because the forces balance (Figure 6·4). The two opposing forces can be equated (6·6 and 6·7, and rearranged) to give a formula for the drag coefficient in terms of the terminal velocity:

$$C_D = \frac{2m_i g}{A\rho_a {w_T}^2}, \tag{6·8}$$

the drag coefficient (C_D) is dependent on both particle and fluid properties, and on particle speed:

$$C_D = 0.25 + \frac{24}{\mathrm{Re}} + \frac{6}{1+\sqrt{\mathrm{Re}}}. \tag{6·9}$$

This formula can be used over a wide range of Reynolds' number ($\mathrm{Re} \sim 10^{-5} - 10^{4}$, White 1974). Re is the dimensionless ratio of inertia forces to viscous forces (for full details see fluid dynamics textbooks, such as Pedlosky (1987)). Reynolds number is expressed here as:

$$\mathrm{Re} = \frac{w_T D}{\nu}, \tag{6·10}$$

in which, ν is the kinematic viscosity of air and D is the insect (particle) diameter $\left(D = \sqrt{4A/\pi}\right)$. In general, Reynolds number indicates the fluid response to a particle moving through the fluid. For viscous fluids (*e.g.* treacle) Re is typically small. In the atmosphere, most particles generate turbulence in their wake because inertial forces dominate over viscous forces. Hence, for a closed-wing moth in free-fall, Re ~ 7000; for aphids Re ~ 100. Both insects are in the turbulent wake regime.

Equating equations 6·8, 6·9, and 6·10 gives an implicit equation for w_T which we wish to solve:

$$\frac{2m_i g}{A\rho_a {w_T}^2} - 0.25 - \frac{12\nu}{w_T\sqrt{A/\pi}} - \frac{6}{1+\sqrt{\frac{2w_T\sqrt{A/\pi}}{\nu}}} = 0\,. \qquad (6{\cdot}11)$$

This equation calculates the free-fall of moths in the atmosphere. Since it cannot be solved analytically, iterative methods are required.

In the solution for w_T, the specific values of m_i and A are required for moths. Hence, the body dimensions of nine specimens of each of the four common species of noctuid were obtained from a preserved collection at the Plant and Invertebrate Ecology Division of Rothamsted Research (§2·3·3). The cross-sectional area was assumed to take two principal forms in free-fall: open and closed wings (Table 6·1).

Table 6·1 – *Mass and cross-sectional area for four species of noctuid moth (consistent with Table 2·3). Values shown are mean ± standard deviation for nine moths of each species.*

	A. exclamations	*A. gamma*	*X. c-nigrum*	*M. pallens*
Mass, m_i [mg]	194 ± 23	142 ± 16	171 ± 22	151 ± 24
Body cross-section, A_b [mm²]	67.4 ± 5.6	47.5 ± 6.8	49.6 ± 9.4	45.6 ± 8.6
Total moth cross-section with opened wings, A_w [mm²]	416 ± 38	361 ± 58	355 ± 41	312 ± 45

In fact, values of open-winged cross-sectional area, A_w, and insect mass, m_i, are closely correlated: hence, A_w can be estimated from m_i for noctuid moths (Figure 6·5). Using equation 6·11, the terminal velocity for a range of noctuid moths was calculated. The linear-log fitted lines can be used as an approximation to estimate w_T (Figure 6·6). Terminal velocities of noctuid moths were found to be $10-12\,\mathrm{m\,s^{-1}}$ if wings were closed and $3-5\,\mathrm{m\,s^{-1}}$ if wings were open. Fitted relationships can be used to estimate w_T from m_i alone:

$$w_{T,c} = 6.26 {m_i}^{0.12}, \qquad (6{\cdot}12)$$

$$w_{T,o} = 0.92 {m_i}^{0.31}, \qquad (6{\cdot}13)$$

for closed and open wings respectively; m_i is in mg. The measurement technique is summarised in Appendix F.

These terminal velocities are large compared to the nocturnal turbulence that noctuid moths will encounter. Any large insects in the atmosphere—particularly noctuids at night—would quickly fall out of the atmosphere. Thus, the moths cannot be held up by the weak nocturnal turbulence and any noctuid moths in the nocturnal atmosphere must be maintained at altitude because of their own flight power. The ratio of terminal velocity to turbulence is discussed in the turbulence section below (§6·4·5). In addition to estimating the values of free-fall speeds for moths, w_T is also needed in later sections to model more accurately the effect of a massive particle in the flow: *i.e.* for the adjustment of the turbulent velocity components.

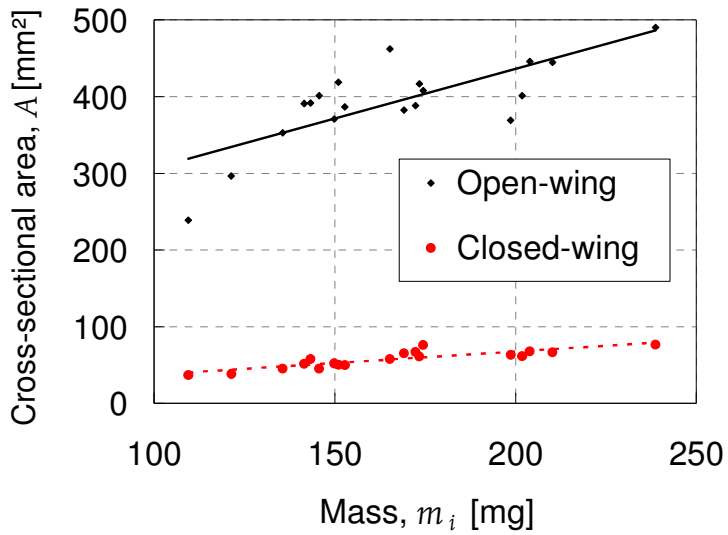

Figure 6·5 – *The cross-sectional area (A_w or A_b for open and closed wings respectively) against moth mass (m_i) for 18 individual noctuid moths. Linear regressions are shown (with R^2 values of 60 % and 70 % respectively).*

6·4·4 Insect-flight as a function of ambient temperature

The vertical insect flight term was modelled as a function of ambient temperature and insect mass. This is analogous to Achtemeier's function (Figure 6·2). The equation was used for all timesteps for each insect in the ensemble (*i.e.* from the surface, through migration, to landing):

$$w_i = \gamma_T \left(T_{amb} - T_0\right) + \gamma_m \left(m_i - \overline{m}\right), \qquad (6·14)$$

where the terms of the equation are defined in the following paragraphs of this section. These parameters have sensitivity tests performed upon them later in this chapter.

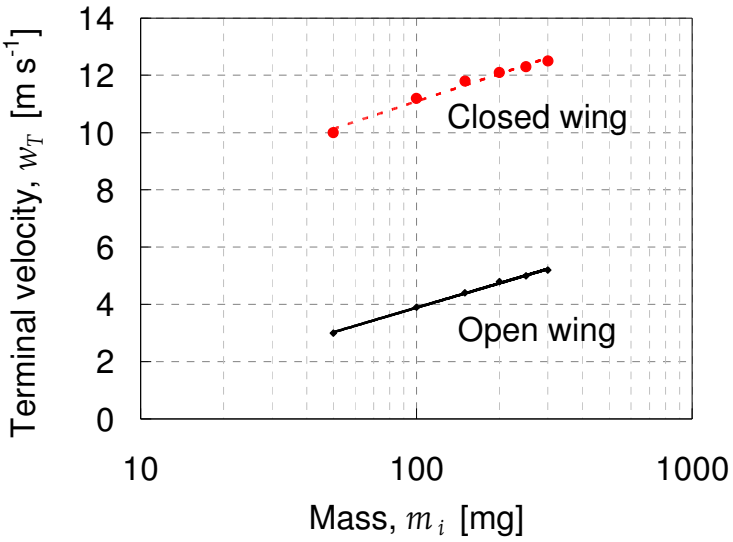

Figure 6·6 – *Terminal velocity against moth mass.*

The preferential minimum temperature, $T_0 = 15\,°\text{C}$, is the temperature at which vertical insect speed is zero (15 °C was chosen following Chapter 4). The ambient temperature, T_{amb}, is the temperature experienced by the insect, and is a function of altitude and time. This value was obtained from the UM data that was linearly interpolated in space and time to where the model-insect was flying.

The rate of change of vertical insect speed with the ambient temperature, $\gamma_T = 0.14\,\text{m s}^{-1}\,\text{K}^{-1}$, was the same as Achtemeier (1998) and is the gradient of the lines in Figure 6·2. It is not known if this value is appropriate in UK cases, because different insect species might have a different γ_T. However, a brief calculation can hone an estimate suitable for UK cases. The maximum UK temperature at the Earth's surface at sunset each year does not exceed 30 °C at Reading, which is an inland site representative of Southern England (from unpublished data records from Reading University Atmospheric Observatory). Therefore, assuming $m_i = \overline{m}$ and using $T_0 = 15\,°\text{C}$ then the slope of $\gamma_T = 0.14\,\text{m s}^{-1}\,\text{K}^{-1}$ is needed so that $w_i > 2\,\text{m s}^{-1}$ only for $T_{amb} > 30\,°\text{C}$. Since moth

speeds of $w_i > 2\,\mathrm{m\,s^{-1}}$ have never been reported, then the given gradient of γ_T seems suitable and consistent with the climatic range of temperatures.

For each member of the ensemble of moths, insect mass, m_i, was randomly picked from an even distribution between 50 and 300 mg. This was used in combination with γ_m (see below) to model the effect that larger insects have faster flight at a given temperature. It is also the case that larger moths can fly in lower temperatures than smaller moths can due to thermal inertia (§1·3). The mean noctuid moth mass was $\overline{m} = 175\,\mathrm{mg}$.

A rate of change of vertical insect speed with insect mass of $\gamma_m = 1000\,\mathrm{m\,s^{-1}\,kg^{-1}}$ was assumed. This gave a range of flight speeds based on noctuid moths for the same range as Δw as in Figure 6·2 and Achtemeier (1998).

6·4·5 Turbulence parametrization

Background

The parametrization of turbulence is based on NAME (**N**umerical **A**tmospheric-dispersion **M**odelling **E**nvironment, see Maryon *et al.* 1999 and §3·1·3), using the Langevin equation (Maryon *et al.* 1999, Aylor and Flesch 2001). The Langevin equation expresses the rate of change of velocity with time as a result of changes in acceleration, in its fundamental form it is expressed as:

$$\frac{\mathrm{d}w}{\mathrm{d}t} = -aw + b\xi(t), \tag{6·15}$$

where a is a damping coefficient, $\xi(t)$ is a random function, and b is a magnitude coefficient. This directly follows from Newton's second law:

$$\underline{\mathbf{F}} = \frac{\mathrm{d}\underline{\mathbf{U}}}{\mathrm{d}t}, \tag{6·16}$$

where $\underline{\mathbf{U}}$ is the velocity and $\underline{\mathbf{F}}$ is the force. Changes in speed with time are the result of accelerations. The Langevin equation has two components. Term 1 is the 'memory term' $(-aw)$ and is an exponential decay of velocity from the initial

acceleration due to viscous forces (Figure 6·7). Term 2 ($b\xi(t)$) is a random/stochastic/generation term using a random-walk* technique (Figure 6·8). Random walks represent changes between timesteps where the speed and direction are randomly picked from a distribution (*cf.* Einstein's work on Brownian motion).

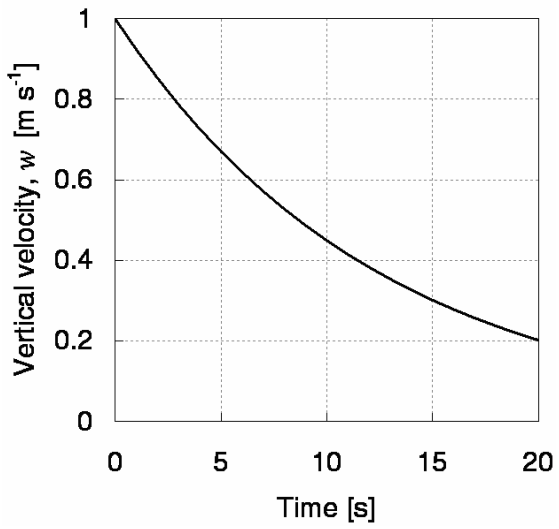

Figure 6·7 – *A schematic decorrelation of the evolution of vertical velocity if only the memory term of the Langevin equation is modelled.*

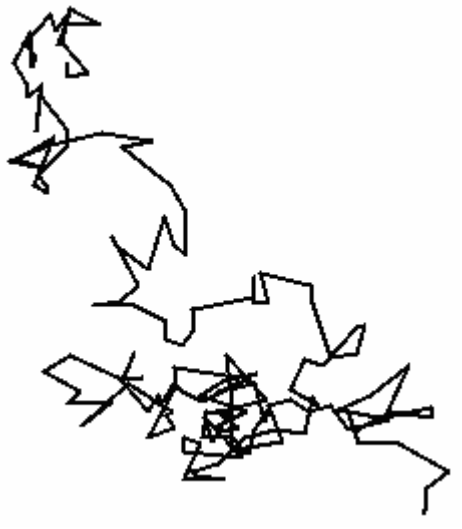

Figure 6·8 – *An example of a random walk with time in 2D space.*

Atmospheric application

In application to atmospheric turbulence, the forward-Euler (see Appendix E for timestepping methods) version of the Langevin equation at the new timestep, $w'(t+1)$, is:

$$\underset{\text{turbulent fluctuation}}{w'(t+1)} = \underset{\text{memory term}}{\left(1-\frac{\Delta t}{\tau_w}\right)w'(t)} + \underset{\text{generation term}}{\sigma_w\left(\frac{2\Delta t}{\tau_w}\right)^{1/2}\xi} \quad . \qquad (6\cdot17)$$

* This method (also known as a drunkard's walk, Brownian motion, a Markov chain, random displacement, or Monte Carlo method) means that at each timestep the direction and distance to the new location from the previous one is random (within a given distribution).

The Lagrangian timescale* is represented by τ_w, the standard deviation of the vertical wind speed is σ_w (see Figure 1·6 for an Eulerian time-series of the turbulent fluctuation of wind speed), and ξ is a number picked randomly from a Gaussian distribution with unit variance. The first term is the memory term; the second term is the generation term.

It is worth noting that $\Delta t < \tau_w$ is required for numerical stability so that—neglecting turbulence generation—the memory component satisfies decay: $w'(t+1) < w'(t)$, *i.e.* decay term always decreases. When the memory term is small (*i.e.* as $\Delta t / \tau_w$ rises to 1), the simulated turbulence field is not correlated at subsequent timesteps. When the memory term is large (*i.e.* as $\Delta t / \tau_w \to 0$) the turbulence field changes more slowly with time and hence there is a high correlation of the turbulence between timesteps.

Turbulence profiles

The Langevin equation requires parametrization for the specific conditions it is used in: in particular the Lagrangian timescale, τ_w, and the standard deviation of vertical wind speed, σ_w. The vertical profiles of τ_w and σ_w can either be simulated as homogeneous (where constant values are used with altitude) or inhomogeneous (where profiles of τ_w and σ_w are simulated as a function of altitude: defined dependent on atmospheric stability). Homogeneous turbulence profiles were used in SLIM (from Panofsky and Dutton 1984, Maryon *et al.* 1999):

$$\sigma_w = u_* \alpha, \qquad (6{\cdot}18)$$

in which $\alpha = 1.25$ for neutral conditions and $\alpha = 0.65$ for stable conditions (see §1·4·3 for stability definitions). Stable conditions were assumed for all nocturnal cases where a surface temperature inversion existed. Following NAME conventions (Maryon *et al.* 1999), τ_w was set to 100 s above the boundary layer. The rationale for this was that turbulent statistics in the residual layer are not well known, but 100 s is used in the free-troposphere in NAME. Hence, the

* The Lagrangian timescale is a timescale over which turbulence is correlated; also called the Lagrangian integral timescale, since it is the integral of the Lagrangian velocity correlation.

residual layer is treated as if it were the free-troposphere: this assumes that there is no effect from the surface on the atmosphere above the inversion (see §1·4·7), which is reasonable given the lack of coupling by turbulence after dusk. Profiles of τ_w and σ_w are shown (Figure 6·9, Figure 6·10). The inversion depth is z_i, thus the stable boundary layer top is at $z/z_i = 1$. Different turbulent statistics are used within and above the stable boundary layer.

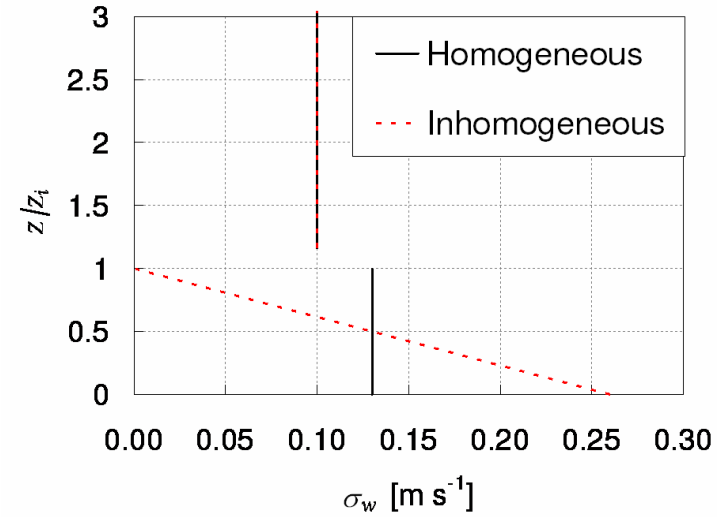

Figure 6·9 – *Stable turbulence profiles for σ_w using the NAME parametrization. The inversion top is z_i.*

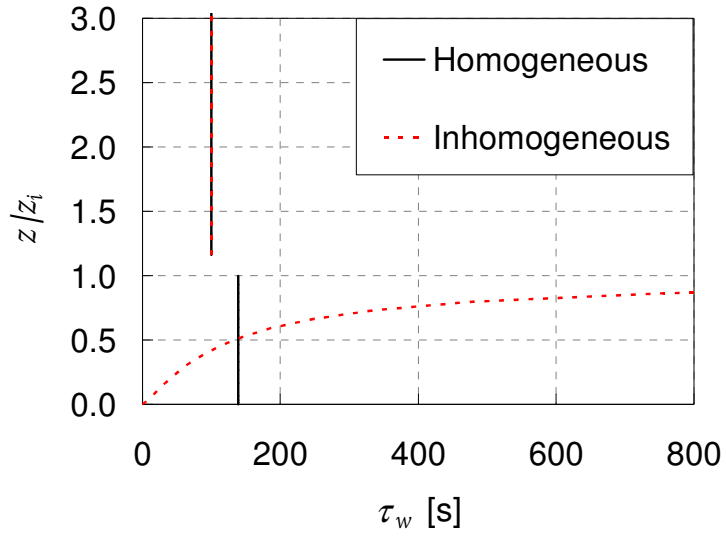

Figure 6·10 – *Stable turbulence profiles for τ_w using the NAME parametrization. The inversion top is z_i.*

Inhomogeneous profiles of σ_w (Figure 6·9, Figure 6·10) within the stable boundary layer can be defined (*e.g.* Panofsky and Dutton 1984). Above the stable

boundary layer (*i.e.* above $z/z_i = 1$) the constant values that are used in the free troposphere were used in the residual layer (Figure 6·9, Figure 6·10). Given that (*i*) moth speeds are greater in magnitude than the turbulent velocities during stable conditions and (*ii*) insect migrations tend to occur above the stable boundary layer (*i.e.* in the residual layer at altitudes above *c.* $100 - 200$ m), the sensitivity of resulting results to a more realistic turbulence profile is assumed to be small. Hence, the homogeneous profiles of τ_w and σ_w were assumed in SLIM.

Adjustments to turbulence parametrizations

Particles are often defined in fluid dynamics models as either massless or massive. Massless particles have negligibly small mass such that they are fluid tracers, *i.e.* their mass does not affect the way the particle moves in the flow. Particles are denoted 'massive' if they do not follow fluid trajectories. For NAME, the theory for alteration of movement in the flow due to a particle's mass has been developed with respect to airborne particulates with size of the order of $0.1 - 100\ \mu$m (Apsley 1989, Maryon 1997, Apsley *et al.* 2005). In SLIM, the insects studied are comparatively large, their size being of the order of a centimetre. Adjustment was made of τ_w and σ_w to account for the insects' mass (described below).

Particles moving through a turbulent medium experience turbulent decorrelation (*e.g.* Figure 6·7) at faster or slower rates depending on the rate of movement of the particle through the fluid. Three free-fall regimes have been defined (Stout *et al.* 1995, Figure 6·11). Very light particles ($\sigma_w >> w_T$) follow atmospheric motion, resulting in 'particle suspension': *i.e.* the particles do not fall to the ground, but instead are transported around by turbulent eddies as if they were fluid elements. For medium-sized particles ($\sigma_w \approx w_T$), the trajectories show particles falling in a 'preferential sweep' regime: these medium-sized particles are little affected by small eddies, but are still swept by larger eddies. Very massive particles' trajectories ($\sigma_w << w_T$) are in the 'eddy-crossing' regime: in the extreme limit

falling vertically downwards, thus cutting through turbulent eddies and being unaffected by them.

Noctuid moths (with size of the order of centimetres) free-fall in the atmosphere in the eddy-crossing regime, due to their large terminal velocities (§6·4·3). By contrast, the movement of small insects—such as aphids in the updraughts of a convective boundary layer—is typically in the suspension regime. Perhaps intermediate insects of size 1–10 mg (*e.g.* lacewings) are likely to free-fall in the preferential sweeping regime.

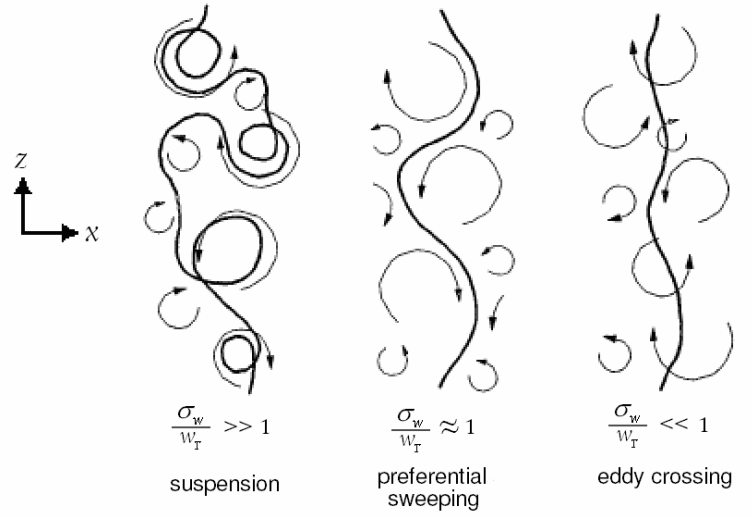

Figure 6·11 – *Three regimes of particles in free-fall through turbulent flow are shown. The ratio used for the definition is* σ_w *(standard deviation of vertical velocity) to* w_T *(terminal velocity of particle). Adapted from Stout et al. 1995. The diagram is not to scale, but plotted as altitude (z) against a generic horizontal dimension (x).*

The effect of free-fall on the turbulent statistics can be calculated. A falling particle effectively reduces the Lagrangian timescale by increasing the rate of decorrelation with itself (Maryon *et al.* 1999). A correction is applied that is larger for particles that are more massive:

$$\tau_w^* = \frac{\tau_w}{\sqrt{1 + w_T^2 / \sigma_w^2}}, \qquad (6\cdot19)$$

in which τ_w^* is the corrected Lagrangian timescale. The above equation can be applied for moths in free-fall.

The effect of turbulent decorrelation calculated in 6·19 is due to eddy-crossing caused by free-fall. Eddy-crossing can also occur due to insect flight. Thus, a correction to τ_w for insects in flight can be made by the replacement of w_T with $|\underline{\mathbf{u}}_i|$ in equation 6·19 to represent eddy-crossing due to insect flight:

$$\tau_w^* = \frac{\tau_w}{\sqrt{1 + |\underline{\mathbf{u}}_i|^2 / \sigma_w^2}}. \qquad (6{\cdot}20)$$

The magnitude of the entire insect vector ($|\underline{\mathbf{u}}_i|$) was chosen (not just the vertical component as one might initially expect). This is because the temporal decorrelation of turbulence with itself occurs due to insect flight in all 3 orthogonal directions (x, y, z).

A second adjustment to the turbulent statistics is required. Due to the increased inertia of massive particles, a moth in a turbulent medium is less affected by the forces acting on it by turbulent accelerations than a less massive particle would be. The turbulence term for large particles in the flow is effectively low-pass filtered*, *i.e.* large particles are only influenced by lower frequency eddies. The turbulence statistics were thus altered for inertial effects as follows (following Maryon *et al.* 1999):

$$\sigma_w^* = \frac{\sigma_w}{\sqrt{1 + \tau_p / \tau_w^*}}, \qquad (6{\cdot}21)$$

in which σ_w^* is the standard deviation of vertical velocity corrected for an inertial particle. The 'particle time constant', τ_p, is given by

$$\tau_p = \frac{w_T(\rho_i - \rho_a)}{g\rho_i}, \qquad (6{\cdot}22)$$

where ρ_i is particle (or insect) density. Massless particles have $\tau_p = 0$ (*i.e.* the eddy-crossing factor, σ_w^*/σ_w, is 1 and thus σ_w remains unchanged) and hence the particle trajectory is the same as a fluid tracer. Massive particles have larger values of τ_p and thus $\sigma_w^* < \sigma_w$, *i.e.* the particle's inertia leads to a reduction in its response to the ambient turbulence.

* A low-pass filter is where low-frequency turbulent fluctuations influence particle trajectories, but high-frequency fluctuations do not affect the trajectories.

For this model, it is assumed that τ_p is representative for an insect in both regimes (*i.e.* replace terminal velocity, w_T, by insect flight speed, $\left|\underline{\mathbf{u}}_i\right|$, when insect is flying).

SLIM assumes a constant atmospheric density of $\rho_a = 1.2\,\mathrm{kg\,m^{-3}}$ for all time and altitudes. Using the atmospheric equation of state ($\rho_a = p/RT$), the atmospheric density variation within the lowest kilometre of the atmosphere is $\rho_a = 1.0 - 1.3\,\mathrm{kg\,m^{-3}}$. However, since $\rho_i >> \rho_a$, equation 6·22 can be simplified to:

$$\tau_p \approx \frac{w_T}{g}. \qquad (6\cdot23)$$

* * * * *

Overall, in this section the modelling of the turbulence statistics used in SLIM have been summarised. Specifically, the quantitative adjustment of the turbulent statistics for insect size is required to model more realistic trajectories.

6·5 Results

SLIM's naturally mixed state was tested, then layers were simulated by modelling vertical insect flight as a function of temperature, testing of model input parameters was then carried-out and finally the results from case study simulations were validated.

6·5·1 A well-mixed case

Passing the well-mixed criterion (Thomson 1987, Rodean 1996) confirms that particles that are initially well mixed in the vertical will remain so. This was used to confirm that no spurious profile features (such as layers) occurred in the resulting particle profiles calculated by SLIM. One method of assessing the distribution of particles in the simulated profile is by using a chi-square statistical test (Fowler *et al.* 1998).

$$\chi^2 = \frac{s^2}{\bar{x}}(N-1), \tag{6·24}$$

in which s^2 is the profile variance, $\bar{x}$ is the profile mean, and N is the number of levels in the profile. Chi-square (χ^2) values are used to interpret the distributions as either (*i*) layered (clustered, contagious, clumped, or grouped); (*ii*) random (well mixed or jumbled); or (*iii*) regular (uniform, even, or ordered). This is shown in Figure 6·12. The test considers the total number of particles, *N*.

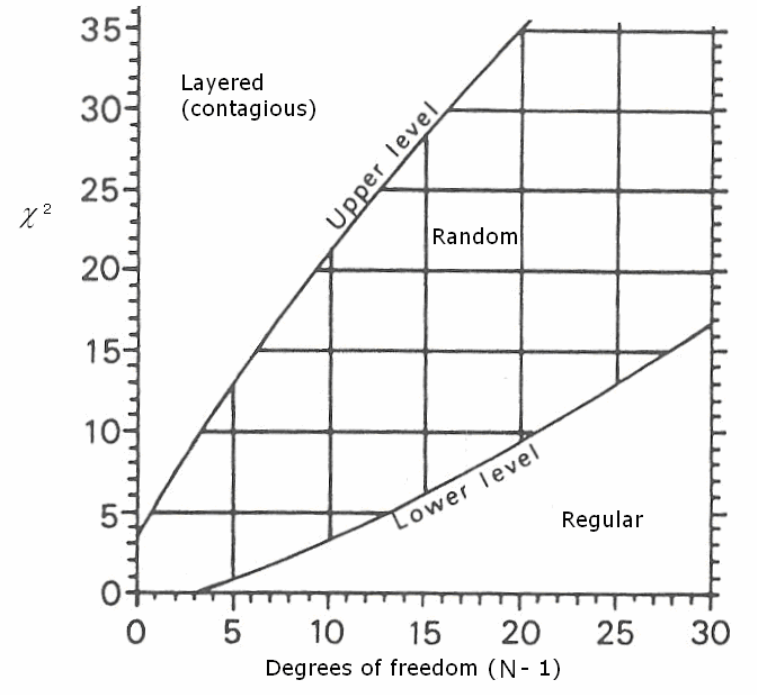

Figure 6·12 – χ^2 *against the degrees of freedom* $(N-1)$. *95 % confidence zones are shown for distributions that are defined as contagious, random, or regular. From Fowler et al. (1998).*

For this test, SLIM was initialised with 200 particles that were regularly spaced within 1 km of altitude from the ground. Reflective conditions were assumed at both virtual boundaries: a 'lid' at the upper boundary, and the Earth's surface as the lower boundary. At the lid, any particle that would have escaped the 1 km domain during a timestep was forced to undergo a perfect elastic collision with the lid: *i.e.* the particle was brought back beneath the lid by the distance it was due to be above the lid in that timestep and its vertical speed was reversed. Similarly, at the bottom boundary, such that the perfect elastic collision gave both z and w values inverted signs.

Particles were massless: only turbulence was modelled. There was no insect flight or free-fall. Model parameters were set at $\Delta t = 10\,\mathrm{s}$, $u_* = 0.2\,\mathrm{m\,s^{-1}}$, and homogeneous stable turbulence profiles were used with $\sigma_w = 0.65u_*$ and $\tau_w = 100\,\mathrm{s}$.

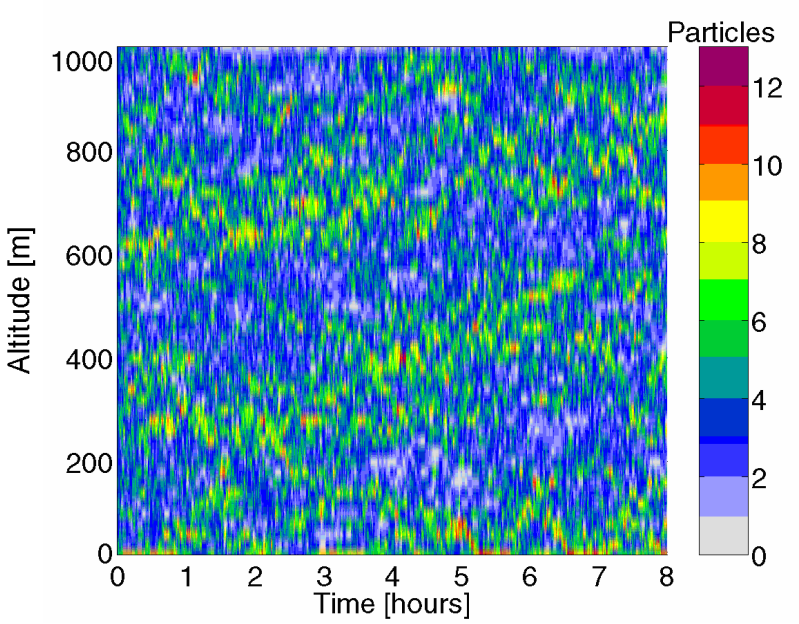

Figure 6·13 – *Particle concentration (particles per twenty-metre vertical bin) for altitude against time. Fifty equally spaced vertical bins were used. N = 200.*

The evolution of the particle concentration for 8 hours shows the distribution of particles in time and altitude (Figure 6·13), with 20 m vertical sampling bins. Qualitatively, no obvious collection of particles occurred anywhere. The particles were tested for contagiousness (*i.e.* spurious layering). The χ^2 time-series is shown in Figure 6·14. Initially, the particles were equally spaced over the vertical domain (hence the low χ^2 values that indicated a regular distribution at the start). Over the time-scale of the test, the profile's χ^2 value fluctuated between 30 and 80, *i.e.* within the random classification. Thus, this test showed that the turbulence parametrization kept particles well-mixed (in the vertical) with time: thus the turbulence scheme will not introduce spurious layering.

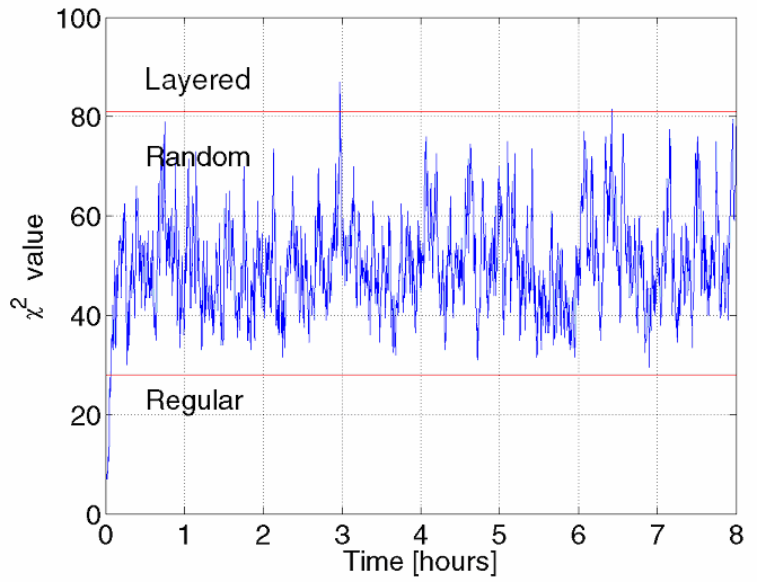

Figure 6·14 – χ^2 *against time for the well-mixed case. Superimposed are lines separating regimes of regular, random, and layered distributions at the 95 % confidence interval.*

6·5·2 Sensitivity studies

Sensitivity studies were carried out in order to identify values of model parameters. These tests were carried out in relation to case study A (Chapter 4). The reason this case was chosen is that it demonstrates the main hypothesis (temperature) for explaining the presence of nocturnal insect layers in the UK (Chapters 4 and 5; Reynolds *et al.* 2005), *i.e.* that the choice of this case means the results of the sensitivity studies are most relevant to cases similar to case study A.

All sensitivity tests assumed the same basic common model parameters, as follows. An ensemble of 200 moths was released at 19:30 UTC (defined as $t = 0$) and flight simulated for 8 hours. Where included, each moth's mass was randomly picked from a uniform distribution between 50 and 300 mg (*cf.* Figure 4·11). The Earth's surface was set as an absorbing boundary: *i.e.* any moth that landed on the ground would not take off again (and would hence cease flight for that night). There was no upper model-bound on the altitude to which moths could fly. A model timestep of $\Delta t = 10$ s was used.

Test for preferential minimum temperature (T_0)

The aim of this test is to assess the sensitivity of the model to variations in T_0. Vertical flight was modelled by including only insect flight and no turbulence: $w = w_i = \gamma_T (T_{amb} - T_0)$. A constant value of $\gamma_T = 0.1\,\mathrm{m\,s^{-1}\,K^{-1}}$ was assumed. The preferential minimum temperature is the temperature at which $w_i = 0$; hence, as T_0 reduces most of the lower altitudes are accessible for insect flight. Large T_0 values imply a restriction on insect flight, and for very large values there is no flight at all (*i.e.* when T_0 is warmer than the dusk surface temperature). Five T_0 values were tested and the resulting trajectories plotted and compared with the layer altitude measured in case study A (Figure 6·15). The trajectories are smooth because there is no turbulence and because the UM temperature data have been interpolated in space and time between model UM values.

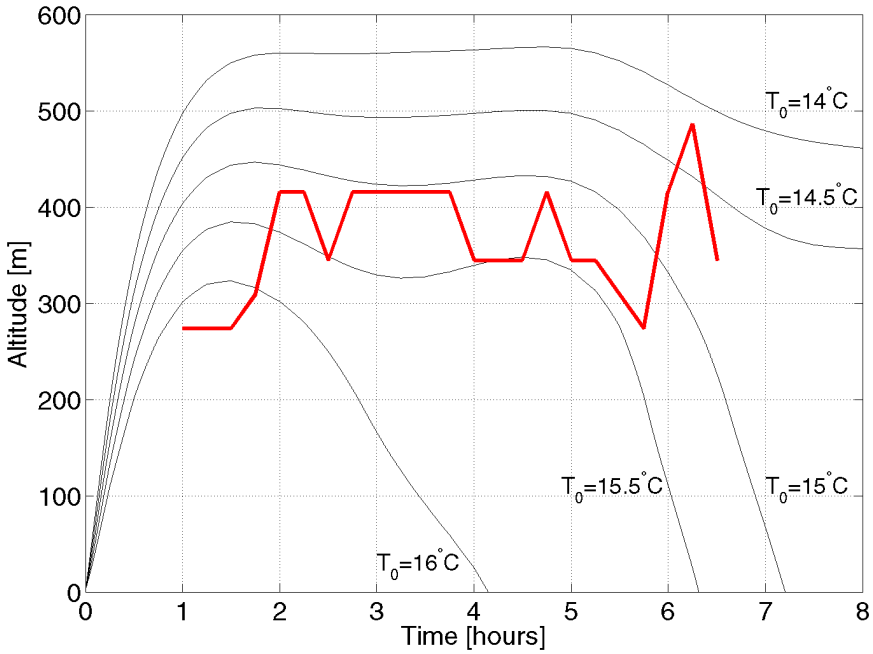

Figure 6·15 – *Altitude against time for trajectories of five different T_0 values. Superimposed is a thick red line that is the radar's diagnosed layer central altitude for 22 August 2000 at Malvern (cf. Figure 4·1).*

$T_0 = 16\,°\mathrm{C}$ was too warm because the trajectory only rose to 310 m before returning to the ground after just 4.1 hours. $T_0 = 14\,°\mathrm{C}$ gave a trajectory that rose too much (to 570 m) and the trajectory did not return to the ground during the 8 hours. The best-matched trajectory to the radar layer was $T_0 = 15\,°\mathrm{C}$ for this case.

Insect flight is clearly sensitive to variations in T_0 of *c.* 1 °C. It follows that there is also sensitivity of insect flight altitude to T_{amb}, since the vertical flight speed is proportional to $(T_{amb} - T_0)$. As the preferential minimum temperature was increased, so the layer decreased in altitude. Furthermore, ascent time* was more rapid for lower preferential minimum temperatures.

Test for the rate of change of vertical speed with ambient temperature (γ_T)

For this test, vertical flight was defined as $w = w_i = \gamma_T(T_{amb} - T_0)$, with a constant value of $T_0 = 15$ °C. Larger values of γ_T (*i.e.* large rates of change of vertical speed with change in ambient temperature) allow a faster response to ambient conditions, whilst smaller γ_T means that the insect responds more slowly to its ambient conditions and flies more slowly. Hence, *a priori* there is an expectation that small γ_T values will lead to slower ascent and a lower layer than large γ_T values. If insect rise too slowly, then the atmospheric temperature cools and thus the layer will be at a lower altitude.

A range of γ_T values were tested, the resulting maximum trajectory altitudes over the eight hour period were recorded (Figure 6·16). Large values of γ_T gave layers at higher altitude. There is a change in behaviour beyond $\gamma_T = 0.05\ \mathrm{m\ s^{-1}\ K^{-1}}$, where layer altitude did not vary substantially with increasing γ_T. Ascent was slower for smaller γ_T (Figure 6·17). An asymptote was found that implied that $\gamma_T > 0.1\ \mathrm{m\ s^{-1}\ K^{-1}}$ did not result in a faster attainment of layer cruising altitude.

* Defined in SLIM as the time of the first occasion where the displacement vector had a downward component in a timestep (*i.e.* $\Delta z < 0$).

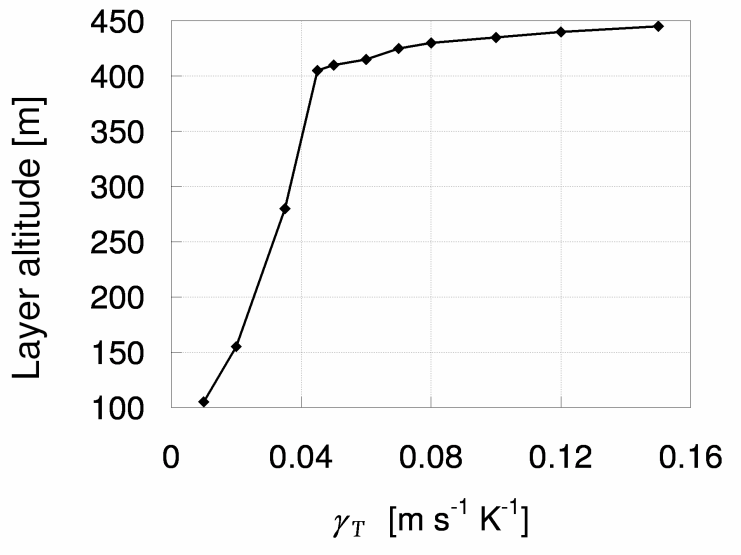

Figure 6·16 – *Sensitivity of maximum layer altitude to* γ_T.

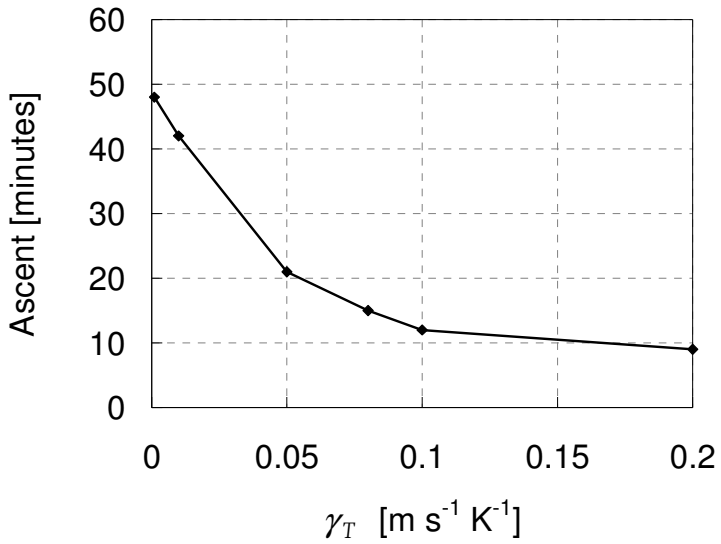

Figure 6·17 – *Sensitivity of ascent time to* γ_T.

Test for layer intensity: turbulent spread

From equation 6·17, it is not straightforward *a priori* to predict what effect the Lagrangian timescale (τ_w) will have on layer intensity (layer intensity is defined as the fraction of the profile that is in the most populous 'virtual'* radar range-gate), due to opposing effects. As $\tau_w \to \infty$, the generation term tends to zero, but also there is no decay: hence existing layer intensity will not alter. As $\tau_w \to 0$, the

* SLIM data have been binned into the same vertical samples as the radar data.

generation term becomes large, but so does the decay. Hence, at the outset, there appears to be opposing effects and perhaps the sensitivity of layer intensity to τ_w will not be large.

In the test for sensitivity of layer intensity to the Lagrangian timescale (τ_w), vertical movement was set to include insect flight and turbulent fluctuations: $w = w_i + w'$. Parameters were set to $T_0 = 15\,°\mathrm{C}$, $\gamma_T = 0.1\,\mathrm{m\,s^{-1}\,K^{-1}}$, and $\sigma_w = 0.1\,\mathrm{m\,s^{-1}}$. Layer intensity changed little for physically-realistic variations in τ_w (Figure 6·18). A small reduction in mean layer intensity (~ 0.1) was observed for an increase in τ_w from 10 to 200 s.

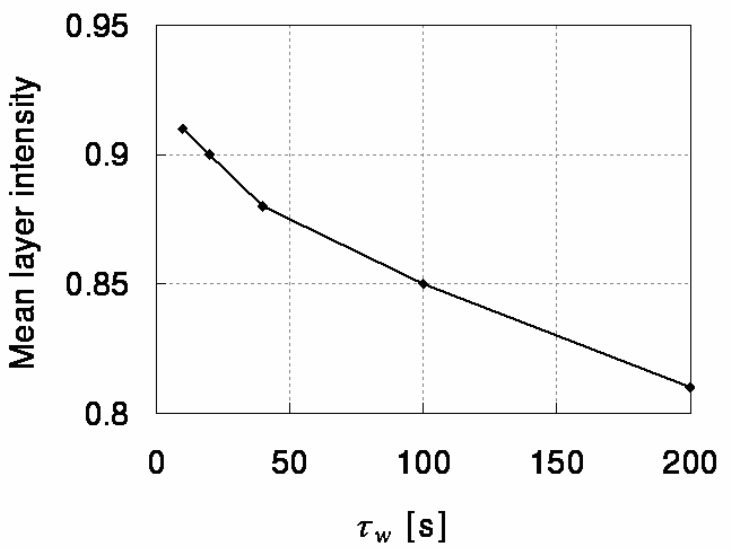

Figure 6·18 – *Sensitivity of mean layer intensity to* τ_w.

The next test was the effect of the 'eddy-crossing factor' on layer intensity (*i.e.* adjustment of τ_w for moving-particle turbulence-decorrelation). A non-moving particle acts as a fluid tracer, whilst a moving particle causes a faster decorrelation of the turbulence field with time (*cf.* Figure 6·11). When flight speed vastly exceeds the magnitude of turbulence, the insect is unaffected by turbulence and hence the eddy-crossing factor is 0: *i.e.* if $w_i >> \sigma_w$, then $\tau_w^* << \tau_w$. The converse is that an insect experiences the full turbulence field if the magnitude of turbulence vastly exceeds the flight speed: it acts as if it was a

fluid tracer and hence the eddy-crossing factor is 1: *i.e.* if $w_i << \sigma_w$, then $\tau_w^* = \tau_w$. This expectation was observed in Figure 6·19 where there was a large change in layer intensity for variation in eddy-crossing factor. For the full range from massless to heavy particle—*i.e.* variation in τ_w^* / τ_w from 0 to 1—the mean layer intensity decreased by 0.55. Hence, as $\tau_w^* / \tau_w \to 0$, the insect has full control over its flight and many insects can form a layer: therefore layers become more intense as $\tau_w^* / \tau_w \to 0$. Using equation 6·20 and given typical values of $\sigma_w = 0.1 - 0.3 \text{ m s}^{-1}$ and $\left|\underline{\mathbf{u}_i}\right| = 1 - 8 \text{ m s}^{-1}$, then typically $\tau_w^* / \tau_w < 0.25$: hence, layer intensity varies by 0.37.

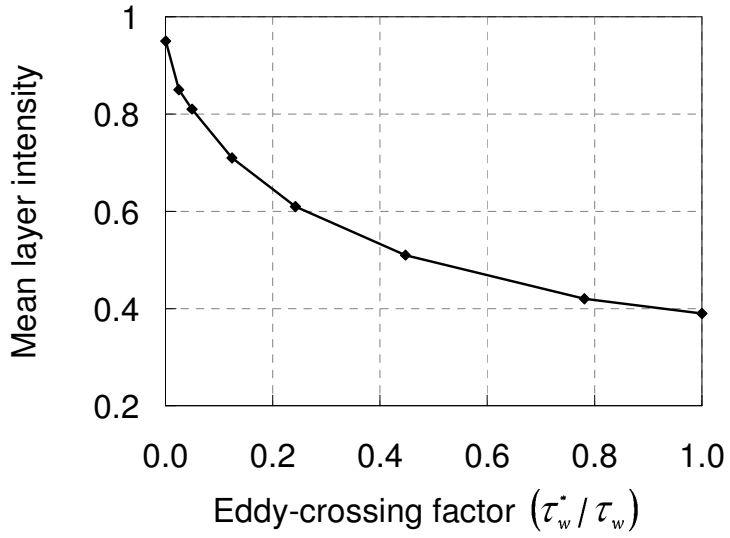

Figure 6·19 – *Sensitivity of mean layer intensity to the eddy-crossing factor* (τ_w^* / τ_w).

The next test was the assessment of the sensitivity of layer spread to σ_w, vertical velocity was set to $w = w_i + w'$: with constant parameters of $T_0 = 15 \text{ °C}$, $\gamma_T = 0.1 \text{ m s}^{-1} \text{ K}^{-1}$, and $\tau_w = 100 \text{ s}$. The initial expectation was that for larger magnitudes of turbulence (large σ_w), insects have less control over their net displacement and hence layers are less intense. Indeed, variation in σ_w had a large effect on mean layer intensity (Figure 6·20). More turbulent flow led to a less intense layer, as expected. From stable to neutral conditions ($\sigma_w : 0.65u_* \to 1.25u_*$) the layer intensity decreased from 0.75 to 0.38: hence,

small adjustments in the turbulence parametrization led to large differences in mean layer intensity.

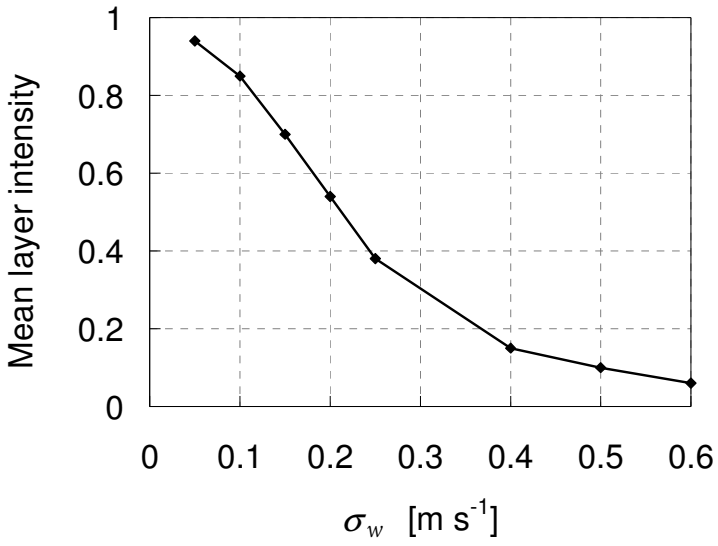

Figure 6·20 – *Sensitivity of mean layer intensity to* σ_w.

A final test of turbulence parametrization was the adjustment of σ_w for insects' inertia—this is done using the 'particle time-constant' τ_p (see equations 6·21 and 6·22). The expectation was that larger insects (with a slower τ_p) have a higher inertia and thus are less reactive to turbulence of a small timescale. Increases in τ_p cause a reduction in the adjusted standard deviation of vertical velocity (σ_w^*). A test assuming $\tau_w = 100$ s found little variation in mean layer intensity for variation in τ_p (Figure 6·21). As τ_p increased (slower), so did the layer intensity: hence, particles with a long (large) particle time-constant (τ_p) are less affected by turbulence. Even a change in τ_p by two orders of magnitude only caused a variation in mean layer intensity by 0.1. But assuming equation 6·23 provides a suitable estimate of the particle time constant, then $\tau_p \approx 0.2 - 1.2$ s. Since the turbulence slowly evolves nocturnally ($\tau_w \sim 100$ s), then $\tau_p > \tau_w$ and thus there is little adjustment for inertia (equation 6·21). Overall, the inertial particle effect was unimportant in the modelling of nocturnal insect layers in SLIM.

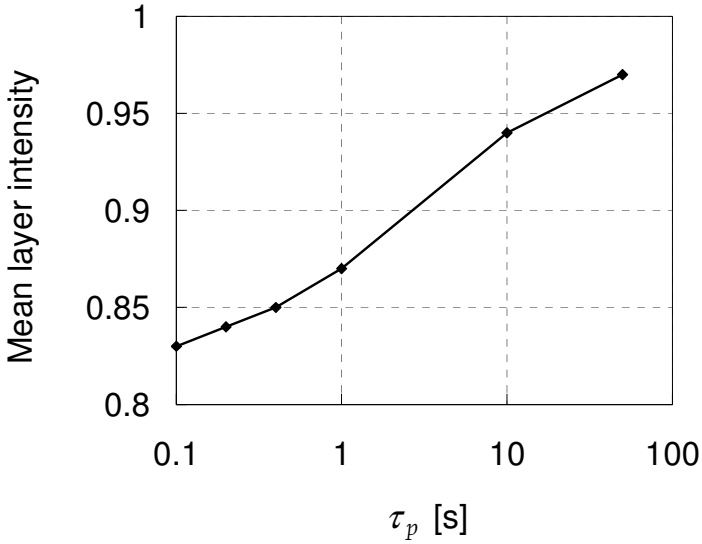

Figure 6·21 – *Sensitivity of mean layer intensity to* τ_p.

Test for layer intensity: sensitivity to mass parametrization

To test the sensitivity of layer spread on the rate of change of vertical velocity with insect mass (γ_m), vertical velocity was modelled ignoring turbulence: $w = w_i = \gamma_T (T_{amb} - T_0) + \gamma_m \left(m_i - \overline{m}\right)$. The following parameters were used: $T_0 = 15\,°\text{C}$, $\gamma_T = 0.1\,\text{m s}^{-1}\,\text{K}^{-1}$, $\sigma_w = 0.1\,\text{m s}^{-1}$, $\tau_w = 100\,\text{s}$, and $\overline{m} = 175\,\text{mg}$. A large value of γ_m means that there is a large range in w_i for a small range in m_i, whilst small γ_m values means there is little adjustment for mass. Hence, the expectation is that larger γ_m leads to less intense layers. Small values of γ_m mean that there is no variation in flight speed with insect mass (Figure 6·22), and hence for $\gamma_m = 0$ there is an infinitely thin layer (layer intensity is 1); layer intensity reduces as γ_m increases (*i.e.* when there becomes a variation in flight speed due to the variation in mass). The slope is steepest for $\gamma_m < 500\,\text{m s}^{-1}\,\text{kg}^{-1}$: a change in mean layer intensity of 0.58. For $\gamma_m = 500 - 1500\,\text{m s}^{-1}\,\text{kg}^{-1}$ there is a smaller reduction, of 0.13, in mean layer intensity. Overall, there are substantial difference in layer intensity when different flight speeds due to mass are included.

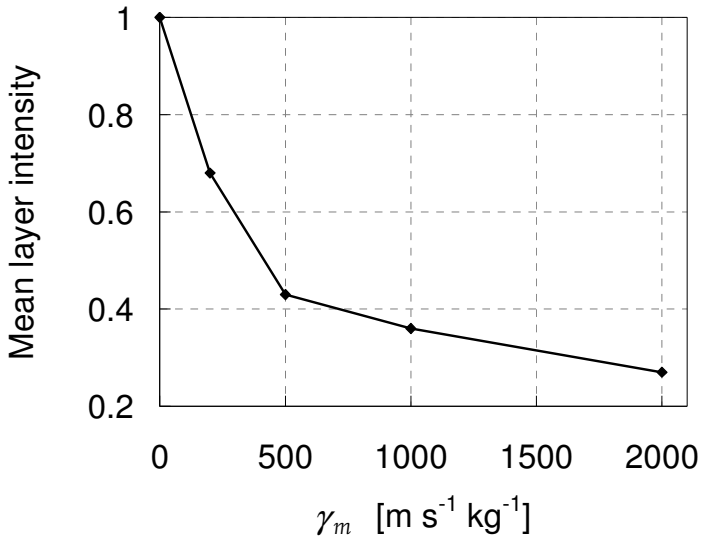

Figure 6·22 – *Sensitivity of mean layer intensity to* γ_m.

Test for layer intensity: temperature gradient

To test the sensitivity of layer spread to the rate of change of vertical velocity with temperature (γ_T), a model equation was used as follows: $w = w_i = \gamma_T(T_{amb} - T_0) + \gamma_m(m_i - \overline{m})$. Parameters were set as: $T_0 = 15\,°\text{C}$, $\gamma_m = 500\,\text{m s}^{-1}\,\text{kg}^{-1}$, $\sigma_w = 0.1\,\text{m s}^{-1}$, $\tau_w = 100\,\text{s}$, and $\overline{m} = 175\,\text{mg}$. A large value of γ_T means that there is fast response of insects to their ambient conditions and can hence quickly find their T_0; small γ_T implies a slower response to change in ambient temperature. There was an increase in layer intensity with an increase in γ_T (Figure 6·23); hence, if vertical flight speed is modelled as a strong function of temperature, layers become more intense. The relationship was nearly linear; mean layer intensity increases from 0.25 to 0.74 for $\gamma_T : 0.01 \rightarrow 0.30\,\text{m s}^{-1}\,\text{K}^{-1}$.

Summary of sensitivity studies

These tests have allowed an assessment of the sensitivity of model parameters, and some honing of their values. There is some variation in ascent time caused by variation in preferential minimum and the rate of change of flight speed with temperature, but there is perhaps little need to simulate ascent time more accurately than to within half an hour.

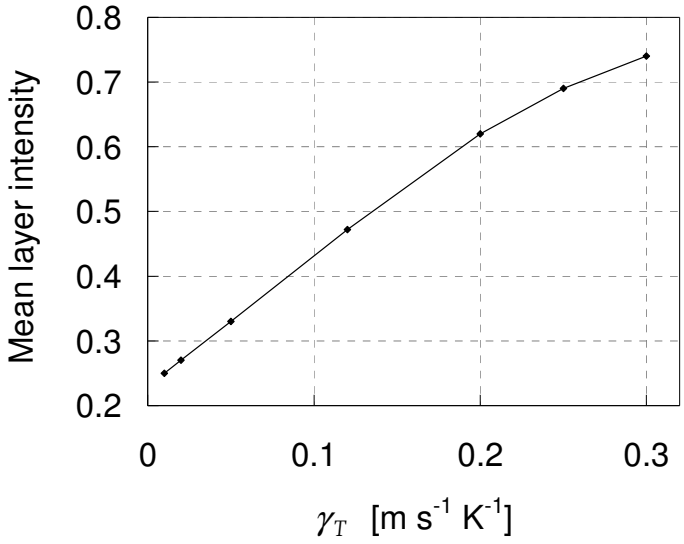

Figure 6·23 – *Sensitivity of mean layer intensity to* γ_T.

The variation in layer altitude is large for changes in preferential minimum temperature: though a value of 15 °C matched the case study most closely. Simulated layers are too low if the rate of change of flight speed with temperature is too low.

Layer intensity is little affected by the Lagrangian timescale for turbulence, but the large values of the magnitude of turbulent fluctuations (σ_w) caused a weak layer intensity. Changes in layer intensity were also caused due to variations in the parameters that caused changes in flight speed with temperature and insect mass.

6·5·3 Case studies

The three case studies analysed in Chapter 4 were replicated using SLIM. For all cases, the same parameters were used, as follows. An ensemble of 300 moths was released at the same time (19:30 UTC), defined as $t = 0$, and subsequently tracked for 8 hours. Each of the 300 moth's masses were randomly selected from an even distribution between 50 and 300 mg. The Earth's surface was set as an absorbing lower model-boundary, so that any moth that landed would not take off again (*i.e.* ceased flight for the night). There was no upper-boundary on the altitude to which moths could fly. A model timestep of $\Delta t = 10\,\mathrm{s}$ was used (recall that

timesteps that are too large are not suitable because there is a requirement that $\Delta t < 0.1\tau_w$ for correct inclusion of turbulent fluctuations). The vertical velocity was set to $w = w' + w_i$ (*i.e.* turbulent fluctuations plus insect flight), where $w_i = \gamma_T (T_{amb} - T_0) + \gamma_m (m_i - \overline{m})$, $\gamma_m = 500 \text{ m s}^{-1} \text{ kg}^{-1}$, and $\gamma_T = 0.12 \text{ m s}^{-1} \text{ K}^{-1}$. A stable homogeneous turbulence profile was set for all altitudes: $\tau_w = 100 \text{ s}$ and $\sigma_w = 0.65 u_*$; where $u_* = 0.2 \text{ m s}^{-1}$.

The model results are shown in Figure 6·24–6·26 alongside the radar-observed data for the same period and altitudes. Calculations of the mean altitude and the layer intensity were averaged over 21:00–23:59 and are shown in Table 6·2. The first two case studies (Figure 6·24, Figure 6·25) showed very close overall agreement, with some small discrepancies. The mean layer altitude in SLIM was similar to the observed situation in case A (only 38 m higher than the observed altitude) and in case B (76 m lower). However, in case C, the altitude predicted by SLIM was considerably greater (440 m) than the observed value. In the last case, SLIM performed poorly: however, this case was expressly chosen in Chapter 4 because the layer altitude did not appear to be correlated with temperature. In this case, the warm temperatures throughout the profile might have led the insects to respond to a different variable (*i.e.* one not modelled in the SLIM insect parametrization). The same vertical sampling bins were used in SLIM as are used for the radar range-gates (see Chapter 2). This led to an anomalous characteristic in Figure 6·26, where the layer was so thin that it passed between virtual range gates 8 and 9 (722–745 m) during 20:00–21:00. This highlights that it is possible that a very thin layer (< 23 m) could potentially pass between radar range gates, but layers as thin as this have not been seen in nature (*e.g.* by use of scanning radars).

Layer cessation in SLIM occurred in both the first two cases, but not for the third case. For case A, the layer in SLIM ended at the correct time; but in case B, the simulated layer ended at 23:00, which was earlier than the radar-observed layer at ~ 02:00.

The layers simulated in SLIM were more intense than in the radar data for all three cases (Table 6·2). A possible reason for the greater intensity in the simulated layers modelled by SLIM is that the methodology employed by SLIM only considers a subset of the nocturnal fauna (50–300 mg, *i.e.* noctuid moths), and that the full spread of the layer in the radar data was caused by a variety of insects that were not modelled by SLIM. To elucidate this hypothesis, the radar data were analysed separately for insects of noctuid moth size (50–300 mg) and smaller (1–50 mg). The radar data for these subsets are shown in Figure 6·27–6·29 and Table 6·2.

In all cases, the radar-observed layers were more intense when only the larger insects were analysed. Layer intensity in SLIM is in closer agreement with this subset of larger insects than with the full range of masses. The layer cessation was the same in case A. In case B, the radar-observed layer ended more suddenly—and at a similar time to SLIM's prediction—than with all analysed insects. The radar observations beyond *c.* 23:00 are not of larger insects. For case C, there was little difference in layer end time in the radar observations between the full distribution of masses and the larger insect subset.

The layers of small insects occurred at altitudes below that of the larger insects (Table 6·2). This indicates that the insects flying at higher altitudes are larger insects. This could be because either larger insects are stronger fliers, or that larger insects tend to have lower minimum temperature preferenda (above the inversion temperature cools with altitude).

Most of the flight activity for small insects was not layered. The distributions show that most of the small insect concentrations occurred at dusk. There was some layering, but that involved few insects compared to the dusk peak (< 10 % of the dusk peak in cases A and C).

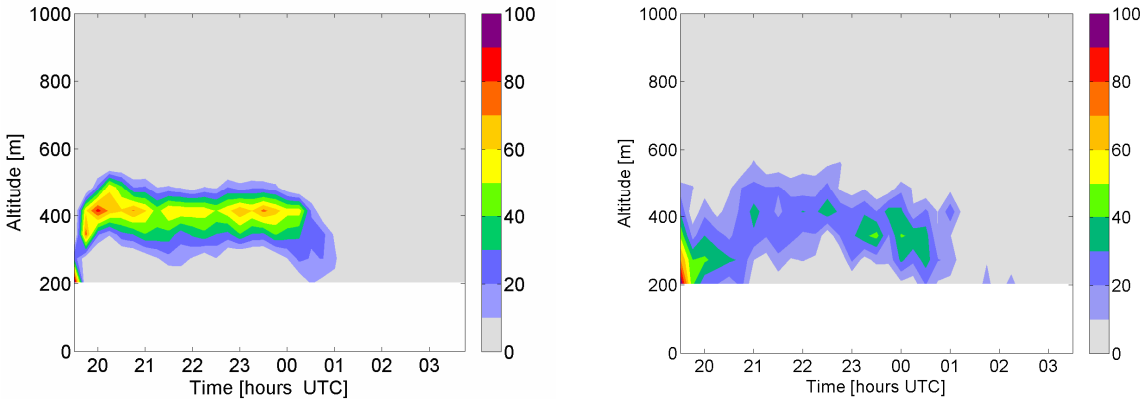

Figure 6·24 – *Altitude of insects against time on 22/23 August 2000 at Malvern: SLIM (left), radar (right). Both expressed as percentages of the maximum value (maximum aerial density in radar data was 187 insects per 10^7 m^3). Dusk was 19:19–19:56; dawn was 4:29–5:05.*

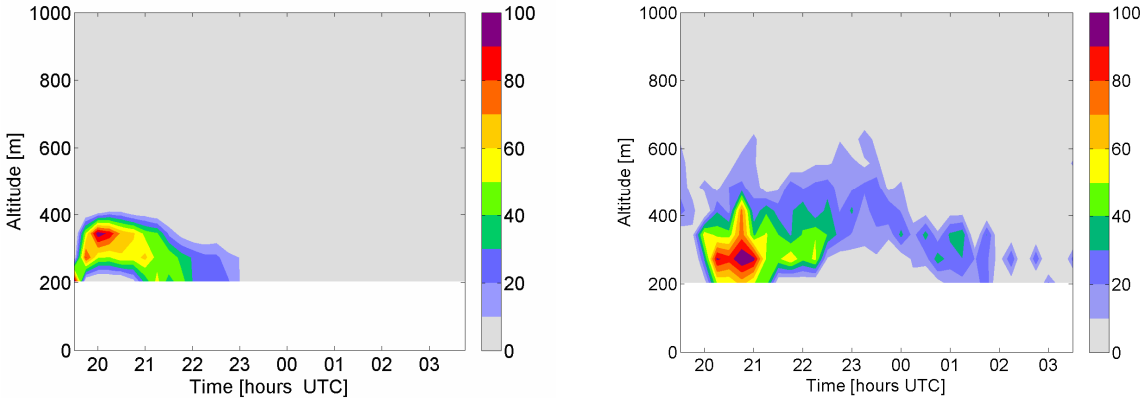

Figure 6·25 – *Altitude of insects against time on 14/15 August 2003 at Malvern: SLIM (left), radar (right). Both expressed as percentages of the maximum value (maximum aerial density in radar data was 98 insects per 10^7 m^3). Dusk was 19:37–20:16; dawn was 4:13–4:51.*

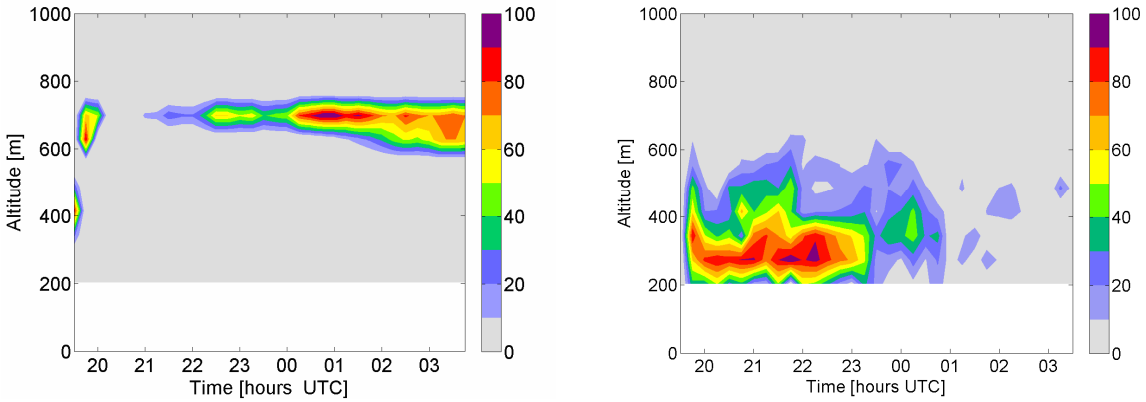

Figure 6·26 – *Altitude of insects against time on 23/24 August 2003 at Malvern: SLIM (left), radar (right). Both expressed as percentages of the maximum value (maximum aerial density in radar data was 126 insects per 10^7 m^3). Dusk was 19:19–19:56; dawn was 4:29–5:06.*

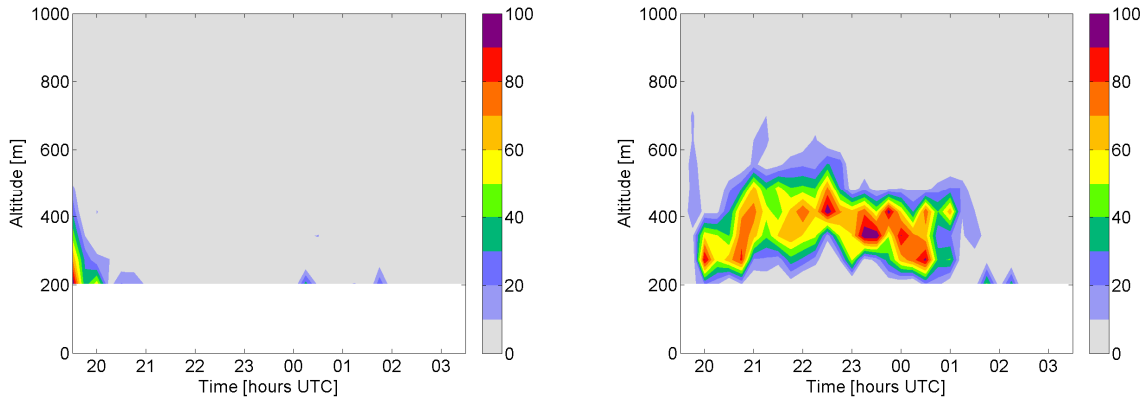

Figure 6·27 – *Altitude of insects against time on 22/23 August 2000 at Malvern above radar: small insects only, 1–50 mg (left), large insects only, 50–300 mg (right). Expressed as percentages of the maximum value.*

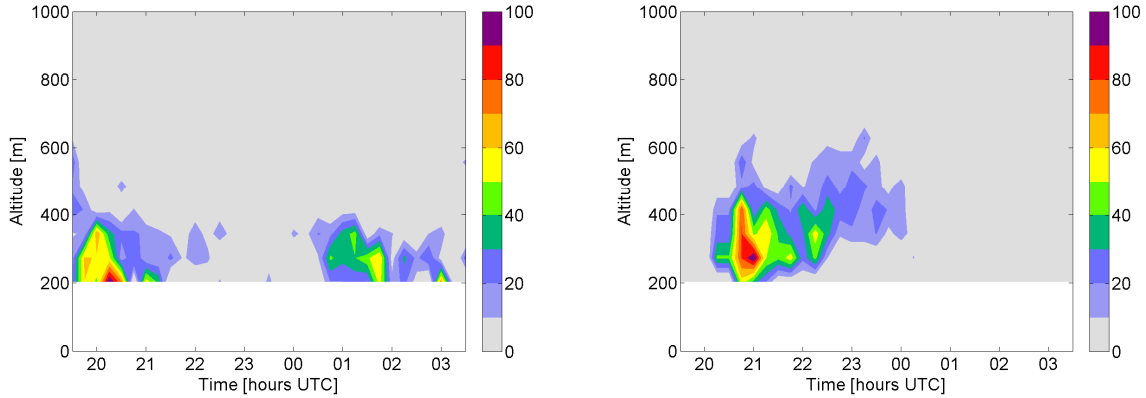

Figure 6·28 – *Altitude of insects against time on 14/15 August 2003 at Malvern above radar: small insects only, 1–50 mg (left), large insects only, 50–300 mg (right). Expressed as percentages of the maximum value.*

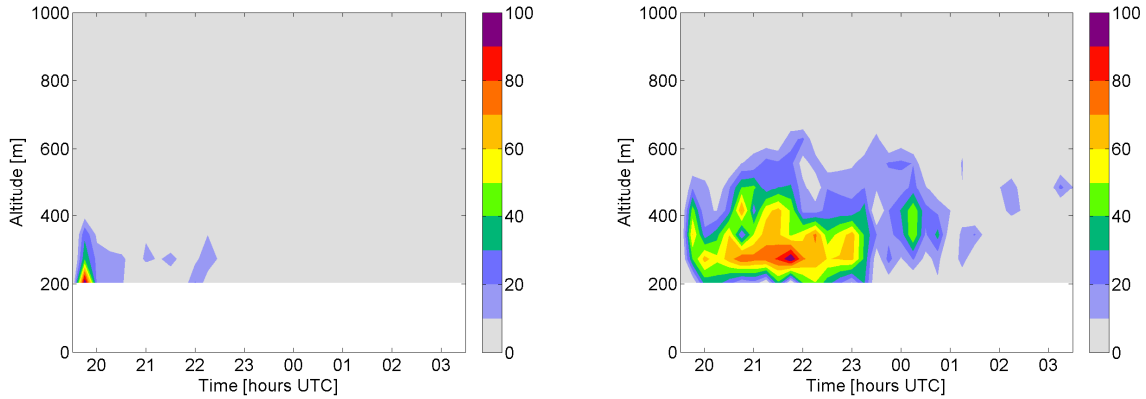

Figure 6·29 – *Altitude of insects against time on 23/24 August 2003 at Malvern above radar: small insects only, 1–50 mg (left), large insects only, 50–300 mg (right). Expressed as percentages of the maximum value.*

Table 6·2 – *Comparison of layer characteristics between radar and SLIM for 3 case studies (all at Malvern).*

			Layer cessation [time, hours UTC]	Mean layer intensity	Mean layer altitude [m]
Case A: 22 August 2000	SLIM		01:00	0.37	430
	Radar:	all insects	01:00	0.29	392
		Larger only (50–300 mg)	01:00	0.31	389
		Smaller only (1–50 mg)	00:30	0.25	327
Case B: 14 August 2003	SLIM		23:30	0.38	280
	Radar:	all insects	01:30	0.24	335
		Larger only (50–300 mg)	00:30	0.25	380
		Smaller only (1–50 mg)	22:30	0.14	344
Case C: 23 August 2003	SLIM		n/a	0.47	784
	Radar:	all insects	01:00	0.22	274
		Larger only (50–300 mg)	00:45	0.26	300
		Smaller only (1–50 mg)	23:30	0.32	282

Of the layering that did occur (which cannot be seen on the figures due to the low insect numbers relative to the dusk peak), two of the three cases (A and B) had layering that was less intense than the full distribution (Table 6·2). This might be caused by larger insects having both better control over their flight and a higher inertia, compared to smaller insects that are more likely to be displaced from a preferred altitude by turbulent fluctuations. Therefore, smaller insects are less likely to be able to stay in a layer—instead being spread due to turbulent fluctuations.

In all cases, the early-evening layer of smaller insects ended before the full distribution's layer did. However, case B exhibited a curious phenomenon. The layer of large insects ended during 23:00–00:00, but there was a subsequent layer of small insects from 00:30 to *c.* 02:00. There was a continuous layer of small insects, but it had few insects (< 10 %) during 22:00–00:30 and increased in intensity later in the night. This result was unexpected: assuming that no take-off occurred after dusk, it suggests heterogeneity in ground populations of the small insects involved in this layer.

6·6 Discussion

In this chapter, the development of SLIM has been described and its parametrization to simulate layer formation by large night-flying insects, particularly noctuid moths, has been investigated. An initial run of the model with a well-mixed atmosphere showed that random turbulence could be created with no spurious simulation of layers. The terminal velocity results (§6·4·3) indicated that free-fall is rapid for noctuid moths. Layering intensity and altitude were found to be sensitive to the turbulent strength, minimum preferential temperature, and to the gradient parameters (γ_T, γ_m). In comparisons with observed cases of moth layering, the model performed with some success.

Moths in free-fall

Noctuid moths of mass $50-300$ mg (*i.e.* mass range focused on species captured on layering nights) in free-fall have been predicted to fall at speeds of 3 to 5 m s^{-1}, with open wings (Figure 6·6). As far as is known, no laboratory studies have measured the actual terminal velocities of noctuid moths. However, a laboratory study for aphids of mean mass 0.49 mg found terminal velocities of 0.82 m s^{-1} and 1.78 m s^{-1} for open and closed wings respectively (Thomas *et al.* 1977). The terminal velocity model in §6·4·3 (equation 6·11) predicts a fall-speed of 1.80 m s^{-1} for closed winged aphids; hence, a high degree of confidence can be expressed in the model (using $A = 3.1$ mm^2, $m_i = 0.49$ mg). The high fall-speeds indicated that noctuid moths must be engaged in active flight in the nocturnal environment, and that the nocturnal turbulence cannot significantly alter the moths' free-fall trajectory (*e.g.* to keep them aloft), *i.e.* $\sigma_w < w_T$. This important result means that nocturnal layers detected by radar were almost certainly not caused by atmospheric flow, but instead by a mechanism related to the flight behaviour (*i.e.* the w_i component) of the migrating moths. The model also predicts a high fall-speed, which might explain why layers can end so dramatically. In as little as half a minute, a large noctuid moth with closed wings could fall from layer altitude (*e.g.* 300 m) to the ground. It is worth noting that

that behaviour is not very likely: it is probably more likely that the moths control their fall, by flying downwards, or at least dropping with their wings open. These fast descents can hence go undetected by the current VLR system with its sampling periods starting every 15 minutes (Chapter 2). Laboratory experiments would be useful in order to validate the values of terminal velocity calculated for noctuid moths.

Sensitivity tests

The sensitivity tests for the environmental-response component of the model showed that careful parametrization is necessary for SLIM to produce consistently realistic model outputs. Layer altitude was extremely sensitive to variations in T_0, the minimum preferential temperature. An error of 1 °C in T_0 caused a single trajectory to lower in altitude from 500 to 300 m above ground in case study A (*i.e.* $T_0 = 15.5 - 14.5$ °C). The error analysis in Chapter 3 revealed that the mean UM error for temperature in the critical region for nocturnal insect layers was just -0.2 °C and that the confidence interval on that error was ±0.4 °C, hence there was no significant bias (Table 3·3). This error in UM is probably smaller than the uncertainty in T_0. A value of $T_0 = 21.5$ °C was used in the study by Achtemeier (1998), which for most nocturnal occasions in the UK would be too high to allow any high-altitude flight at all. The differences between different species probably mean that a single T_0 value is not realistic, which is why a variation was proposed here for the modelling of vertical flight as a function of moth masses, which gave a range of flight speeds to the same ambient conditions: thus giving a less intense layer. The γ_T parameter (the gradient term for the variation of vertical flight with changes in ambient temperature) showed asymptotic behaviour beyond $0.05\,\mathrm{m\,s^{-1}\,K^{-1}}$ for layer altitude and $0.10\,\mathrm{m\,s^{-1}\,K^{-1}}$ for ascent time. Thus, layer intensity was not very sensitive to changes in γ_T beyond those values. Indeed, $0.14\,\mathrm{m\,s^{-1}\,K^{-1}}$ was used in the Achtemeier (1998) study. Gradients of $0.1 - 0.2\,\mathrm{m\,s^{-1}\,K^{-1}}$ are seen in Figure 6·1 (data from Carpenter *et al.* 1981), although those gradients were associated with a threshold temperature of a

physiological nature for take-off and could be less relevant to the minimum preferential temperature here (T_0).

The layer intensity (related to the vertical depth of layers) showed some sensitivity to the parametrization of turbulence. It is important to parametrize the vertical depth of layers correctly because there is often large vertical wind shear at night, and hence insects flying at different altitudes will have different potential migration displacements. The turbulence parametrization has two main components: Lagrangian timescale (τ_w) and turbulent strength (σ_w). The Lagrangian timescale had only a small effect on layer intensity: there was a $10\,\%$ variation in layer intensity for $\tau_w = 10 - 200\,\mathrm{s}$ (NB. τ_w is limited to a maximum of $100\,\mathrm{s}$ in the NAME-4 dispersion model, Maryon *et al.* 1999). Overall, the value of τ_w did not have a large effect on layer intensity. When inertial effects (*i.e.* allowing for variation in insect size) were taken into account, the change in layer intensity was also small: a $14\,\%$ variation in layer intensity was observed for a variation in the particle time constant, τ_p, from 0.1 to $50\,\mathrm{s}$. However, the range of masses of noctuids probably only gives a range of τ_p from 0.3 to $0.5\,\mathrm{s}$; clearly the inertia effect is a less important one in this model than other parametrizations.

The strength of turbulence—represented by the standard deviation of the vertical velocity, σ_w—had a large effect on layer intensity. Homogeneous profiles were used. The stable scenario ($\sigma_w = 0.65u_*$, and assuming $u_* = 0.2\,\mathrm{m\,s^{-1}}$) produced a layer intensity of 0.8 compared to a neutral scenario ($\sigma_w = 1.25u_*$) of 0.38. A daytime convective boundary layer's homogeneous turbulent statistic* gives values in the region $\sigma_w = 0.5 - 1.2\,\mathrm{m\,s^{-1}}$. Perhaps this indicates why less insect layering occurs in the day compared to night-time (*cf.* Figure 2·9), because the stronger turbulence in the day could spread even some larger insects (of the

* For daytime convective boundary layers in NAME, the following homogeneous profile is used: $\sigma_w = \left(0.4w_*^2 + 1.1u_*^2\right)^{1/2}$; where w_* is a characteristic velocity scale (dependent on variables *H, z,* and *T*).

order of tens of milligrams) that might try to maintain constant altitude. Clearly, the magnitude of turbulence is very important for layer modelling; identification of turbulent statistics in and above the nocturnal boundary layer would improve the model's accuracy. The fact that insect flight is least affected by turbulence at night is probably one of the most important reasons that moths migrate at night (amongst other reasons reviewed in Chapters 1 and 2, such as reduced risk of predation). The impact of turbulence on the horizontal component of moth flight is not analysed here, but would clearly produce a horizontal spread in final insect locations.

A large change in mean layer intensity occurred for large changes in the eddy-crossing factor (*cf.* Figure 6·11), *i.e.* where insects cut through the turbulent field and hence experience different turbulent fluctuations than a fluid tracer. Hence, layers were more intense for an in-flight insect. The eddy-crossing factor was calculated to be less than 0.1 for these moths in flight (assuming a range of 50 to 300 mg), indicating that the Lagrangian timescale was only 10 % of the value that a fluid tracer would have.

Given the full insect velocity model (equation 6·14), both gradient parameters (γ) had an effect on mean layer intensity. When γ_m is large, there is a spread of insect flight speeds and hence a spread layer. Layer intensity changed by 60 % for $\gamma_m < 500\,\mathrm{m\,s^{-1}\,kg^{-1}}$ and then there was relatively little change (of 0.13) in mean layer intensity from $500-2000\,\mathrm{m\,s^{-1}\,kg^{-1}}$. Large γ_T causes a more intense layer. There was an increase in mean layer intensity of 0.22 from $\gamma_T = 0.1-0.3\,\mathrm{m\,s^{-1}\,K^{-1}}$.

Case studies

In all three cases studies, the model successfully simulated a layer. However, the model parameters were chosen based on sensitivity studies of the first case study, and so case study A was expected to perform well. In the final case study, the model layer was too elevated compared with the radar data; but that case was deliberately chosen in Chapter 4 because it did not appear to match the

temperature hypothesis and the layer was correlated with a nocturnal jet. Hence, credence can still be given to the hypothesis of a hierarchical response to alternative factors (once temperature is warm enough) in determining the altitude of nocturnal layers on some occasions.

From the radar, it was shown that layers of large insects were found higher than layers of small insects, this was also found in Taylor *et al.* (1979). It is possible that this effect is due to either (*i*) larger insects flying higher because of increased flight power; or (*ii*) different temperature thresholds giving smaller insects a higher preferential minimum temperature than larger insects: thus smaller insects tending to fly in a ceiling layer at lower altitude. Point (*i*) is captured in the γ_m parameter. The second point is consistent with the increased endothermic warming in larger insects (*e.g.* Bartholomew and Heinrich 1973, May 1979). It is not fully clear which of these two effects is most likely to cause the differences in flight altitudes in insects of different sizes. Altogether, larger moths can fly to higher altitudes and in colder ambient temperatures; hence, this formed the basis of a spread in modelled flight characteristics based on moth mass.

In cases A and B, SLIM predicted layer altitudes and timings similar to those of radar observations, but layer intensity was too high in SLIM across all case studies. The increased intensity of layers in SLIM was partly explained by the fact that SLIM was only including insects of mass $50-300\,\mathrm{mg}$. The remaining difference in intensity between SLIM and radar-observed layers of large insects could be explained by the sensitivity of the model to turbulence.

For cases A and C, the radar data showed a dusk peak of many small insects, many of these small insects then returned to the Earth's surface leaving a layer of large insects. This compares well with the breakdown of masses early and late in the night in Chapter 4 (Figure 4·12) that revealed that smaller insects became less abundant with time.

Case B was quite distinct. The layer of large insects ended at 23:00–00:00. But there was a preponderance of small insects after 01:00 in a layer formation. Assuming that there was no take-off of insects after dusk, a possible explanation is that there was surface source heterogeneity upwind of the radar.

Flight duration could be determined either by a neurophysiological factor or fatigue; Johnson (1969) suggested that the estimation of duration of migration based on fuel supply might bear little relation to nature. For the first two case studies, the parametrization of insect response to environmental conditions caused termination of flight at about the right time in cases A and B, but this was not so in the last case study. Hence, a key hypothesis for the mechanism of layer cessation is due to ambient temperatures cooling to below the preferential minimum temperature value.

In some specific cases, lack of insect sources upwind of a coast is a further explanation (case A and C in particular) for sudden layer cessation: further work is required to investigate this phenomenon. Fatigue cannot be ruled out entirely, because radar studies have shown that wing-beat frequency often decreases with time for migrating insects (Riley *et al.* 1981). However, these decreases might be due to a reduced metabolic rate caused by a cooler atmosphere (at night under clear-skies, longwave radiation loss causes the whole atmosphere to cool, see §1·4·7). Further work is required to elucidate this (possibly by the inclusion of an additional parameter in SLIM).

The SLIM-simulated layer for case C was too high and is unlikely to be due to error in UM data: because a shift in most of the profile in the UM of ~ 5 °C would be needed—which is well above any errors found in temperature (Chapter 3). It is most likely that on this occasion, the insect layer was determined by another variable because temperatures were well above the preferential minimum temperature.

Further modelling of other behavioural mechanisms in insects

When adapting this model to the full four dimensions (*i.e.* x, y, z, t), the common orientation phenomenon will need to be taken into account (Riley 1989) so that horizontal displacements can be predicted accurately.

More detailed turbulence modelling should provide increases in accuracy. The strength of turbulence, σ_w, could be parametrized as a function of local stability. Furthermore, insects have been hypothesised to respond to anisotropies in turbulence due to Kelvin-Helmholtz waves (Riley 1989). This has not been included in SLIM, but there might be a requirement to parametrize an insect-flight response to turbulence.

Overall, the SLIM approach shows promise and has been used to model insect layers on 3 occasions: two with success. Temperature does indeed seem to be important predicting layers of insects. Further work should include the systematic testing of SLIM over a larger data-set to further hone its parametrizations.

7: Conclusions

7·1 Summary

The work in this thesis has demonstrated that some species of nocturnal high-flying insect migrants have evolved strategies that often result in migration at a particular altitude range in the atmospheric boundary layer. Consequently, the insects tend to form narrow and well-defined layers hundreds of metres above the ground. Clearly, flight in these layers has many benefits for the migrants involved, such as usually allowing faster (and thus further) movement than would be possible at other altitudes in the atmosphere. It is important for society that we more fully understand these migration pathways in order to forecast outbreaks of pestilence and disease. Considering larger-sized (radar-detectable) insects, noctuid moths are probably the most important constituent of the layers observed over the UK. It has been suggested by many authors (reviewed in Chapter 1) that ambient meteorological conditions influence the formation of insect layers, although there has been much speculation about the precise role played by specific meteorological variables. However, much of the work on insect layering has been carried out in tropical and subtropical regions of the world, and there has been just one previous study of layering in temperate northern Europe (Reynolds *et al.* 2005). Therefore, in this thesis, the specific objectives were to:

1. study the diel cycle of UK high-altitude insect migration;
2. ascertain the likely fauna comprising nocturnal layers over the UK;
3. investigate if and how insect response to ambient meteorological conditions can lead to nocturnal layers;
4. use continuous data-sets to study insect layering—and the role of meteorological conditions—over several years, rather than by the traditional approach of analysis by case studies of single occasions;
5. investigate the influence of atmospheric turbulence on nocturnal layers of insects;
6. develop a model to simulate nocturnal layer formation by noctuid moths.

In Chapter 2, the key technique that provided the insect flight data used in this thesis was outlined: namely the use of vertical-looking entomological radar (VLR). A method for qualitatively assessing the large amounts of VLR data was devised, *i.e.* the 'Quickview' database (these Quickviews have already been used in research tasks outside the scope of the present thesis, *e.g.* an examination of dawn layering (Reynolds *et al.* 2007)). Subsequently, using several years of VLR data, an analysis was made of the diel cycle of insect migration above two sites in southern Britain. Four reasonably discrete periods of migratory activity were observed over the diel cycle—dawn, day, dusk, and night. Analysis revealed that most layering occurred following the dusk peak and at a critical time and altitude. This 'critical region' was defined as occurring during summertime, between 20:00 and 22:00 hours UTC and at 200–500 m above ground level (a.g.l.). In this thesis, analysis of the role played by meteorological conditions on the initiation and maintenance of nocturnal layering events was restricted to events and conditions in this 'critical region'.

Meteorological data were required for comparison with VLR-observed insect layering. Although radiosonde ascents were useful for specific occasions, a numerical weather prediction model—the UK Met Office's unified model (UM)—was used to provide profiles with much better temporal and spatial resolution than the sparser radio-soundings. In Chapter 3, the UM was introduced and then validated for 17 nocturnal occasions where a radiosonde profile was available at the same time and location as a UM profile. Despite some deficiencies, the UM data was found to be sufficiently accurate in the critical region used for the analyses required for this thesis.

Three case studies of nocturnal insect layers were analysed in Chapter 4, and these studies presented evidence for the hypotheses that layers predominantly occurred (*i*) at the same altitude as a nocturnal jet, (*ii*) at an inversion top, and (*iii*) in a ceiling layer (where ascent to higher altitudes is prevented or constrained because temperatures are below a threshold for flight).

In Chapter 5, four years of VLR and UM data were analysed to investigate the correlations between particular meteorological conditions and the initiation and maintenance of nocturnal insect layering in the critical region. In this analysis, temperature was shown to explain the most variance in a variable (NLQ) representing the intensity and duration of nocturnal layering. However, the influence of the nocturnal jet could be important on nights where temperatures did not constrain migratory flight.

Chapter 6 saw the development of a stochastic Lagrangian insect model (SLIM) to simulate development of the three nocturnal layers studied in detail in Chapter 4. The 'virtual layers' of moths produced by the model were then subjected to sensitivity studies, where the parameters were adjusted to determine the robustness of the model. These results showed that layering was sensitive to the turbulence parametrization. Even though there was no modelled physiological response of insects to ambient turbulence, the insects were spread vertically by the turbulent wind. Hence, it was shown that—due to the weak nocturnal turbulence—the layers of insects detected by the VLR were not formed by passive mechanisms (such as layers caused by vertical shears in wind speed and direction). Thus, the insects forming the nocturnal layers must have been fliers that actively chose their altitude of flight.

Throughout this work, a consistent theme has been the strong (often over-arching) influence of temperature on nocturnal layering. This was partially expected (see review in Chapter 1) because insects are poikilothermic and because night-time temperatures in Britain, even in summer, might be rather marginal for high-altitude flight. Results in Chapter 5 showed that the inferences made of the case study data were consistent with the analysis over a much longer period (four years' data). Finally, in Chapter 6, numerical modelling results showed that nocturnal insect layers could be simulated by prescribing the vertical component of insect flight-speed as being proportional to the ambient temperature.

7·2 Discussion

7·2·1 Aerial insect activity

Analysis of radar data revealed four discrete high-altitude migratory flight events during each 24-hour period by macro-insects in the UK. Dawn, day, dusk, and night emigrations were distinct over several months' (and years') data: particularly in the summer. Diel periodicity analysis of a large number of individual species have been carried out by Lewis and Taylor (1964), but these studies used suction trapping data collected near the ground, and some of the flights would have been foraging or mating flights rather than migratory in nature. The radars only detect flight above about 150 m, and therefore produce data purely on migratory flight activity.

The discrete nature of the emigration phases was utilised during the high-altitude aerial netting campaigns, by collecting discrete samples of insects from each phase (Chapter 2; Chapman *et al.* 2004a). It is worth noting that the nocturnal transition of the atmospheric boundary layer (ABL) occurs during a period near dusk when conditions rapidly change: particularly near the surface where the temperatures rapidly cool and wind speeds decrease (*e.g.* Lapworth 2003). Both of these features do not favour long-distance migratory flights at low altitude after dusk, and thus it is not surprising that dusk emigration usually leads to climbing flights and migration at high altitude.

Most of the radar-observed nocturnal insect fauna weighed in the region of 50 to 200 mg and were capable of speeds of up to 5–6 m s^{-1} (Chapter 4). These relatively large speeds mean that in many situations, an insect's flight speed would contribute a considerable component to its flight trajectory. Owing to the observed size and speed of the insects, large moths—especially noctuids—are most likely to be major constituents of nocturnal layers in the UK. Based on material presented in Chapter 4, including relevant light-trap catches, four of the most likely species in the aerial layers are *Autographa gamma, Agrotis exclamations*, *Xestia c-nigrum*, and *Mythimna pallens*. The typical mass, body size, and wing-size of

these species were therefore obtained, to give representative values for noctuid migrants in the UK (Chapter 2). Given these data, the free-fall speed of noctuid moths could be estimated.

It was shown that in the nocturnal atmosphere, the terminal velocity of free-falling noctuid moths greatly exceeds that of the turbulent fluctuations (Chapter 6). Due to their mass, the moths are less affected by nocturnal turbulence (which is weaker at night than by day). Thus, noctuid-sized moths in the nocturnal atmosphere would very quickly descend to the ground if they ceased flying, in contrast to smaller day-flying insects during periods of strong turbulence (which could be held aloft without flight if caught in an updraught). Large nocturnally-flying moths are clearly at the top end of a mass spectrum, where they generally have good control over the altitude to which they fly (in fine weather at night, active flight is clearly a requirement in order to reach the observed migration altitudes: *cf.* Gatehouse 1997). Studies of this group are therefore required if one is to understand the interactions between insect behaviour and meteorological conditions in determining the altitude of flight.

A fuller understanding of the physical and behavioural characteristics of aerial insect fauna is clearly required in order to improve parametrization of insect migration trajectory models. The development of insect migration trajectory models and improvement of knowledge of aerial insect migration is generally important because many insects are vectors of plant, animal, and human diseases (*e.g.* Reynolds *et al.* 2006) or are agricultural pests (*e.g.* Pedgley 1993).

7·2·2 Layers

One characteristic of high-latitude migration is that flight often occurs in layers at specific altitudes. It has previously been recognized (Drake and Rochester 1994) that a 'climatology' of insect layers is required in order to improve our understanding of the processes affecting layer properties. This thesis goes some way to providing a climatology of insect layering for the UK (Chapter 2).

Layering is most commonly observed during the night-time and daytime periods (as compared to the dawn and dusk peaks of activity). Nocturnal layers tend to be a much more temporally continuous feature, whilst daytime layers seem to be more sporadic in nature (although no detailed study of insect layers during the day has been undertaken here or elsewhere). Although nocturnal layers can occur at altitudes of 800–1000 m (Reynolds *et al.* 2005 and see below), the systematic studies reported here showed that the nocturnal layers occurred most frequently at lower altitudes. A critical region (*i.e.* 200–500 m, 20:00–22:00 UTC) was defined indicating where future studies (most particularly in the UK) should focus efforts in analysing nocturnal insect layers.

Nocturnal layers were not observed beyond about midnight or 01:00 (Chapter 4; Reynolds *et al.* 2005). Flights of moths continuing through the whole night until dawn or beyond which have been observed in other regions of the world are apparently uncommon in the UK (Figure 2·9 showed that dawn is the least likely time of day to observe layering). Since Britain is an island, some of the more abrupt flight terminations might be due to a lack of source areas beyond the coasts—indeed this was inferred from the back-trajectory analysis in the case studies (Chapter 4)—rather than because air temperatures have dropped below thresholds for sustained flight or because flight fuel reserves have been exhausted. However, on many occasions, a lack of source areas upwind is unlikely to have been the cause for layer cessation, and falling temperatures are likely to have played a major role.

Layering was not detected at dusk or dawn, presumably because large numbers of emigrants tend to be ascending at these times, and thus they are occupying a range of altitudes. Indeed, there is often a monotonic decrease of insect numbers with altitude at dusk and dawn.

Previous studies of layers around the world have been on a case study basis, usually during field campaigns lasting a few weeks, and therefore this thesis can claim to be the first study in the world to embark upon a systematic study of

layers from an entomological point of view. The VLRs have been running continuously since the year 2000 at 2 UK locations and have hence gathered an unrivalled data-set. This has enabled hundreds of days to be studied to provide an analysis of layers that is generic and not specific to case study occasions.

Furthermore, access to meteorological data has also enabled more generic study of insect layers than ever before. The Met Office's UM provided data that was temporally continuous, thus providing an excellent data-set for comparison with the VLR data-set. Thus, for the first time, a systematic approach has been possible for elucidating the mechanisms causing nocturnal layering in the UK.

7·2·3 Meteorological mechanisms for nocturnal layer formation and intensity

The key question addressed in this thesis was thus: which meteorological factors present in the first kilometre of the nocturnal atmosphere will have the most influence on the migration altitude of large insects?

Temperature

The case studies (Chapter 4) took place in southern UK and hence in a cooler climate than most previous radar entomology studies. It was to be expected that noctuid moth migration would be strongly constrained by temperatures on many occasions.

From a systematic analysis of the large VLR dataset (Chapter 5), temperature was found to be the most important variable in explaining the presence of insect layers in the critical region (200–500 m, 20:00–22:00). Temperature explained the most variance in layer formation, intensity, and duration. Even in statistical analyses where variance due to other meteorological factors was allowed for first, there was still significant variance in NLQ explained by temperature.

The simplest hypothesis for insect layering is that the insects have selected the altitude of the warmest air. At night, this often occurs at the top of a surface

temperature inversion (Chapter 4; Schaefer 1976, Drake 1984, Drake and Farrow 1988, Feng *et al.* 2003, Reynolds *et al.* 2005). Accumulation of migrants at the warmest altitude appears to be most likely to occur in relatively cool conditions (*e.g.* case study A), causing the insects to become concentrated at a particular altitude—particularly if there is cooling from below (*i.e.* radiative cooling on clear nights).

There are, however, many references in the literature in which insects, particularly moths, have ascended above the altitude of the temperature maximum. On some of these occasions, insects might be forming so-called 'ceiling layers', *i.e.*, ascent has continued until insects reached an altitude corresponding to the lowest temperature at which they can sustain flight: the preferential minimum. This probably occurred in the case study B in Chapter 4 and it is the basis of the parametrization in SLIM.

Overall, it is concluded that temperature is the most important meteorological variable affecting the nocturnal insect layering observed by radar over the UK.

Wind speed

Despite the conclusion above, there are many reports in the literature (from non-UK case studies) where insect layers have been closely associated with wind speed and conspicuously *unrelated* to air temperature profiles. Consequently, it is hypothesised here that the night-time air temperatures in these case-studies were significantly above flight thresholds for the taxa concerned, thus freeing the insects of the need to migrate at warm altitudes. It seems conceivable that large insects—such as migratory noctuid moths—could detect altitudes of wind speed maxima (perhaps related to the optomotor effect or detection of anisotropic turbulence) and thence fly preferentially within them (Chapter 4; Wolf *et al.* 1986). This would be an adaptive strategy for maximizing the insects' displacement. Furthermore, the binary analysis of the VLR dataset (Chapter 5) showed that when layering did occur, nocturnal jets were more intense than when layers did not occur.

In most cases, it can be difficult to distinguish the effects of wind speed from those of temperature: not least because the nocturnal jet usually occurs near to and just above the top of surface inversions (Chapter 1). A hypothesis can be postulated that layers are associated with a nocturnal jet in situations where (*i*) the migrants were flying above the level of the warmest temperatures, and (*ii*) 'ceiling layer' effects were unlikely due to temperatures being well above the preferential minimum at and above the flight altitude.

It seems likely therefore that a hierarchical effect is the most parsimonious explanation for layer altitude. The following is the most likely scenario: on nights when temperatures throughout the boundary layer are well above the flight threshold, migrating moths may select their flight-altitude based on wind speed, to maximise their displacement distance. However, the precise mechanism by which they detect zones of fast wind-speed still remain to be elucidated. Evidence for this hierarchical mechanism comes from the data presented in Chapter 5: only when air temperatures were warm in the critical region were faster wind speeds and more intense jets correlated with larger NLQ values (recall that large NLQ values mean that layers are more intense and are longer in duration).

For passive material in the atmosphere, shears in wind speed and direction can create layers in the vertical profile—due to the process of differential advection. This seems highly unlikely as a mechanism for producing insect layers. It was estimated in Chapter 5 (using typical wind shear values) that heterogeneity in surface insect populations on scales of order 16 km would be needed for differential advection to produce layers that could be observed by the radar: indeed, horizontal correlations in insect populations are typically high over hundreds of kilometres (Taylor 1973). There was no significant correlation between the shear of wind direction and insect layering (Chapter 5).

Humidity

In case studies, relationships were found between layering and low relative humidity (Chapter 4). But there is a strong physical (inverse) relationship between

temperature and relative humidity. In many cases where an inversion exists, there will be a co-located layer of low relative humidity; since high temperatures give a higher saturated vapour pressure, and hence a lower relative humidity (for the same specific humidity). The binary layer analysis revealed that lower relative humidity and high specific humidity were correlated with layer presence. However, the ANOVA showed that neither specific nor relative humidity explained any variance in layer intensity once the variance due to temperature had first been taken into account. Finally, no hierarchical relationships (statistical interactions) could be found between humidity and temperature.

These results, and the fact that a strong relationship between humidity and insect layers has not been described in the literature, suggest that any relationships with humidity are merely surrogates for temperature.

Turbulence and stability

It is well known that turbulent mixing in the atmosphere can spread material (*e.g.* pollen, pollution). Layers of any material can become less concentrated in the vertical when encountering turbulence: as was observed for moths in aircraft-based radar observations in the USA (Wolf *et al.* 1990). It was shown in Chapter 6 that modelled layers were less intense during stronger turbulence. The results of an ANOVA (Chapter 5) showed that during cases of less intense turbulence, insect layers were more concentrated and long-lasting. Turbulence can be suppressed or enhanced by buoyancy (hence, gradient of potential temperature) and generated mechanically (*i.e.* wind speed shear). Therefore, these quantities (potential temperature gradient and wind speed shear) were also analysed in Chapter 5: both were consistent with reduced turbulence during layering occasions. Altogether these results suggest that even without any insect response to turbulence, the effects of turbulent fluctuations can move individual trajectories slightly off course and thus produce a vertical spread in an insect layer.

Overall, this suggests that for trajectory modelling of aerial insect migrations, turbulence is a significant factor that should be included in models.

7·2·4 Potential for future modelling of insect migration

The UK Met Office's dispersion model, NAME (Numerical Atmospheric Modelling Environment), was used as the basis for the insect model developed in Chapter 6: SLIM. Hence, the results discussed in this thesis (particularly the outputs from SLIM) could be used to make adaptations to NAME for more realistic insect trajectory modelling. SLIM is unique in going beyond the approach of just using back-trajectory analysis (see review by Scott and Achtemeier 1987). SLIM includes both turbulence parametrization (identified as necessary in Nathan *et al.* 2005) and a parametrization for insect responses to ambient conditions (*cf.* Achtemeier 1998).

Other UK migrant species could be investigated in a similar manner to the studies carried out here. The turbulence results in Chapter 6 showed that parametrization of turbulence in trajectory models gave a spread of insects, which became more like the layers detected by the radars. Applications to issues of emerging importance include the spread of the bluetongue virus by the vector *Culicoides* (Mellor *et al.* 2000). Obviously, these insects are not large enough to be detected by the VLR used in this study; although other methods could be used to provide data for a numerical model (*e.g.* sampling using an aeroplane or other aerial platform).

The UM data have been found to be highly suitable for comparison with insect data from the radar, since the UM's vertical resolution is similar to that of the VLR and there were no significant biases in the nocturnal cases studied for most of the variables (Chapter 3). Both data-sets are rich resources and hold much promise for future analyses in the biometeorology of high-altitude insect migration.

7·3 Further work

This thesis has improved our understanding of the meteorological mechanisms influencing insect layering, and has led to the identification of a number of areas of possible further research.

It has been assumed in this thesis that layers can only form following a peak in high-altitude emigratory insect activity at dusk: the dusk peak. This will depend on the numbers of flight-ready individuals which have recently emerged, but the surface meteorology (particularly temperature and wind speed) would also explain some of the properties of the dusk peak, such as insect concentration and duration of peak. Nocturnal layers in the UK have only been observed following the dusk peak, hence prediction of dusk peak occasions might lead to an increased predictability in layering.

The mechanisms and adaptive significance of common orientation behaviour were not studied in this thesis. Migrants are often able either to align themselves in a downwind direction, or to orient at an angle to the wind (but generally one which avoids gross backwards (tail-first) displacement (Riley and Reynolds 1986)). In some cases, this occurs under severely reduced illumination. It is conceivable that insects are able to use non-visual cues to detect wind speed and direction, such as anisotropies in turbulence due to Kelvin-Helmholtz waves (Riley 1989). If large insects are indeed able to interpret these turbulence properties, this might have an influence on the choice of flight altitude.

The mechanisms involved in the formation of daytime layers were not studied in this thesis and thus these still remain unclear. Chapter 2 showed that daytime layers were more sporadic in time than night-time layers. Turbulent structure in the convective boundary layer (CBL) during the daytime is important: insects probably respond to updraughts in the CBL leading to concentrations of insects at the updraught top (Geerts *et al.* 2005a, 2005b). Clearly, there is still much

research to be done in explaining the existence and structure of daytime layers of insects.

Model development

It would be useful to validate SLIM beyond the case study approach carried out here. The next step would be to design experiments that enable validation of SLIM in a systematic way. For example, one approach would be to examine correlations between SLIM outputs and radar data for layer altitude, intensity, and duration.

Thus far, layer cessation has only been investigated on a case study basis. A systematic study of layer cessation mechanisms could be performed to attempt to find which of the following hypotheses have most support: (*i*) internal energy resource depletion (*i.e.* fatigue or exhaustion of migrants), (*ii*) an innate (genetically-determined) flight period, (*iii*) lack of insect source populations (*e.g.* coastal effects), and/or (*iv*) increased illumination caused by sunrise. It is probable that a systematic exploration of the dataset would show that a combination of these hypotheses would be involved in layer cessation.

The inclusion of further dimensions would give a full 3D (and time) trajectory model. In addition to being able to provide UK-wide predictions, specific phenomena could be investigated, *e.g.* at what scales of heterogeneity in surface population can differential advection lead to insect layers?

Improvements in the turbulence parametrization in SLIM would strengthen conclusions made from model results, and allow a more accurate prediction of trajectories. For example, analysis could be performed to test if the gradient Richardson number (from UM data) could be used to estimate the turbulent statistics for an inhomogeneous profile.

Laboratory studies of the response of noctuid moth flight to ambient temperature would help in several ways, for example in ascertaining the value of a

preferential minimum temperature for some species of UK noctuid moth. This would aid interpretation of radar data and refine the preferential minimum temperature parameter used in SLIM. In addition, the establishment of a gradient for the insect flight-speed response to ambient temperature would prove a useful development to SLIM.

7·4 Concluding remarks

Most other insect layering studies have been conducted in sub-tropical zones using azimuthally-scanning radars. Prior to the development of vertical-looking, insect-monitoring radar in the UK, little was known about high-altitude flight in the UK, and it was suspected that northern temperate regions of Europe would be rather marginal for insect migration. As this thesis has revealed, there is in fact considerable migratory activity over the UK in the summer months, and a range of fascinating phenomena can be observed. This thesis represents the first substantial analysis of insect migration and layering in the north temperate zone of Europe. Thus, as far as high-altitude nocturnal insect migration is concerned, the UK has moved from one of the least studied to perhaps the best studied environments in the world.

Appendix A: Quickview database

All the radar data (Chapter 2) were used to form a visual database of radar data, an example is shown below (Figure A1).

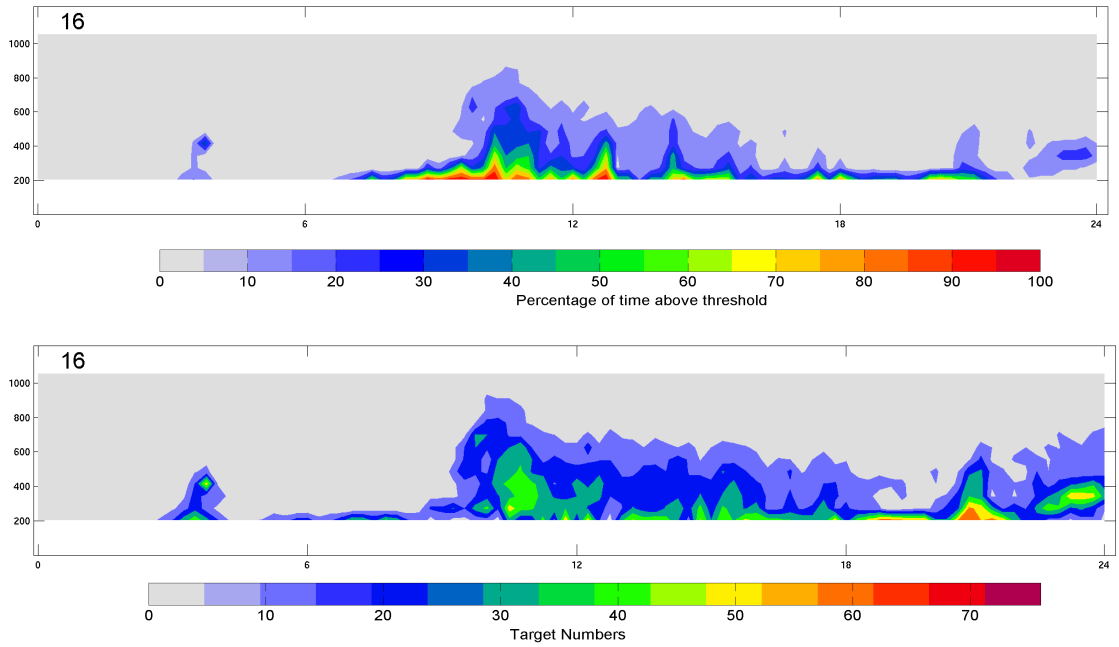

Figure A1 – *An example of Quickview database plots for one day. Insect target number evolution (bottom) and 'percentage-above-threshold' (above) is shown for the Malvern radar, for June 16 2000 (00:00–23:50 hours UTC, x-axis). The first 13 radar range gates are shown (altitude on y-axis), showing data from the centre of range gate 1 (202.5 m) to the centre of range gate 13 (1053.9 m).*

Appendix B: LQ definitions

The threshold values used by the algorithm to set layer quality (LQ) are—of necessity—somewhat arbitrary, based on experience (of the Rothamsted Radar Entomology Unit) of profiles and knowledge of the radar's characteristics. During testing, and the current analysis, they have produced results that appeared to be appropriate when qualitatively compared to the data. LQ values are defined from 0–7. This LQ method is used extensively in Reynolds *et al.* (2005), and in Chapter 5 of this thesis.

LQ = 0: radar not operating.

LQ = 1: 'percentage above –80 dBm threshold' values > 10 % in all range gates. When the percentage above threshold is > 10 %, the target numbers are likely to be seriously affected by interference, and are considered to be unreliable. In particular, a uniformly high percentage above threshold in all range gates is virtually always caused by precipitation, and it is important to exclude these periods from the analysis. (The module does attempt, however, to identify occasions when an insect layer is present, but masked by inter-target interference—see below, LQ = 7.) Altitudes higher than the point at which the percentage above threshold falls below 10 % are subsequently inspected for Layer Qualities of 2–6, using targets numbers.

LQ = 2: no layer, as no (unit) increase in analysable target numbers with altitude.

LQ = 3: no layer; the number of targets in each of the range gates inspected ≤ 5 or the variation in target numbers ≤ 5. This excludes range gate 1 (150 to 195 m) because there are often high numbers of targets at low altitudes for reasons unrelated to the layering of migrants.

LQ = 4: poorly-defined layer; a peak (in a single range gate) has been detected, containing more than 5 targets, but less than 15 % of the total number of targets detected in the profile.

LQ = 5: layer; a peak (in a single range gate) has been detected, containing between 15 % and 25 % of the total targets detected in the profile; or a peak containing > 25 % of the total targets but composed of < 10 targets.

LQ = 6: well-defined layer; a peak (in a single range gate) has been detected with at least 10 targets, and with at least 25 % of total targets. If target numbers are unreliable due to inter-target interference the module then inspects the percentage above threshold data for evidence of a layer.

LQ = 7: possible layer. 'Percentage above –80 dBm threshold' values > 10 % in all gates, and there is a rise of at least 10 % within the profile. The LQ = 7 output is useful when very high insect densities create inter-target interference, preventing the analysis of individual targets. Occasionally an LQ = 7 may also be generated by precipitation in the high altitude range gates, but these occasions can be identified and excluded from analysis because they are usually singletons, preceded and followed by periods with low LQ scores.

Appendix C: One-way ANOVA

GenStat® was used to carry out 1-way ANOVAs (Chapter 5) for NLQ with the factors listed in Table C1; full results are listed. The commands used in GenStat for wind factor are shown below:

```
BLOCK "No Blocking"
TREATMENTS u_cat
COVARIATE "No Covariate"
ANOVA [PRINT=aovtable,information; FPROB=yes] NLQ
```

This represents a no-blocking ANOVA for categorised wind speed with NLQ as the y-variate. Some terms are defined here (see also Fowler *et al.* 1998):

df: degrees of freedom is equal N–1 (where N is the number in the sample)

SS: the sums of squares

ms: mean sum of squares (SS ÷ df)

F: a test statistics calculated by dividing the variance between samples by the variance within samples

p: the probability/significance value

Table C1 – *One-way ANOVA results for NLQ with the listed factors (i.e. meteorological variables in the critical region for nocturnal layering). Emboldened p-values mean a significant result (p < 0.05).*

Factors	df	SS	ms	F	p
A. Wind speed	2	1.385	0.679	0.27	0.767
Residual	276	706.719	2.561		
B. Temperature	2	55.401	27.700	11.71	**<0.001**
Residual	276	652.676	2.365		
C. Relative humidity	2	13.456	6.728	2.67	0.071
Residual	276	694.622	2.517		
D. Specific humidity	2	20.486	10.243	4.11	**0.017**
Residual	276	687.591	2.491		
E. Potential temperature gradient	2	29.564	14.782	6.01	**0.003**
Residual	276	678.513	2.458		
F. Vertical shear of wind speed	1	1.621	1.621	0.64	0.426
Residual	277	706.456	2.550		
G. Richardson Number	1	12.245	12.245	4.87	**0.028**
Residual	277	695.832	2.512		
H. Jet variable	2	9.583	4.792	1.89	0.153
Residual	276	698.494	2.531		
I. Vertical shear of wind direction	2	14.423	7.211	2.87	0.058
Residual	276	693.654	2.513		
Total	**278**	**708.077**			

Appendix D: Two-way ANOVA

An unbalanced ANOVA design was needed when using GenStat for two-way ANOVA with these data. An unbalanced design was used because the order of consideration of variance matters (*i.e.* the results of lines 1 and 4 do not give the same result as they would in a balanced test). The numerical GenStat code used is of the form shown below (the temperature and jet example shown):

```
1 TREATMENTS T_cat*jet_cat
2 COVARIATE "No Covariate"
3 AUNBALANCED [PRINT=aovtable; PSE=diff; FPROB=yes] NLQ; SAVE=_ausave
4 TREATMENTS jet_cat*T_cat
5 COVARIATE "No Covariate"
6 AUNBALANCED [PRINT=aovtable; PSE=diff; FPROB=yes] NLQ; SAVE=_ausave
```

The first line analyses temperature factor first, line 2 is jet factor allowing for temperature, then line 3 is the interaction. Line 4 analyses jet factor first, then temperature allowing for jet factor in line 5, and lastly the interaction in line 6. The variate is NLQ. Temperature was compared to each of the leading factors (see main body text).

Table D1 – *Two-way ANOVA results for NLQ with temperature and other listed factors (i.e. meteorological variables in the critical region for nocturnal layering). Emboldened p-values mean a significant result ($p < 0.05$).*

Factors			df	SS	ms	F	p
A. Wind speed	1st	T	2	55.401	27.700	11.75	**<0.001**
	2nd	u	2	1.598	0.799	0.34	0.713
	Interaction		4	14.585	3.646	1.55	0.189
	1st	u	2	1.358	0.679	0.29	0.750
	2nd	T	2	55.641	27.820	11.80	**<0.001**
	Residual		270	636.493	2.357		
C. Relative humidity	1st	T	2	55.401	27.700	11.77	**<0.001**
	2nd	RH	2	1.549	0.775	0.33	0.720
	Interaction		4	15.583	3.896	1.66	0.161
	1st	RH	2	13.456	6.728	2.86	0.059
	2nd	T	2	43.494	21.747	9.24	**<0.001**
	Residual		270	635.545	2.354		
D. Specific humidity	1st	T	2	55.401	27.700	11.61	**<0.001**
	2nd	q	2	2.078	1.039	0.44	0.647
	Interaction		4	6.412	1.603	0.67	0.612
	1st	q	2	20.486	10.243	4.29	**0.015**
	2nd	T	2	36.993	18.496	7.75	**<0.001**
	Residual		270	644.186	2.386		
E. Potential temperature gradient	1st	T	2	55.401	27.700	11.76	**<0.001**
	2nd	thetagrad	2	12.331	6.166	2.62	0.075
	Interaction		3	2.129	0.710	0.30	0.824
	1st	thetagrad	2	29.564	14.782	6.28	**0.002**
	2nd	T	2	38.168	19.084	8.10	**<0.001**
	Residual		271	638.216	2.355		
G. Richardson number	1st	T	2	55.401	27.700	11.76	**<0.001**
	2nd	Ri	1	5.406	5.406	2.29	0.131
	Interaction		1	1.619	1.619	0.69	0.408
	1st	Ri	1	12.245	12.245	5.20	**0.023**
	2nd	T	2	48.561	24.281	10.30	**<0.001**
	Residual		274	645.651	2.356		
H. Jet variable	1st	T	2	55.401	27.700	11.81	**<0.001**
	2nd	j	2	5.752	2.876	1.23	0.295
	Interaction		4	13.618	3.404	1.45	0.217
	1st	j	2	9.583	4.792	2.04	0.132
	2nd	T	2	51.569	25.784	10.99	**<0.001**
	Residual		270	633.307	2.346		
Total		Total	278	708.077	2.547		

Appendix E: Numerical methods

The different methods for solving the equation of motion during a timestep are numerous (*e.g.* Durran 1999). Three fundamental methods were considered for use in this model. Consider the memory term differential equation:

$$\frac{\mathrm{d}u'}{\mathrm{d}t} = -\frac{u'}{\tau_u}. \qquad \text{(E1)}$$

Equation E1 is an exponential decay, the new velocity values are related to the previous one through the timescale as a decorrelation process. Large timescales give a slowly evolving velocity field and small timescales give fast temporal decorrelation. Considering a velocity time-series (Figure E1a) with magnification to a single timestep (Figure E1b), the variation within the timestep can thus be seen.

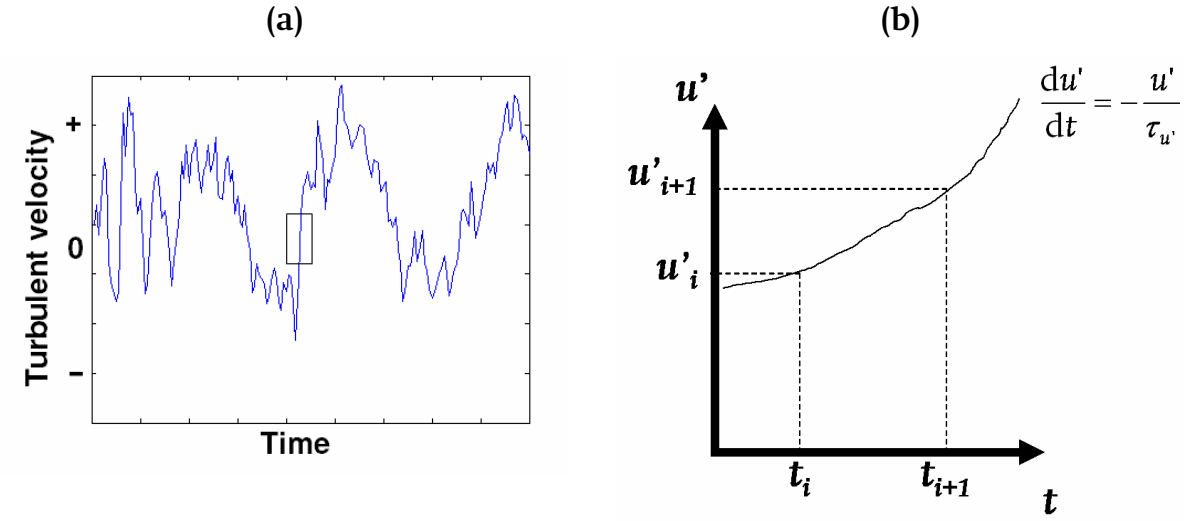

Figure E1 – *(a) Example of turbulent velocity evolution (the box is magnified in figure b). (b) Schematic of evolution of u' within a timestep.*

The area under the curve between t_i and t_{i+1} can be calculated to give the displacement during that timestep–i.e. $\Delta s = \bar{u}\Delta t$, where the overbar represents a mean value. It is physically fundamental that as $\Delta t \to 0$, the changes in u are infinitesimal; hence, the smaller the timestep is, then the smaller any errors in wind speed calculations will be.

Three fundamental finite difference timestepping methods are:

1. Forward-Euler (explicit) is the most straightforward scheme: the area under the curve is calculated using the velocity at previous timestep, $u'(t_i)$: see Figure E2a. This scheme is numerically stable on the condition that $\Delta t < \tau_u$.

$$u'(t_{i+1}) = u'(t_i)\left(1 - \frac{\Delta t}{\tau_u}\right) \tag{E2}$$

2. Backward-Euler (implicit) is an unconditionally stable numerical scheme, the area under the curve is calculated using $u'(t_{i+1})$.

$$u'(t_{i+1}) = u'(t_i) - \frac{u'(t_{i+1})\Delta t}{\tau_u} \tag{E3}$$

3. Trapezoidal, or Crank-Nicolson (mixed implicit/explicit), is unconditionally stable, which allows larger timesteps without the model developing numerical instabilities. The area under the curve is calculated with trapezoid shapes using both timesteps.

$$u'(t_{i+1}) = \left(\frac{1 - \frac{\Delta t}{2\tau_u}}{1 + \frac{\Delta t}{2\tau_u}}\right) u'(t_i) \tag{E4}$$

Even though larger timesteps are numerically stable, accuracy can be at risk because as $\tau \to 0$, then turbulent eddies cannot be resolved. Hence, there is a physical restraint that $\Delta t < \tau_u$ in order to represent turbulent eddies.

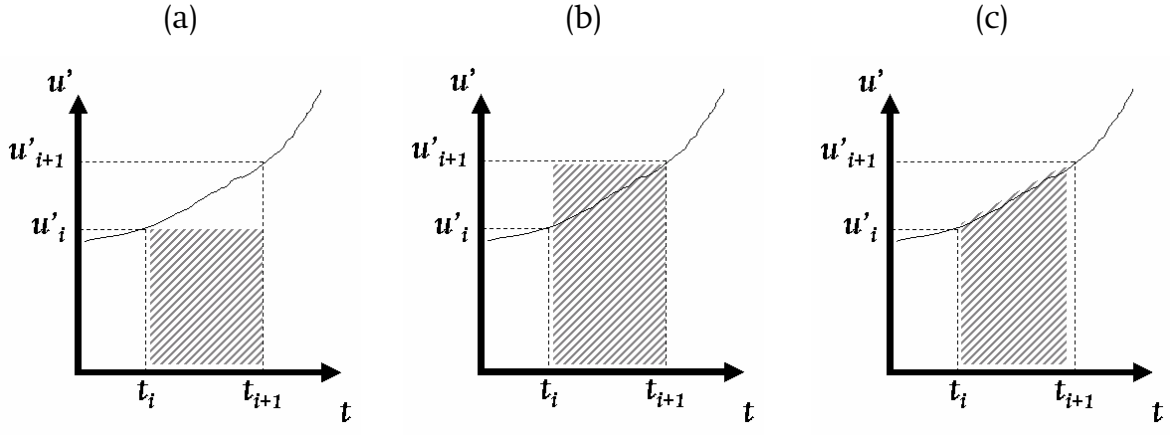

Figure E2 – *Three timestepping schemes: (a) forward-Euler, (b) backward-Euler, (c) trapezoidal. The area under the curves (grey hatching) is equal to the displacement during the timestep.*

Appendix F:
Moth size measurements

For free-fall calculations (Chapter 6), moth dimensions were required to be measured (Figure F1). The thorax width (w_t) was measured at its widest value. Body length (l_b) was measured including abdomen, thorax, and head (antennae were not included). True wing-length (l_w) was taken from wing-tip to the close edge of the thorax. Wing-span (s_w) can be calculated by assuming two wing-lengths plus a thorax width: *i.e.* $s_w = 2l_w + w_t$.

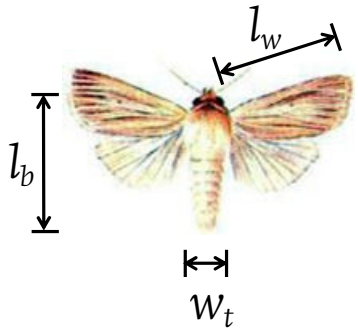

Figure F1 – *Schematic of moth measurements.*

Cross-sectional area can be calculated as open-wing or closed-wing. Open-wing cross-section was calculated as:

$$A_o = 0.7 s_w l_b, \tag{F1}$$

where the value of 0.7 is used as a correction for the fact that the cross-sectional area is smaller than wing-span multiplied by body length. Closed-wing cross-section was calculated as follows:

$$A_c = 0.9 w_t l_b, \tag{F2}$$

in which the value of 0.9 was used because the body width is not constant, but tapers, particularly in the abdomen. For the closed-wing cross-section it was assumed that the wings fold onto the body area.

The volume of moth was required in order to estimate moth density in the free-fall calculations. It was assumed that the wings were of negligibly small mass and volume, and that the moth dimensions could be assumed as a cylinder (Figure F2). Hence, the volume of the moth was estimated as:

$$V_m = 0.9\pi\left(\frac{w_t}{2}\right)^2 l_b, \tag{F3}$$

where the 0.9 is another parameter to adjust for variable body width.

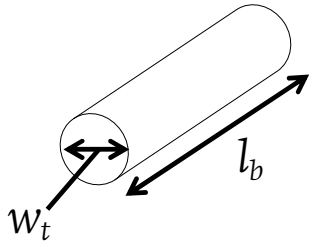

Figure F2 – *Schematic for volume calculation.*

Glossary of symbols

This section is split into categories to aid searching (general, subscripts, radar, profiles, meteorology, statistics, and entomology). The symbols are described in more detail in the main body of the thesis.

1. General

a.g.l.	Above ground level
a.s.l.	Above sea level
A	Cross-sectional area, perpendicular to the flow [m^2]
C_D	Dimensionless drag co-efficient
CSD	Circular standard deviation
f	Coriolis parameter [~ 10^{-4} s^{-1} in mid-latitudes]
F_g	Gravitational force [N]
F_d	Drag force [N]
g	Gravitational acceleration [9.8 m s^{-2}]
Re	Reynolds number
$\underline{\mathbf{s}} = x, y, z$	Displacement vector, decomposed into the three standard orthogonal distances (sometimes with x defined as in the direction of mean flow) [m]
t	Time [s]
UTC or GMT	Universal time co-ordinated or Greenwich mean time
$\underline{\mathbf{u}} = u, v, w$	Velocity vector, decomposed into three orthogonal parts [ms^{-1}]
z	Altitude [m]
ν	Kinematic viscosity of air [1.01 x 10^{-6} m^2 s^{-1}, at 20 °C]
ξ	Random number with unit variance
π	3.14
ρ_a	Air density [1.20 kg m^{-3}, at 20 °C]

ψ	Hypothetical variable
$\overline{\psi}$	Mean of property ψ
$\Delta\psi$	A finite increment in property ψ
ψ'	Turbulent fluctuation of property ψ
$\psi \to 0$	Property ψ tends to zero
ψ_s	Surface value of property ψ
ψ_0	Reference value of property ψ
$\psi = \mathrm{f}^{\mathrm{n}}(\alpha, \beta)$	Property ψ is a function of α and β
$\partial\psi/\partial z$	Rate of change of property ψ with respect to altitude, z
$\underline{\psi}$	Vector property
ψ	Scalar property
$\lvert\underline{\psi}\rvert$	Magnitude of vector: becomes scalar
$\psi(t)$	Property ψ, as a function of time, t
$\psi(t)$ or $\psi(t_i)$	Property ψ at time t
$\psi(t+1)$ or $\psi(t_{i+1})$	Property ψ after an increment of time

2. Subscripts

i	Insect
int	Interaction (in ANOVA)
l	Low-frequency meander term
UM	Unified Model, *i.e.* model-derived wind speed
1,2,3	Category number (in ANOVA)

3. Radar

d*Bm*	The power level in decibels, referenced to 1 mW

4. Profiles

C	A scale factor denoting the general size of insect population
LQ	Layer quality
NLQ	Nocturnal layer quality
z_e	A shift of the insect profile
λ	The regression coefficient of log density on log altitude

5. Boundary-layer meteorology

BL	Boundary layer (sometimes atmospheric BL: hence, ABL)
c_p	Specific heat capacity of air at constant pressure [1004 J kg^{-1} K^{-1}]
CBL	Convective boundary layer
e	Turbulent kinetic energy [J]
EZ	Entrainment zone (atop the convective boundary layer)
FA or FT	Free atmosphere or free troposphere (*i.e.* above the boundary layer)
G	Geostrophic wind speed [m s^{-1}]
H	Sensible heat flux [W m^{-2}]
j	Jet strength
k	Von kármán's constant [0.41]
K_H	Eddy diffusivity/viscosity for heat [m^2 s^{-1}]
K_M	Eddy diffusivity/viscosity for momentum [m^2 s^{-1}]
L	Obukhov length [m]
M	Horizontal wind speed (momentum) [m s^{-1}]
ML	Mixed layer (the largest portion of the convective boundary layer)
NBL	Nocturnal boundary layer (often becomes a stable BL: hence, SBL)
p	Atmospheric pressure [Pa]
p_0	Reference pressure [10^5 Pa]
q	Specific humidity [g kg^{-1}]
r	Humidity mixing ratio [g kg^{-1}]

R	Dry gas constant [287 J kg^{-1} K^{-1}]
RH	Relative humidity [%]
Ri	Richardson number
Ri_B	Bulk Richardson number
Ri_c	Critical Richardson number
Ri_f	Flux Richardson number
Ri_T	A sub-critical Richardson number
SL	Surface layer (layer where friction with the Earth is important)
T	Absolute temperature [K]
u_j	Wind speed at jet maximum [m s^{-1}]
$u_{\min\uparrow}$	Wind speed at minimum above jet [m s^{-1}]
u_*	Friction velocity [m s^{-1}]
z_i	Altitude of lowest inversion [m]
z_0	Roughness length [m]
z_T	Roughness length for temperature [m]
ε	Dissipation energy [J]
ζ	Monin-Obukhov stability parameter, $\zeta = z / L$
θ	Potential temperature [K]
θ_*	Potential temperature scale in the surface layer [K]
σ_w	Standard deviation of vertical velocity [s]
$\sigma_w{}^*$	Revised standard deviation of vertical velocity for inertia [s]
τ_s	Surface momentum stress [N m^{-2}]
τ_w	Lagrangian timescale for vertical turbulence decorrelation [s]
$\tau_w{}^*$	Revised Lagrangian timescale for eddy-crossing effect [s]
ϕ_h	Function of ζ for heat
ϕ_m	Function of ζ for momentum
ϕ	Wind direction [° from north, bearing]

6. Statistics

F	A test statistic calculated by dividing the variance between samples by the variance within samples (particularly in ANOVA)
ms	Mean sum of squares: SS ÷ df (particularly in ANOVA)
N	Sample size
p	p-value for statistical significance
r	Correlation coefficient
r^2	Coefficient of determination (amount of variance explained)
s	Sample variance
sk	Skewness
SS	The sums of squares (particularly in ANOVA)
ν (or df)	Degrees of freedom, $\nu = \mathrm{N} - 1$
χ^2	Probability distribution for statistical significance tests

7. Entomology

CEW	Corn earworm, a noctuid moth
FAW	Fall armyworm, a noctuid moth
m_i	Insect mass [kg]
T_{amb}	Ambient temperature (*e.g.* for Lagrangian insect) [°C]
TBW	Tobacco budworm, a noctuid moth
T_0	Insect preferential minimum temperature [°C]
w_T	Terminal velocity [m s^{-1}]
$w_{T,o}$	Terminal velocity, for open wings [m s^{-1}]
$w_{T,c}$	Terminal velocity, for closed wings [m s^{-1}]
γ_m	Gradient for relationship between w_i and m_i [m s^{-1} kg^{-1}]
γ_T	Gradient for relationship between w_i and T_{amb} [m s^{-1} K^{-1}]
ρ_i	Insect body density [kg m^{-3}]

References

Achtemeier, G. L. (1998). A framework for standardizing flight characteristics for separating biology from meteorology in long-range insect transport. In *13th Conference of Biometeorology and Aerobiology*, pages 360-363. American Meteorological Society.

Andre, J. C. and Mahrt, L. (1982). The nocturnal surface inversion and influence of clear-air radiative cooling. *J. Atmos. Sci.*, **39**, 864-878.

Apsley, D. D. (1989). Modelling airborne dispersion of coarse particulate material. Technical Report RD/L/3481/R89, CEGB.

Apsley, D. D., Dyster, S. J., and McHugh, C. (2005). Modelling dry deposition. Technical Report P17/13E/05, ASMS3: National Power and CERC.

Arya, S. P. (1988). *Introduction to micro-meteorology*. Academic Press.

Aylor, D. E. and Flesch, T. K. (2001). Estimating spore release rates using a Lagrangian stochastic simulation model. *J. Appl. Meteorol.*, **40**, 1196-1208.

Bartholomew, G. A. and Heinrich, B. (1973). A field study of flight temperatures in moths in relation to body weight and wing loading. *J. Exp. Biol.*, **58**, 123-135.

Bean, B. R., McGavin, R. E., Chadwick, R. B., and Warner, B. D. (1971). Preliminary results of utilizing the high resolution FM radar as a boundary layer probe. *Bound-Layer Meteorol.*, **1**, 466-473.

Beerwinkle, K. R., Lopez, J. D., Witz, J. A., Schleider, P. G., Eyster, R. S., and Lingren, P. D. (1994). Seasonal radar and meteorological observations associated with nocturnal insect flight at altitudes to 900 metres. *Environ. Ento.*, **23**(3), 676-683.

Bowen, B. M., Baars, J. A., and Stone, G. L. (2000). Nocturnal wind direction shear and its potential impact on pollutant transport. *J. Appl. Meteorol.*, **39**, 437-445.

Browning, K. A. (1981). Ingestion of insects by intense convective updraughts. *Antenna*, **5**, 14-17.

Burt, P. J. A. and Pedgley, D. E. (1997). Nocturnal insect migration: effects of local winds. *Advances in Ecological Research*, **27**, 61-92.

Campistron, B. (1975). Ingestion of insects by intense convective updraughts. *Antenna*, **5**, 14-17.

Carpenter, J. E., Sparks, A. N., and Harrell, E. A. (1981). The effect of temperature on wingbeat frequency and sustained flight on certain Lepidopterous insects. *J. Ga. Entomol. Soc.*

Carson, D. J. (1973). The development of a dry inversion-capped convectively unstable boundary layer. *Q. J. R. Meteorol. Soc.*, **99**, 450-467.

Chapman, J. W., Smith, A. D., Woiwod, I. P., Reynolds, D. R., and Riley, J. R. (2002a). Development of vertical-looking radar technology for monitoring insect migration. *Comp. Electron. Agric.*, **35**, 95-110.

Chapman, J. W., Reynolds, D. R., Smith, A. D., Riley, J. R., Pedgley, D. E., and Woiwod, I. P. (2002b). High-altitude migration of the diamondback moth *Plutella xylostella* to the U.K.: a study using radar, aerial netting, and ground trapping. *Ecol. Ento.*, **27**, 641-650.

Chapman, J. W., Reynolds, D. R., and Smith, A. D. (2003). Vertical-looking radar: A new tool for monitoring high-altitude insect migration. *Bioscience*, **53**, 503-511.

Chapman, J. W., Reynolds, D. R., Smith, A. D., Smith, E. T., and Woiwod, I. P. (2004a). An aerial netting study of insects migrating at high altitude over England. *Bull. Ento. Res.*, **94**, 123-136.

Chapman, J. W., Reynolds, D. R., and Smith, A. D. (2004b). Migratory and foraging movements in beneficial insects: a review of radar monitoring and tracking methods. *Int. J. Pest Manag.*, **50**(3), 225-232.

Chinery, M. (1993). *Field Guide: Insects of Britain and Northern Europe*. Collins, 3rd edition.

Clark, D. P. (1969). Night flights of the Australian plague locust, *Chortoicetes terminifera* Walk., in relation to storms. *Aust. J. Zool.*, **17**, 329-352.

Coad, B. R. (1931). Insects captured by airplane are found at surprising heights. *Yb. of Agric.*, **U.S. Dept. Agric.**, 320-323.

Coombs, M. (1993). Endothermy and flight thresholds for *Helicoverpa punctigera* and H. armigera (Lepidoptera:Noctuidae). *Aust. J. Zool.*, **41**, 577-587.

Cullen, M. J. P., Davies, T., Mawson, M. H., James, J. A., Coulter, S. C., and Malcolm, A. (1997). *Numerical methods in atmospheric and ocean modelling: The Andre J. Robert memorial volume.*, chapter An overview of numerical methods for the next generation UK NWP and climate model., pages 425-444. Canadian Meteorological and Oceanographic Society, Ottawa, Canada.

Davies, P. A. (2000). Development and mechanisms of the nocturnal jet. *Meteorol. Appl.*, **7**, 239-246.

Dingle (1996). *Migration: biology of life on the move*. OUP, NY.

Dingle, H. and Drake, V. A. (2007). What is migration? *Biocience*, **57**, 113-121.

Drake, V. A. (1984). The vertical distribution of macro-insects migrating in the nocturnal boundary layer: a radar study. *Bound-Layer Meteorol.*, **28**, 353-374.

Drake, V. A. (1985a). Radar observations of moths migrating in a nocturnal low-level jet. *Ecol. Ento.*, **10**, 259-265.

Drake, V. A. (1985b). Solitary wave disturbances of the nocturnal boundary layer revealed by radar observations of migrating insects. *Bound-Layer Meteorol.*, **31**, 269-286.

Drake, V. A. (2002). Automatically operating radars for monitoring insect pest migrations. *Entomol. Sinica*, **9**, 27-39.

Drake, V. A. and Farrow, R. A. (1983). Nocturnal migration of the Australian plague locust, *Chortoicetes terminifera* (Walker) (Orthoptera: Acrididae): quantitative radar observations of a series of northward flights. *Bull. Ento. Res.*, **73**, 567-585.

Drake, V. A. and Farrow, R. A. (1985). A radar and aerial-trapping study of an early spring migration of moths (Lepidoptera) in inland New South Wales. *Aust. J. Ecol.*, **10**, 223-235.

Drake, V. A. and Farrow, R. A. (1988). The influence of atmospheric structure and motions on insect migration. *Ann. Rev. Ento.*, **33**, 183-210.

Drake, V. A. and Rochester, W. A. (1994). The formation of layer concentrations by migrating insects. In *21st Conference on Agricultural & Forest Meteorology and the 11th Conference of Biometeorology and Aerobiology*, pages 411-414. American Meteorological Society.

Drake, V. A., Helm, K. F., Readshaw, J. L., and Reid, D. G. (1981). Insect migration across Bass Strait during spring: a radar study. *Bull. Ento. Res.*, **71**, 449-466.

Dudley, R. (2001). *Insect Movement: Mechanisms and Consequences*, chapter 2: The Biomechanics and Functional Diversity of Flight. CABI Publishing.

Durran, D. R. (1999). *Numerical methods for wave equations in geophysical fluid dynamics*. Springer-Verlag.

Edwards, J. M., Beare, R. J., and Lapworth, A. J. (2006). Simulation of the observed evening transition and nocturnal boundary layers: Single-column modelling. *Q. J. R. Meteorol. Soc.*, **132**, 61-80.

Enserink, M. (2006). During a hot summer, bluetongue virus invades northern Europe. *Science*, **313**, 1218-1219.

Essery, R., Best, M., and Cox, P. (2001). Moses 2.2 technical documentation. Technical Report 30, UK Met Office Hadley Centre.

Farrow, R. A. (1986). *Insect Flight: Dispersal and Migration*, chapter Interactions between synoptic scale and boundary-layer meteorology on micro-insect migration., pages 185-195. Berlin/Heidelberg: Springer-Verlag.

Feng, H. Q., Wu, K. M., Cheng, D. F., and Guo, Y. Y. (2003). Radar observations of the autumn migration of the beet armyworm *Spodoptera exigua* (Lepidoptera:Noctuidae) and other moths in northern China. *Bull. Ento. Res.*, **93**, 115-124.

Feng, H. Q., Wu, K. M., Cheng, D. F., and Guo, Y. Y. (2004a). Northward migration of *Heliocoverpa armigera* (Lepidoptera:Noctuidae) and other moths in early summer observed with radar in northern China. *Ecology and Behaviour*, **97**, 1874-1883.

Feng, H. Q., Wu, K. M., Cheng, D. F., and Guo, Y. Y. (2004b). Spring migration and summer dispersal of *Loxostege sticticalis* (Lepidoptera:Pyralidae) and other insects observed with radar in northern China. *Population Ecology*, **33**, 1253-1265.

Fitt, G. P. (1989). The ecology of *Heliothis* species in relation to agroecosystems. *Ann. Rev. Ento.*, **34**, 17-52.

Fitt, G. P., Dilon, M. L., and Hamilton, J. G. (1995). Spatial dynamics of *Helicoverpa* populations Australia: simulation modelling and empirical studies of adult movement. *Comp. Electron. Agric.*, **13**, 177-192.

Fowler, J., Cohen, L., and Jarvis, P. (1998). *Practical statistics for field biology*. John Wiley and Sons.

Freeman, J. A. (1946). The distribution of spiders and mites up to 300 ft. in the air. *J. Anim. Ecol.*, **15**, 69-74.

French, R. A. (1969). Migration of *Laphygma exigua* Hübner (Lepidoptera:Noctuidae) to the British Isles in relation to large-scale weather systems. *J. Anim. Ecol.*, **38**(1), 199-210.

Gallagher, F. W., Bowers, J. F., Laufenberg, E. J., Argenta, E. P., Storwold, D. P., and McLaughlin, S. A. (2004). Possible detection of insects in an urban environment by a frequency modulated-continuous wave radar. In *16th Conference on Biometeorology and Aerobiology*, Vancouver, BC, Canada. American Meteorological Society.

Garratt, J. R. (1992). *The atmospheric boundary layer*. Cambridge atmospheric and space series. Cambridge University Press.

Gatehouse, A. G. (1997). Behavior and ecological genetics of wind-borne migration by insects. *Ann. Rev. Ento.*, **42**, 475-502.

Geerts, B. and Miao, Q. (2005a). Airborne radar observations of the flight behavior of small insects in the atmospheric convetive boundary layer. *Quant. Ecol.*, **34**, 361-377.

Geerts, B. and Miao, Q. (2005b). A simple numerical model of the flight behavior of small insects in the atmospheric convective boundary layer. *Quant. Ecol.*, **34**, 353-360.

Götz, K. G. (1972). Principles of optomotor reaction in insects. *Bibl. Ophthalmol.*, **82**, 251-259.

Grant, A. L. M. (1994). Wind profiles in the stable boundary layer, and the effect of low relief. *Q. J. R. Meteorol. Soc.*, **120**, 27-46.

Grant, A. L. M. (1997). An observational study of the evening transition boundary-layer. *Q. J. R. Meteorol. Soc.*, **123**, 657-677.

Greenbank, D. O., Schaefer, G. W., and Rainey, R. C. (1980). *Spruce budworm (Lepidoptera:Tortricidae) moth flight and dispersal: new understanding from canopy observations, radar and aircraft*. Entomological Society of Canada, Ottawa.

Gregg, P. C., Del Socorro, A. P., and Rochester, W. A. (2001). Field test of a model of migration of moths (Lepidoptera:Noctuidae) in inland Australia. *Aust. J. Entomol.*, **40**, 249-256.

Gregory, D. and Rowntree, P. R. (1990). A mass flux convection scheme with representation of cloud ensemble characteristics and stability-dependent closure. *Mon. Weath. Rev.*, **118**, 1483-1506.

Gullan, P. J. and Cranston, P. S. (2000). *Insects: an outline of entomology*. Blackwell Science.

Harrington, R. and Woiwod, I. P. (1995). Insect crop pests and the changing climate. *Weather*, **50**, 200-208.

Hobbs, S. E. and Wolf, W. W. (1989). An airborne radar technique for studying insect migration. *Bull. Ento. Res.*, **79**, 693-704.

Hobbs, S. E. and Wolf, W. W. (1996). Developments in airbourne entomological radar. *J. Atmos. Oceanic Technol.*, **13**, 58-61.

Holton, J. R. (1992). *Dynamic meteorology*. Academic Press.

Irwin, M. E. and Thresh, J. M. (1988). Long-range dispersal of cereal aphids as virus vectors in North America. *Phil. Trans. Royal Soc. London B*, **321**, 421-446.

Johnson, C. G. (1957). The distribution of insects in the air and the empirical relation of density to height. *J. Anim. Ecol.*, **26**, 479-494.

Johnson, C. G. (1969). *Migration and dispersal of insects by flight*. Metheun and Co, London.

Kaimal, J. C. and Finnigan, J. J. (1994). *Atmospheric boundary layer flows*. Oxford University Press.

Kennedy, J. S. (1961). A turning point in the study of insect migration. *Nature*, **189**, 785-791.

Kennedy, J. S. (1985). *Migration: mechanisms and adaptive significance (Ed. M.A. Rankin)*, volume 27, chapter Migration, behavioural and ecological, pages 5-26. Contributions in Marine Science Suppl.

Kondo, J., Kanechica, O., and Yasuda, N. (1978). Heat and momentum transfer under strong stability in the atmospheric surface layer. *J. Atmos. Sci.*, **35**, 1012-1021.

Lapworth, A. (2003). Factors determining the decrease in surface wind speed following the evening transition. *Q. J. R. Meteorol. Soc.*, **129**, 1945-1968.

Lee, D. R., Stull, R. B., and Irvine, W. S. (1979). Clear air turbulence forecasting techniques. Afgwc/tn-79/001, Air Force Global Weather Central, Offutt AFB, NE 68113.

Lewis, T. and Taylor, L. R. (1964). Diurnal periodicity of flight by insects. *Trans. R. Ento. Soc. London*, **116**, 393-479.

Lingren, P. D., Raulston, J. R., Popham, T. W., Wolf, W. W., Lingren, P. S., and Esquivel, J. F. (1995). Flight behaviour of corn earworm (Lepidoptera:Noctuidae) moths under low wind speed conditions. *Environ. Ento.*, **24**, 851-860.

Lock, A. P., Brown, A. R., Bush, M. R., Martin, G. M., and Smith, R. N. B. (2000). A new boundary layer mixing scheme. part 1: Scheme description and single-column model tests. *Mon. Weath. Rev.*, **128**, 3187-3199.

Luhar, A. K. (2002). The influence of vertical wind direction shear on dispersion in the convective boundary layer, and its incorporation in coastal fumigation models. *Bound-Layer Meteorol.*, **102**, 1-38.

Luis Yela, J. and Holyoak, M. (1997). Effects of moonlight and meteorological factors on light and bait trap catches of nocturnal moths (Lepidoptera:Noctuidae). *Environ. Ento.*, **26**(6), 1283-1290.

Mahrt, L. (1981). The early evening boundary layer transition. *Q. J. R. Meteorol. Soc.*, **107**, 329-343.

Mardia, K. V. (1972). *Statistics of Directional Data.* Academic Press, London.

Maryon, R. H. (1997). The gravitational settling of particulates: towards a parameterisation for the 'NAME' dispersion model. Turbulence and Diffusion Note 244, Met Office (PMSR).

Maryon, R. H. (1998). Determining cross-wind variance for low frequency wind meander. *Atmos. Environ.*, **32**, 115-121.

Maryon, R. H., Ryall, D. B., and Malcolm, A. L. (1999). The NAME 4 dispersion model: science documentation. Turbulence and Diffusion Note 262, Met Office (PMSR).

Matthews, R. W. and Matthews, J. R. (1978). *Insect Behaviour*. John Wiley and Sons.

May, M. L. (1979). Insect thermoregulation. *Ann. Rev. Ento.*, **24**, 313-349.

McCorcle, M. D. and Fast, J. D. (1989). Prediction of pest distribution in the corn belt: a meteorological analysis. In *Proceedings of the 9th conf. on biometeorology and aerobiology*, pages 298-302.

McIlveen, R. (1992). *Fundamentals of weather and climate*. Stanley Thornes Publisher Ltd.

Mellor, P. S., Boorman, J., and Baylis, M. (2000). *Culicoides* biting midges: Their role as arbovirus vectors. *Ann. Rev. Ento.*, **45**, 307-340.

Mel'nichenko, A. N. (1936). Regularities of mass flying of the adults of *Loxostege stictalis* L. and the problems of the prognosis of their flight migrations. *Bull. Plant. Prot.*, **17**, 56.

Nathan, R., Sapir, N., Trakhtenbrot, A., Katul, G. G., Bohrer, G., Otte, M., Avissar, R., Soons, M. B., Horn, H. S., Wikelski, M., and Levin, S. A. (2005). Long-distance biological transport processes through the air: can nature's complexity be unfolded *in silico*? *Diversity Dist.*, **11**, 131-137.

Otuka, A., Watanabe, T., Suzuki, Y., Matsumura, M., Furuno, A., Chino, M., Kndon, T., and Kamimuro, T. (2006). A migration analysis of *Sogatella furcifera* (Horvath) (Homoptera:Delphacidae) using hourly catches and a three-dimensional simulation model. *Agric. and Forest Ento.*, **8**, 35-47.

Panofsky, H. A. and Dutton, J. A. (1984). *Atmospheric turbulence*. John Wiley and Sons.

Payne, R. W., Baird, D. B., Cherry, M., Gilmour, A. R., Harding, S. A., Kane, A. F., and Lane, P. W. (2003). *The guide to GenStat® release 7.1. Part2:Statistics.* VSN International, Oxford, U.K.

Pedgley, D. E. (1993). Managing migratory insect pests - a review. *Int. J. Pest Manag.*, **39**, 3-12.

Pedlosky, J. (1987). *Geophysical fluid dynamics*. Springer-Verlag.

Petty, G. W. (2004). *A first course in atmospheric radiation.* Sundog publishing.

Rainey, R. C. (1974). Biometeorology and insect flight: some aspects of energy exchange. *Ann. Rev. Ento.*, **19**, 407-439.

Rainey, R. C. (1989). *Migration and Meteorology*. Clarendon Press, Oxford.

Reynolds, D. R. and Riley, J. R. (1997). The flight behaviour and migration of insect pests: radar studies in developing countries. NRI bulletin 71, Natural Resources Institute, Chatham, UK.

Reynolds, D. R., Chapman, J. W., Edwards, A. S., Smith, A. S., Wood, C. R., Barlow, J. F., and Woiwod, I. P. (2005). Radar studies of the vertical distribution of insects migrating over southern Britain: the influence of temperature inversions on nocturnal layer concentrations. *Bull. Ento. Res.*, **95**, 259-274.

Reynolds, D. R., Chapman, J. W., and Harrington, R. (2006). The migration of insect vectors of plant and animal viruses. *Advances in Virus Research*, **67**, 453-517.

Reynolds, D. R., Smith, A. D., and Chapman, J. W. (2007). A radar study of emigratory flight and layer formation by insects at dawn over southern Britain. *Bull. Ento. Res.*, **in press**.

Riley, J. R. (1975). Collective orientation in night-flying insects. *Nature*, **253**, 113-114.

Riley, J. R. (1989). Orientation by high-flying insects at night: observations and theories. In *Orientation and Navigation - Birds, Humans and other animals*, volume Conference of the Royal Institute of Navigation, Cardiff, 6-8 April 1989. The Royal Institute of Navigation, London.

Riley, J. R. and Reynolds, D. R. (1979). Radar-based studies of the migratory flight of grasshoppers in the middle Niger area of Mali. *Proc. Royal Soc. London B*, **204**, 67-82.

Riley, J. R. and Reynolds, D. R. (1986). *Insect Flight: Dispersal and Migration*, chapter Orientation at night by high-flying insects, pages 71-87. Berlin/Heidelberg: Springer-Verlag.

Riley, J. R., Reynolds, D. R., and Farmery, M. J. (1981). Radar observations of *Spodoptera exempta*, Kenya, March-April 1979.

Riley, J. R., Reynolds, D. R., and Farmery, M. J. (1983). Observations of the flight behaviour of the armyworm moth, *Spodoptera exempta*, at an emergence site using radar and infra-red optical techniques. *Ecol. Ento.*, **8**, 395-418.

Riley, J. R., Cheung, X. N., Zhang, X. X., Reynolds, D. R., Xu, G. M., Smith, A. D., Cheng, J. Y., Bao, A. D., and Zhai, B. P. (1991). The long-distance migration of *Nilaparvata lugens* (Stål) (Delphacidae) in China: radar observations of mass return flight in the autumn. *Ecol. Ento.*, **16**, 471-489.

Riley, J. R., Reynolds, D. R., Smith, A. D., Edwards, A. S., Zhang, X. X., Cheng, X. N., Wand, H. K., Cheng, J. Y., and Zhai, B. P. (1995). Observations of the autumn migration of the rice leaf roller *Cnaphalocrosis medinalis* (Lepidoptera:Pyralidae) and other moths in eastern China. *Bull. Ento. Res.*, **85**, 397-414.

Rochester, W. A. (1999). *The migration systems of* Helicoverpa punctigera *(Wallengren) and* Helicoverpa armigera *(Hübner) (Lepidoptera:Noctuidae) in Australia*. Ph.D. thesis, The University of Western Australia.

Rochester, W. A., Dillon, M. L., Fitt, G. P., and Zalucki, M. P. (1996). A simulation model of the long-distance migration of Helicoverpa spp. moths. *Ecol. Modelling*, **86**, 151-156.

Rodean, H. C. (1996). *Stochastic Lagrangian models of turbulent diffusion*, volume 26 of *Meteorological Monographs*. American Meteorological Society, Boston.

Saunders, W. E. (1952). Some further aspects of night cooling under clear skies. *Q. J. R. Meteorol. Soc.*, **78**, 603-612.

Schaefer, G. W. (1976). Radar observations of insect flight. *Symp. R. Ento. Soc. London*, **7**, 157-197.

Schaefer, G. W. (1979). An airborne radar technique for the investigation and control of migrating pest insects. *Phil. Trans. Royal Soc. London B*, **287**, 459-465.

Scott, R. W. and Achtemeier, G. L. (1987). Estimating pathways of migrating insects carried in atmospheric winds. *Environ. Ento.*, **16**, 1244-1254.

Showers, W. B. (1997). Migration ecology of the black cutworm. *Ann. Rev. Ento.*, **42**, 393-425.

Smith, A. D., Riley, J. R., and Gregory, R. D. (1993). A method for routine monitoring of the aerial migration of insects by using a vertical-looking radar. *Phil. Trans. Royal Soc. London B*, **340**, 393-404.

Smith, A. D., Reynolds, D. R., and Riley, J. R. (2000). The use of vertical-looking radar to continuously monitor the insect fauna flying at altitude over southern England. *Bull. Ento. Res.*, **90**, 265-277.

Southwood, T. (1977). Habitat, the templet for migration strategies? *J. Anim. Ecol.*, **46**, 337-365.

Sparks, A. N., Westbrook, J. K., and Wolf, W. W. (1985). Atmospheric transport of biotic agents on a local scale. In *The Movement and Dispersal of Agriculturally Important Biotic Agents*, An International Conference on The Movement and Dispersal of Biotic Agents, pages 203-217, Louisiana.

Stout, J. E., Arya, S. P., and Genikhovich, E. L. (1995). The effect of nonlinear drag on the motion and settling velocity of heavy particles. *J. Atmos. Sci.*, **52**, 3836-3848.

Stull, R. B. (1997). *An Introduction to Boundary Layer Meteorology*. Kluwer Academic Publishers.

Stull, R. B. (2000). *Meteorology for Scientists and Engineers*. Brooks/Cole.

Symmons, P. M. and Luard, E. J. (1982). The simulated distribution of night-flying insects in a wind convergence. *Aust. J. Zool.*, **30**, 187-198.

Taylor, L. R. (1973). Monitoring change in the distribution and abundance of insects. *Rep. Rothamsted exp. Stn for 1973, Part 2.* 202-239.

Taylor, L. R. (1974). Insect migration, flight periodicity and the boundary layer. *J. Anim. Ecol.*, **43**(1), 225-238.

Taylor, L. R. and Carter, C. I. (1961). The analysis of numbers and distribution in an aerial population of macrolepidoptera. *Trans. R. Ento. Soc. London*, **113**, 369-386.

Taylor, P. S. and Sheilds, E. J. (1990). Flight thresholds of the armyworm (Lepidoptera: Noctuidae). *Environ. Ento.*, **19**, 1410-1417.

Taylor, R. A. J. (1979). A simulation model of locust migratory behaviour. *J. Anim. Ecol.*, **48**, 577-602.

Thomas, A. A. G., Ludlow, A. R., and Kennedy, J. S. (1977). Sinking speeds of falling and flying *Aphis fabae* scopoli. *Ecol. Ento.*, **2**, 315-326.

Thomas, C. F. G., Brain, P., and Jepson, P. C. (2003). Aerial activity of linyphiid spiders: modelling dispersal distances from meteorology and behaviour. *J. App. Ecol.*, **40**, 912-927.

Thomson, D. J. (1987). Criteria for the selection of stochastic models of particle trajectories in turbulent flows. *J. Fluid Mech.*, **180**, 529-556.

Thorpe, A. J. and Guymer, T. H. (1977). The nocturnal jet. *Q. J. R. Meteorol. Soc.*, **103**, 633-653.

Turner, R., Song, Y. H., and Uhm, K. B. (1999). Numerical model simulations of brown planthopper *Nilaparvata lugens* and white-backed planthopper *Sogatella furcifera* (Hemiptera: Delphacidae) migration. *Bull. Ento. Res.*, **89**, 557-568.

Van der Hoven, I. (1957). Power spectrum of horizontal wind speed in the frequency range from 0.0007 to 900 cycles per hour. *J. Met.*, **14**, 160-164.

Vaughn, C. R. (1985). Birds and insects as radar targets: A review. *Proc. IEEE*, **73**, 205-227.

Westbrook, J. K., McCraken, G. F., and Kunz, T. H. (2006). Aerobiology of predator and prey: bats and insects. In *17th Conference on Biometeorology and Aerobiology*, San Diego, CA, USA. American Meteorological Society.

White, F. M. (1974). *Viscous fluid flow*. McGraw-Hill.

Williams, C. B. (1930). *The Migration of Butterflies*. Oliver and Boyd: Edinburgh.

Williams, C. B. (1958). *Insect Migration*. Collins London.

Wilson, D. R. and Ballard, S. P. (1999). A microphysically based precipitation scheme for the UK Meteorological Office Unified Model. *Q. J. R. Meteorol. Soc.*, **125**, 1607-1636.

Woiwod, I. P. and Harrington, R. (1994). *Long-term experiments in agricultural and ecological sciences*, chapter Flying in the Face of Change – The Rothamsted Insect Survey, pages 321-342. CAB International, Wallingford.

Wolf, W. W., Westbrook, J. K., and Sparks, A. N. (1986). Relationship between radar entomological measurements and atmospheric structure in south Texas during March and April 1982. In *Proc. of Entomological Societies of America and Canada, Toronto*, pages 84-97.

Wolf, W. W., Westbrook, J. K., Raulston, J., Pair, S. D., and Hobbs, S. E. (1990). Recent airborne radar observations of migrants pests in the United States. *Phil. Trans. Royal Soc. London B*, **328**, 619-630.

Wood, C. R., Chapman, J. W., Reynolds, D. R., Barlow, J. F., Smith, A. D., and Woiwod, I. P. (2006). The influence of the atmospheric boundary layer on nocturnal layers of noctuids and other moths migrating over southern Britain. *Int. J. Biometeorol.*, **50**, 193-204.